



US Army Corps
of Engineers
Waterways Experiment
Station

Technical Report CERC-93-12
August 1993

AD-A269 839



(2)

In-House Laboratory Independent Research Program

Surf Beat in Coastal Waters

by Edward F. Thompson, Michael J. Briggs
Coastal Engineering Research Center

DTIC
ELECTE
SEP 2 8 1993
S A D

Approved For Public Release: Distribution Is Unlimited

93 9 27 091

021150 93-22423
184P8



The contents of this report are not to be used for advertising, publication, or promotional purposes. Citation of trade names does not constitute an official endorsement or approval of the use of such commercial products.



PRINTED ON RECYCLED PAPER

Surf Beat in Coastal Waters

by Edward F. Thompson, Michael J. Briggs
Coastal Engineering Research Center

U.S. Army Corps of Engineers
Waterways Experiment Station
3909 Halls Ferry Road
Vicksburg, MS 39180-6199

Accesion For	
NTIS GRADE	V
DATA FORM	23
U.S. GOVERNMENT	23
JOINT SOURCE	23
SEARCHED	
INDEXED	
SERIALIZED	
FILED	
By	
DRAFTED	
RECORDED	
APPROVED FOR RELEASE	
DISTRIB	
A-1	

DTIC QUALITY INSPECTED 3

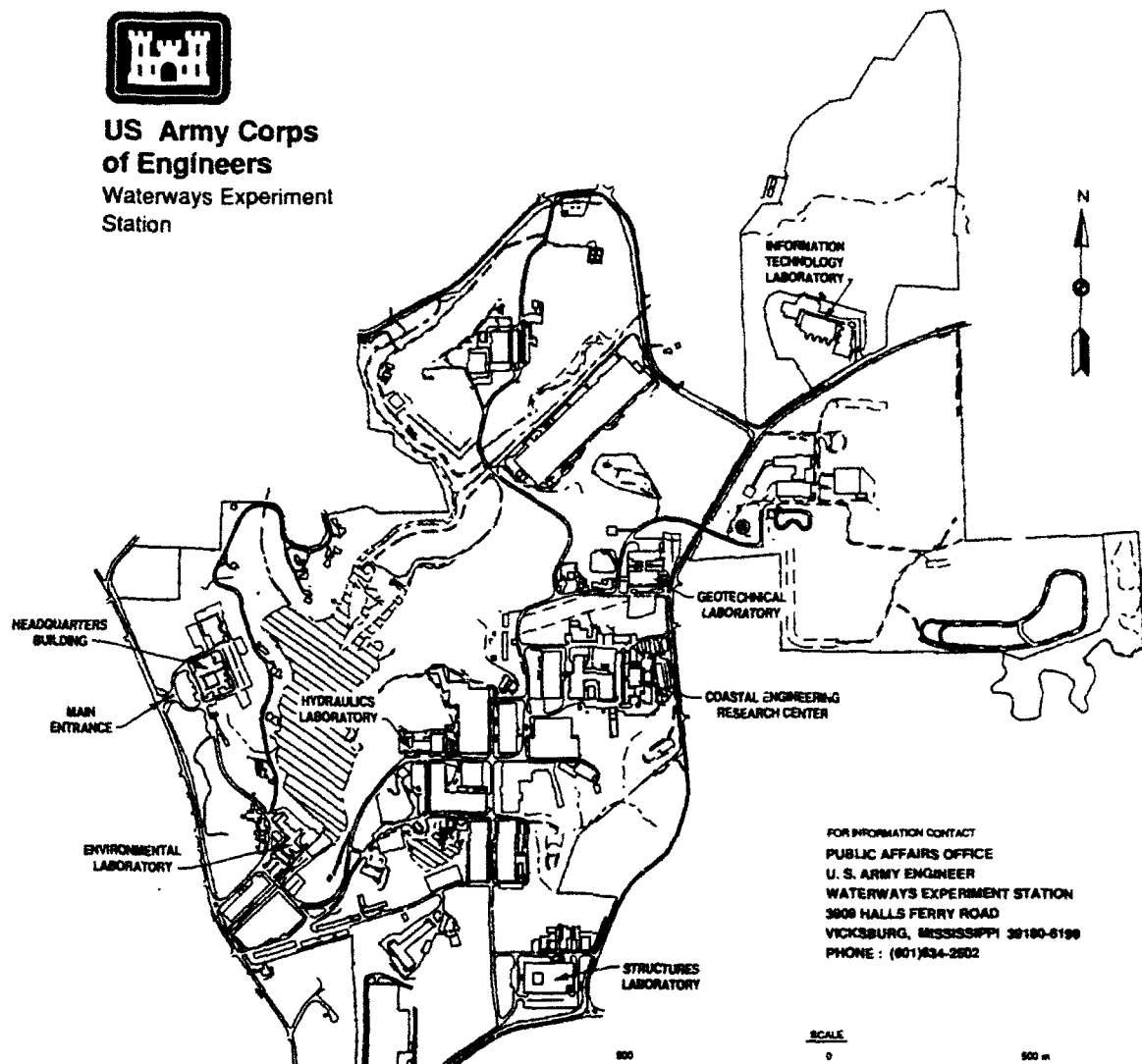
Final report

Approved for public release; distribution is unlimited



**US Army Corps
of Engineers**

Waterways Experiment
Station



Waterways Experiment Station Cataloging-in-Publication Data

Thompson, Edward F.

Surf beat in coastal waters / by Edward F. Thompson, Michael J. Briggs, Coastal Engineering Research Center ; prepared for Assistant Secretary of the Army (R&D).

182 p. : ill. ; 28 cm. -- (Technical report ; CERC-93-12)

Includes bibliographical references.

1. Ocean waves -- Mathematical models. 2. Spectral energy distribution. 3. Water waves -- Mathematical models. 4. Amphibious warfare. I. Briggs, Michael Jeffrey. II. United States. Assistant Secretary of the Army (Research, Development and Acquisitions) III. Coastal Engineering Research Center (U.S.) IV. U.S. Army Engineer Waterways Experiment Station. V. In-house Laboratory Independent Research Program (U.S. Army Engineer Waterways Experiment Station) VI. Title. VII. Series: Technical report (U.S. Army Engineer Waterways Experiment Station) ; CERC 93-12.

TA7 W34 no.CERC-93-12

Contents

Preface	vii
Conversion Factors, Non-SI to SI Units of Measurement	ix
1 - Introduction	1
Background and Purpose	1
Previous Studies	2
Procedure	5
2 - Theory	7
Theoretical Development	7
Computer Program	10
3 - Laboratory Experiments	14
Laboratory Tests	14
Results	23
Comparison with Theory	32
4 - Field Measurements	40
Field Experiment	40
Results	49
Comparison with Theory	56
5 - Conclusions	61
References	63
Appendix A: Offshore and Nearshore Array Directional Spectra	A1
Appendix B: Offshore Array Directional Spectra Over 360-deg Arc	B1

Appendix C: Short and Long Wave Significant Heights from Field Data	C1
Appendix D: Short and Long Wave Spectra from Field Data, Gage 181	D1
Appendix E: Short and Long Wave Spectra from Field Data, Gage 2904	E1
Appendix F: Short and Long Wave Spectra from Field Data, Gage 2804	F1
Appendix G: Short and Long Wave Spectra from Field Data, Gage 2704	G1
Appendix H: Short and Long Wave Spectra from Field Data, Gage 2504	H1
Appendix I: Short and Long Wave Spectra from Field Data, Gage 2404	I1
Appendix J: Short and Long Wave Spectra from Field Data, Gage 2304	J1
Appendix K: Short and Long Wave Spectra from Field Data, Gage 2204	K1
Appendix L: Short and Long Wave Spectra from Field Data, Gage 2104	L1

List of Figures

Figure 1. Main steps in processing time series	11
Figure 2. Basin and gage layout	15
Figure 3. Target and measured frequency spectra at OGA a) S0105; b) S0905; c) S3705; d) S4505	16
Figure 4. Measured frequency spectra offshore (Gage 4) and nearshore (Gage 20), S0105	18
Figure 5. Distribution of period between successive runup maxima above a threshold value, RUNUP 6. Several different thresholds are represented. Analyses were performed by: a) Operator 1; b) Operator 2; c) Operator 3	21

Figure 6. Distribution of period between successive runup maxima above a threshold value, RUNUP 7. Several different thresholds are represented. Analyzed by Operator 1	22
Figure 7. Significant wave height, short waves: a) 0-deg approach; b) 20-deg approach	24
Figure 8. Directional spectrum, S0105, OGA: a) Short waves; b) Long waves	25
Figure 9. Directional spectrum, S0105, NGA: a) Short waves; b) Long waves	25
Figure 10. Significant wave height, long waves, 0-deg approach: a) Swell; b) Sea	26
Figure 11. Significant wave height, long waves, 20-deg approach: a) Swell; b) Sea	27
Figure 12. Measured long wave spectra, 0-deg approach: a) S0105; b) S0905; c) S3706; d) S4504	28
Figure 13. Measured long wave spectra, 20-deg approach: a) S2505; b) S3305; c) S6105; d) S6905	30
Figure 14. Time series from short waves (measured) and long waves (predicted), S3705: a) Gage 4; b) Gage 10	33
Figure 15. Predicted and measured long wave spectra, 0-deg approach: a) S0105; b) S0905; c) S3706; d) S4504	35
Figure 16. Predicted and measured long wave spectra, 20-deg approach: a) S2505; b) S3305; c) S6105; d) S6905	37
Figure 17. DELILAH gage locations and bathymetry, 12 Oct 90	42
Figure 18. Directional wave spectrum from array in 8-m depth, 12 Oct 90. Local wind vector and variability also shown	44
a) 1300 hr; $H_{m0}=1.54\text{m}$; $T_p=15.6\text{ sec}$; b) 1600 hr; $H_{m0}=2.18\text{m}$; $T_p=13.6\text{ sec}$; c) 1900 hr; $H_{m0}=2.42\text{m}$; $T_p=13.6\text{ sec}$; d) 2200 hr; $H_{m0}=2.45\text{m}$; $T_p=13.6\text{ sec}$;	
Figure 19. Significant wave height, 1600-1900 12 Oct 90, 17-min records: a) Short waves; b) Long waves	50
Figure 20. Significant wave height variation with cross-shore location, 17-min records beginning at 1651 (Gage 181) and 1658 (nearshore gages)	51

Figure 21. Significant wave height variation with depth, 17-min records from all nearshore gages	53
Figure 22. Variation of H_{m0LW}/H_{m0} with time, 17-min records	53
Figure 23. Variation of H_{m0LW}/H_{m0} with H_{m0}/d , 17-min records, all nearshore gages	54
Figure 24. Variation of H_{m0LW}/H_{m0} at Gage 2904 with offshore H_{m0} , 17-min records	54
Figure 25. Variation of $H_{m0LW}/(H_{m0})_{\text{Gage } 181}$ with depth	55
Figure 26. Short wave spectrum, 17-min records beginning at 1658	56
Figure 27. Long wave spectrum, 102-min records a) Gages 181, 2904, and 2804; b) Gages 2704, 2504, and 2404; c) Gages 2304, 2204, and 2104	57
Figure 28. Predicted and measured significant height, long waves, 17-min records: a) Gage 181; b) Gage 2904; c) Gage 2804	58
Figure 29. Predicted and measured long wave spectra, 102-min records beginning at 1651 (Gage 181) and 1658 (Gage 2804)	60

Preface

This study was performed by the Coastal Engineering Research Center (CERC) of the US Army Engineer Waterways Experiment Station (WES) under the In-House Laboratory Independent Research Program, Project A91D, Work Unit No. 4A161101A91D-003.

This report was prepared by Dr. Edward F. Thompson, Coastal Oceanography Branch (COB), Research Division (RD), CERC, and Mr. Michael J. Briggs, Wave Processes Branch (WPB), Wave Dynamics Division (WDD), CERC. The work was performed under the direct supervision of Dr. Martin C. Miller, Chief, COB, Mr. H. Lee Butler, Chief, RD; Mr. Dennis G. Markle, Chief, WPB; and Mr. C. E. Chatham, Jr., Chief, WDD; and under the general supervision of Mr. Charles C. Calhoun, Jr., Assistant Director, CERC, and Dr. James R. Houston, Director, CERC.

Special acknowledgement is due to Mses. Karen Huff and Panola Rivers, COB, for extensive contributions to laboratory and field data collection, analysis, and interpretation. Ms. Lori Hadley provided valuable assistance in preparing material for this report. Mr. Francis E. Sargent, WPB, provided a computer program for band-pass filtering of time series, and Dr. Steven A. Hughes, WDD, provided a computational code for nonlinear interactions in a wave spectrum.

This limited study was able to include state-of-the-art laboratory and field data sets because of the dedicated efforts of a number of people. Mr. David A. Daily, Electronic Technician in the WES Instrumentation Services Division, and Mrs. Debra R. Green, WPB, assisted in laboratory data collection and analysis. Mrs. Brenda J. Wright, Wave Research Branch, WDD, and Mr. Kent K. Hathaway, Field Research Facility (FRF), Engineering Development Division, assisted in video data collection and analysis. Special appreciation is extended to participants in the DELILAH field experiment for collaborating to collect an excellent set of field data. Dr. Edward B. Thornton, Naval Postgraduate School, Monterey, CA, with the assistance of many others, acquired the data from the nearshore pressure gages. Messrs. William A. Birkemeier, Kent K. Hathaway, Clifford F. Baron, and Dr. Charles E. Long, FRF; and Dr. Robert T. Guza, Scripps Institution of Oceanography, La Jolla, CA, provided critical support during the experiment.

At the time of publication of this report, Director of WES was
Dr. Robert W. Whalin. Commander was COL Bruce K. Howard, EN.

Conversion Factors, Non-SI to SI Units of Measurement

Non-SI units of measurement used in this report can be converted to SI units as follows:

Multiply	By	To Obtain
feet	0.3048	meters
inches	25.4	millimeters

1 Introduction

Background and Purpose

As ocean wind waves propagate into shallow water, they exhibit increasingly strong nonlinearities. One important nonlinear effect is the emergence of low frequency energy as a consequence of interactions between higher frequency incident wave components. While wind wave periods are between 1 sec and 30 sec, the low frequency energy is typically characterized by periods between 30 sec and several minutes. This low frequency energy is often referred to as "long waves" because the wave lengths at these frequencies are considerably longer than those associated with wind waves. Similarly, wind waves are usually termed "short waves" in this context. Another often-used term synonymous with long waves is "infragravity waves."

Approaching a beach, incident wind waves ultimately break and their maximum height nearshore is limited by water depth. However, the emerging low frequency components never break and continue to grow as offshore wave conditions intensify. The low frequency components, often called surf beat, can dominate the inner surf zone during storm conditions.

While models can predict wind wave growth and propagation reasonably well, the evolution of surf beat is not easily modeled at present. A major barrier to progress is the difficulties involved in collecting hydrodynamic data in the surf zone. The surf zone is characterized by strong turbulence and intense dissipation of energy. Measuring devices, besides being very rugged, must maintain accuracy despite the presence of sand in suspension and air bubbles entrained during the breaking process.

Laboratory and field data provide essential documentation and insights on nonlinear processes. Major advances in laboratory and field wave data collection and analysis over the last decade have greatly enhanced the value of these tools for investigating second order nonlinear phenomena. With the acquisition of a directional wave laboratory basin, the U.S. Army Engineer Waterways Experiment Station (WES) has a capability matched by only a few laboratories in the world to investigate coastal hydrodynamics under controlled conditions. Irregular wave conditions which closely resemble those in nature can be generated. Further WES has a Field Research Facility (FRF) at Duck, NC, which greatly facilitates development of field expertise and collection of

high-quality field measurements. Both of these facilities are valuable tools in investigating surf beat.

The purpose of this study was to develop a practical predictive relationship between offshore wave conditions and nearshore long waves, including surf beat. Since offshore wave conditions are usually known or can be estimated with reasonable accuracy at a site and they are the primary forcing mechanism for nearshore long waves, they are an appropriate basis for predicting surf beat. The objectives were to develop and test a relatively simple predictive model in order to demonstrate the feasibility of predicting surf beat and to provide a first-level tool for surf zone modeling applications.

Surf beat has a strong impact on both military and civil works activities in the Corps of Engineers. In the military sphere, amphibious landing operations and Logistics Over The Shore (LOTS) activities can be seriously impacted by strong currents, water level variations, and runup induced by surf beat. Examples include vessel maneuverability, vessel motions, and forces on vessel and causeway mooring lines, pipelines, and pilings. Scour around pipelines and pilings can also be a concern.

Besides the evident importance of long waves in surf zone processes, long waves can impact operations outside the surf zone. Typically long waves are a concern when operations involve equipment with resonant periods that fall within the range of long wave periods. They also cause problems in harbors with resonant oscillation frequencies in the long wave range.

Military LOTS applications impacted by long waves outside the surf zone include vessel motions during transfer of cargo to lighterage, forces on vessel mooring lines, and dredge motions which can damage bottom-contacting equipment. When protected or semi-protected harbors are available in a military operation, long waves are always a potential source of excessive motions and mooring forces for docked vessels.

The work described in this report impacts three active work units in the WES military research program on Sustainment Engineering. The key application is in LOTS, the movement of personnel and material from ships to shore. The work units affected are Real-Time Forecasting of Sea States, Water Levels and Currents for LOTS Operations, and Simulation Model for LOTS Operations.

Previous Studies

Low frequency nearshore motions were first observed by Munk (1949) and Tucker (1950). They documented surf beat with measurements. Further, they suggested a link between incident wind wave grouping and surf beat. Some subsequent studies have more formally defined surf beat as the low frequency nearshore motions occurring in the cross shore direction. Low frequency nearshore motions which propagate in the longshore direction are referred to as "edge waves," however edge waves are difficult to distinguish from surf beat

without comprehensive measurement and analysis. Recent reviews of the subject of low frequency nearshore motions are provided by Oltman-Shay and Hathaway (1989) and Kobayashi (1988).

Field studies have confirmed the presence of significant surf beat motions in the surf zone, as manifested in both surface fluctuations, velocities, and runup. The motions are most important on gently sloping beaches. While wind waves lose most of their energy in traversing the surf zone, surf beat maintains or increases its energy and can dominate the inner surf zone (particularly the swash zone) during storms. Goda (1975) found surf beat heights in 1 m depth which were between 20 and 40 percent of the offshore wave height. Guza and Thornton (1985), using reasonably detailed measurements from 3 California beaches, found surf beat heights of 37 and 32 percent of the offshore (10-m depth) wave height in water depths of 0-1 m and 1-2 m, respectively. Holman and Bowen (1984) analyzed runup data collected along the Oregon coast. Holman and Sallenger (1985), using measurements at Duck, NC, demonstrate a linear dependence of setup and swash height scaled by incident height on the surf similarity parameter

$$\xi_0 = \frac{\beta}{\sqrt{\frac{H_0}{L_0}}} \quad (1)$$

where

- ξ_0 = surf similarity parameter,
- β = foreshore slope (typically $\beta < 1$),
- H_0 = incident deep water wave height (taken as the significant height measured in 20-m depth),
- L_0 = incident deep water wavelength.

Guza and Thornton (1985) cite a number of other field studies in which surf beat was identified as an important feature.

The process by which short (wind) waves create long waves has been explained theoretically by two mechanisms. First, radiation stress forces a depression of local mean water level under high short waves and an elevation under low short waves (Longuet-Higgins and Stewart 1962, 1964). Thus grouping in wind waves induces a low frequency component of sea surface motion in any water depth. The low frequency motions, or long waves, are tied to the short wave groups. They propagate at the short wave group velocity. They are commonly referred to as "bound" long waves. The importance of bound long waves is confirmed by Huntley and Kim's (1984) field measurements from St. Margaret's Bay, Nova Scotia, showing a strong correlation between low frequency cross shore velocities and the short wave envelope. List (1986) validated the importance of bound long waves with field

measurements from Duck, NC. Okihiro, et al. (1992) and Elgar, et al. (1992) also investigated the presence of bound long waves in field data from a variety of shallow water measurement sites.

It is generally accepted that the bound waves can give rise to freely propagating long waves in shallow water when short wave energy is dissipated, as in the surf zone, or partially blocked, as at a harbor entrance. The process by which bound long waves become free long waves is not well understood. Since free long waves are effectively reflected by a coast, seaward-propagating long waves are also expected. They can be partially reflected back toward the coast by depth variations. Long shore propagating free long waves (edge waves) may also be formed.

The second theoretical mechanism for generating long waves from short waves was proposed by Symonds, et al. (1982). The source is the relatively slow variation in time of the point of nearshore wave breaking as groups of high short waves alternate with groups of low short waves. This mechanism is a function of nearshore bottom slope as well as incident short wave characteristics. The long waves thus generated are freely propagating. The authors also predict a shore-reflected long wave and, hence, a standing long wave in the surf zone. It was suggested that the standing long wave may play a role in shaping nearshore morphology, particularly the location of nearshore bars. Symonds and Bowen (1984) extended the model to include representation of a linear, shore-parallel bar. Similarly, edge waves have been postulated as a mechanism for the formation of beach cusps. The existence of cross shore standing wave patterns is reasonably well documented (e.g. Guza and Thornton 1985).

Since short wave information is much more widely available and better understood than long wave information, it is highly desirable to have a short wave driven model for predicting long waves. A number of theoretical approaches have been suggested. These can be distinguished in terms of whether they address long waves in the frequency or time domain.

Hasselmann (1962) used a perturbation approach extended to fifth order to formulate the weak nonlinear couplings between spectral components in the frequency domain. Assumptions include small wave slopes and horizontally unbounded ideal fluid of constant depth. The nonlinear couplings result in transfer of energy from short to long wave frequencies. The transfer is highly dependent on water depth and directional spread of spectral energy, with stronger transfer to long waves occurring as the depth decreases and the directional spread narrows (Okihiro, et al. 1992).

Theoretical expressions for second-order, group-induced long waves from nonlinear interactions within a short wave spectrum were presented by Sand (1982a) based on earlier work by Ottesen Hansen (1978). The expressions arise from solution of Laplace's equation with nonlinear surface condition and boundary conditions expanded to second order. Assumptions inherent in the theory include no breaking, constant local water depth, and no directional spread. The theory was extended by Sand (1982b) to include directional

spreading. An expression for the long wave spectrum as a function of the local wind wave spectrum was given by Sand (1982c). The long wave spectrum depends on Fourier "a" and "b" coefficients from the short wave spectrum. Hence it depends on phases as well as amplitudes of short wave components. Sand's work, which parallel's Hasselmann's (1962), is described more fully in Chapter 2.

Additional theoretical developments based in the frequency domain include van Leeuwen and Battjes (1990) and Agnon, et al. (1993). van Leeuwen and Battjes (1990) extended the work of Longuet-Higgins and Stewart (1962, 1964) and Symonds, et al. (1982) to include a continuous spectrum of short waves. Agnon, et al. (1992) derived an evolution equation describing spectral shoaling which includes quadratic interactions. In the limit of shallow water, the quadratic interactions approach a Boussinesq model. The model presented is restricted to unidirectional waves approaching normal to parallel depth contours.

The calculation of surf beat arising from irregular short waves was investigated in the time domain by Lo (1981). His primary focus was the simplified case of a periodically modulated (bichromatic) short wave train. Subsequent studies include those by Mei and Benmoussa (1984), Liu (1989), and Schaffer and Jonsson (1990).

Madsen, et al. (1991a, 1991b) used a new form of the Boussinesq equations to develop long wave evolution models in both the frequency and time domains. The models apply to unidirectional, shoaling waves. Other unidirectional time domain models capable of treating a realistic random sea state are given by Kobayashi, et al. (1989) and Mase and Kobayashi (1991).

A recent study by Okihiro, et al. (1992) indicates that long waves predicted from directionally spread short waves using Hasselmann's (1962) approach to second order are consistently lower than measurements in 8- to 13-m depths. Less than half of the observed long wave energy could be attributed to bound waves. The importance of bound long waves increases as incident swell wave energy increases. Predictions from unidirectional theory provide an upper limit on the expected bound long waves. Coincidentally, the unidirectional predictions also provide a better approximation to the total long wave energy observed in the data. The relative dominance of free long wave energy and the correlation between swell energy and bound long wave energy are also discussed by Elgar, et al. (1992) using additional field data sets.

Procedure

The research procedure includes collection and analysis of laboratory and field data complemented by investigation of theory. The theoretical approach is taken from the work of Sand (1982a, 1982c) based on the nonlinear transfer of energy from short to long waves. It is assumed that the waves are unidirectional and they propagate over a flat bottom for a sufficient distance for the nonlinear transfers to stabilize. The theoretical approach and the

Fortran computer program in which it has been implemented are described in Chapter 2.

Data were collected in the WES directional wave laboratory basin over a plane, 1:30 slope, which is representative of natural beaches. A variety of controlled offshore wave conditions was generated and wave measurements were collected through the surf zone. The advantage of working in a laboratory basin is positive control of bottom configuration, gage placement, and wave generation. The disadvantage is possible distortion by influences in the laboratory which would not be present in nature. Primary concerns are reproducing low frequency energy correctly and minimizing multiple reflections of low frequency waves in the confined basin. The laboratory experiments and results are described in Chapter 3.

Field data were obtained in the multi-agency Duck Experiment on Low-frequency and Incident-band Longshore and Across-shore Hydrodynamics (DELILAH) experiment at the WES FRF during the fall of 1990. Hurricane swell measured along a cross-shore gage array represented a near ideal test case. The data provide perspective on the limitations of the theory and on possible laboratory effects such as shortcomings in the reproduction of incident low frequency energy and reflections of low frequency waves in the confined basin. The field experiment and results are described in Chapter 4.

Theoretical predictions were compared to laboratory and field measurements to develop guidelines for predicting surf beat. The comparisons are presented as part of respective laboratory and field results (Chapters 3 and 4). Conclusions are given in Chapter 5.

2 Theory

Theoretical Development

The theoretical approach used in this study is based on the work of Ottesen Hansen (1978) and Sand (1982a, 1982c). This approach provides a predictive linkage between short waves and long waves in shallow water which is suitable for examining the basic mechanisms underlying surf beat. A formulation for control of laboratory wavemakers to correctly simulate both long and short waves is also examined by Sand (1982a).

A general expression for bound long waves induced by short waves can be derived from a perturbation analysis of the Laplace equation. When the nonlinear boundary conditions are expanded to second order, subharmonic terms appear. These terms describe the group-induced long waves.

A single short wave component can be described as

$$\eta_n(t) = a_n \cos(\omega_n t - k_n x_1) + b_n \sin(\omega_n t - k_n x_1) \quad (2)$$

where

$\eta_n(t)$	= time series of water surface elevation;
t	= time;
a_n, b_n	= Fourier a and b coefficients;
ω_n	= frequency of the n'th spectral component, in radians;
k_n	= wavenumber of the n'th spectral component;
x_1	= spatial coordinate of the point of interest.

If two short wave components are combined, a grouped time series is created of the form

$$\begin{aligned} \eta_{nm}(t) = & a_n \cos(\omega_n t - k_n x_1) + b_n \sin(\omega_n t - k_n x_1) \\ & + a_m \cos(\omega_m t - k_m x_1) + b_m \sin(\omega_m t - k_m x_1) \end{aligned} \quad (3)$$

where the n and m subscripts denote the n 'th and m 'th spectral components, respectively. The second order long wave time series corresponding to this group is given by

$$\frac{\eta_{LB_{nm}}(t)}{d} = G_{nm}d \left[\frac{a_n a_m + b_n b_m}{d^2} \cos(\Delta\omega_{nm}t - \Delta k_{nm}x_1) + \frac{a_m b_n - a_n b_m}{d^2} \sin(\Delta\omega_{nm}t - \Delta k_{nm}x_1) \right] \quad (4)$$

where

- $\eta_{LB_{nm}}(t)$ = time series of long wave surface elevations;
- d = water depth;
- G_{nm} = nonlinear transfer function;
- $\Delta\omega_{nm}$ = $\omega_n - \omega_m$;
- Δk_{nm} = $k_n - k_m$.

The long wave frequency can be expressed as

$$\Delta f_{nm} = f_n - f_m = \frac{\Delta\omega_{nm}}{2\pi} \quad (5)$$

where

- Δf_{nm} = long wave frequency, in Hertz;
- f_n, f_m = short wave frequencies, in Hertz.

It is convenient to work with the nonlinear transfer function as the product $G_{nm}d$, which renders it dimensionless. This product can be calculated as

$$G_{nm}d = \frac{4\pi^2 D_n D_m \Delta k_{nm} d \cosh(\Delta k_{nm}d)}{\cosh(k_n d + k_m d) - \cosh(\Delta k_{nm}d)} \cdot \frac{\Delta k_{nm} d (D_n - D_m)(k_n d D_m + k_m d D_n) \coth(\Delta k_{nm}d)}{2 D_n D_m} \quad (6)$$

$$- 2\pi^2 (D_n - D_m)^2 \Delta k_{nm} d \left[4\pi^2 (D_n - D_m)^2 \coth(\Delta k_{nm}d) - \Delta k_{nm} d \right]^{-1}$$

where

$$D_n = \sqrt{\frac{d}{g}} f_n \quad (7)$$

$$D_m = \sqrt{\frac{d}{g}} f_m$$

and

g = acceleration due to gravity.

Graphical displays of the functional dependence of $G_{nm}d$ on nondimensional depth and Δf_{nm} are available in the literature (Sand 1982a, 1982c). Generally $G_{nm}d$ decreases slightly as waves propagate from deep to intermediate water depth and then rapidly increases as waves continue to shoal in shallow water.

The time series of long wave surface elevations in an irregular sea state composed of many different frequency components can be expressed as

$$\eta_{LB}(t) = \sum_{n=n_1}^{n_2} \sum_{m=n_1}^{n_2} \eta_{LBnm}(t) \quad (8)$$

where

- $\eta_{LB}(t)$ = time series of long wave surface elevations;
- n_1 = $f_1/\Delta f$;
- f_1 = lowest frequency in the short wave spectrum, an integer multiple of Δf ;
- Δf = basic frequency increment in spectral analysis, = T_R^{-1} ;
- T_R = record length;
- n_2 = $f_2/\Delta f$;
- f_2 = highest frequency to be included in the short wave spectrum, an integer multiple of Δf ;

and $\eta_{LBnm}(t)$ is obtained from equation 4.

An expression for components of the energy density spectrum of long waves was given by Sand (1982c) as

$$S_{\eta, LB}(\Delta f_{nm}) = \frac{\left[\sum_{m=n}^{n_2} G_{nm} (a_m a_m + b_m b_m) \right]^2 + \left[\sum_{m=n}^{n_2} G_{nm} (a_m b_m - a_m b_m) \right]^2}{2 \Delta f} \quad (9)$$

where

$S_{\eta, LB}(\Delta f_{nm})$ = group bound low frequency spectral density at frequency Δf_{nm} .

These equations allow short wave information to be used in calculating bound long waves, including the time series (equation 8) and the spectrum (equation 9). The long wave information depends directly on Fourier a and b coefficients from the short wave time series, and hence is dependent on short wave amplitude and phase.

Computer Program

The Fortran computer program LONGWV was written for analysis of long waves in this study. Major operations in the program are diagrammed in Figure 1. Input time series can be read in either of two standard WES formats: the Coastal Engineering Research Center (CERC) laboratory data format, and the FRF field data format. A variety of input parameters is specified to define and control the analysis. The mean is computed and subtracted from each time series.

The frequency spectrum is computed with a Fourier Transform (FT) routine written by A. Yfantis, University of Nevada, Las Vegas, and Leon Borgman, University of Wyoming, Laramie, Wyoming. The FT routine is capable of performing both direct and inverse transforms. It can transform any number of points up to the record total as long as that number can be factored into powers of 2, 3, and 5. Hence it is considerably more general than the traditional FT routines which require the number of points to be an even power of 2. The FT routine returns estimates of the a and b coefficients defined by

$$\eta(t) = \sum_{i=1}^{\frac{N}{2}-1} (a_i \cos \omega_i t + b_i \sin \omega_i t) \quad (10)$$

where

$\eta(t)$ = time series of water surface elevations;

N = number of data points in time series;

a_i, b_i = Fourier a and b coefficients;

ω_i = frequency of i 'th spectral component.

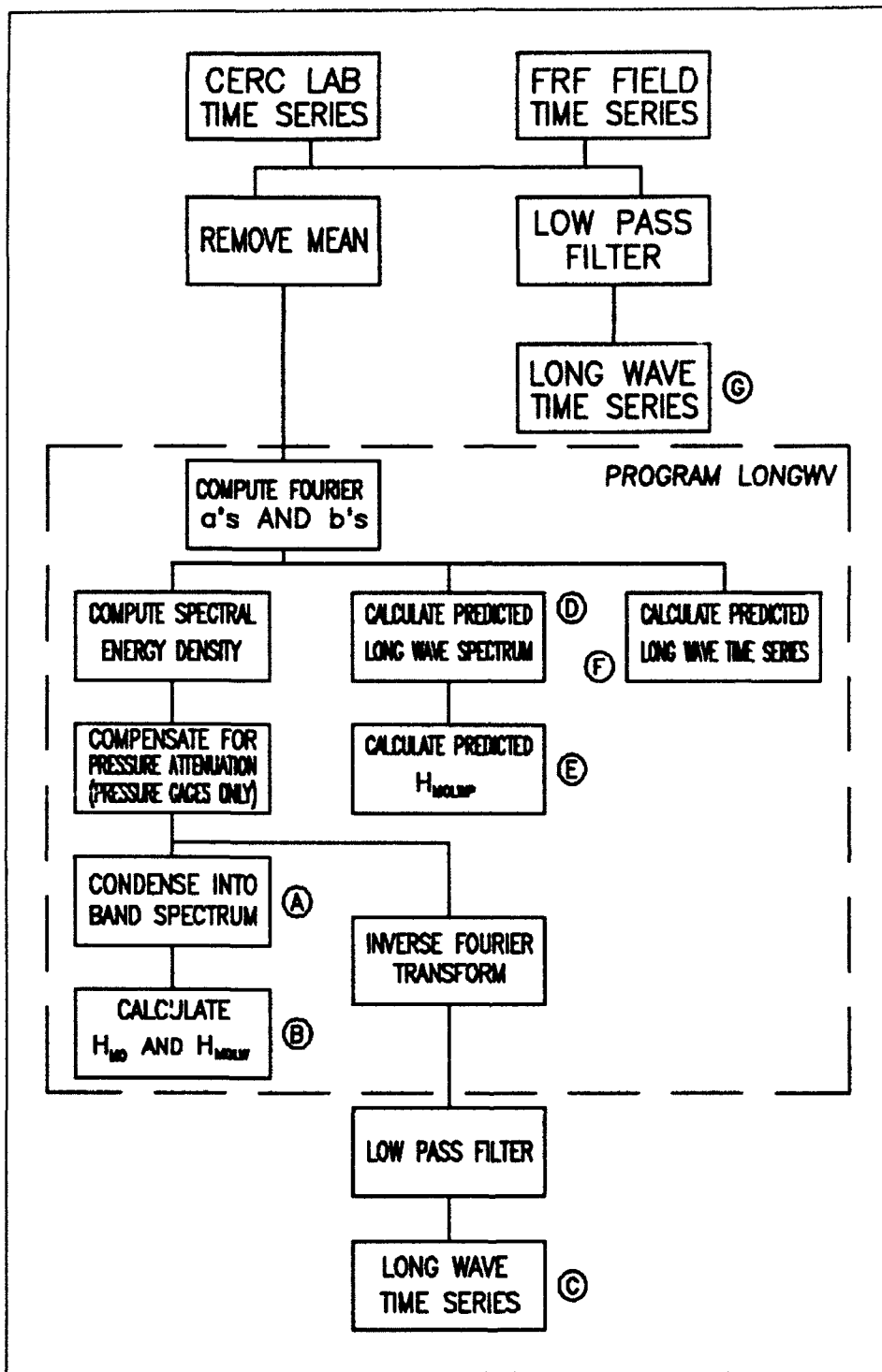


Figure 1. Main steps in processing time series

Spectral energy and energy density are computed from the FT components. Energy is compensated for pressure attenuation with depth if subsurface pressure gages are being analyzed (needed for FRF data). Energy is summed in both the short and long wave portions of the spectrum. Short and long wave significant heights are estimated as follows (B in Figure 1):

$$H_{mo} = 4.0 \left(\sum_{i=n_1}^{n_2} S_i(f) \right)^{\frac{1}{2}} \quad (11)$$

where

- H_{mo} = significant wave height, short waves;
- $S_i(f)$ = spectral energy for i 'th frequency component;
- n_1 = low frequency limit of short wave spectrum;
- n_2 = high frequency limit of short wave spectrum;

and

$$H_{mOLW} = 4.0 \left(\sum_{i=n_{1LW}}^{n_{2LW}} S_{nLW_i}(f) \right)^{\frac{1}{2}} \quad (12)$$

where

- H_{mOLW} = significant wave height, long waves;
- $S_{nLW_i}(f)$ = spectral energy for i 'th frequency component;
- n_{1LW} = low frequency bound of long wave spectrum;
- n_{2LW} = high frequency bound of long wave spectrum.

Spectral energy is condensed into bands, which decreases spectral resolution but increases stability of the spectral estimate (A in Figure 1). Critical parameters summarizing this process, following the notation recommended by IAHR (1986), are given in Table 1. The number of degrees of freedom is a measure of stability or confidence level of the spectral estimates. The larger the number of degrees of freedom, the higher the spectral stability. The IAHR (1986) recommends a minimum of 20 degrees of freedom.

Table 1 Critical Parameters Related To Spectral Computation	
Symbol	Description
T_R	Record length
b	Spectral bandwidth
v	Number of degrees of freedom

The bound long wave spectrum is predicted in LONGWV using the Fourier a and b coefficients from the short wave spectrum and equation 9 (D in Figure 1). A predicted long wave significant height is calculated from the predicted spectrum as (E in Figure 1)

$$H_{mOLW_p} = 4.0 \left(\sum_{i=R_{LB}}^{n_{LB}} S_{\eta LB_i}(f) \right)^{\frac{1}{2}} \quad (13)$$

where

H_{mOLW_p} = predicted long wave significant height;
 $S_{\eta LB_i}(f)$ = predicted low frequency spectral density for i'th component;

As with the measured spectra, the predicted long wave spectrum is condensed into bands to yield more stable estimates.

An option is available in LONGWV to use the Fourier a and b coefficients to predict the long wave time series rather than the spectrum (F in Figure 1). The procedure is based on equations 4 and 8.

The last main step in LONGWV is calculation of the inverse Fourier transform. When all of the Fourier a and b coefficients are used in the inverse transform, the original time series is recreated. This procedure is helpful for verifying proper operation of the FT routine. Alternatively, the Fourier coefficients for a selected range of frequencies can be used in the inverse transform to recreate a filtered time series. This procedure can be used to create a time series of measured long waves (C in Figure 1). A measured long wave time series can also be extracted more directly from the original time series by applying a low pass filtering routine (G in Figure 1).

3 Laboratory Experiments

Laboratory Tests

GBM Test Series

Data Collection. Laboratory tests were conducted as part of the Generalized Beach Model (GBM) series in the WES directional wave basin (Briggs and Smith 1990; Briggs, Smith, and Green 1991). The 28 m by 40 m basin contained a fixed, mortar bottom which was flat within 4.5 m of the wavemaker and then formed a plane 1:30 slope (Figure 2). Water depth at the wavemaker was 50 cm. Absorber material lined the basin back and sides. The sides had no solid walls but were open to adjacent basins to help minimize reflections. The model scale was approximately 1 to 25. Twenty surface wave gages were arranged in one cross-shore array and two linear longshore arrays, similar to the arrangement used in field experiments at Torrey Pines Beach, California (Pawka 1982). The longshore array nearest the wavemaker is termed the Offshore Gage Array (OGA). The shoreward longshore array is called the Nearshore Gage Array (NGA).

The tests of greatest interest in this study were single-peaked wave conditions normally incident to the slope. Unidirectional, narrow, and broad directional spreading were included. Energy appears in the low frequency portion of the spectrum during shoaling and visibly grows with continued shoaling. This process is indicative of the low frequency surf beat motions which are the subject of this study.

Eight wave conditions are considered in this study (Table 2). All cases were generated with the TMA spectral form using a gamma value of 3.3 (Bouws, et. al. 1985). The cases are characterized by peak period, where the 2.50-sec period represents swell and the 1.25-sec period sea. They are further characterized by approach direction (zero degrees is normal to shore) and directional spread (40 degrees represents a locally-generated sea). Wave data were collected at the sampling rate of 10 Hz to give a usable record length of 500 sec for swell and 250 sec for sea. Four additional unimodal cases, with wave direction of 10 deg, are available in the GBM data set. They were not considered in this study because the cases in Table 2 adequately cover the range of conditions. Analysis of these data for long wave information is also discussed by Thompson and Briggs (1991).

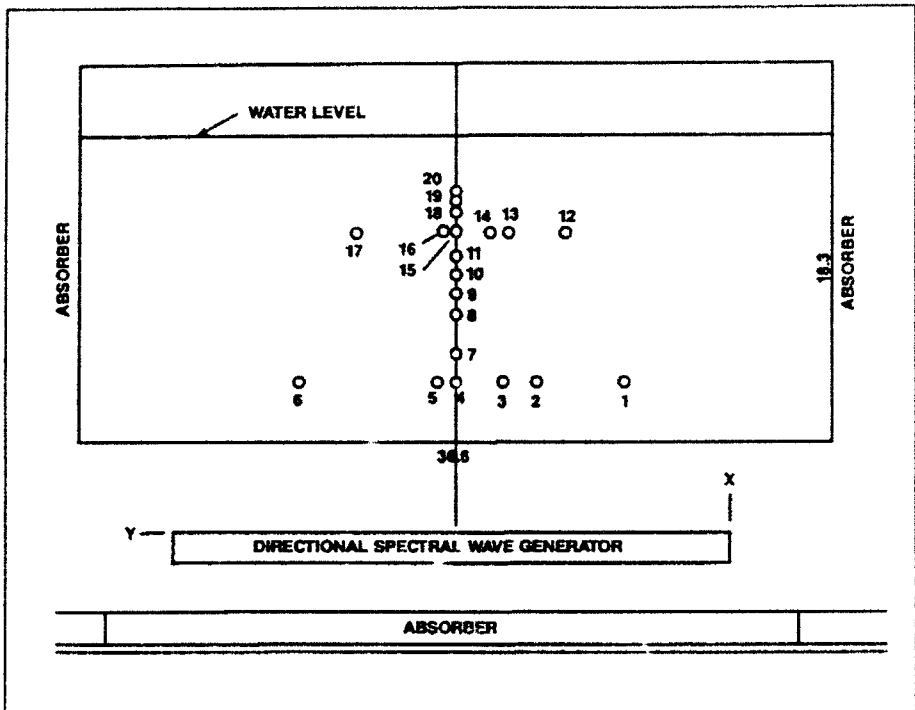
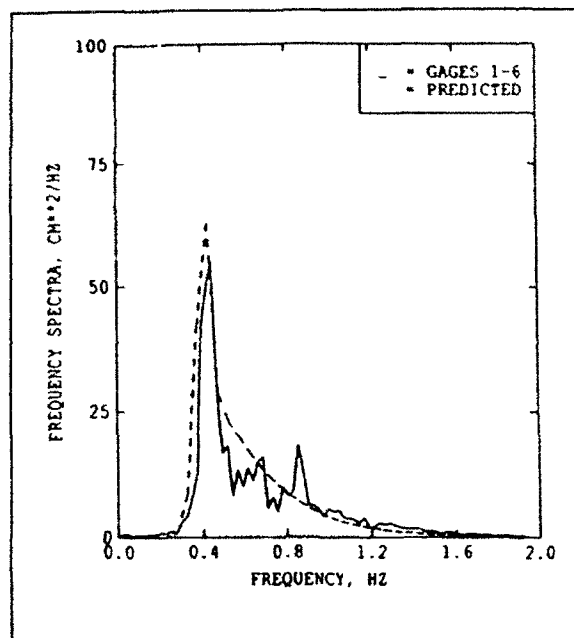


Figure 2. Basin and gage layout

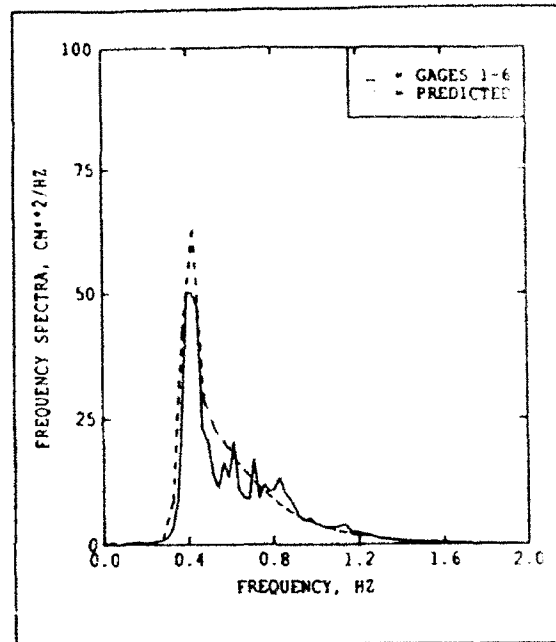
Table 2
Target Model Wave Conditions

Case	Peak Period sec	Significant Height cm	Direction deg	Directional Spread deg
S0105	2.50	15.2	0	0
S0905	2.50	15.2	0	40
S3705	1.25	12.2	0	0
S4505	1.25	12.2	0	40
S2505	2.50	15.2	20	0
S3305	2.50	15.2	20	40
S6105	1.25	12.2	20	0
S6905	1.25	12.2	20	40

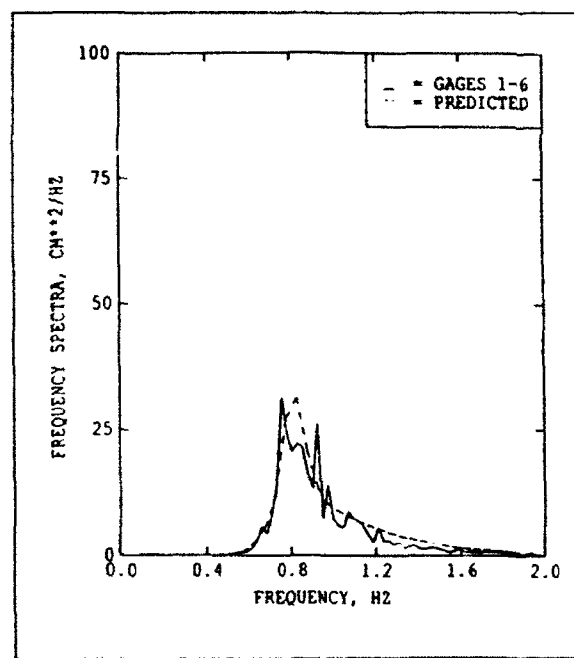
The wavemaker control signal was calculated to reproduce the target TMA spectrum at the OGA. The signal was then iteratively corrected as described by Briggs and Jensen (1988) until target and measured spectra approximately matched at the OGA. Corrections extended to frequencies as low as 0.05 Hz. The target and OGA spectra are adequately matched, as shown in Figure 3 for the 0-deg cases.



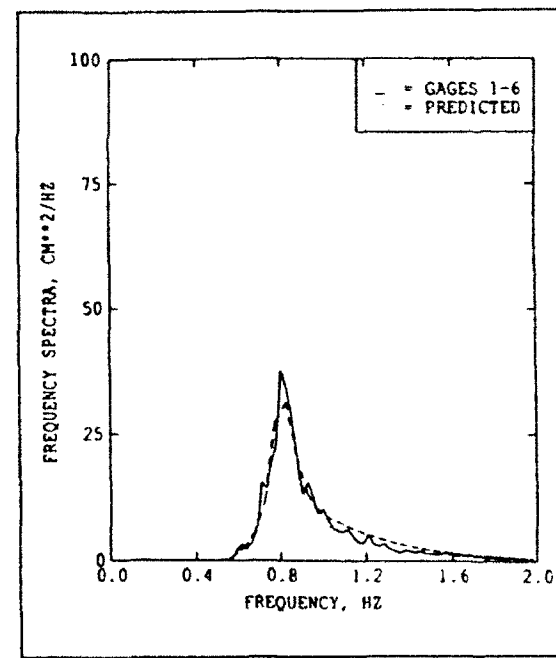
a) S0105



b) S0905



c) S3705



d) S4505

Figure 3. Target and measured frequency spectra at OGA

Data Analysis. Laboratory time series from the GBM cases were subjected to initial spectral analysis for this study using a FT routine with no windowing and 24 degrees of freedom. In terms of Table 1, the spectral analysis parameters were $T_R=500$ sec and $b=0.024$ Hz for the swell cases; $T_R=250$ sec and $b=0.048$ Hz for the sea cases; and $v=24$ for both cases. A larger value of v is desirable, but cannot be obtained without collecting longer time series records or overly reducing the spectral frequency resolution. The justification for using $v=24$ is as follows. If one assumes that wave groups repeat at time intervals of at least $4T_p$ and at most $15T_p$, where T_p is the peak period, then the long wave spectrum should adequately cover the frequency range

$$\frac{1}{15} f_p \quad \text{through} \quad \frac{1}{4} f_p \quad (14)$$

where f_p is the peak frequency (the reciprocal of T_p). For the long period cases

$$T_p = 2.5 \text{ sec} \quad f_p = 0.4 \text{ Hz} \quad (15)$$

$$\text{Range of long wave frequencies} \sim 0.028 - 0.100 \text{ Hz} \quad (16)$$

The analysis with $v=24$ corresponds to a frequency resolution of 0.024 Hz, a reasonable tradeoff between statistical confidence and resolution for these records. The same values are adequate for the cases in which T_p is 1.25 sec.

Significant wave height was calculated for both the short and long wave parts of the spectrum as discussed in Chapter 2. Frequencies less than half the peak frequency were considered as part of the long wave spectrum. This cutoff is arbitrary, but it includes most long wave energy without significant contamination from the low frequency tail of the wind wave spectrum. An example of spectra from one case helps illustrate the increase in low frequency energy in shallow water (Figure 4).

RUNUP Tests

The GBM tests have some important limitations in addition to short record lengths. Wave gages could not be placed across the entire surf zone for practical reasons. The most landward gages were in the outer part of the surf zone or, for low energy wave conditions, outside the surf zone. Also the GBM record length is shorter than needed for detailed analysis of low frequency components.

Data Collection. An opportunity for some additional tests arose as part of a cooperative study between WES, Scripps Institution of Oceanography, and

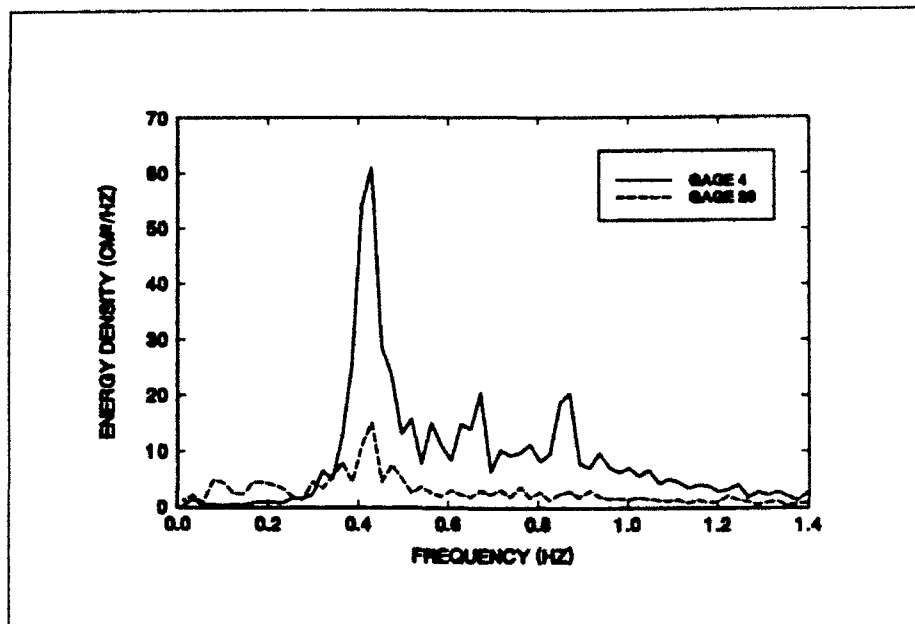


Figure 4. Measured frequency spectra offshore (Gage 4) and nearshore (Gage 20), S0105

Washington State University. This study, known as the Nonlinear Evolution of Refracting Directional Spectra (NERDS) study, was concerned only with the evolution of the short wave part of the spectrum (Elgar, et al. 1992). However, it provided an experimental setup similar to GBM and a promising chance for this study to gather data more suitable to long wave analysis. The primary objectives in modifying the GBM procedures were:

- 1) Increase the record length;
- 2) Collect data in the inner surf zone so that surf beat can be analyzed at the location where it is expected to be most intense.

The first objective is easily accomplished. The second objective is challenging.

Some novel approaches to accomplishing the second objective were tested during the NERDS runs. The approaches are based on the premise that surf beat is most visible and most easily measured in wave runup on the beach. Surf beat is strongly imprinted on wave runup. It is strongest in the inner surf zone. Also its effect is magnified in the runup. For example, a surf beat with height of 1 cm on a 1:30 sloped beach will move the mean runup location through a distance of 30 cm up or down the beach, depending on the phase of the surf beat wave. This periodic 30-cm variation in mean runup location may be more readily measured than a 1-cm surface variation, though neither can be measured by conventional techniques.

Two independent measurement techniques were tested during the NERDS experiments. Both techniques rely on novel applications of existing

equipment. Development of new equipment was beyond the scope of this study. The techniques are:

- a. runup gage was fabricated as an elongated staff gage which could be laid on the slope.
- b. tripod-mounted video camera was aimed at the runup zone.

The runup gage was laid along painted scale markers perpendicular to the water line. It was as close to the smooth beach slope as possible without touching. It provided time series records similar to the wave gages but with a much different scaling. The primary flaw of the runup gage was that it missed a substantial part of the upper runup of most waves. This runup occurs in thin sheets where the water surface is nearly parallel to the beach and the elevation is below the gage wire. Despite the clipping of upper runups from the record, it was hoped that the runup signal would still have a significant surf beat imprint.

The video camera was located at mean water level in the on/offshore direction and mid-basin in the alongshore direction. After some experimentation, the camera was placed at an elevation 0.5 m above the beach. The camera angle and zoom were adjusted so that scale markers painted on the beach were clearly visible and the runup/rundown levels approached the limits of the video frame. An oblique angle gave better runup visibility than a primarily downward-looking angle. With a video record in which the time-varying beach/water interface is sufficiently clear, a runup time series could be extracted. A video camera with 3/4-in.¹, broadcast quality tapes was used. Within the limits of the scope of this study, the approach drew on experience gained by Hathaway and Walton (1990) in earlier video runup tests in the laboratory.

Both measurement techniques tested were sufficiently successful that the NERDS tests were followed by a series of nine tests (referred to as the RUNUP tests) run strictly for this study. Wavemaker control signals were taken directly from selected GBM tests with changes of gain in some cases so that the limits of the runup gage were not exceeded. Thus the tests could be directly compared with previous GBM results.

The video camera zoom setting in the RUNUP tests was optimized by using an initial run of each test to insure the video frame was slightly larger than the range of extreme runup/rundown. Horizontal reference lines, helpful for later analysis, were created by encompassing the runup gage and the shadow of the frame supporting the cross-shore gage array. Each video included a static calibration segment in which a yardstick was placed against the runup gage support bar to verify cross-shore dimensions and linearity of the video frame.

¹ A table of factors for converting non-SI units of measurement to SI units is presented on page ix.

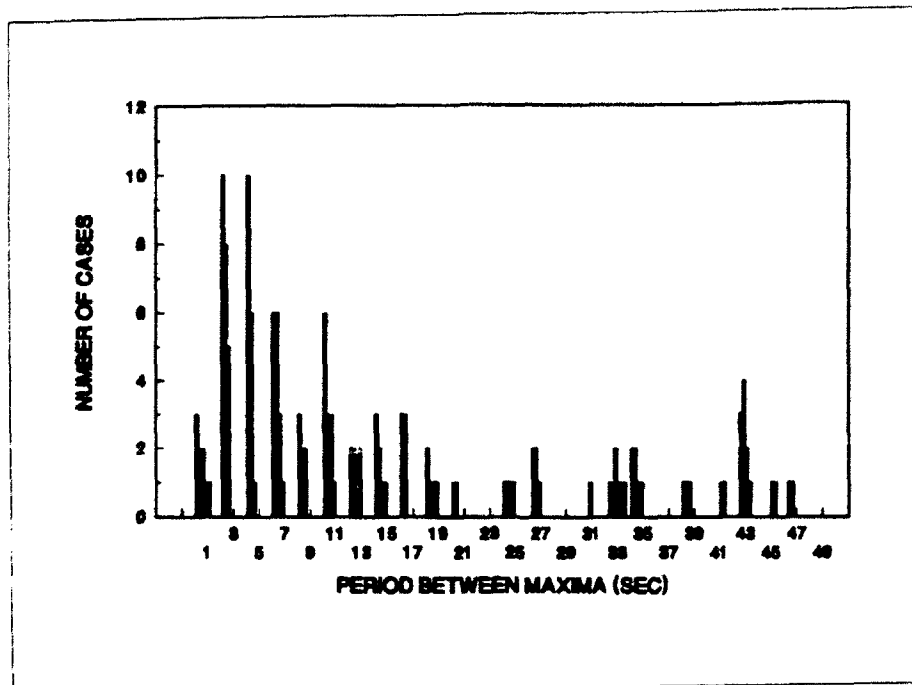
Data Analysis. Time series from the RUNUP tests were analyzed in the frequency and time domains with standard programs. The runup gage signal was included in the analysis. The runup gage analysis and examination of the time series plots did not give encouraging results because of the severe underestimation of upper runups, and this technique was not pursued further.

The initial approach to analyzing the video records was to use the automated WES FRF system. A trial tape was sent to the FRF. Despite some experimentation with options, the visual contrast at the land/water interface was too weak to be consistently recognized. This approach could be revisited in future experiments, especially if the interface visibility could be further optimized by such things as dying the water, painting the beach, and adjusting lighting. Anticipated improvements to the FRF automated system would also increase the probability of success in future efforts.

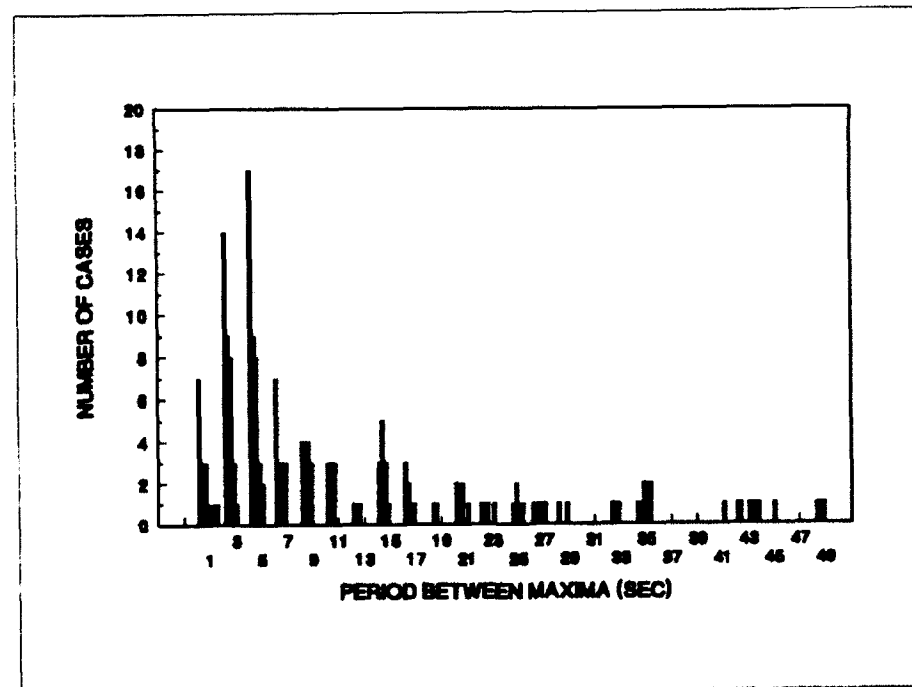
A manual digitization procedure was developed to analyze the video runup data. A WES video editing machine, which allows frame-by-frame control of the playback, was used. Because of the tedium and imprecision in the manual procedure, only the high and low values were extracted for each runup. The operator identified each frame in which a high or low value occurred. The horizontal location of each extreme was read from a scale grid on clear acetate superimposed on the video screen. The time of each extreme (relative to the record start) was read from the playback machine digital display. Maximum runup values could be accurately identified but extreme rundown values were often imprecise because the rundown did not have a distinct edge. In the operational procedure, the operator verbally read the position and time values for each runup extremum and an assistant typed the values into a computer file as they were read.

Two records (RUNUP No. 6 and No. 7) were selected and manually analyzed. These RUNUP tests used the S0105 wavemaker control signal with gains of 0.4 (RUNUP No. 6) and 0.35 (RUNUP No. 7). Three different operators independently analyzed No. 6 to help develop confidence intervals on the results. The distribution of time period between successive maxima was computed for each record. In each case, the analysis was done with several different thresholds below which the maxima were ignored. Thus the tendency for a periodicity in the higher runups could be examined. The distributions, in 2-sec intervals, obtained for No. 6 by the three operators are given in Figure 5. The cluster of bars at each period interval represents results for different thresholds. Similar results for No. 7 are given in Figure 6. At the longer periods which would typify surf beat in these laboratory tests (longer than 10 sec), there are no dominating peaks in the distribution. There is some evidence of a concentration in the 15-17 sec range. Energy in this range could be affected by basin oscillations.

The basin configuration during the NERDS and RUNUP tests differed from the original GBM configuration in two possibly important ways: 1) a solid side wall was added because of new model construction in an adjacent basin sector; and 2) the floor was elevated and the wavemaker was moved further shoreward to accommodate NERDS test objectives. Despite the advantages of

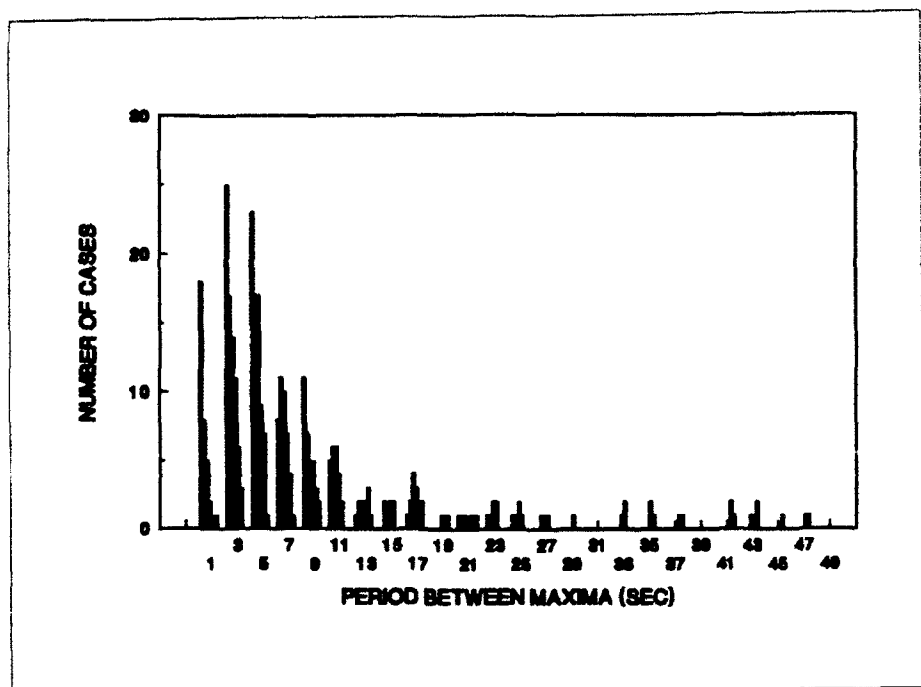


a) Analyzed by Operator No. 1



b) Analyzed by Operator No. 2

Figure 5. Distribution of period between successive runup maxima above a threshold value, RUNUP No. 6. Several different thresholds are represented (Continued)



c) Analyzed by Operator No. 3

Figure 5. (Concluded)

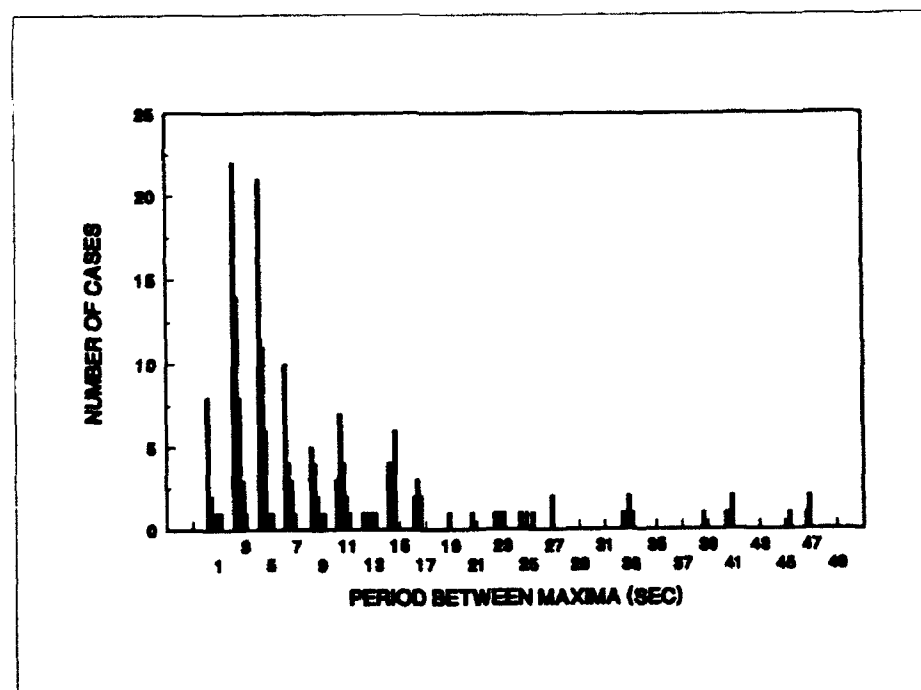


Figure 6. Distribution of period between successive runup maxima above a threshold value, RUNUP No. 7. Several different thresholds are represented. Analyzed by Operator No. 1

the RUNUP data set, it was finally decided that concerns about possible distortion of low frequency energy due to long wave reflections from the basin walls are sufficiently great that detailed analysis of surf beat should be done only with the original GBM data set.

Results

The following results are from the GBM tests summarized in Table 2. Variation of wind wave significant height with water depth along the cross-shore array for 0-deg approach is shown in Figure 7a. Visible wave breaking occurred shoreward of Gage 10 (22.6-cm depth) in all cases. A similar display for 20-deg approach is shown in Figure 7b. A three-dimensional perspective plot of the directional spectrum from Case S0105 at the OGA indicates the desired characteristics were reasonably well reproduced in frequency and direction (Figure 8a). A similar plot for just the low frequency spectrum is given in Figure 8b. Directional spread is greater for the low frequency spectrum than for the wind wave spectrum. The analysis for these plots was done by the Maximum Likelihood Method with 24 degrees of freedom. Another pair of plots for the same case at the NGA is given in Figure 9. Depth-induced changes are evident in both the short and long wave spectra. A full set of plots for all the cases considered is given in Appendix A.

The array of gages can be used to investigate the importance of wave reflection. Plots for the full 360-deg directional spread of energy were produced by including gage 7 in the OGA analysis (Appendix B). No strong presence of energy moving toward the wavemaker was evident.

Long wave significant height, H_{mOLW} , increases as depth decreases (Figures 10 and 11). The H_{mOLW} is consistently higher for unidirectional waves than for directionally-spread waves. Also H_{mOLW} is generally higher for waves approaching at 0 deg than 20 deg although the differences are small.

Some evidence of possible low frequency basin oscillation was observed in long wave spectra at the shallower gages. Long wave spectra for offshore, nearshore, and intermediate depth gages for the 0-deg approach cases show the spectral structure (Figure 12). Natural frequency for the first mode of oscillation between the wavemaker and the beach was estimated as 0.064 Hz. The shallower gage shows a spectral peak near the natural basin frequency in several cases, particularly Case S0105, in which the oscillations would most likely be a problem. Similar plots for the 20-deg approach are given in Figure 13. The peaks around 0.064 Hz are less prominent than in Figure 12. Reduction of the peak in Figure 13 is attributed to the oblique wave approach and open basin side boundaries, which should help reduce oscillations.

Interesting nonlinearities emerge in the short as well as the long wave spectrum during shoaling. The importance of these nonlinearities in predicting nearshore field spectra was recently demonstrated by Freilich et al. (1990). Although these processes are embedded in the short wave spectra discussed in this study, they are not investigated here. Further detail on nonlinearities in a shoaling short wave spectrum are presented by Elgar, et al. (1992). They used

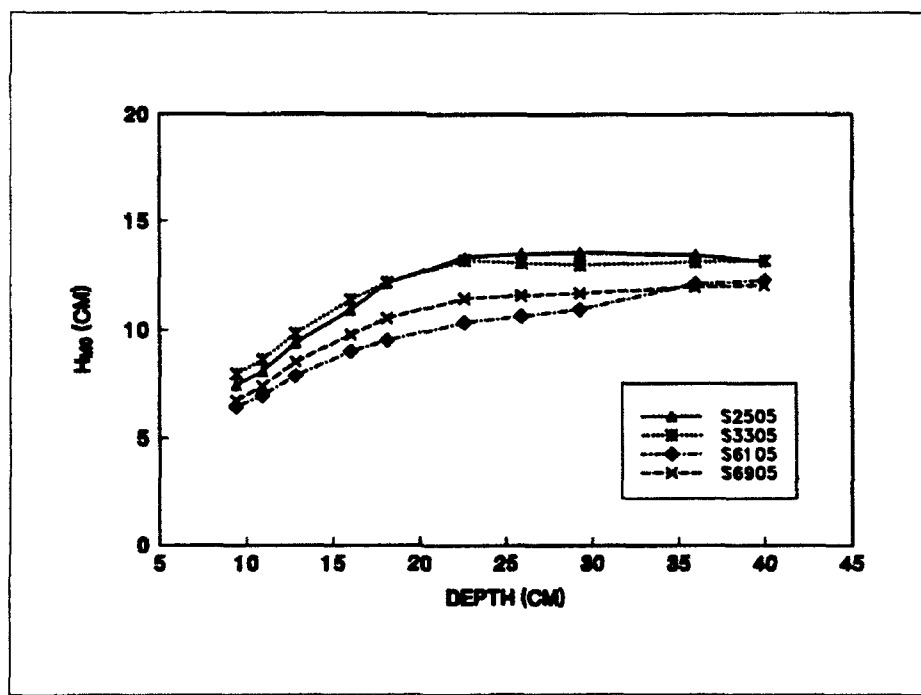
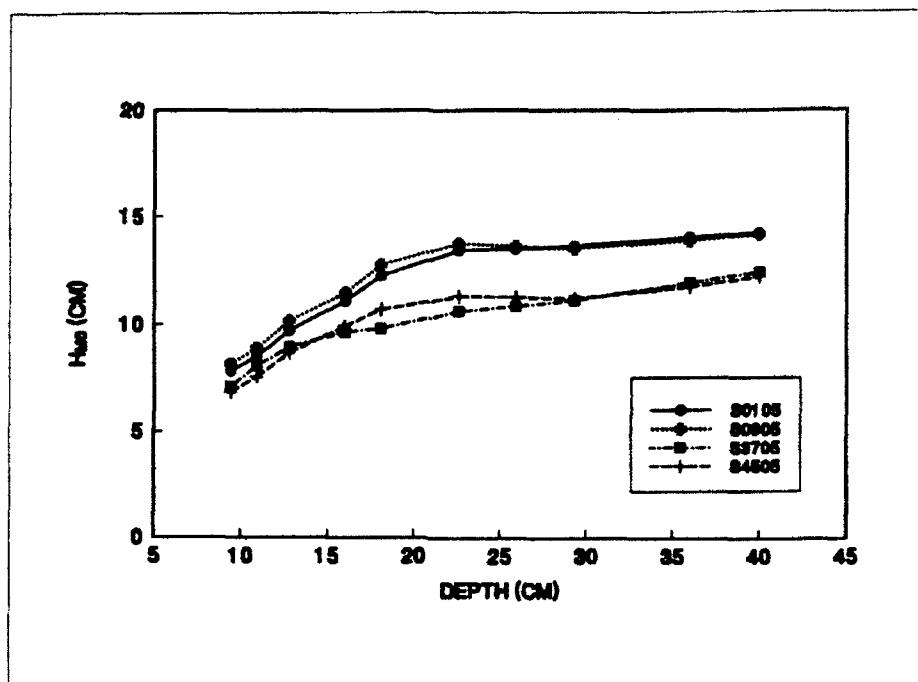


Figure 7. Significant wave height, short waves

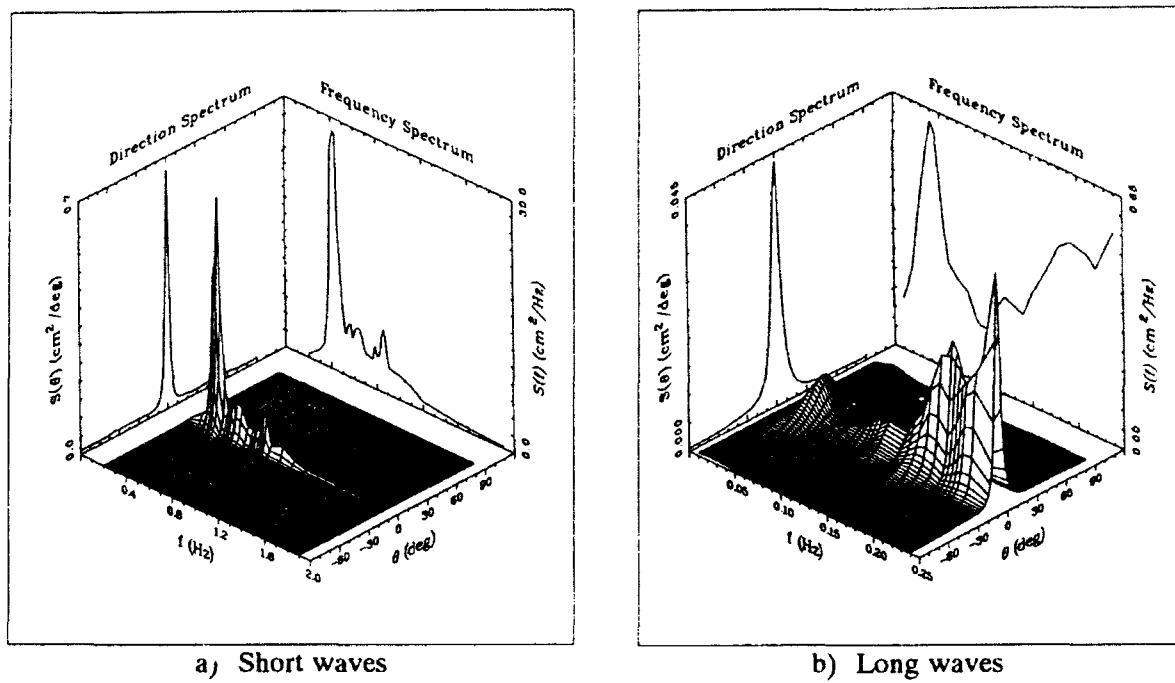


Figure 8. Directional spectrum, S0105, OGA

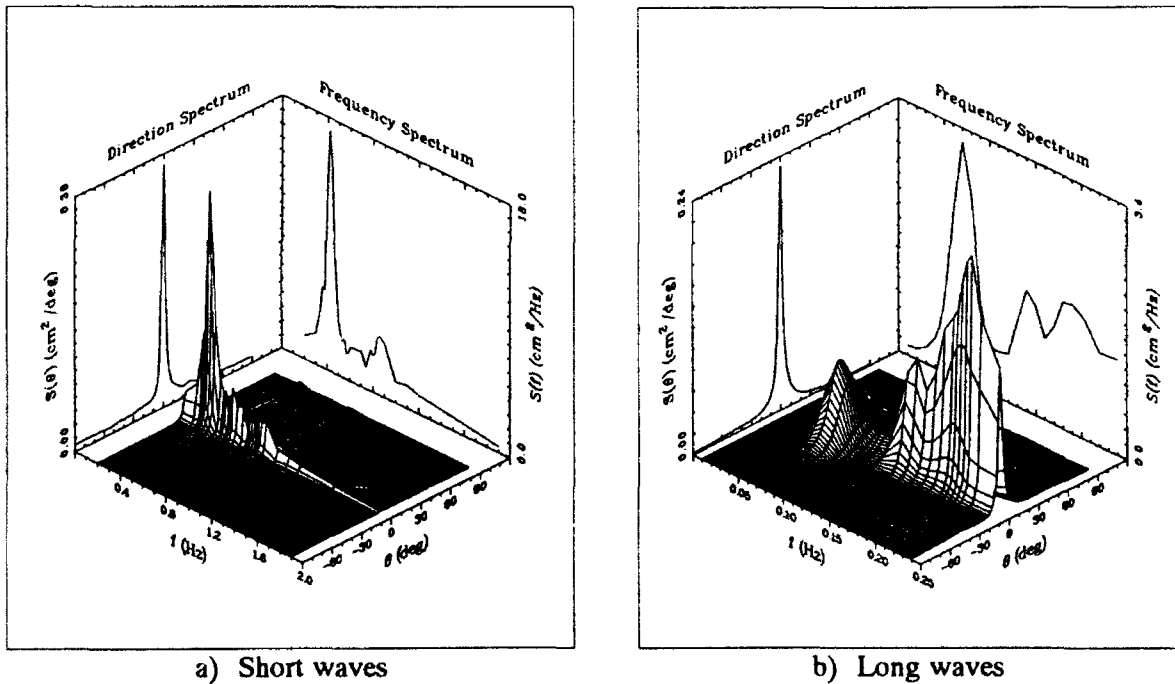
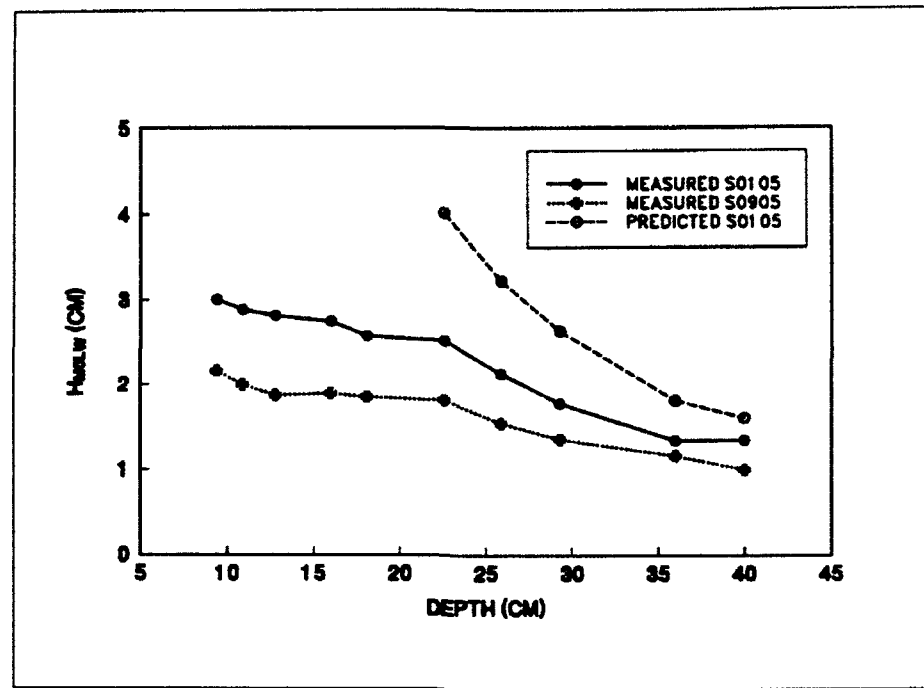
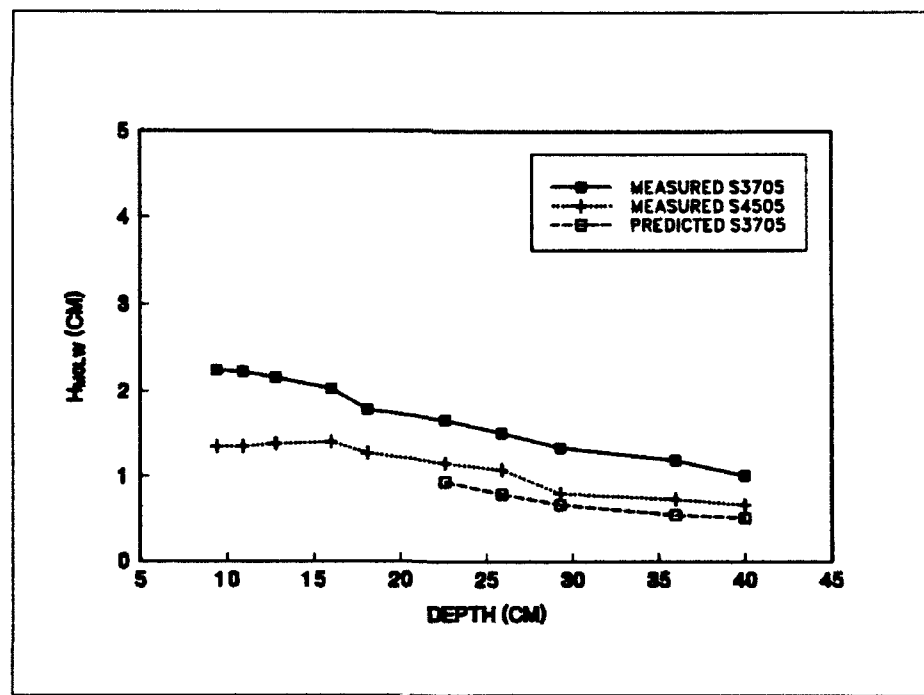


Figure 9. Directional spectrum, S0105, NGA

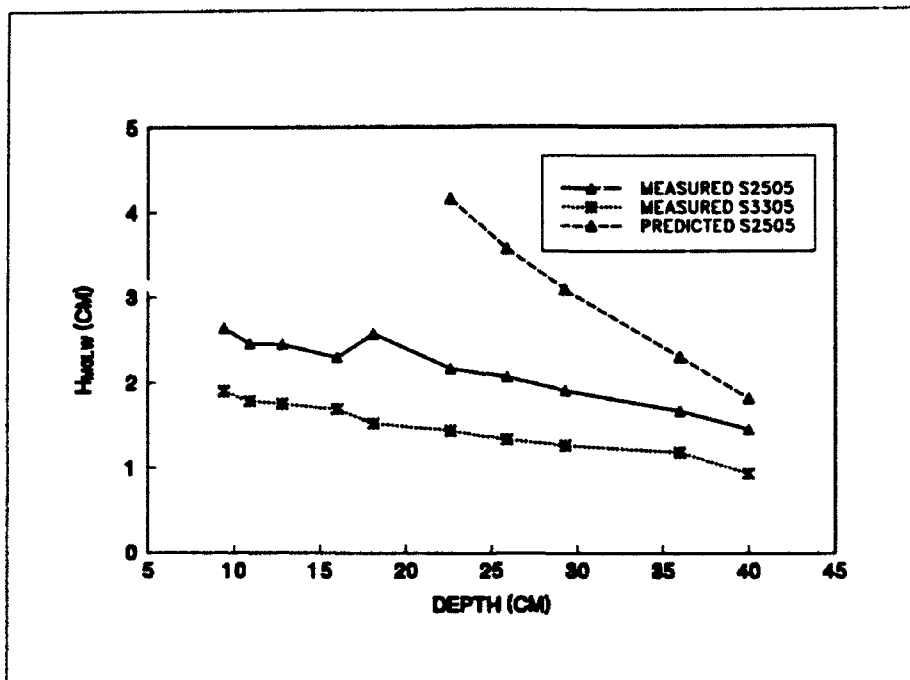


a) Swell

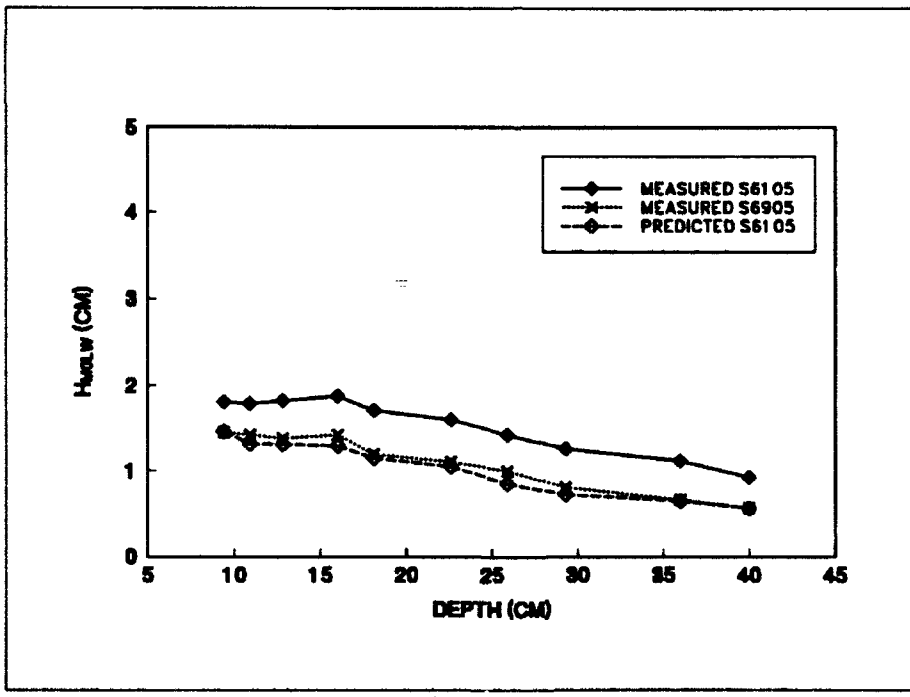


b) Sea

Figure 10. Significant wave height, long waves, 0-deg approach

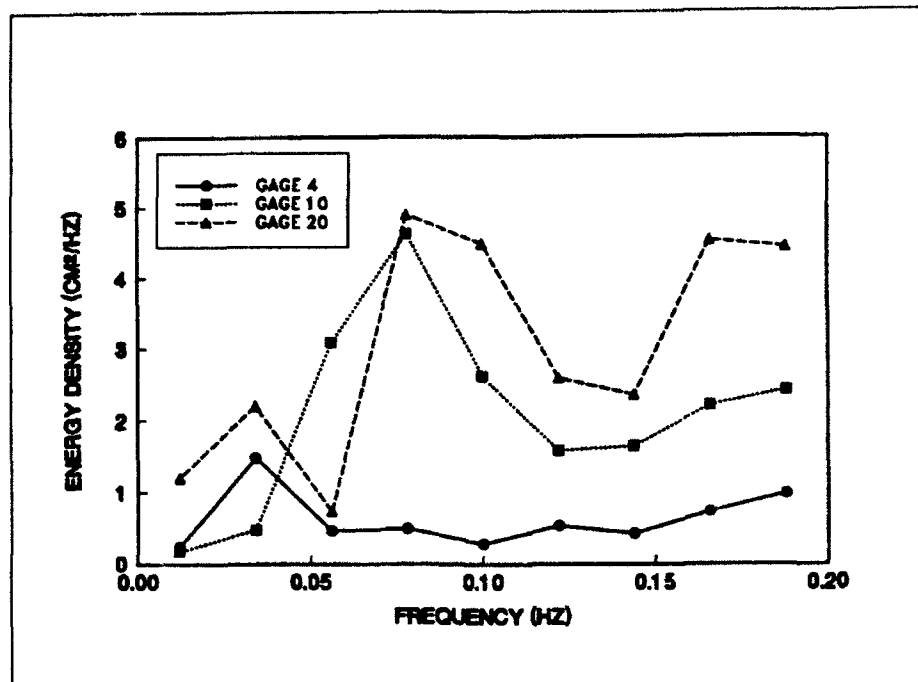


a) Swell

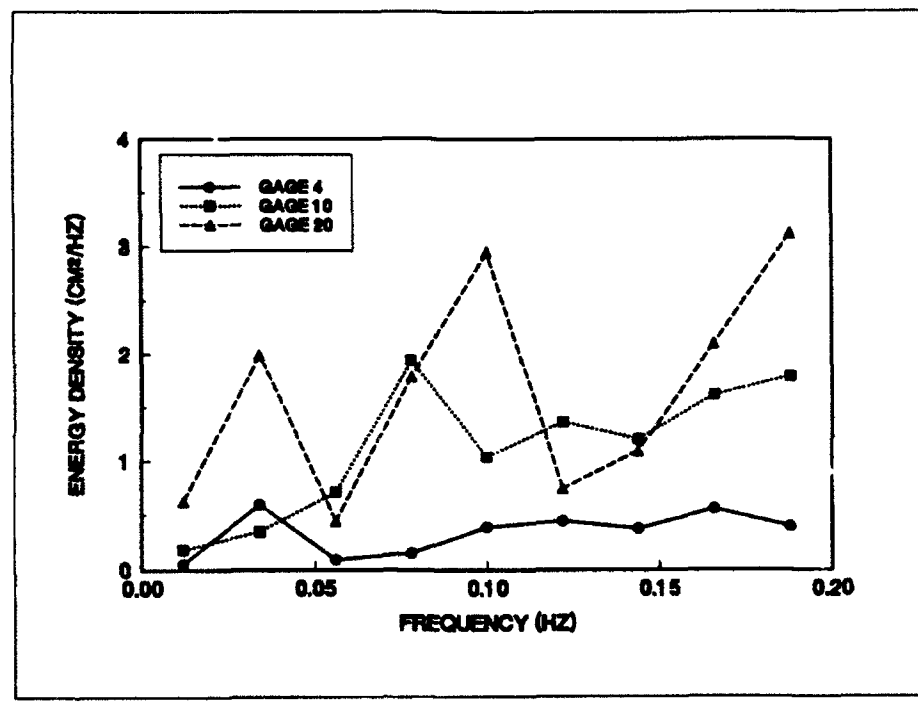


b) Sea

Figure 11. Significant wave height, long waves, 20-deg approach

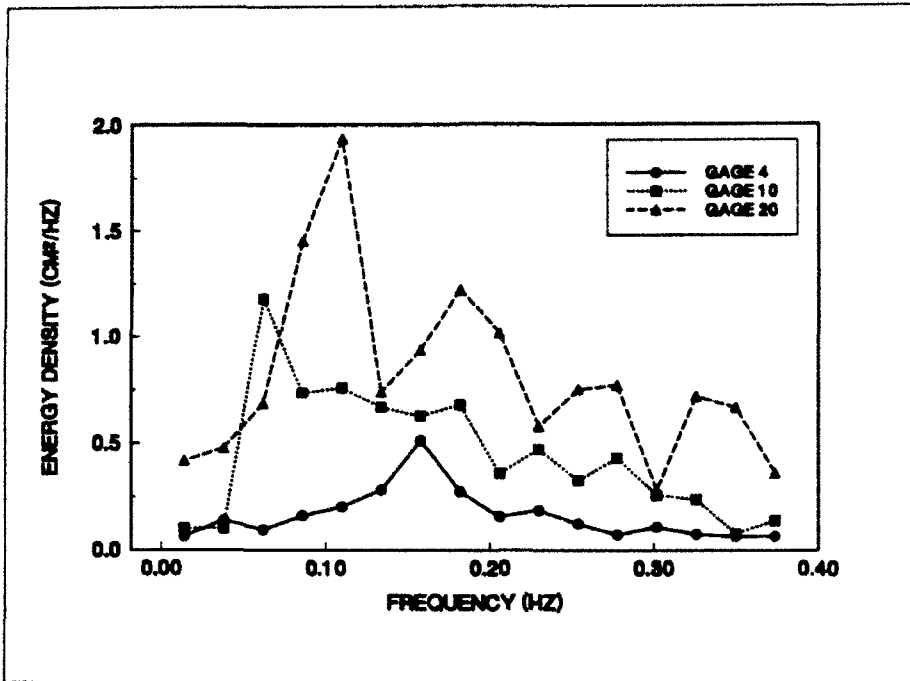


a) S0105

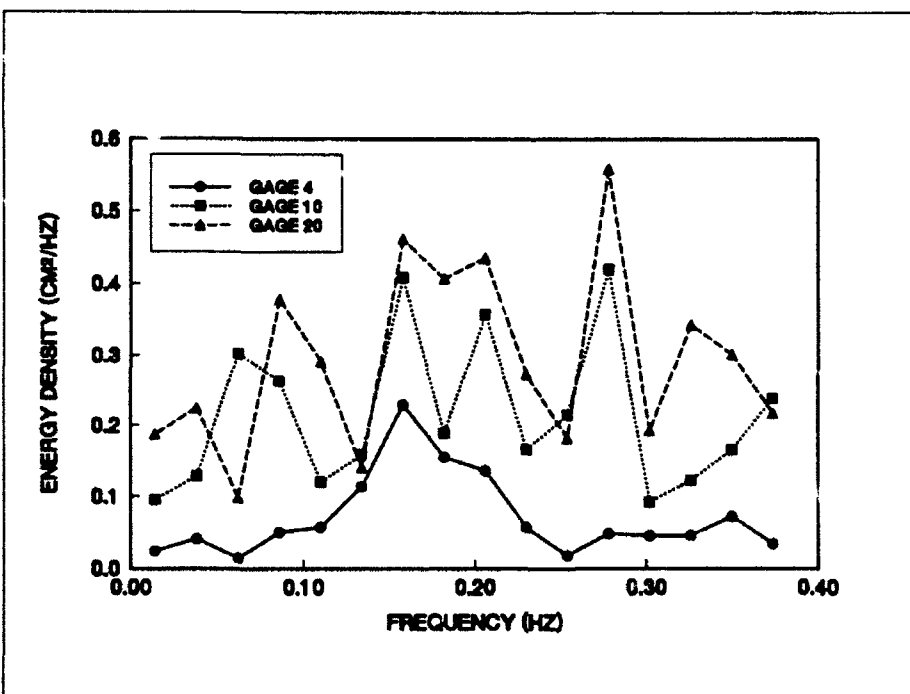


b) S0905

Figure 12. Measured long wave spectra, 0-deg approach (Continued)

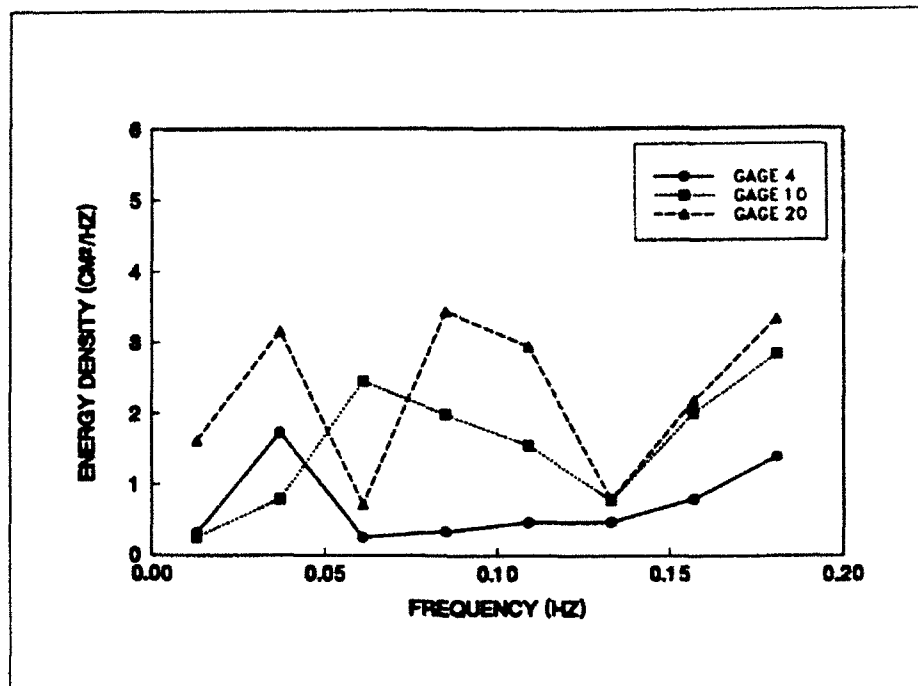


c) S3706

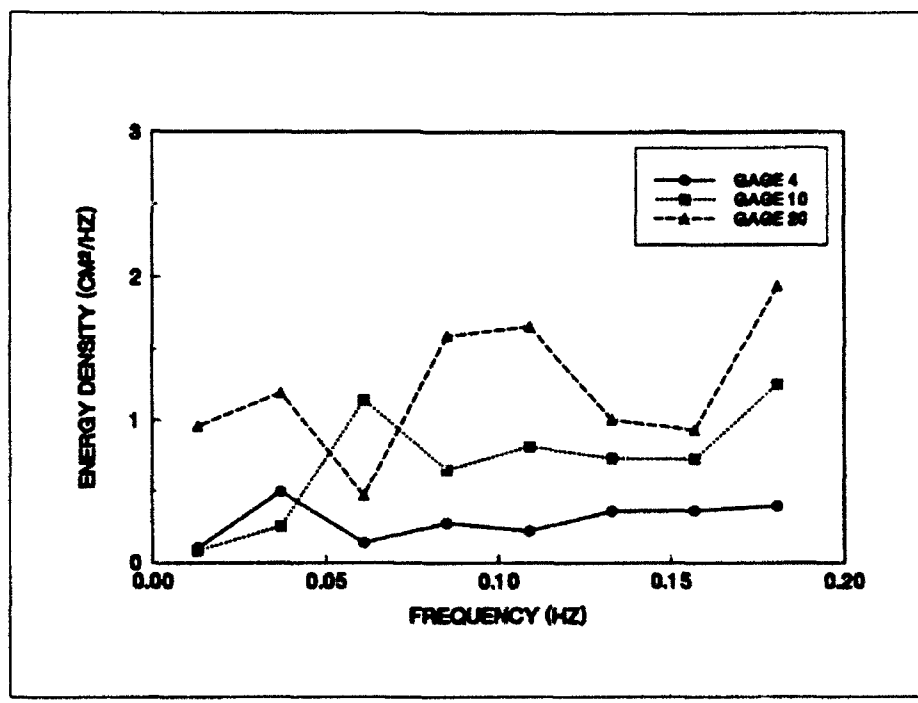


d) S4504

Figure 12. (Concluded)

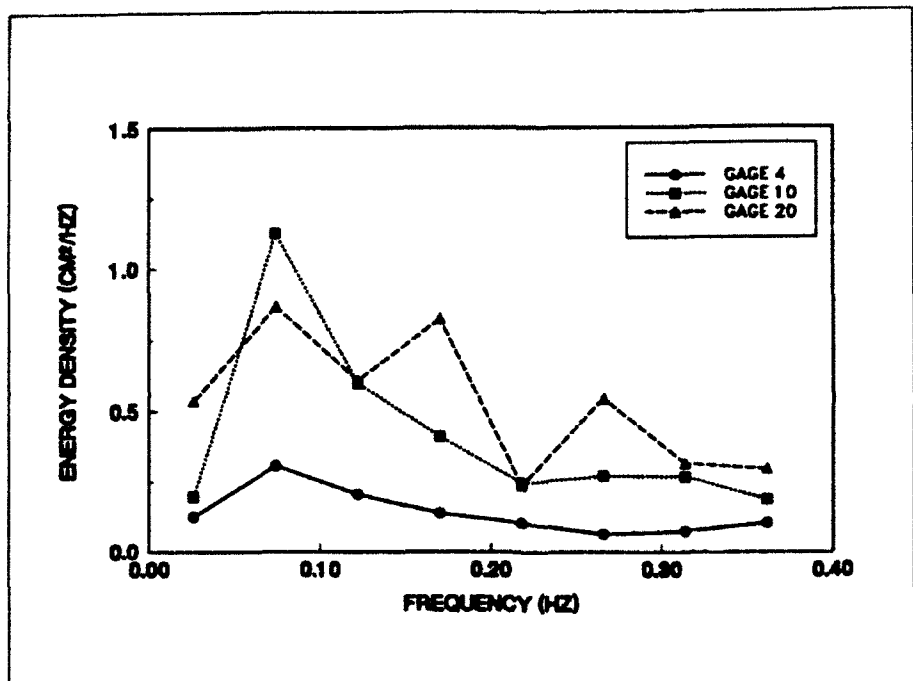


a) S2505

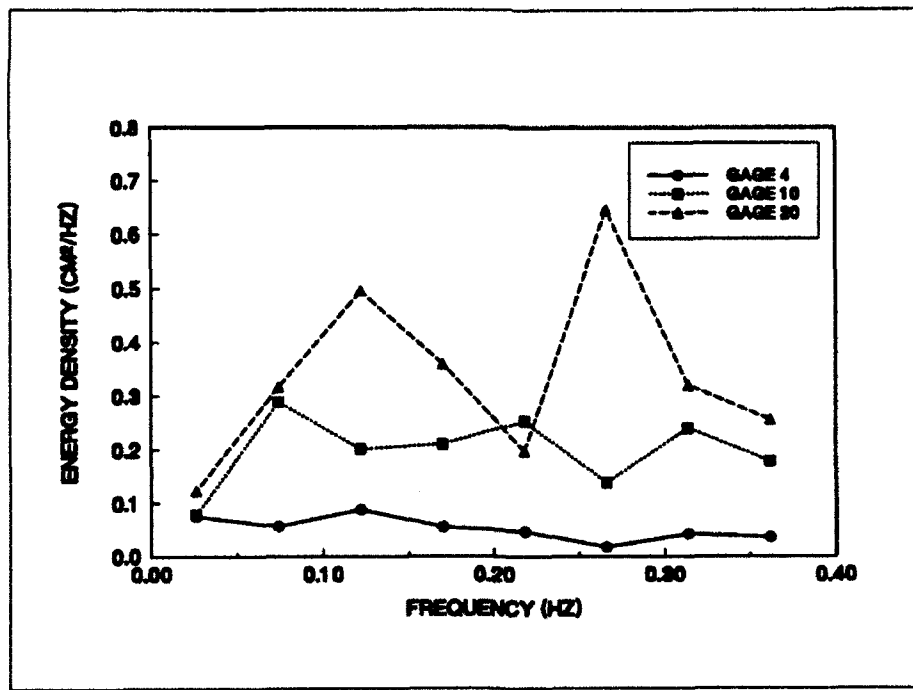


b) S3305

Figure 13. Measured long wave spectra, 20-deg approach (Continued)



c) S6105



d) S6905

Figure 13. (Concluded)

the same GBM laboratory basin to run tests with incident spectra scaled from field measurements at Torrey Pines Beach. These experiments validated the accuracy of WES laboratory simulation of nonlinear processes in shoaling short wave spectra.

Comparison with Theory

The equations of Sand (1982a, 1982c) were used to predict bound long waves at each gage on the cross-shore array. As with measurements, predicted significant heights increase with decreasing depth (Figures 10 and 11). Predictions of H_{MOLW} from unidirectional theory, shown in the figures, should be compared to the unidirectional laboratory results. Predictions based on theory for directionally spread waves would be significantly lower. Predictions are only shown at points seaward of the surf zone. Predictions and measurements are the same order of magnitude. However the details are not consistent; predictions exceed measurements for swell but the reverse is true for sea.

Theoretical predictions of several other long wave properties can be compared to measurements. Predicted long wave time series are shown against measured short wave time series in Figure 14. The elevation scale has been expanded for the long wave time series to make it visible. Radiation stress theory predicts that crests in the long wave time series should coincide with groups of low short waves and long wave troughs should fall under groups of high short waves. Qualitatively, the results confirm this pattern.

Predicted long wave spectra are compared to measurements in Figures 15 and 16. Predicted and measured long wave spectra are generally similar at Gage 4. Predictions significantly exceed measurements at Gage 10 for the swell cases and the reverse is generally true for sea cases. A possible explanation is given in the following paragraphs.

Sand's (1982a) work has been used successfully to program wavemakers in flumes for proper generation of bound long waves. Proper long wave generation is more difficult in a large directional basin because of increased complexity, leakage under and around the wavemaker, and more severe limits on paddle stroke. Aside from iterative corrections of the measured spectra to minimize the amount of long wave energy, described above, GBM tests in the WES basin do not include explicit control of second order long waves. Thus, long waves measured in the laboratory basin could have three main components: 1) bound long waves induced by grouping in the wind waves; 2) free long waves to counterbalance the bound waves at the wavemaker (180 deg out of phase); and 3) free long waves reflected from the beach, including possible basin oscillations.

Observed differences between the sea and swell cases may be explained as follows. The wavemaker control signal was empirically adjusted to give very low long wave energy at the wavemaker. However the irregular wave train being generated requires a bound long wave component arising from radiation stresses under a grouped wavetrain (component No. 1). This component

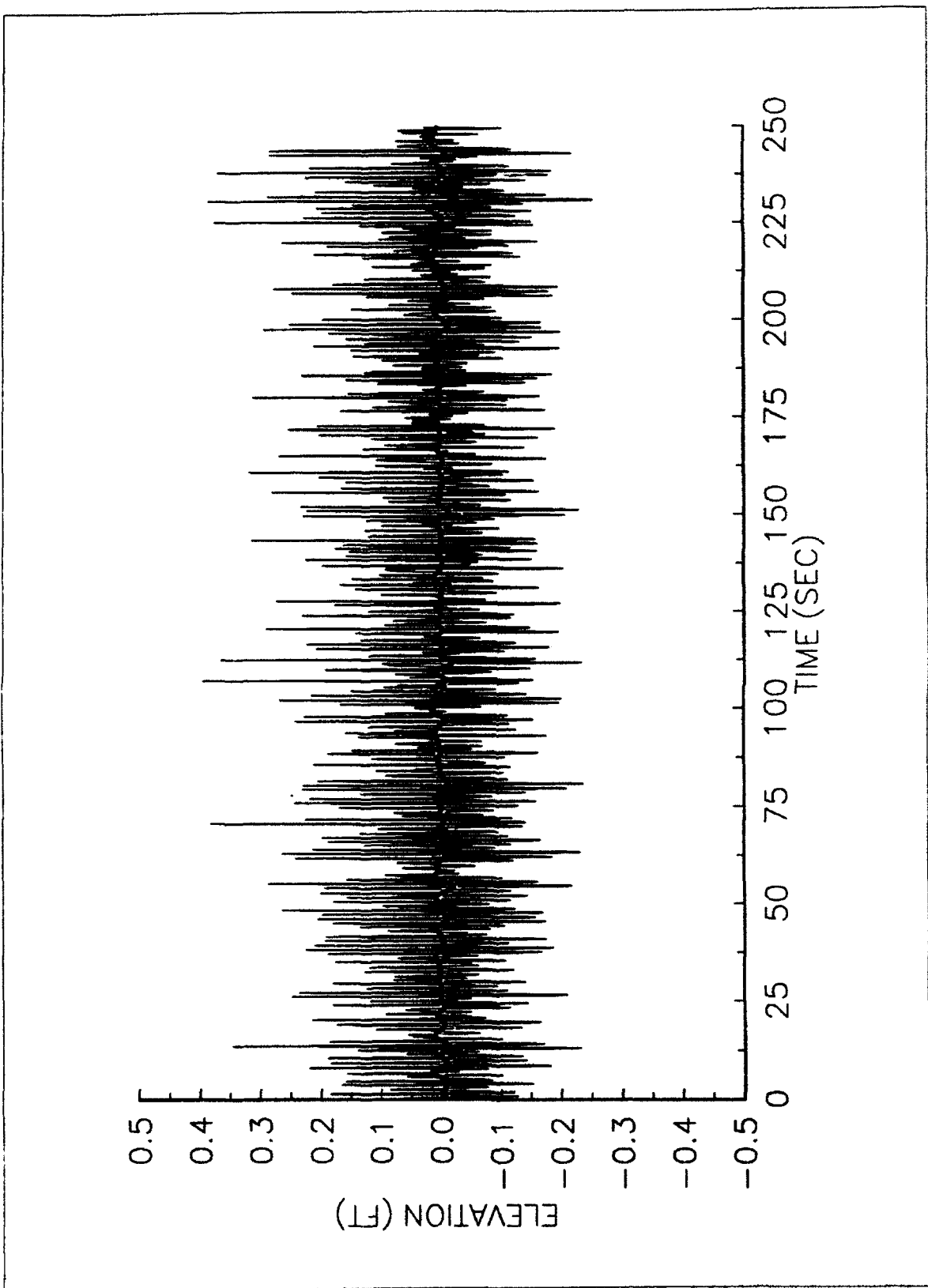
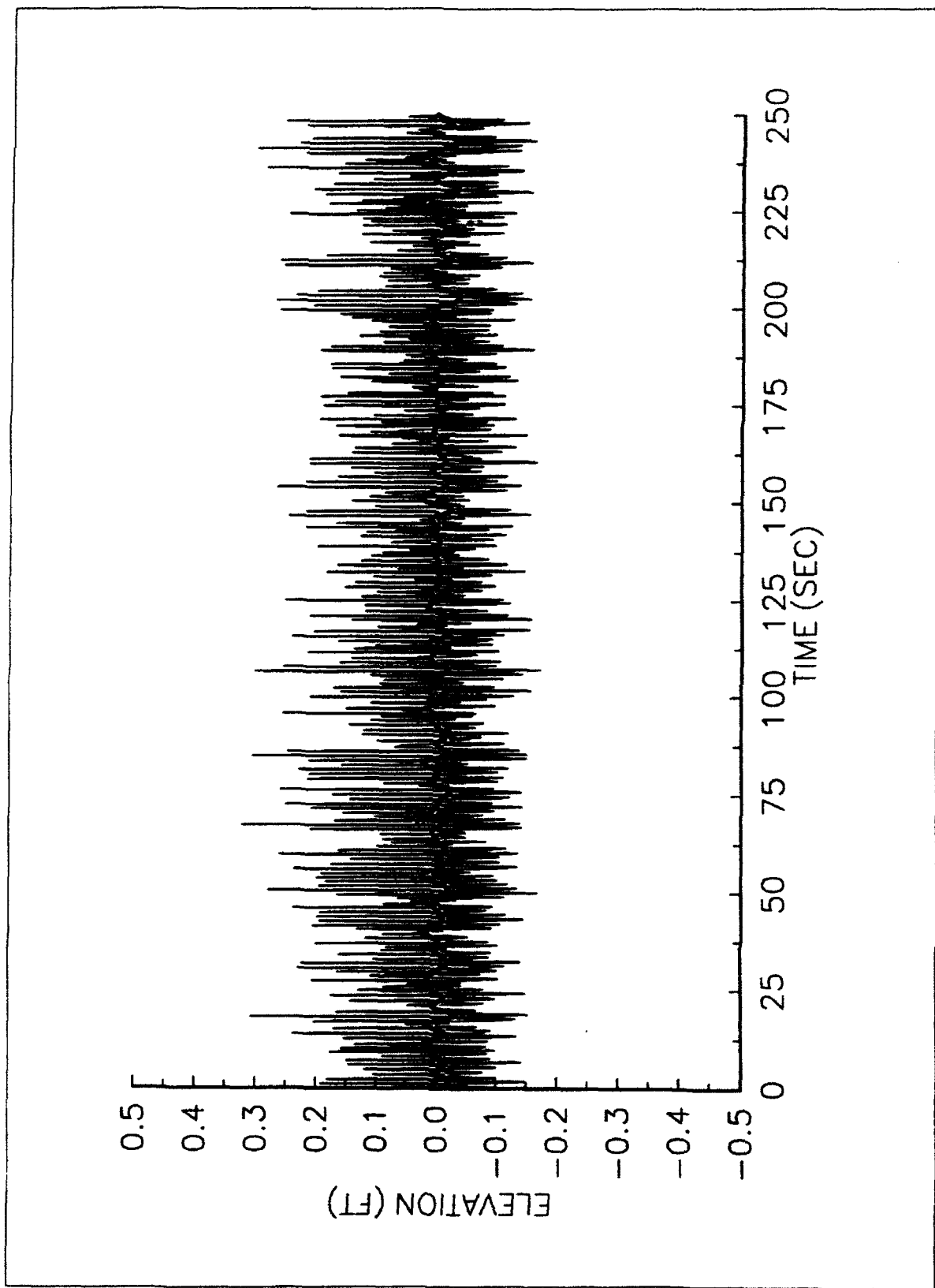
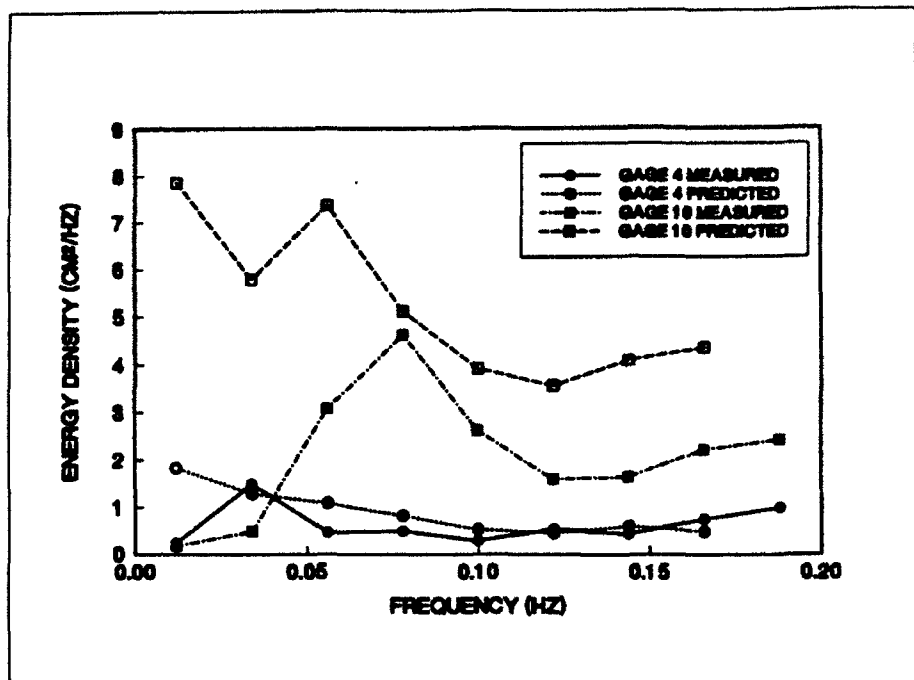


Figure 14. Time series from short waves (measured) and long waves (predicted), S3705 (Continued)

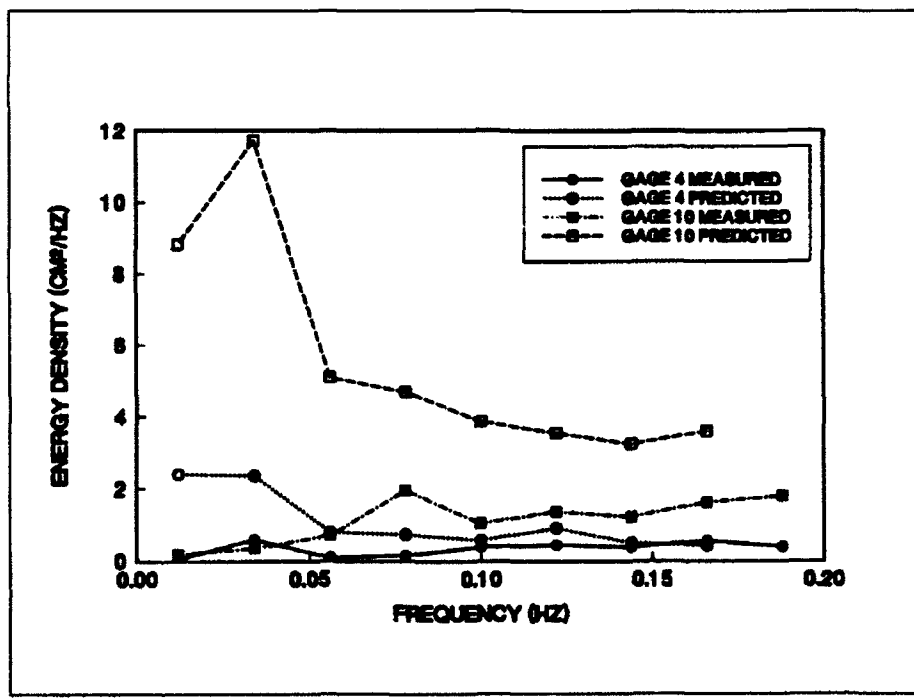


b) Gage 10

Figure 14. (Concluded)

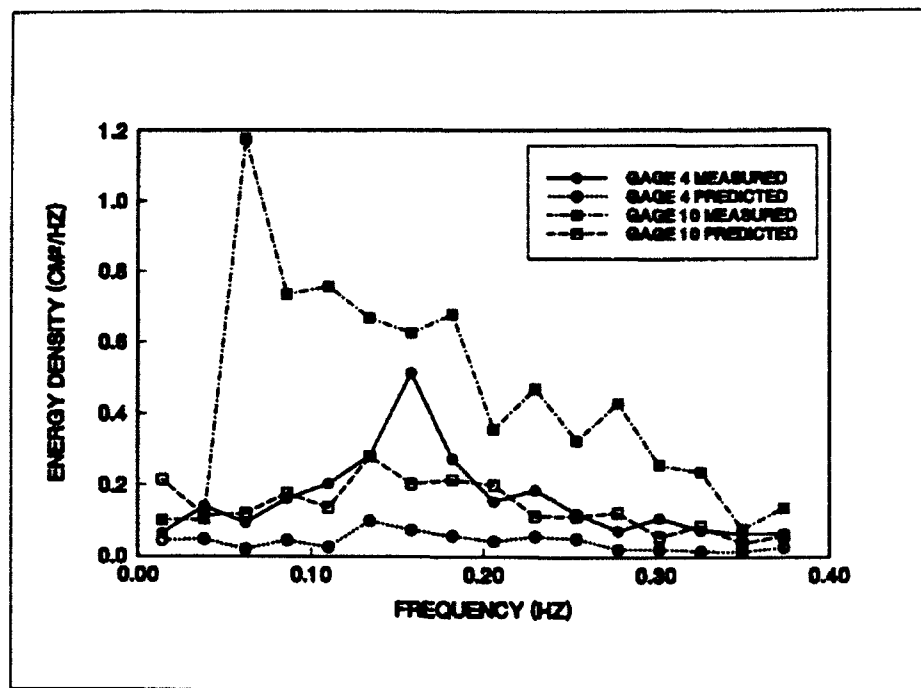


a) S0105

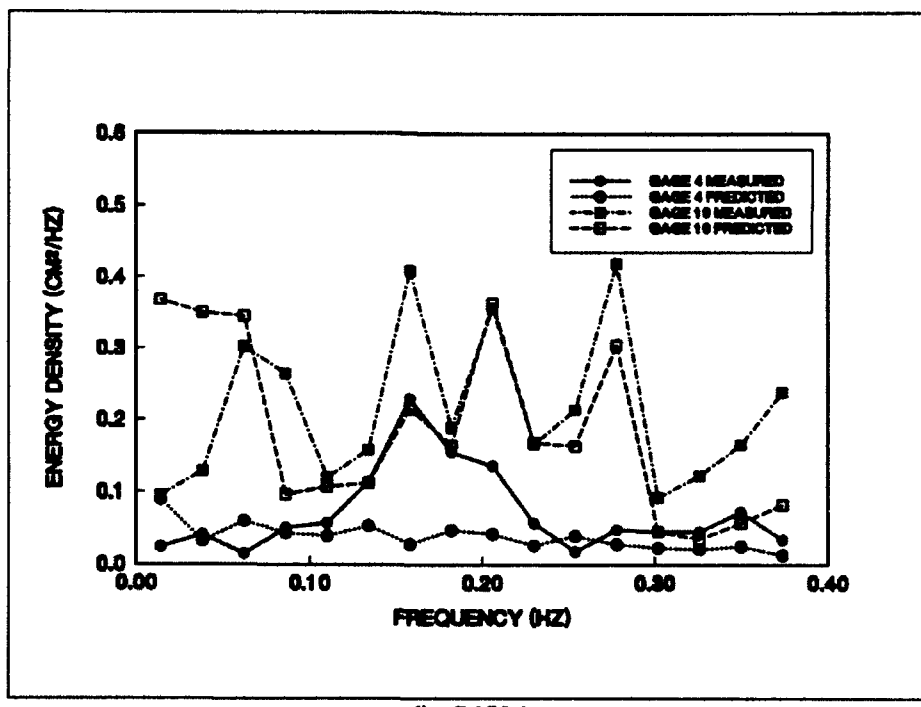


b) S0905

Figure 15. Predicted and measured long wave spectra, 0-deg approach
(Continued)

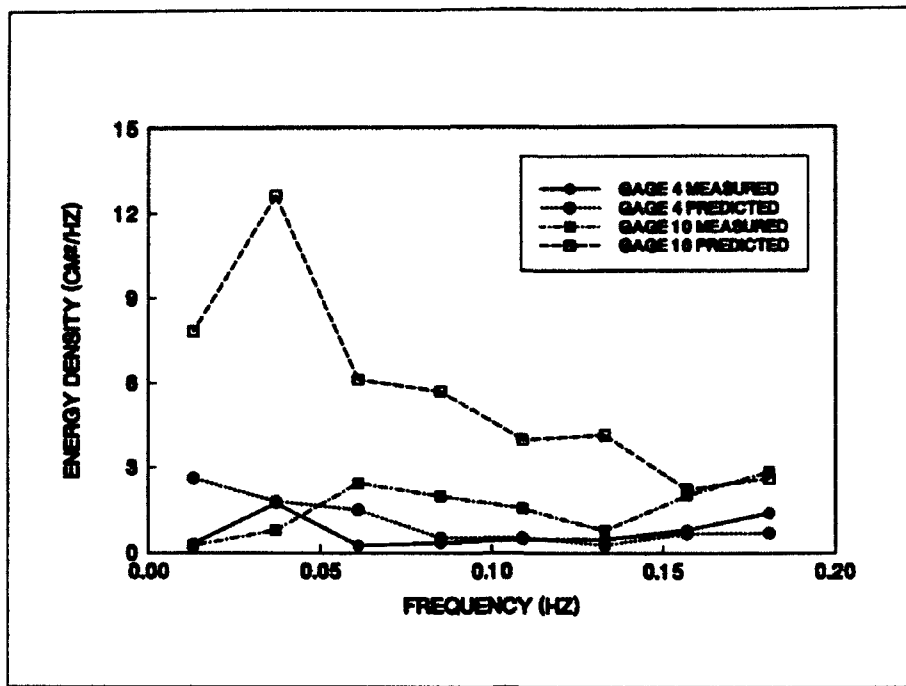


c) S3706

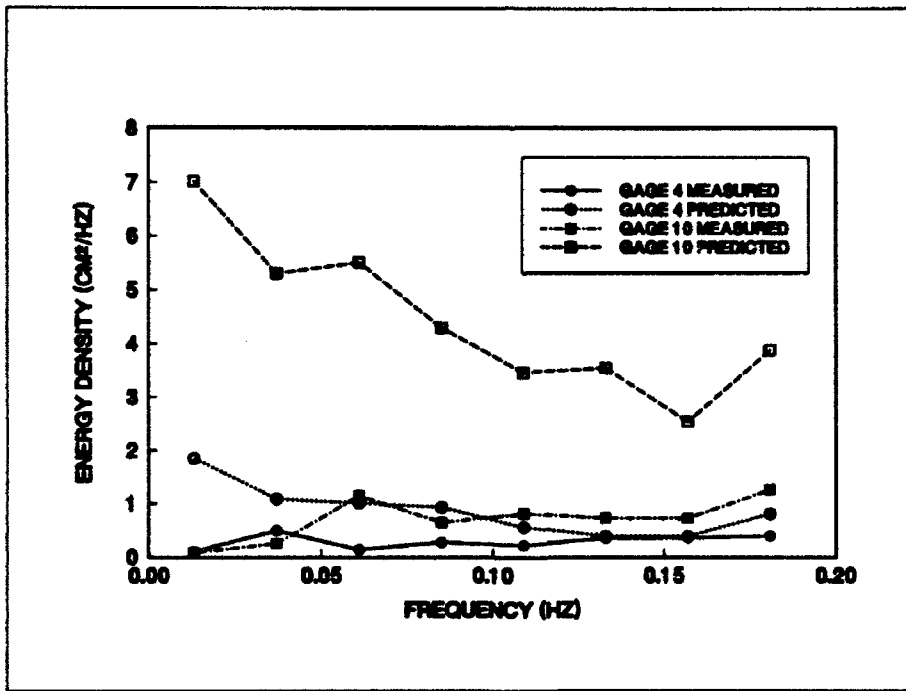


d) S4504

Figure 15. (Concluded)

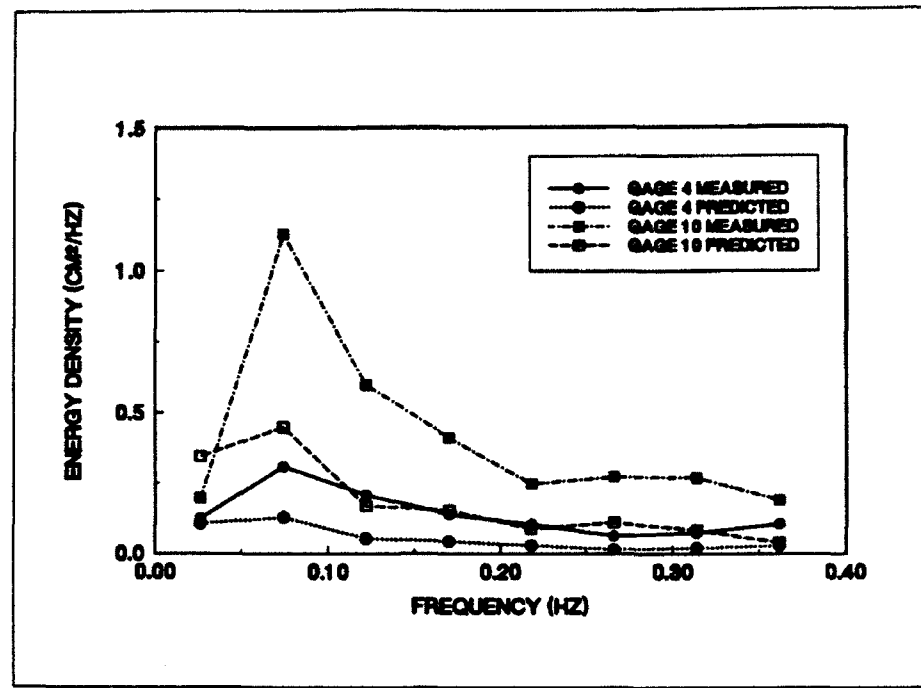


a) S2505

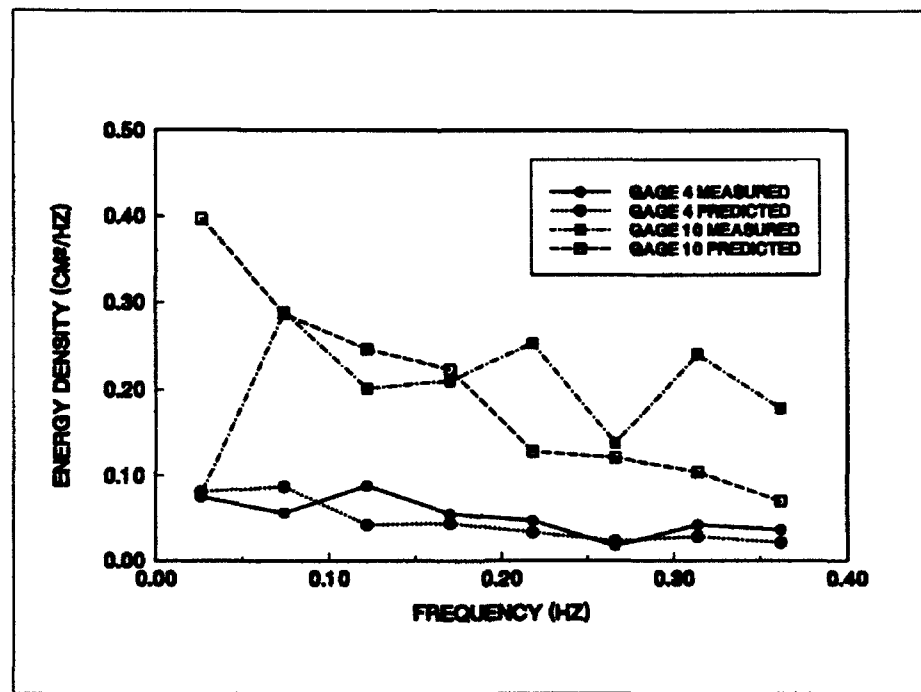


b) S3305

Figure 16. Predicted and measured long wave spectra, 20-deg approach (Continued)



c) S6105



d) S6905

Figure 16. (Concluded)

was not explicitly generated by the wavemaker. To satisfy the condition of no net long wave energy at the wavemaker boundary, a free long wave must also appear (component No. 2). The free and bound long waves are opposite in phase at the wavemaker. The free long wave travels at the group velocity appropriate to its frequency. The bound long wave travels at the group velocity of the short waves.

In the case of the swell tests, the two group velocities are nearly the same, approximately equal to the depth limited velocity. Thus the phase differences between free and bound long wave components persist as the waves propagate away from the wavemaker up onto the slope. Because the free and bound waves continue to counter-balance each other, the net measured long wave energy is less than the bound wave energy. The theory predicts only bound long wave energy. Hence the overpredictions relative to the swell measurements is not surprising. Calculations based on group velocities and analysis by the procedures of Sand (1982a) account for an excess of predictions over measurements in the swell cases (S0105 and S2505).

For the sea tests, the group velocities of the free and bound waves differ significantly. By the time waves propagate from the wavemaker to the most seaward gages, phase differences between free and bound long waves are no longer preserved. The net measured long wave energy is greater than the bound long wave energy alone. The underprediction of theory relative to measurements in this case is not surprising. Calculations confirm that this process is a likely explanation for the high values of measured long wave height relative to predictions for sea cases (S3705 and S6105). This process was documented by Bowers and Huntington (1987).

4 Field Measurements

Field Experiment

An excellent opportunity for acquiring outstanding field data arose during the early part of this surf beat investigation. The DELILAH nearshore experiment, a large, multiagency effort, was conducted at the FRF during October 1990. The experiment was designed to investigate the physics of the surf zone using a variety of techniques including a large array of fixed and mobile instruments, video and radar systems, and precision surveys. The experiment yielded a high quality data base including nearshore waves, currents, runup, and winds.

The stated objectives of DELILAH were:

To measure the wave and wind forced three-dimensional nearshore dynamics with specific emphasis on infragravity waves, shear waves, mean circulation, set-up, runup, and wave transformation. To also monitor the bathymetric response to these processes.

The success of DELILAH depended on the dedicated efforts of the FRF staff and a relatively small number of other investigators. The DELILAH investigators (most of whom were on site for much of the experiment), their organizations, and general areas of scientific interest are listed in Table 3.

Experiment Plan

The DELILAH experiment plan is described by Birkemeier, et al. (1991). In addition to the long term FRF directional wave array in 8-m depth, a variety of gages was located in the surf zone area. As in past experiments, nearshore gages were placed north of the FRF pier, directly shoreward of the directional array. The area is exposed to storm waves from the northeast without interference from the pier. Bottom contours are typically shore parallel.

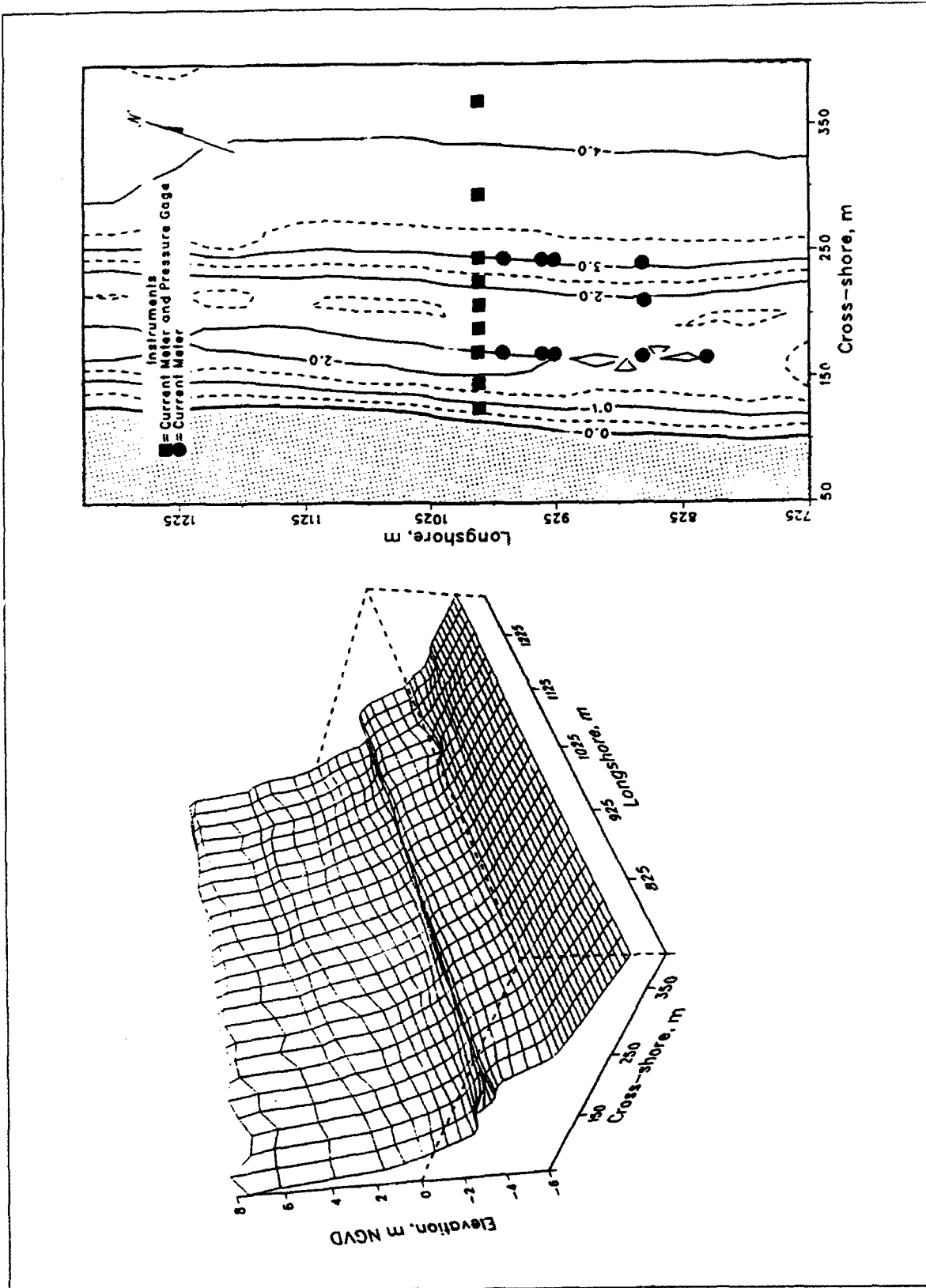
Nine current meters and pressure wave gages were placed along a cross shore line (Figure 17). They extended across the typical position of the nearshore bar and were designed to encompass surf zone widths due to 1.5-m

Table 3
DELILAH Investigators and Areas of Interest

Investigator	Areas of Scientific Interest
Coastal Engineering Research Center	
W. Birkemeier	Morphology
K. Hathaway	Runup, infragravity waves, morphology, remote sensing
C. Long	Incident and reflected directional wave spectra
N. Kraus	Longshore currents
J. Smith	Vertical current profile, 2-D circulation
T. Walton	Runup
E. Thompson	Surf beat modelling
Naval Postgraduate School	
E. Thornton	Mean circulation, shear waves, rip currents
K. Scott	Mean circulation, shear waves, rip currents
Naval Research Laboratory	
D. Trizna	Radar measurements of waves and currents
Oregon State University	
R. Holman	Morphology, runup, shear waves, infragravity waves, video remote sensing
P. Howd	Infragravity waves, morphology
T. Lippman	Morphology, infragravity waves, video remote sensing
T. Holland (also with USGS)	Runup, cusp formation
Scripps Institution of Oceanography	
R. Guza	Cross shore and longshore currents, infragravity waves, wave transformation
Quest Integrated, Inc.	
J. Oltman-Shay	Shear waves, infragravity waves
Washington State University	
S. Elgar	Incident and reflected directional wave spectra

significant wave heights. Another 10 current meters were placed at selected points in the alongshore direction. Current meters were mounted on pipes and positioned to be below low tide level and above the highest expected bed level.

Fixed instruments were supplemented with a sled-mounted wind meter, staff wave gage, and vertical array of five current meters. The sled was intermittently deployed at the seaward end of a cross shore transect. It was towed



incrementally back to shore, stopping to collect a data record at each increment. The Coastal Research Amphibious Buggy (CRAB) deployed the sled and a large front end loader was used to tow it back.

Video cameras located on the FRF observation tower recorded swash and other surf zone processes. The Naval Research Laboratory tested radar systems to remotely sense waves, currents, and bathymetry. The CRAB ran daily surveys of nearshore bathymetry in a small 550-m by 375-m minigrid area encompassing the fixed DELILAH gages.

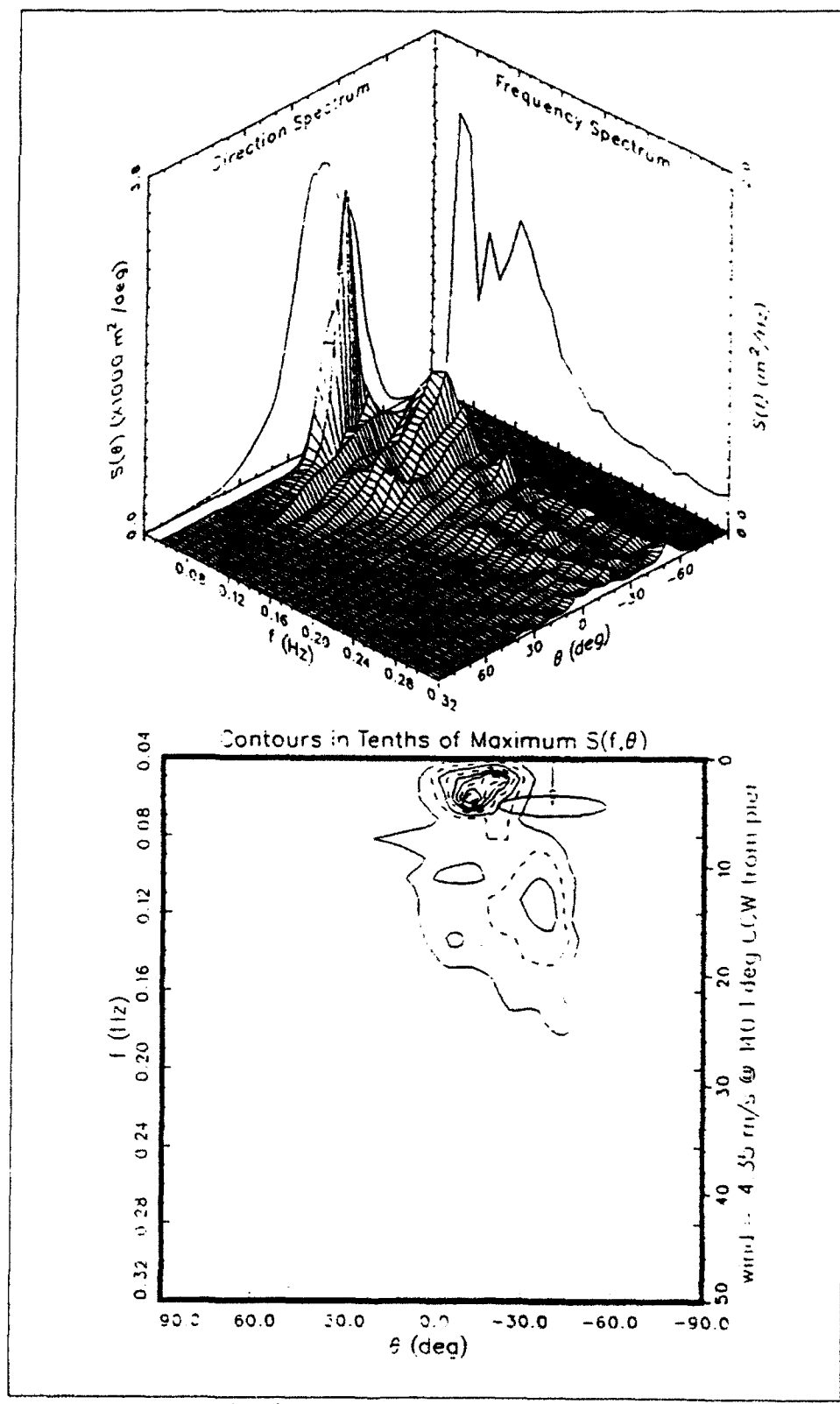
Experiment Conditions

Overall conditions during the experiment are summarized by Birkemeier, et al. (1991). The particular episode chosen for this study occurred on the afternoon of 12 October 1990. Hurricane Lilli was located 500 km southeast of the FRF and heading toward the north. Large, regular swell waves were arriving from a direction nearly perpendicular to shore but with a slight southerly slant. The H_{m0} at the directional array was between 2.0 m and 2.5 m. Unusually high wave runup was observed along the beach. Also the runup appeared to be more nearly uniform along the beach than usual; the runup crested simultaneously at about the same elevation along a fairly long stretch of beach. The nearshore bar was relatively linear and uniform in the longshore direction (Figure 17). Local winds were light, about 5 m/sec from the east-southeast. Wave measurements at the directional array confirm the presence of swell with an exceptionally narrow spread in frequency and direction (Figure 18). The time interval 1600-1900 hr EST was chosen for detailed analysis in this study because it comes unusually close to matching the assumptions of the unidirectional theory being considered.

The FRF archive tapes are written in records of 4096 points. Data from the DELILAH wave gages were collected at a sampling rate of 8 Hz, giving 8.533 min of data in each record. Data from the 8-m directional array were collected at a rate of 4 Hz, giving records of 17.066-min length. Data were collected near continuously during the experiment. Additional details and formats are given by Birkemeier, et al. (1991). For this study, gages along a cross shore transect including the 8-m array were selected (Table 4). Significant wave breaking during the selected event began at around gage 2804.

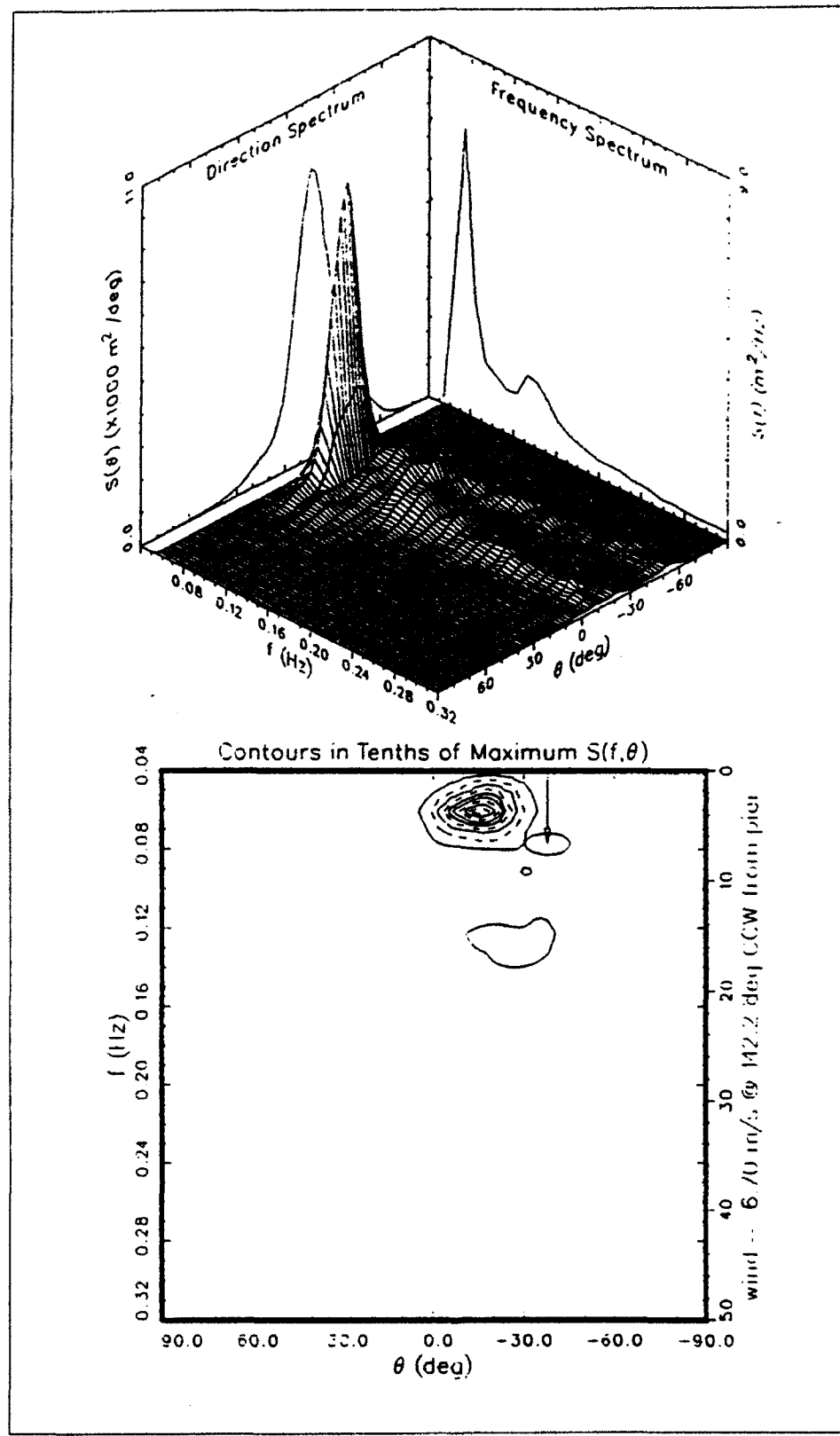
Data Analysis

Data records for the selected times and gages were extracted from the FRF archive tapes. Data from Gage 181 nearly covers the full 3-hour episode. Data from the nearshore gages begins at 1658 hours, corresponding to the start of a data tape. Gage 2604 was inoperative during this episode. The other nearshore gage records had occasional small blocks of missing data. The gap lengths were at most 1.6 percent of the record. Record means, needed for determining water depth and compensating the pressure records, were computed bypassing the gaps. The mean was removed from each time series and zero data values were added in the gaps. Mean values from Gage 181 are



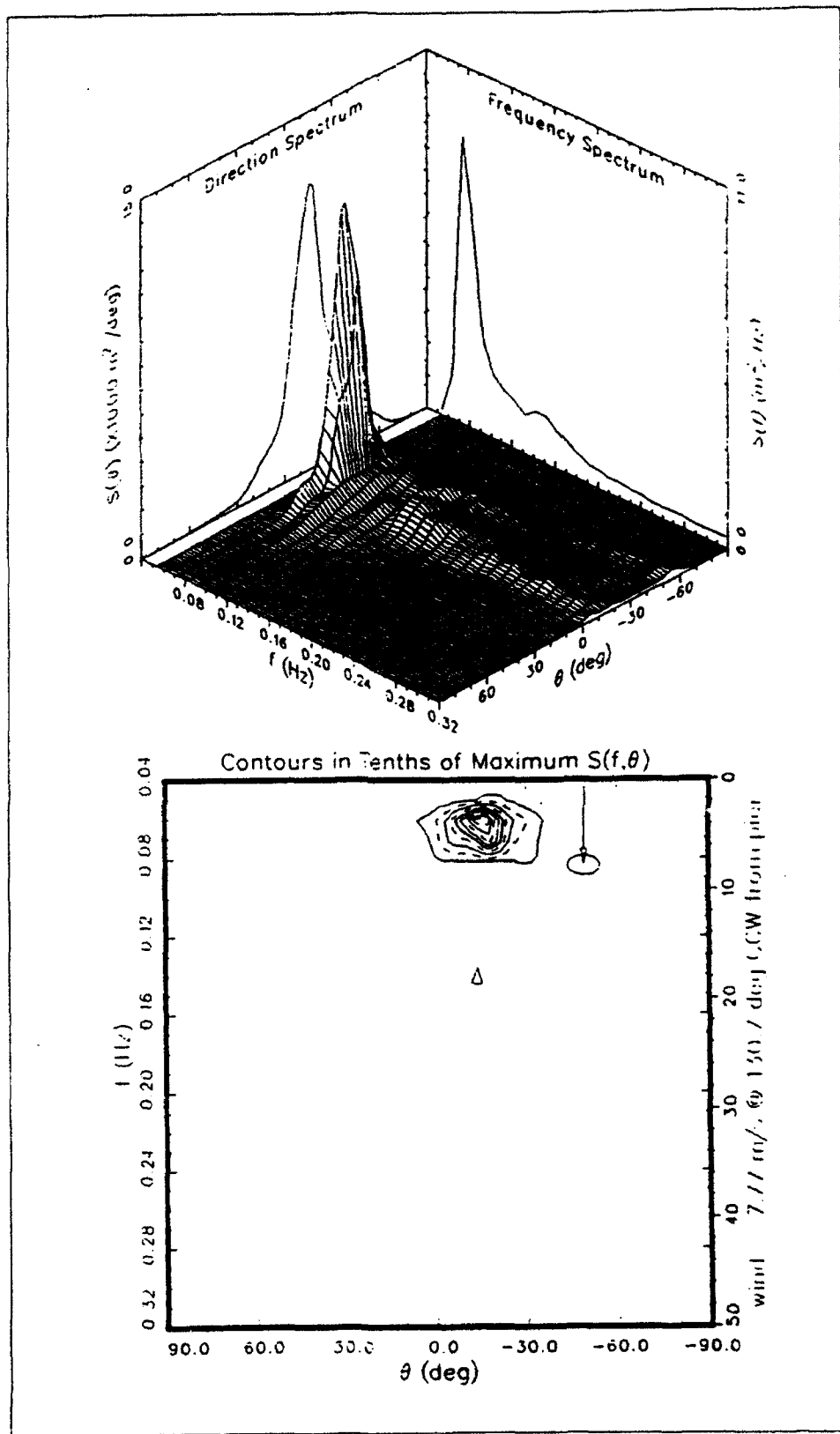
a) 1300 hr; $H_{m0}=1.54 \text{ m}$; $T_p=15.6 \text{ sec}$

Figure 18. Directional wave spectrum from array in 8-m depth, 12 Oct 90. Local wind vector and variability also shown (Continued)



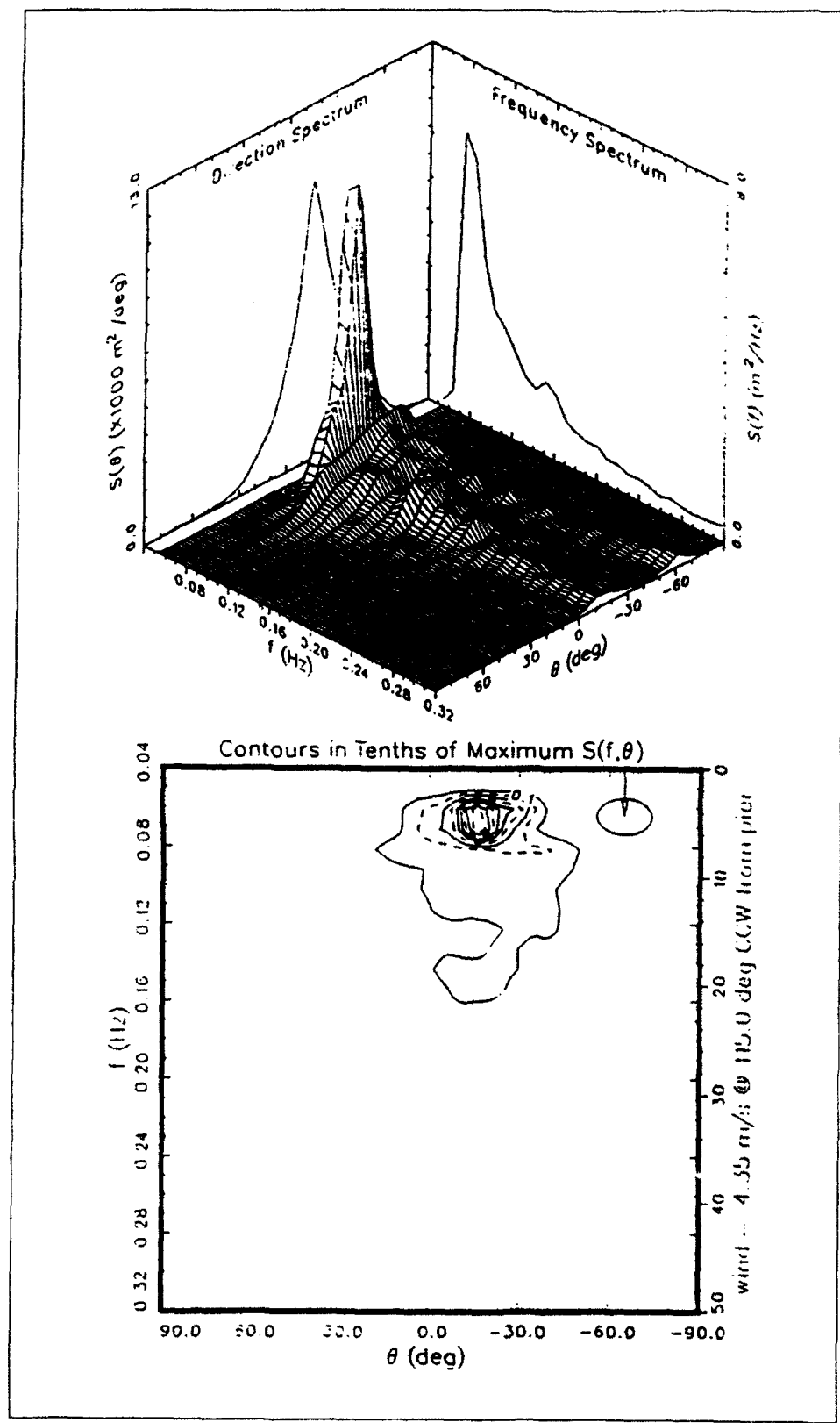
b) 1600 hr; $H_{m0}=2.18 \text{ m}$; $T_p=13.6 \text{ sec}$

Figure 18. (Continued)



c) 1900 hr; $H_{m0}=2.42 \text{ m}$; $T_p=13.6 \text{ sec}$

Figure 18. (Continued)



d) 2200 hr; $H_{m0}=2.45 \text{ m}$; $T_p=13.6 \text{ sec}$

Figure 18. (Concluded)

Table 4
Field Gages Used in
This Study

Gage Number	Water Depth ¹ m
8-m Directional Array	
181	7.67
Nearshore DELILAH Gages	
2104	0.28
2204	1.39
2304	0.87
2404	1.32
2504	1.88
2604	2.33
2704	3.03
2804	3.68
2904	4.25

¹ Depths relative to NGVD (8 cm above MSL)

relative to NGVD. Means from the nearshore gages are in absolute pressure and must be adjusted for atmospheric pressure.

Data records were subjected to spectral analysis with program LONGWV discussed in Chapter 2. The program was adapted to FRF data. Capabilities for varying water level between records and for combining an arbitrary number of successive records together to make longer records were added. Band spectra were computed using 12 frequencies per band, giving $\nu=24$.

A routine was added to compensate pressure spectra for hydrodynamic attenuation due to submergence of the gage so that surface wave conditions can be represented. Atmospheric pressure for the selected event, needed for compensation, was taken from the FRF barometer record (Gage 616) as 1017.0 mb. Compensation of energy at the high frequency end of the short wave spectrum was stopped when the compensation factor became greater than 100. The compensation was applied in calculating spectra, band spectra, and significant heights for both long and short waves. It was not applied to the Fourier a and b coefficients used to predict the long wave characteristics because: 1) the compensation is expected to be negligible for long waves in shallow depths; and 2) altering the a's and b's might unfavorably impact the inverse Fourier transform.

As with the laboratory data, it was necessary for stability to confine the calculation of nonlinear interactions between short wave components to frequencies less than a cutoff value. A high frequency cutoff of 0.04 Hz was used with the FRF data.

Output files from LONGWV were run in the postprocessing program CONVERTSP, which provides options for units conversion and further band averaging of measured and predicted spectra. The CONVERTSP output files are in a format to facilitate plotting.

Results

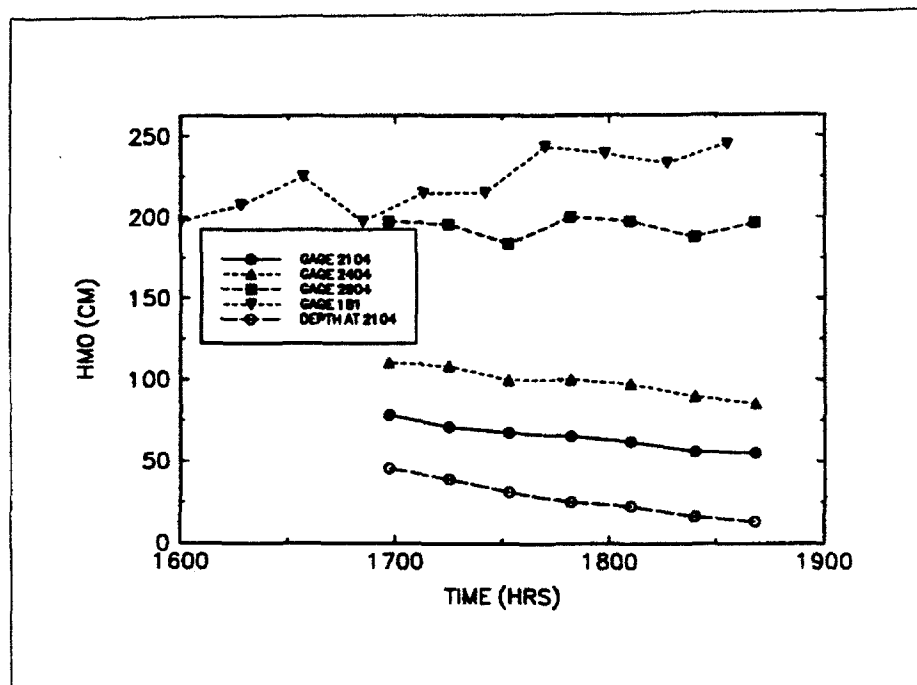
Variation of short wave significant height with depth is illustrated in Figure 19a. Significant height at Gage 181 was between about 2.0 and 2.5 m during the episode. Heights were somewhat higher toward the end of the episode than near the beginning. Heights were nearly constant at the most seaward nearshore gages. Heights decreased with time at the inner nearshore gages. The decrease is due to depth decreases of between 30 and 40 cm during the time period covered by the nearshore gages. Depth changes are primarily a result of the ebbing tide.

The variation of long wave significant height with depth is shown in Figure 19b. As with the short wave height, the long wave height at Gage 181 tends to increase during the episode. Tendencies at the nearshore gages are opposite to those observed for the short wave heights. Heights increase closer to shore, and heights increase with time. The dramatic difference in behavior of short and long wave heights during shoaling is further illustrated in Figure 20. Similar plots for all 17-min records are given in Appendix C. The full data set on short and long wave significant heights from 17-min records is given in Tables 5-8.

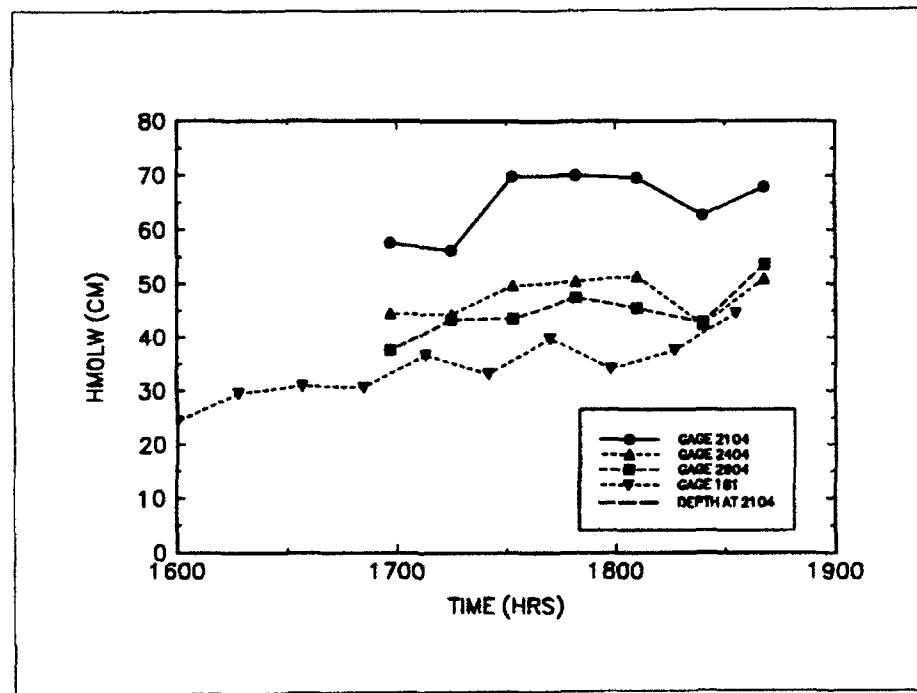
The overall effect of water depth on short and long wave significant height is shown by plotting results from all 17-min nearshore gage records together (Figure 21). The rapid decrease in short wave significant height during breaking and the insensitivity of long wave significant height to breaking are evident. Long wave height exceeds short wave height in the shallowest depths.

Variation of the ratio H_{m0LW}/H_{m0} is examined in Figures 22-25. The increase in the inner surf zone with time during the episode is shown in Figure 22. Variation with relative depth shows a consistent trend (Figure 23). The ratio H_{m0LW}/H_{m0} appears to approach an upper limit of about 1.2 in the inner surf zone. The ratio at Gage 2904, outside the surf zone, shows some correlation with H_{m0} offshore at Gage 181 (Figure 24), which accounts for some of the scatter in Figure 23.

In Figure 25, the ratio of H_{m0LW} to H_{m0} at Gage 181 is shown as a function of water depth. The ratio is between about 0.20 and 0.25 across the nearshore gages with the exception of the shallowest gage. There, in depths of less than 0.5 m, the ratio increased to an average of nearly 0.30. These values are



a) Short waves



b) Long waves

Figure 19. Significant wave height, 1600-1900 12 Oct 90, 17-min records

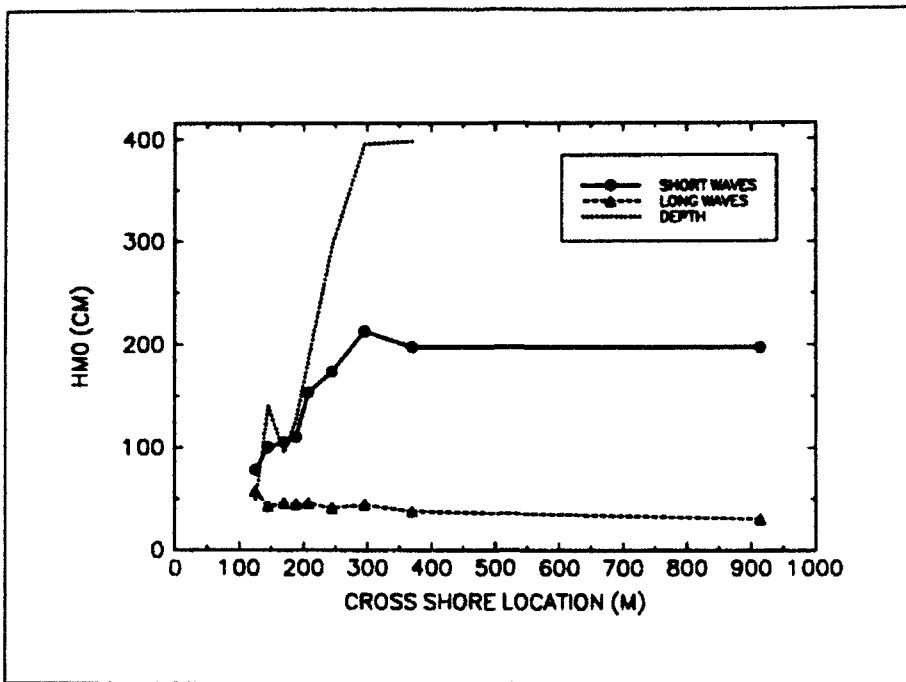


Figure 20. Significant wave height variation with cross shore location, 17-min records beginning at 1651 (Gage 181) and 1658 (nearshore gages)

Table 5
Short Wave Significant Heights, Gage 181, 12 Oct 90, 17 Minute Records¹

Time (EST)									
1600	1617	1634	1651	1708	1725	1742	1759	1816	1833
196.9	207.6	224.7	197.3	214.8	215.0	243.4	239.1	233.2	244.8

¹ Significant heights are given in cm

Table 6
Long Wave Significant Heights, Gage 181, 12 Oct 90, 17 Minute Records¹

Time (EST)									
1600	1617	1634	1651	1708	1725	1742	1759	1816	1833
24.3	29.5	30.9	30.6	36.6	33.1	39.8	34.1	37.6	44.5

¹ Significant heights are given in cm

Table 7
Short Wave Significant Heights, Nearshore Gages,
12 Oct 90, 17 Minute Records¹

Gage Number	Time (EST)						
	1651	1708	1725	1742	1759	1816	1833
2104	78.2	71.1	67.5	65.2	61.9	55.9	54.9
2204	100.4	97.2	87.9	89.9	88.7	78.5	78.9
2304	105.2	110.8	91.6	92.1	90.9	82.3	78.0
2404	110.1	108.1	99.5	99.9	97.2	89.5	85.0
2504	153.4	150.4	138.6	133.6	132.0	117.3	108.5
2704	173.7	170.2	167.2	161.3	162.9	159.4	141.5
2804	212.9	209.4	203.8	213.5	211.4	207.3	198.3
2904	197.4	195.8	183.8	200.0	197.6	187.7	196.6

¹ Significant heights are given in cm

Table 8
Long Wave Significant Heights, Nearshore Gages,
12 Oct 90, 17 Minute Records¹

Gage Number	Time (EST)						
	1651	1708	1725	1742	1759	1816	1833
2104	57.6	56.2	69.9	70.1	69.7	62.8	67.9
2204	42.7	36.3	52.6	50.1	46.9	47.5	54.7
2304	45.7	39.8	52.4	50.2	51.6	42.1	51.5
2404	44.5	44.3	49.7	50.5	51.5	42.4	51.0
2504	45.8	47.9	52.7	51.7	47.6	44.7	49.7
2704	41.2	46.0	55.5	53.8	50.7	52.4	44.5
2804	44.4	43.9	51.2	56.0	45.6	50.8	52.6
2904	37.6	43.3	43.6	47.5	45.5	42.8	53.6

¹ Significant heights are given in cm

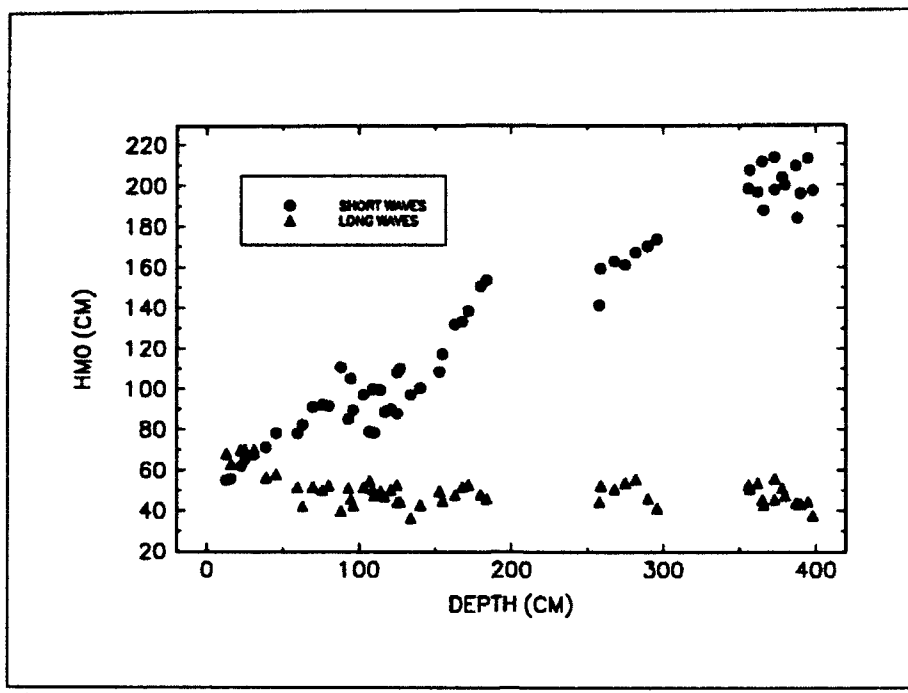


Figure 21. Significant wave height variation with depth, 17-min records from all nearshore gages

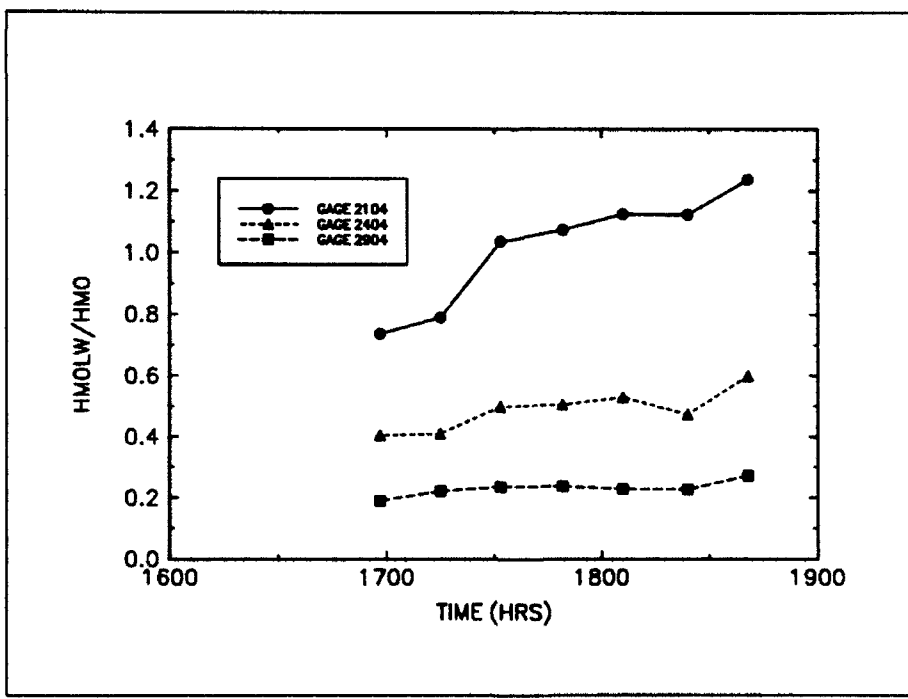


Figure 22. Variation of H_{sOLW}/H_{s0} with time, 17-min records

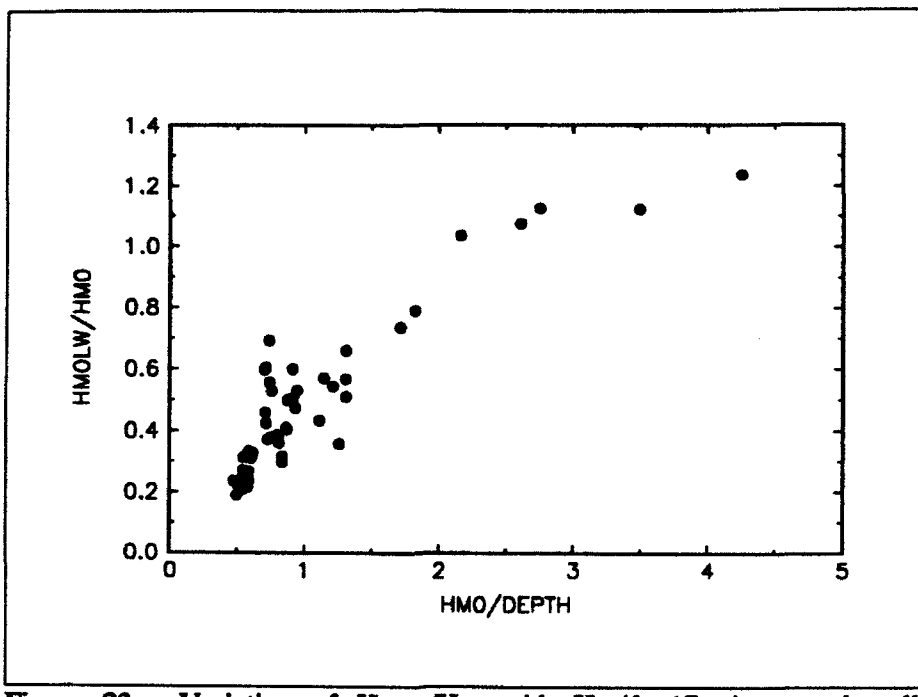


Figure 23. Variation of H_{molw}/H_{m0} with H_{m0}/d , 17-min records, all nearshore gages

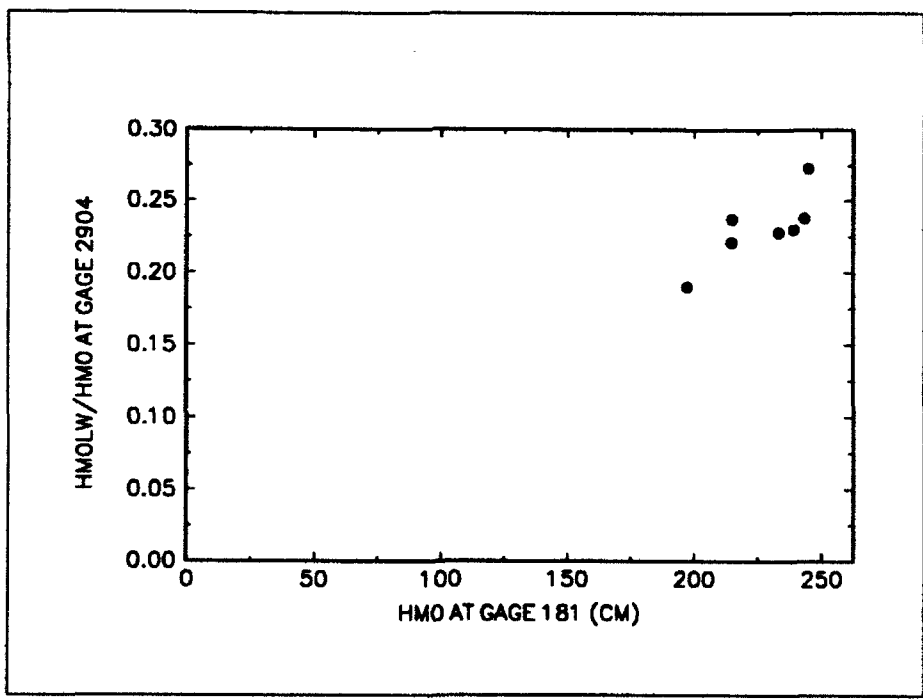


Figure 24. Variation of H_{molw}/H_{m0} at Gage 2904 with offshore H_{m0} , 17-min records

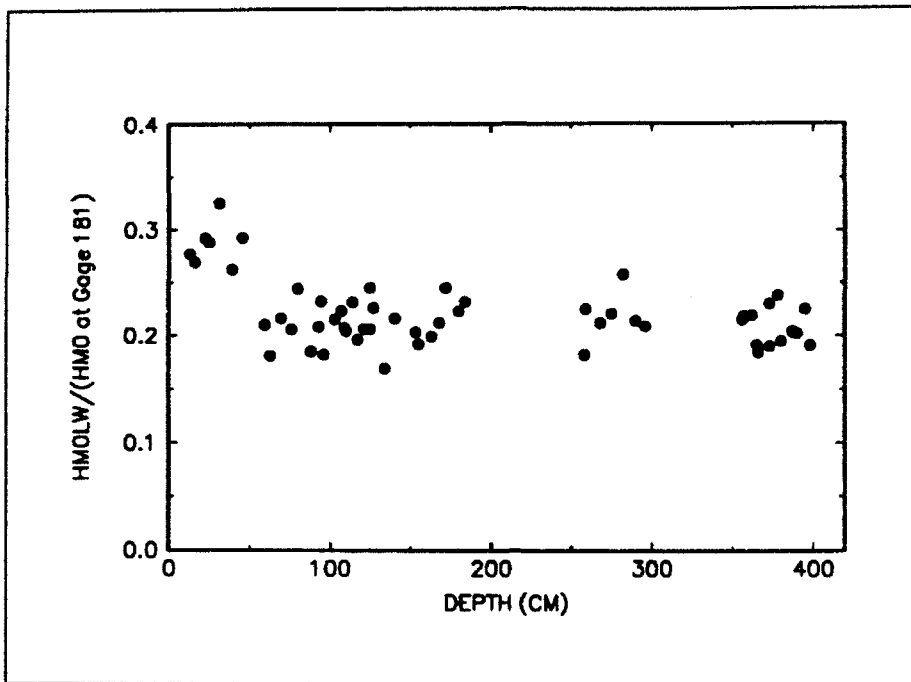


Figure 25. Variation of $H_{\text{mol},w}/(H_{\text{mol}})_{\text{Gage 181}}$ with depth

consistent with Goda's (1975) results from 3 field sites of $H_{\text{mol},w}/(H_{\text{mol}})_{\text{offshore}}$ ranging from 0.2 to 0.4. Guza and Thornton (1985) considered a range of cases from 3 U.S. field sites and found that $H_{\text{mol},w}/(H_{\text{mol}})_{\text{offshore}}$ in 0-1 m depth and 1-2 m depth were 0.37 and 0.32, respectively. Their offshore measurements were in depths of 7-19 m, comparable to Gage 181 in this study. It is not evident why the $H_{\text{mol},w}/(H_{\text{mol}})_{\text{offshore}}$ values in this study are lower than Guza and Thornton's (1985) results, but it is noted that offshore significant heights in Guza and Thornton's data were all lower than those in this study. Also Guza and Thornton (1985) used a high frequency cutoff of 0.05 Hz for the long wave spectrum as opposed to about 0.04 Hz in this study. This difference would tend to elevate Guza and Thornton's (1985) $H_{\text{mol},w}$ values relative to those computed in this study.

Short and long wave spectra for all the gages are given in Appendices D through L. Short wave spectra are given for all record lengths analyzed. Long wave spectra are shown for record lengths from 34 min through 102 min. The 17, 51, and 102-min records are included for all gages. Additional record lengths of 34, 68, and 85 min are included only for gages 181 and 2904. Short wave spectra from 4 gages are illustrated in Figure 26. The spectrum changes little between gages 181 and 2904. Inside the surf zone (gages 2404 and 2104), the short wave spectrum loses considerable energy and the long wave spectrum gains energy.

Long wave spectra are usually difficult to calculate with confidence. Long time series are required during a time period when wave conditions are stationary. Except for tidal variations, this episode meets the requirements fairly well. Therefore long wave spectra computed from 102-min records are

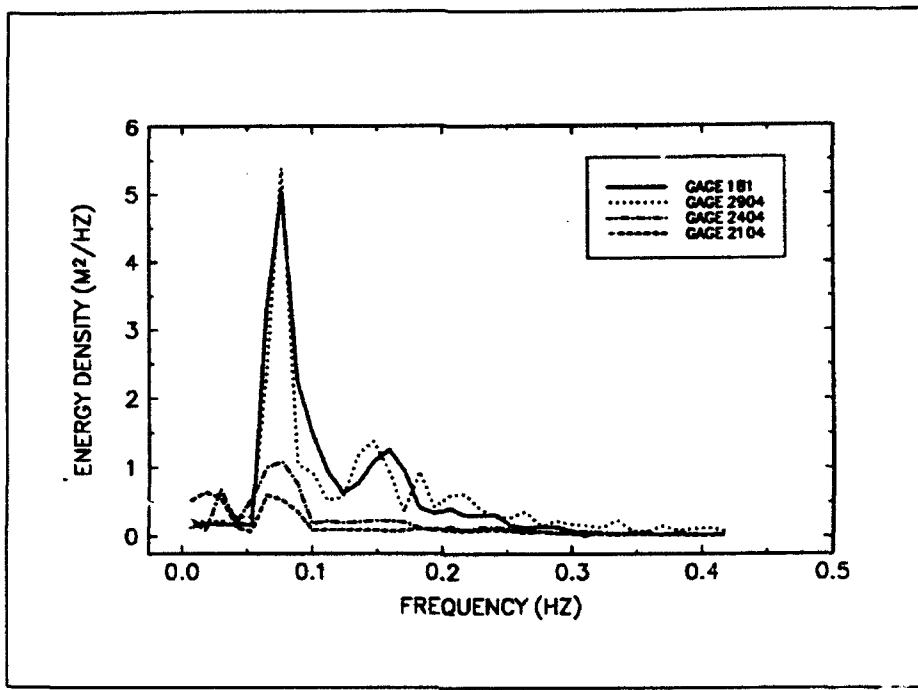


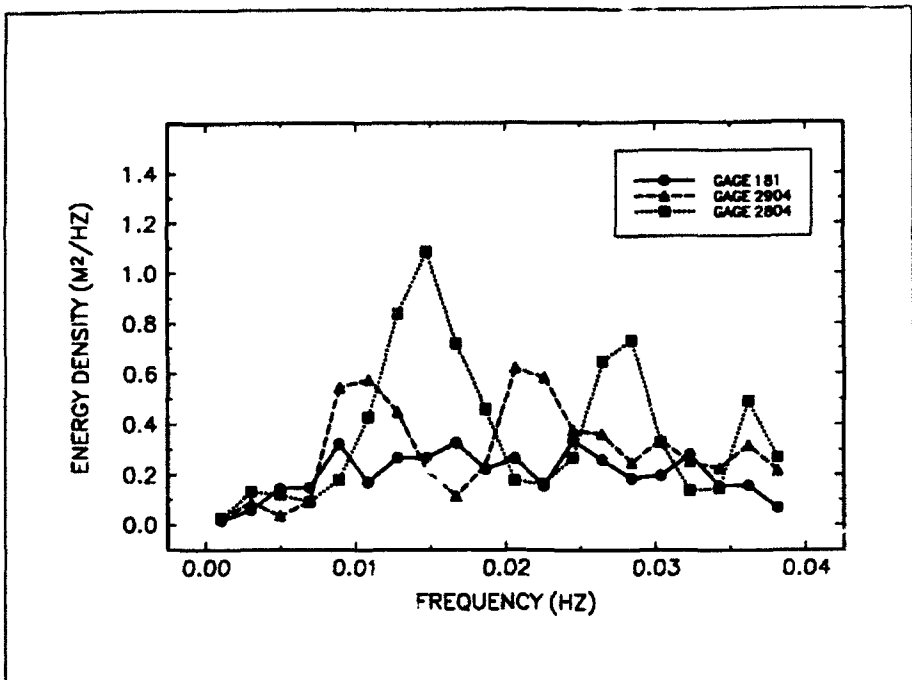
Figure 26. Short wave spectrum, 17-min records beginning at 1658

presented (Figure 27). The offshore long wave spectrum (Gage 181) is broad with no prominent peaks. However all of the nearshore long wave spectra have at least one prominent peak. Many have two peaks. At the outer nearshore gages (Gages 2904, 2804, and 2704), the higher frequency peak is at a frequency of about twice that of the lower frequency peak. There appears to be a steady migration of the peaks toward higher frequency as the waves shoal, with emergence of a new peak at low frequency (around 0.005 Hz) at Gage 2704.

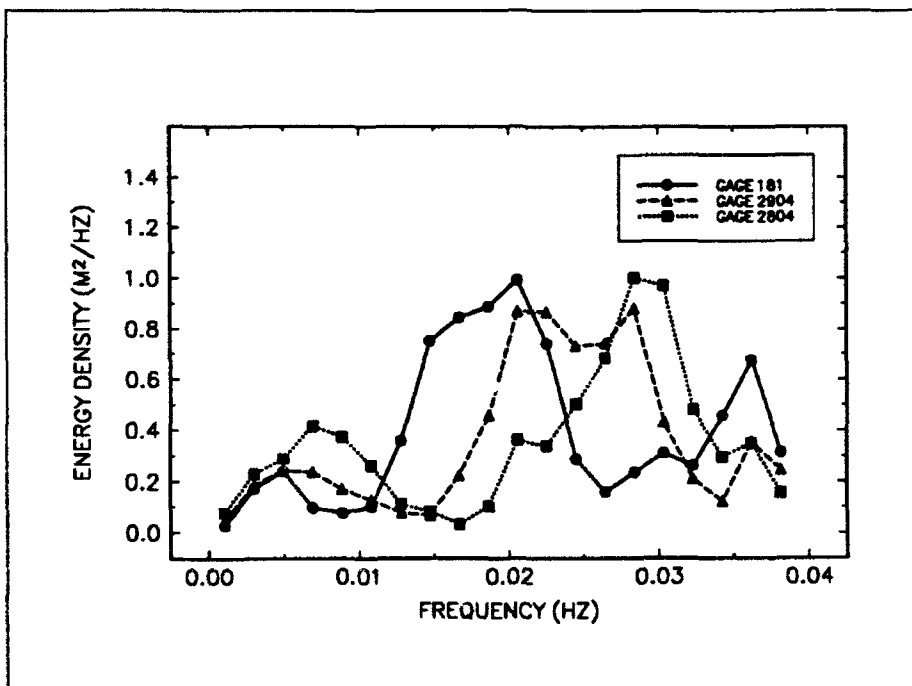
Comparison with Theory

The equations of Sand (1982a, 1982c) were used to predict long waves at each gage on the cross shore array. Because of limitations of the theory, comparisons are presented only for those gages seaward of the surf zone. Predictions are shown on each plot in Appendix C. Scatter plots of measured and predicted H_{m0LW} are given in Figure 28. Measurements exceeded predictions by an average of about 20 percent at Gage 181. The one case for which measurement and prediction coincide is at 1600 hours. At the nearshore gages, predictions exceeded measurements by an average of about 40 percent.

The underprediction at Gage 181 can be explained by considering that long waves are effectively reflected seaward from the nearshore slope. Thus the record from Gage 181 includes some seaward-propagating long wave energy. It also can be expected to include some free long wave energy from other sources. Hence, it is not surprising that the measurements, including both bound and free long waves, exceed the theoretical prediction which includes only bound long waves.

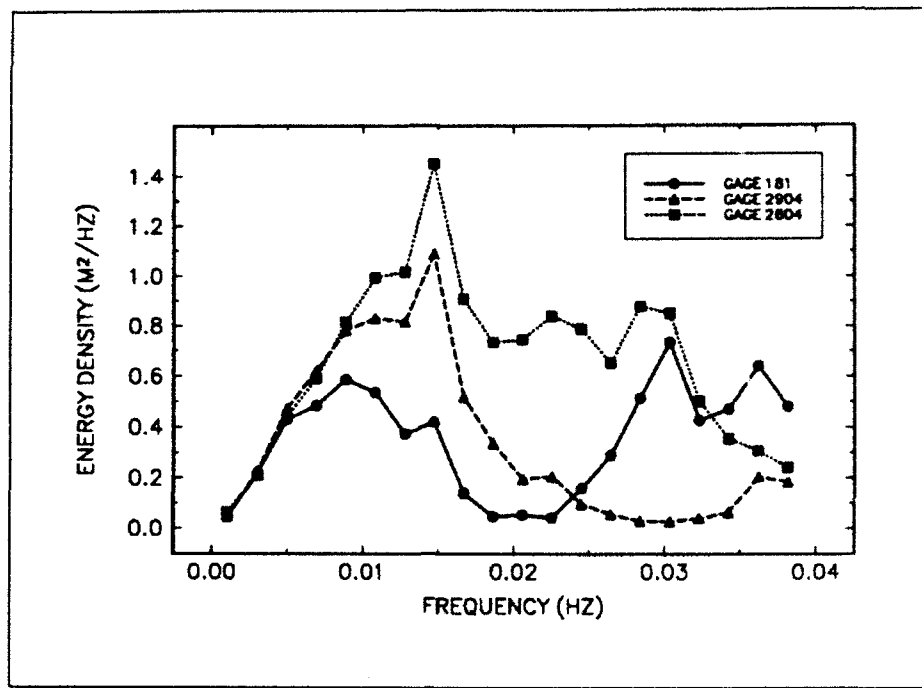


a) Gages 181, 2904, and 2804



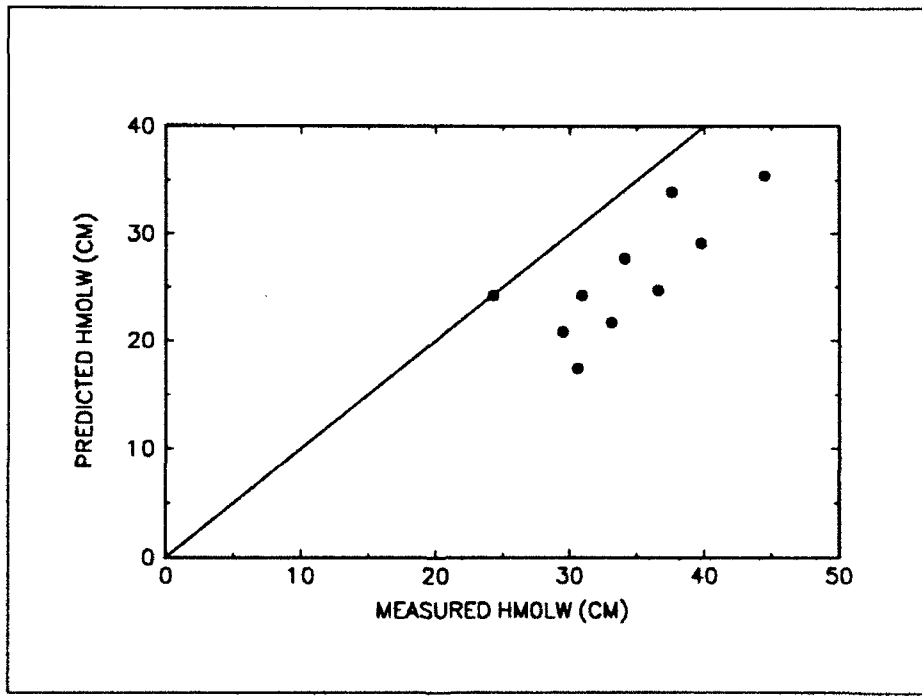
b) Gages 2704, 2504, and 2404

Figure 27. Long wave spectrum, 102-min records (Continued)



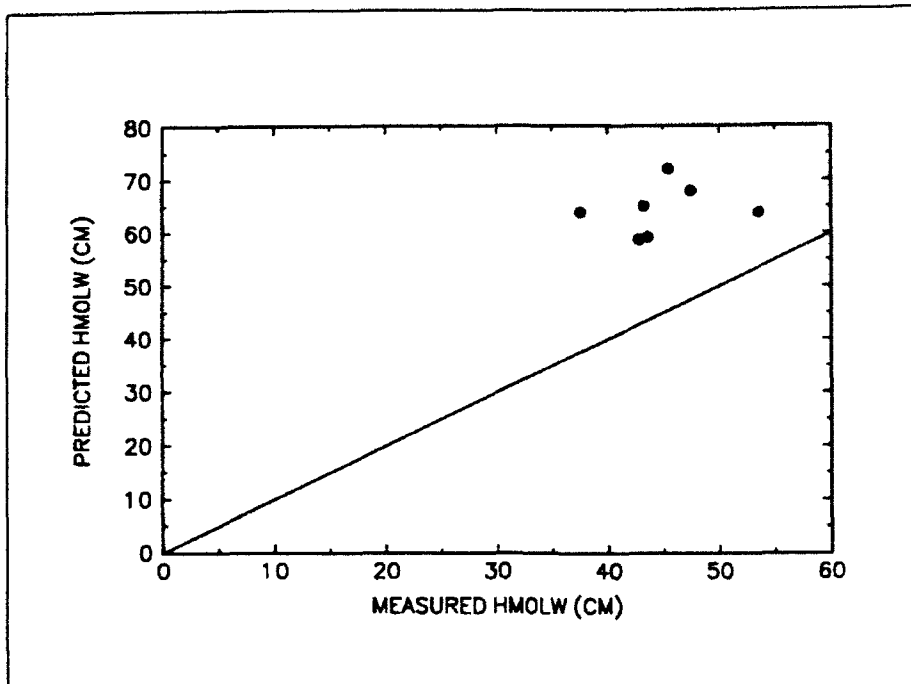
c) Gages 2304, 2204, and 2104

Figure 27. (Concluded)

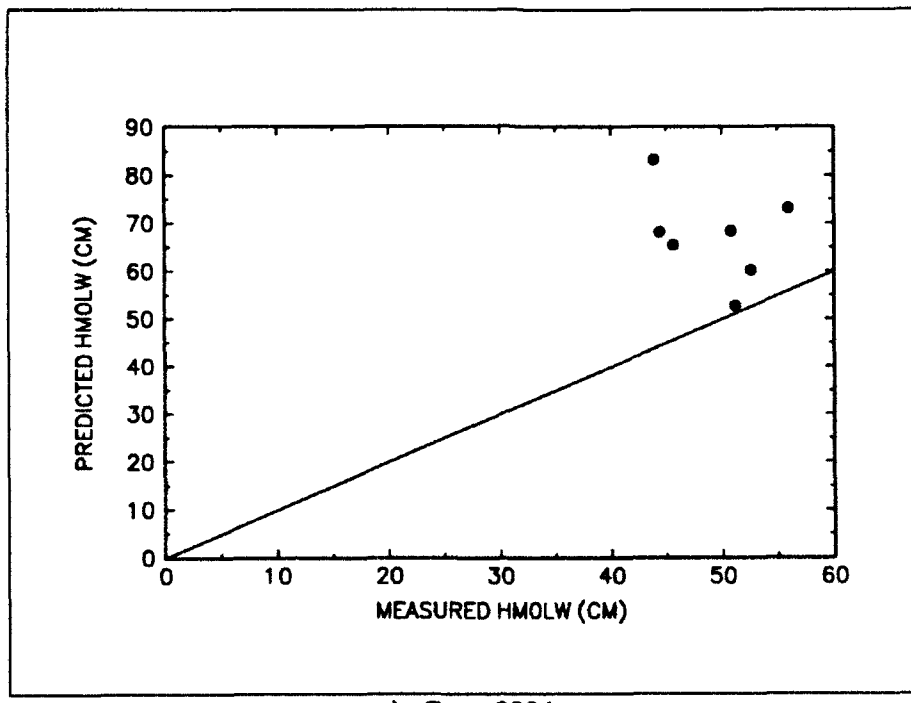


a) Gage 181

Figure 28. Predicted and measured significant height, long waves, 17-min records (Continued)



b) Gage 2904



c) Gage 2804

Figure 28. (Concluded)

bound and free long waves, exceed the theoretical prediction which includes only bound long waves.

The overprediction at Gages 2904 and 2804 can be attributed to the the sloped bottom which prevents the long waves from reaching an equilibrium for the local depth. Thus at any given depth on the nearshore slope, the long waves are a consequence of the deeper depths somewhat seaward and hence are less strongly developed than would be expected from the "flat bottom" theory. This hypothesis is supported by the small improvement in predictions at Gage 2804 over Gage 2904, after the waves have propagated over another 75 m of constant depth.

Predicted and measured long wave spectra at two gages are shown in Figure 29. Gage 2804 is shown instead of Gage 2904 because the bottom was relatively flat between the two gages, giving waves at Gage 2804 somewhat more opportunity to adjust to local water depth. Predicted spectra are a rough approximation to the measurements with the exception of a high energy tail in the predictions for Gage 2804 at very low frequency (below 0.008 Hz) which is not evident at all in the measurements. Other than this tail, the predicted Gage 2804 spectrum shows two prominent peaks similar to those in the measured spectrum, but shifted toward low frequency.

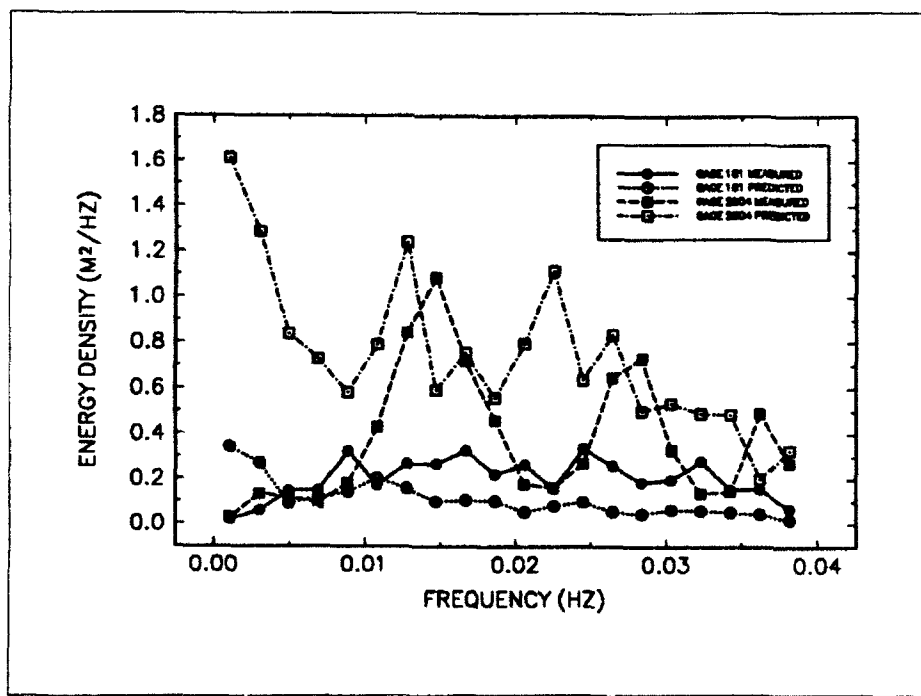


Figure 29. Predicted and measured long wave spectra, 102-min records beginning at 1651 (Gage 181) and 1658 (Gage 2804)

5 Conclusions

Based on wind wave shoaling tests in a directional basin with open side boundaries, the following conclusions are reached:

1. Long wave energy (surf beat) increases significantly during shoaling and breaking of a short wave spectrum.
2. More long wave energy is generated by unidirectional short wave spectra than by directionally-spread short wave spectra.
3. The general magnitude of long wave energy, but not the details, is predicted near the beginning of the slope by the bound long wave equations of Sand (1982a, 1982c).
4. For applications in which nearshore long waves are important, attention should be paid to bound long wave phases as well as energy during laboratory generation.

Based on analysis of an episode of energetic swell during the DELILAH field experiment, the following conclusions are reached:

5. Nearshore long wave energy increases with decreasing depth and increasing offshore short wave height.
6. The ratio H_{m0LW}/H_{m0} approaches a limit of about 1.2 in the inner surf zone in these data (Figure 23). Thus the local short wave height may be used to predict an upper bound on long wave height.
7. The ratio of H_{m0LW} to H_{m0} at the offshore Gage 181 tends toward a constant value through most of the surf zone and then increases in very shallow depth. The data and other studies suggest that H_{m0LW} inside the surf zone can be coarsely approximated by

$$H_{m0LW} \sim 0.3 (H_{m0})_{8-m \text{ depth}} \quad d > 1 \text{ m} \quad (17)$$

$$H_{m0LW} \sim 0.4 (H_{m0})_{8-m \text{ depth}} \quad d \leq 1 \text{ m}$$

8. The theory of Sand (1982a, 1982c) provides a useful approximation to the long wave significant height and spectrum just outside the surf zone. Since H_{m0LW} appears to change relatively little across the surf zone, the theoretical predictions could apply across the surf zone too.

Future investigations should be directed toward:

1. Consider a wider range of field wave conditions.
2. Analyze field data to separate bound and free long wave energy and to identify propagation direction.
3. Develop a more realistic theory-based model of long wave evolution in the nearshore zone.

References

Agnon, Y., Sheremet, A., Gonsalves, J., and Stiassnie, M. (1993). "Nonlinear evolution of a unidirectional shoaling wave field," accepted for publication in *Coastal Engineering*.

Birkemeier, W. A., Hathaway, K. K., Smith, J. M., Baron, C. F., and Leffler, M. W. (1991). "DELILAH Experiment: Investigator's summary report," draft technical report, U.S. Army Engineer Waterways Experiment Station, Vicksburg, MS.

Bouws, E. H., Gunther, H., Rosenthal, W., and Vincent, C. L. (1985). "Similarity of the wind wave spectrum in finite depth water, Part I-Spectral form," *J. Geophysical Research* 90(C1), 975-86.

Bowers, E. C., and Huntington, S. W. (1987). "The representation of set-down beneath wave groups in harbour modelling." *Proc., XXII Congress. IAHR, Lausanne, Switzerland.*

Briggs, M. J., and Jensen, R. E. (1988). "Simulation of extreme storm events in coastal structural models." *Proc., Ocean Structural Dynamics Symposium. Corvallis, OR.*

Briggs, M. J., and Smith, J. M. (1990). "The effect of wave directionality on nearshore waves." *Proc., 23rd Coastal Engineering Conf. ASCE, Delft, The Netherlands.*

Briggs, M. J., Smith, J. M., and Green, D. R. (1991). "Wave transformation over a generalized beach," Technical Report CERC-91-15, U.S. Army Engineer Waterways Experiment Station, Vicksburg, MS.

Elgar, S., Guza, R.T., Freilich, M.H., and Briggs, M.J. (1992). "Laboratory simulations of directionally spread shoaling waves," *J. Waterway, Port, Coastal and Ocean Engineering* 118(1), 87-103.

Elgar, S., Herbers, T.H.C., Okihiro, M., Oltman-Shay, J., and Guza, R.T. (1992). "Observations of Infragravity Waves," *J. Geophysical Research* 97(C10), 15573-15577.

Freilich, M.H., Guza, R.T., and Elgar, S.E. (1990). "Observations of non-linear effects in directional spectra of shoaling gravity waves," *J. Geophysical Research* 95(C6), 9645-56.

Goda, Y. (1975). "Irregular wave deformation in the surf zone," *Coastal Engineering in Japan* 18, 13-27.

Guza, R. T., and Thornton, E. B. (1985). "Observations of surf beat," *J. Geophysical Research* 90(C2), 3161-72.

Hasselmann, K. (1962). "On the non-linear energy transfer in a gravity wave spectrum. Part 1. General theory," *J. Fluid Mechanics* 12, 481-500.

Hathaway, K. K., and Walton, T. L. (1990). "Evaluation of video camera technique in the laboratory," Memorandum for Record, U.S. Army Engineer Waterways Experiment Station, Vicksburg, MS.

Holman, R. A., and Bowen, A. J. (1984). "Longshore structure of infragravity wave motions," *J. Geophysical Research* 89(C4), 6446-52.

Holman, R. A., and Sallenger, A. H. (1985). "Setup and swash on a natural beach," *J. Geophysical Research* 90(C1), 945-53.

Huntley, D. A., and Kim, C. S. (1984). "Is surf beat forced or free." *Proc., 19th Coastal Engineering Conf.* ASCE, 871-85.

IAHR. (1986). "List of sea state parameters," Suppl. to PIANC Bull. 52, pub. jointly by IAHR and PIANC, Brussels, Belgium. Also *J. Waterway, Port, Coastal and Ocean Engineering* 115(6), 793-808.

Kobayashi, N. (1988). "Review of wave transformation and cross-shore sediment transport processes in surf zones," *J. Coastal Research* 4(3), 435-45.

Kobayashi, N., DeSilva, G., and Watson, K. D. (1989). "Wave transformation and swash oscillation on gentle and steep slopes," *J. Geophysical Research* 94(C1), 951-66.

List, J. H. (1986). "Groupiness as a source of nearshore long waves." *Proc., 20th Coastal Engineering Conf.*, 497-511.

Liu, P. L.-F. (1989). "A note on long waves induced by short-wave groups over a shelf," *J. Fluid Mechanics* 205, 163-70.

Lo, J.-M. (1981). "Surf beat: numerical and theoretical analysis," Ph.D. diss., University of Delaware, Newark, DE.

Longuet-Higgins, M. S., and Stewart, R. W. (1962). "Radiation stress and mass transport in gravity waves, with application to 'surf beats,'" *J. Fluid Mechanics* 13, 481-504.

Longuet-Higgins, M. S., and Stewart, R. W. (1964). "Radiation stresses in water waves; a physical discussion, with applications," *Deep-Sea Research* 11, 529-62.

Madsen, P. A., Murray, R., and Sorensen, O. R. (1991a). "A new form of the Boussinesq equations with improved linear dispersion characteristics," *Coastal Engineering* 15, 371-88.

Madsen, P. A., Sorensen, O. R., and Yang, Z. (1991b). "Wave-wave interaction in shallow water." *Proc., 24th Congress. IAHR*, Madrid, Spain, B, 1-10.

Mase, H., and Kobayashi, N. (1991). "Transformation of random breaking waves and its empirical numerical model considering surf beat." *Proc., Coastal Sediments Conf. ASCE*, 688-702.

Mei, C. C., and Benmoussa, C. (1984). "Long waves induced by short-wave groups over an uneven bottom," *J. Fluid Mechanics* 139, 219-35.

Munk, W. H. (1949). "Surf beats." *Transactions, American Geophysical Union*. 30(6), 849-54.

Okiihro, M., Guza, R.T., and Seymour, R.J. (1992). "Bound Infragravity Waves," *J. Geophysical Research* 97(C7), 11453-11469.

Oltman-Shay, J., and Hathaway, K. K. (1989). "Infragravity energy and its implications in nearshore sediment transport and sandbar dynamics," Technical Report CERC-89-8, U.S. Army Engineer Waterways Experiment Station, Vicksburg, MS.

Ottesen Hansen, N.-E. (1978). "Long period waves in natural wave trains," Progress Report No. 46, Institute of Hydrodynamical and Hydraulic Engineering, Technical Univ. of Denmark, Denmark, 13-24.

Pawka, S. S. (1982). "Wave directional characteristics on a partially sheltered coast," Ph.D. diss., Scripps Institution of Oceanography, La Jolla, Calif.

Sand, S. E. (1982a). "Long wave problems in laboratory models," *J. Waterway, Port, Coastal and Ocean Engineering* 108(WW4), 492-503.

Sand, S. E. (1982b). "Long waves in directional seas," *Coastal Engineering* 6(3), 195-208.

Sand, S. E. (1982c). "Wave grouping described by bounded long waves," *Ocean Engineering* 9(6), 567-80.

Schaffer, H. A., and Jonsson, I. G. (1990). "Theory versus experiments in two-dimensional surf beats." *Proc., 22nd Coastal Engineering Conf. ASCE*, 1131-43.

Symonds, G., Huntley, D. A., and Bowen, A. J. (1982). "Two-dimensional surf beat: Long wave generation by a time-varying breakpoint," *J. Geophysical Research* 87(C1), 492-8.

Symonds, G., and Bowen, A. J. (1984). "Interactions of nearshore bars with incoming wave groups," *J. Geophysical Research* 89(C2), 1953-9.

Thompson, E.F., and Briggs, M.J. (1991). "Long waves in laboratory wave basin shoaling tests." *Proc., 24th Congress. IAHR*, Madrid, Spain.

Tucker, M. J. (1950). "Surf beats: Sea waves of 1 to 5 minute period." *Proc., Royal Society, London*. Series A, 214, 79-97.

van Leeuwen, P. J., and Battjes, J. A. (1990). "A model for surf beat." *Proc., 22nd Coastal Engineering Conf. ASCE*, 32-40.

Appendix A

Offshore and Nearshore Array

Directional Spectra

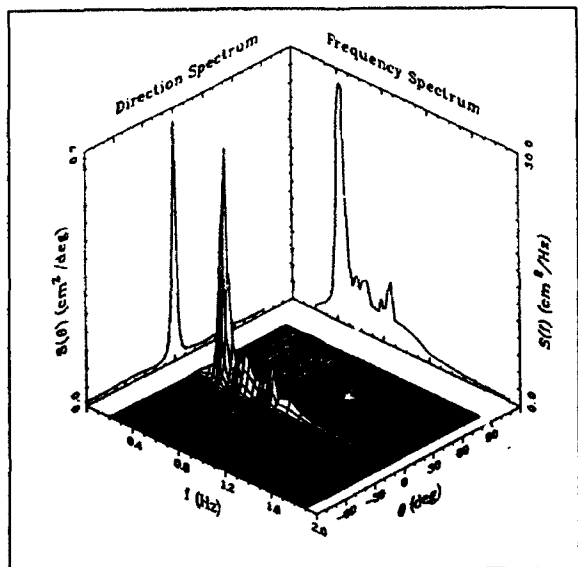


Figure A1. OGA, S0105, short waves

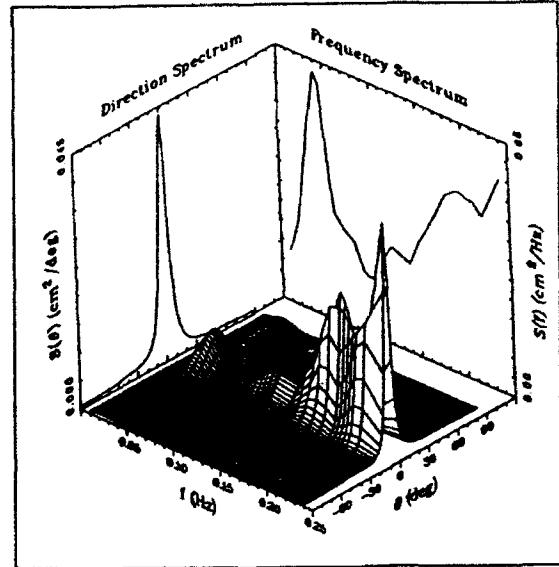


Figure A2. OGA, S0105, long waves

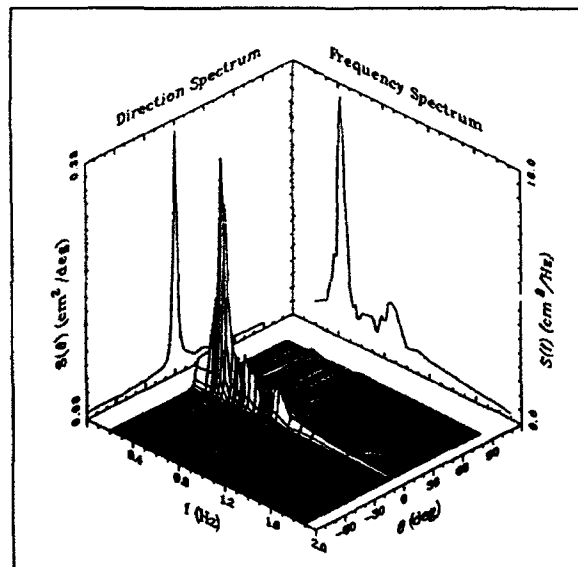


Figure A3. NGA, S0105, short waves

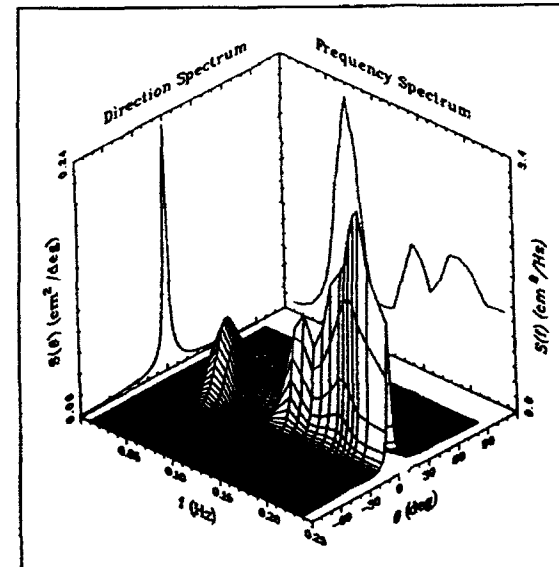


Figure A4. NGA, S0105, long waves

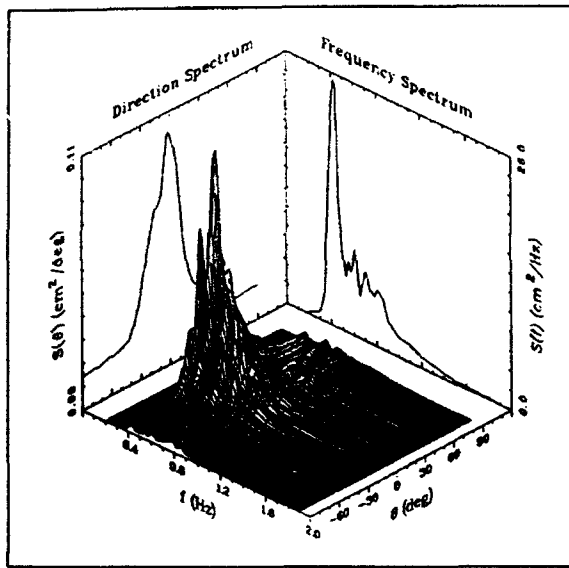


Figure A5. OGA, S0905, short waves

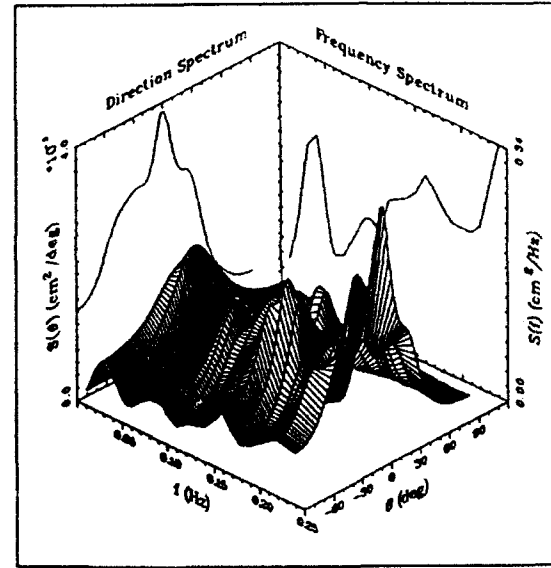


Figure A6. OGA, S0905, long waves

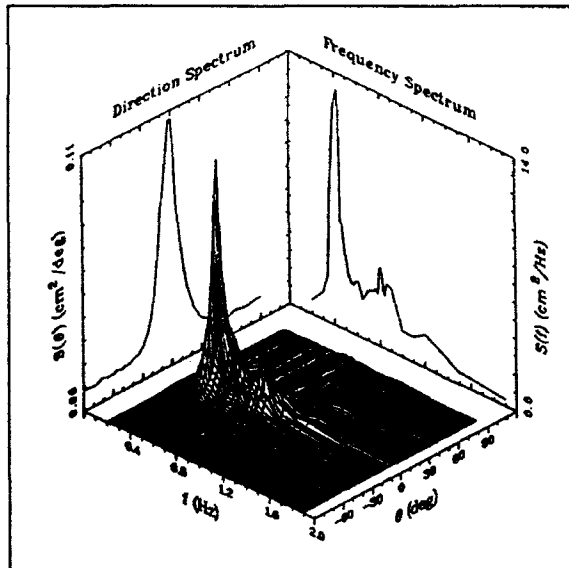


Figure A7. NGA, S0905, short waves

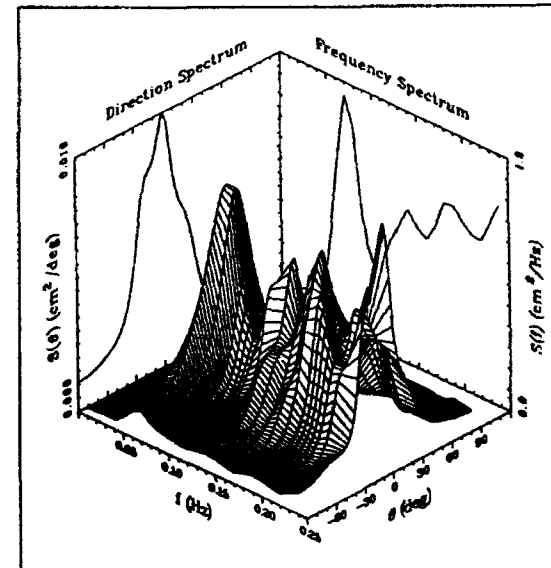


Figure A8. NGA, S0905, long waves

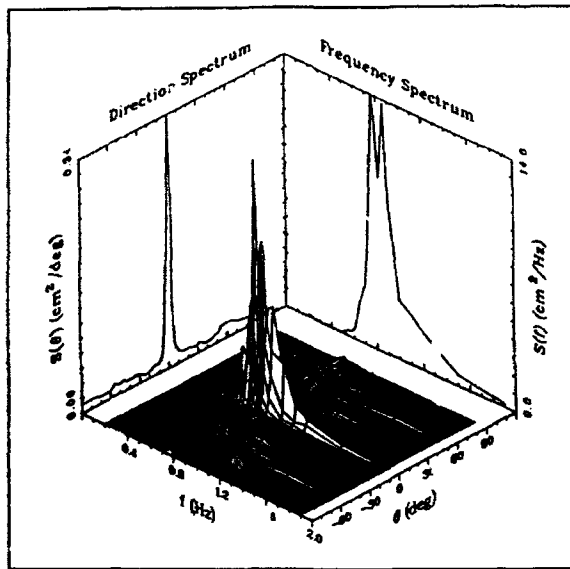


Figure A9. OGA, S3705, short waves

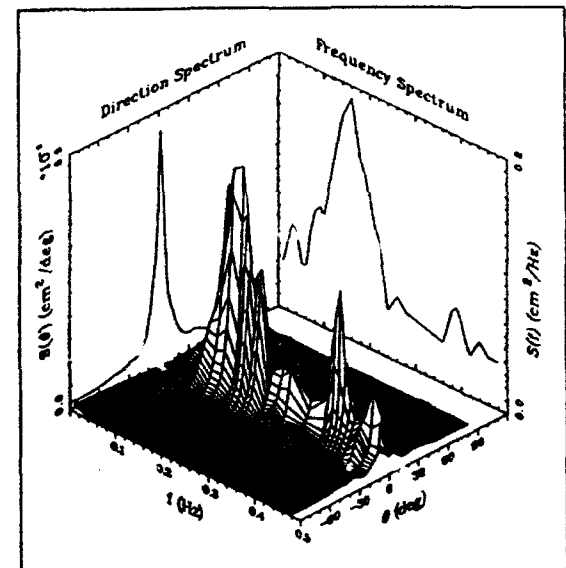


Figure A10. OGA, S3705, long waves

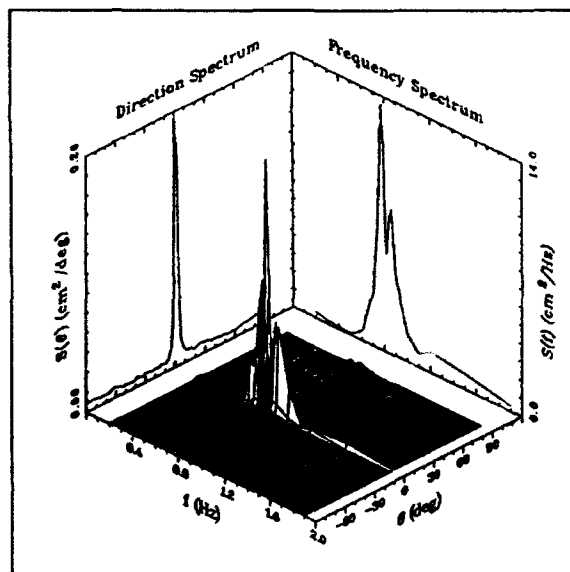


Figure A11. NGA, S3705, short waves

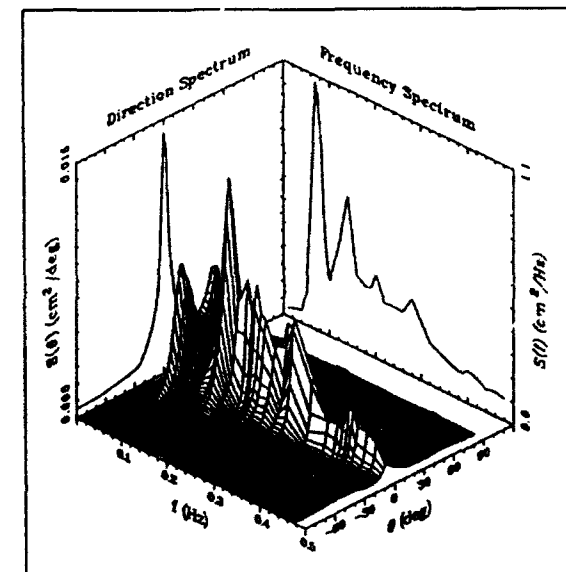


Figure A12. NGA, S3705, long waves

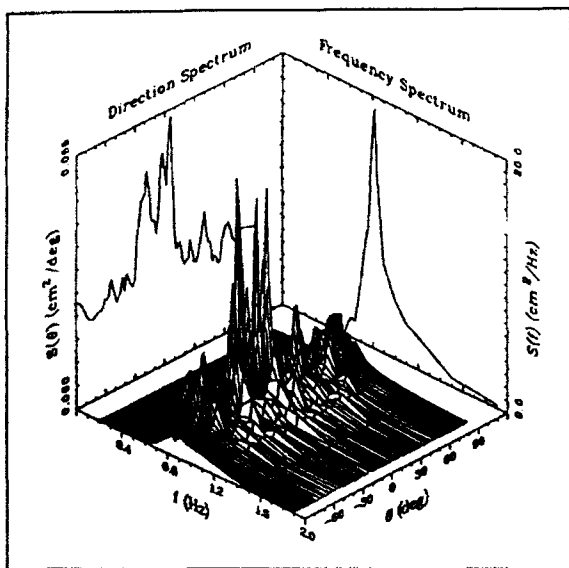


Figure A13. OGA, S4505, short waves

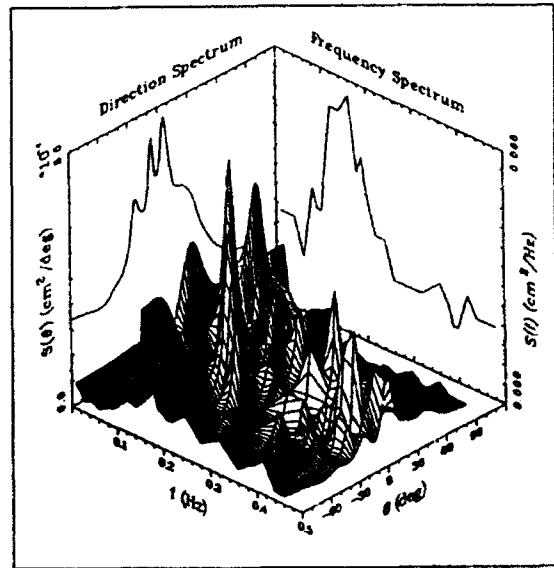


Figure A14. OGA, S4505, long waves

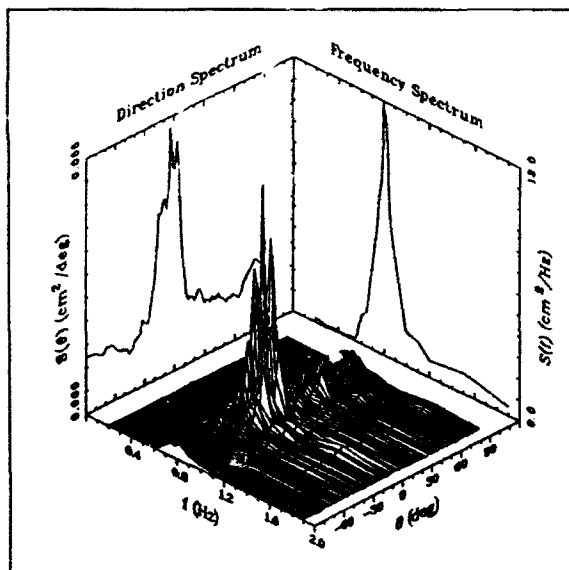


Figure A15. NGA, S4505, short waves

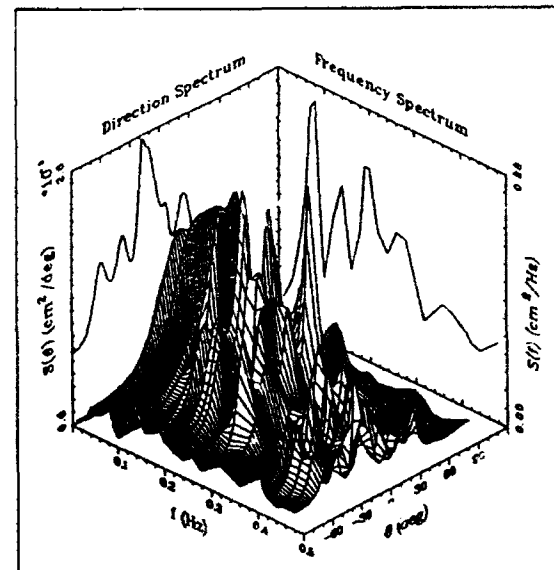


Figure A16. NGA, S4505, long waves

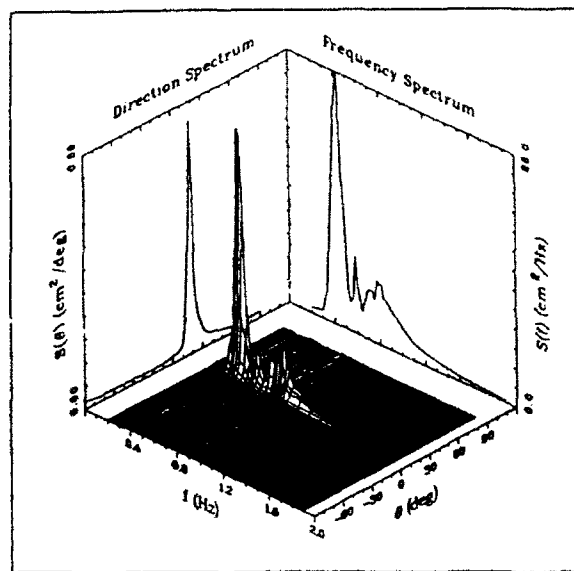


Figure A17. OGA, S2505, short waves

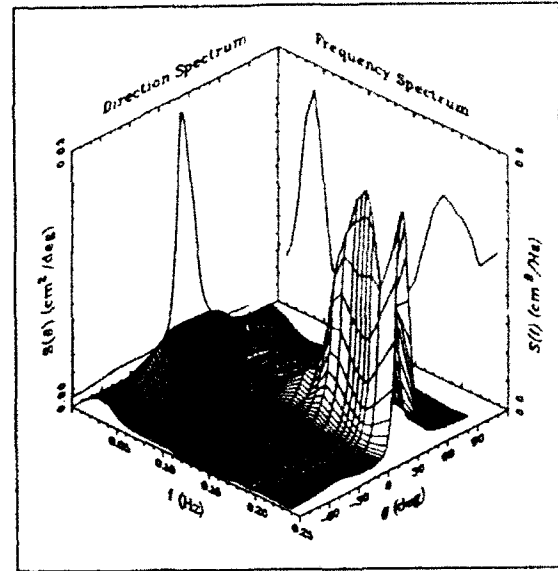


Figure A18. OGA, S2505, long waves

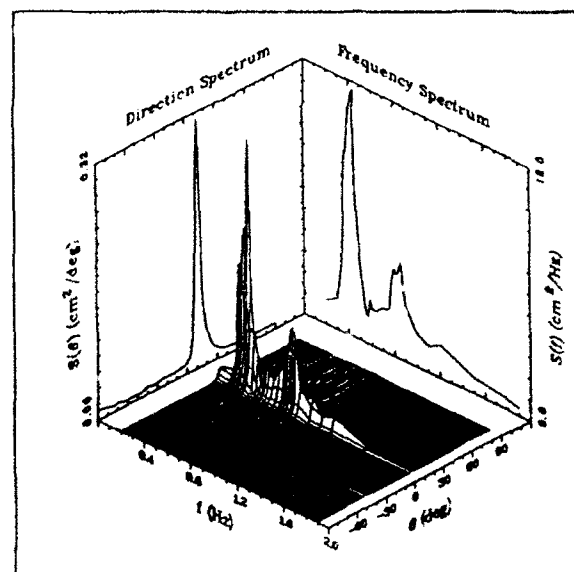


Figure A19. NGA, S2505, short waves

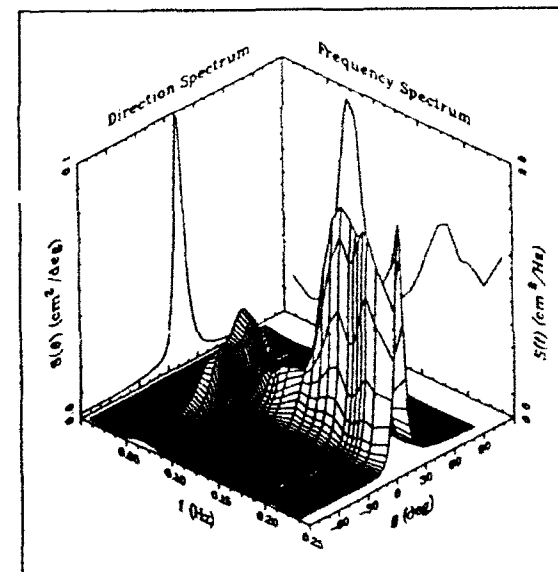


Figure A20. NGA, S2505, long waves

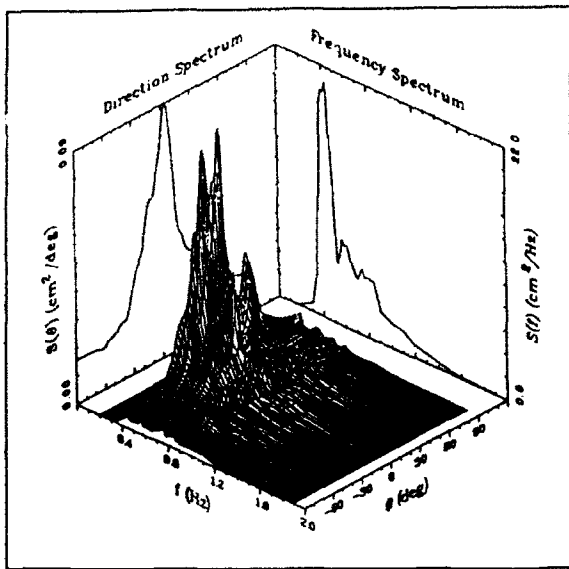


Figure A21. OGA, S3305, short waves

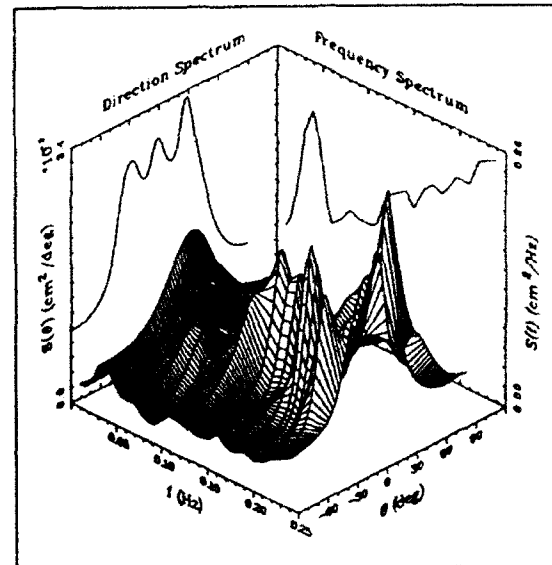


Figure A22. OGA, S3305, long waves

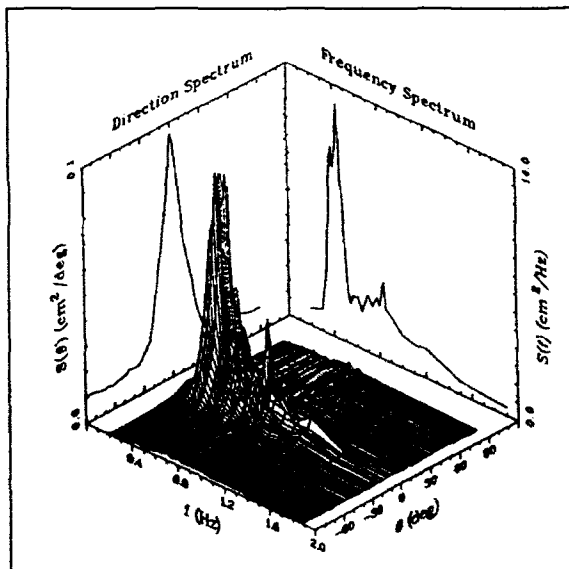


Figure A23. NGA, S3305, short waves

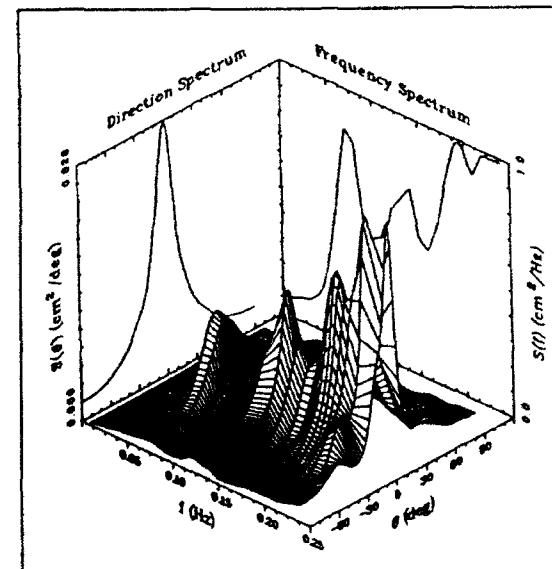


Figure A24. NGA, S3305, long waves

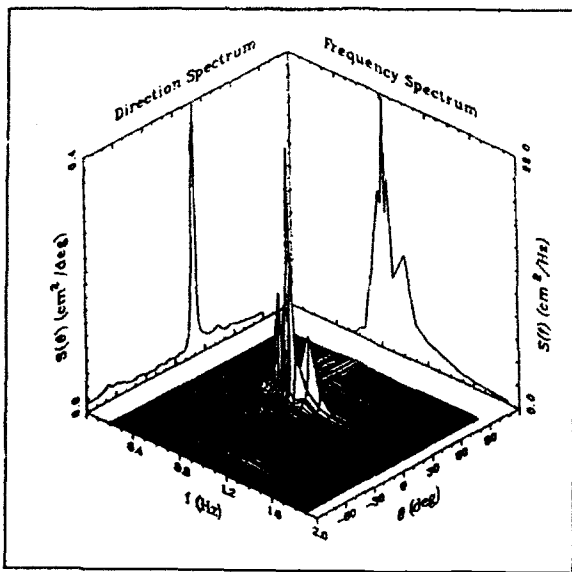


Figure A25. OGA, S6105, short waves

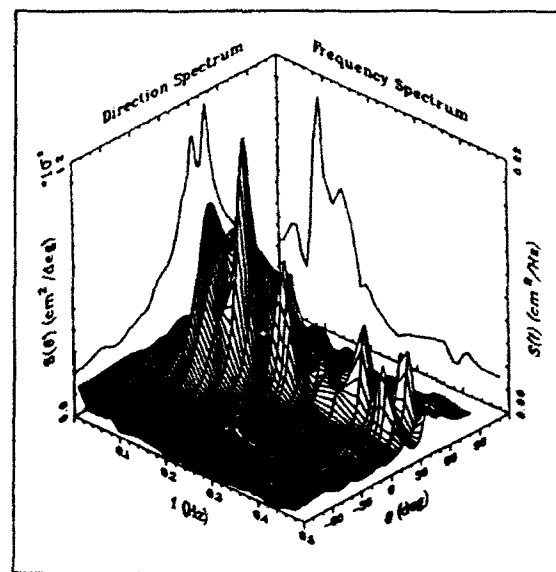


Figure A26. OGA, S6105, long waves

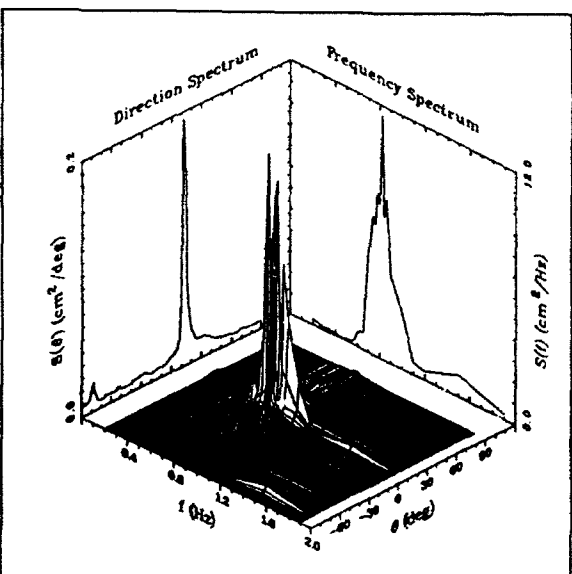


Figure A27. NGA, S6105, short waves

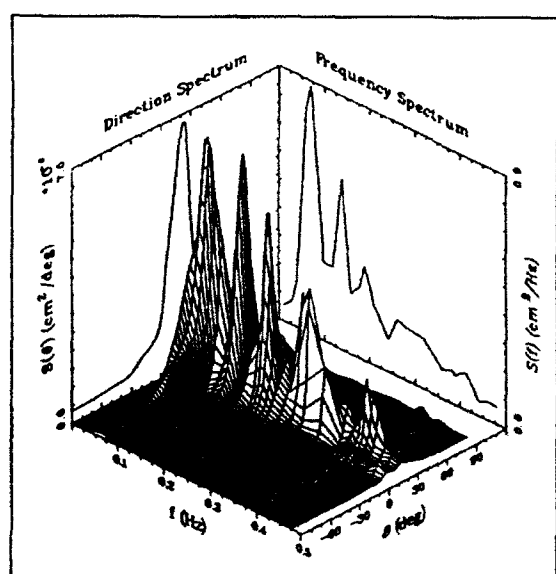


Figure A28. NGA, S6105, long waves

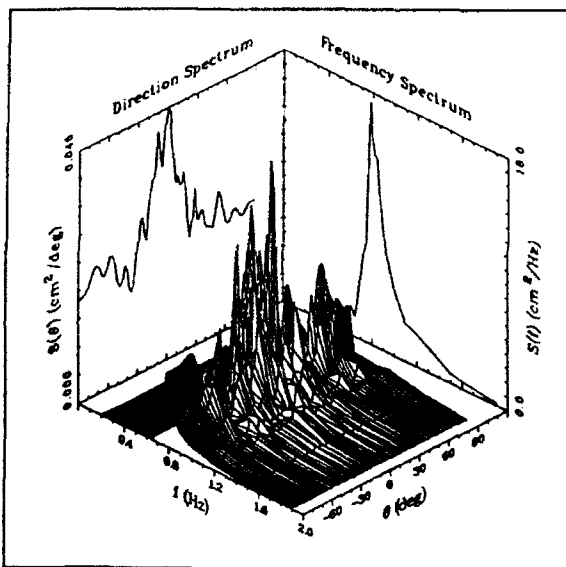


Figure A29. OGA, S6905, short waves

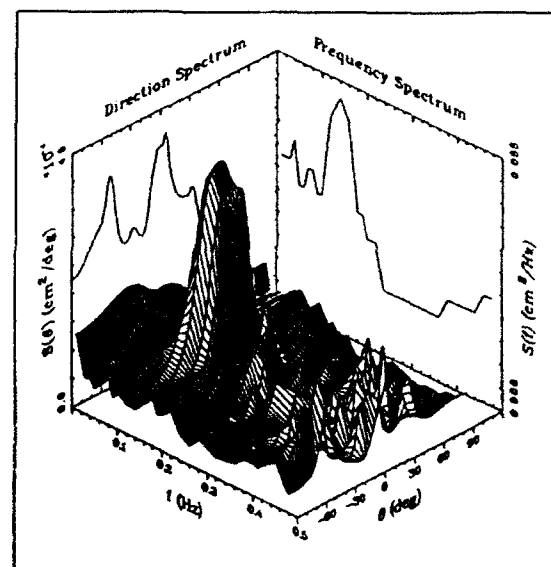


Figure A30. OGA, S6905, long waves

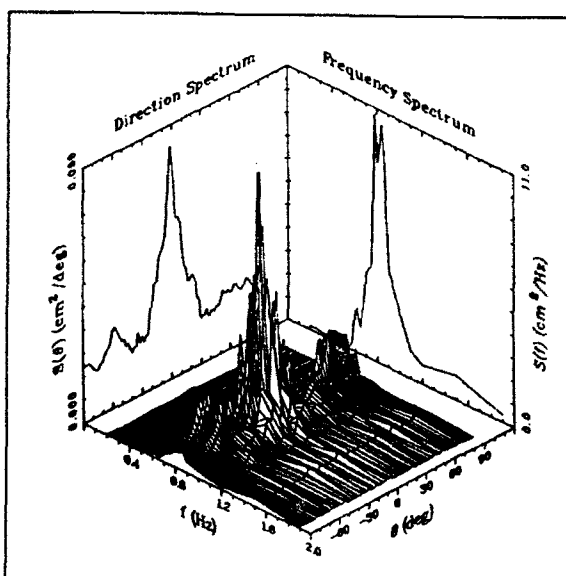


Figure A31. NGA, S6905, short waves

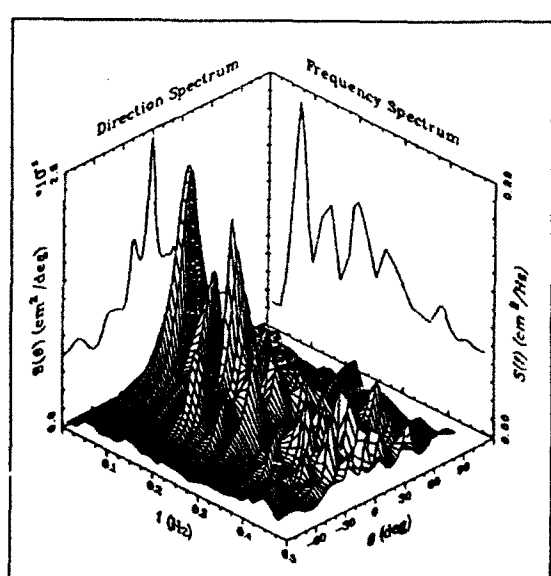


Figure A32. NGA, S6905, long waves

Appendix B

Offshore Array Directional Spectra Over 360-deg Arc

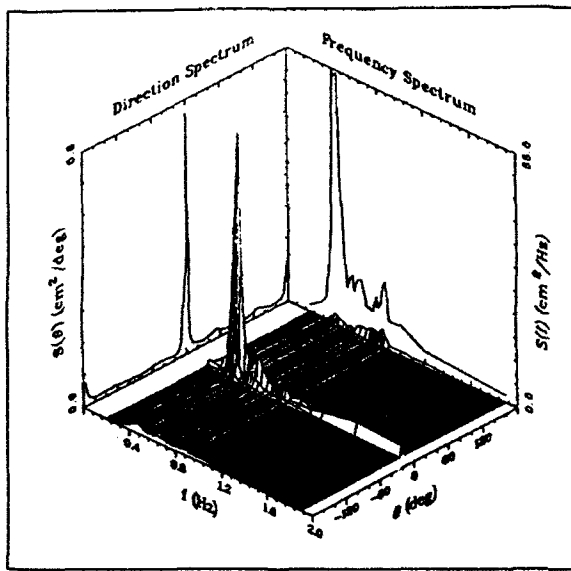


Figure B1. OGA, S0105, short waves

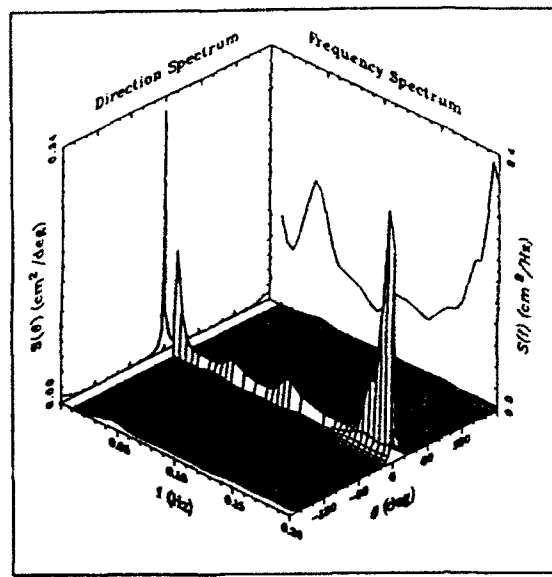


Figure B2. OGA, S0105, long waves

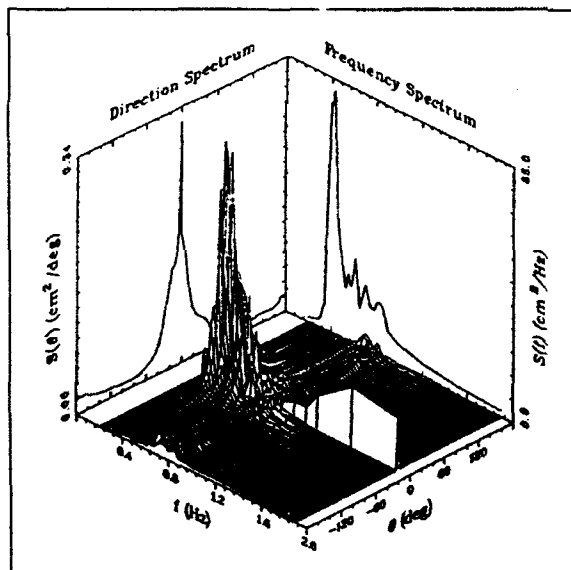


Figure B3. OGA, S0905, short waves

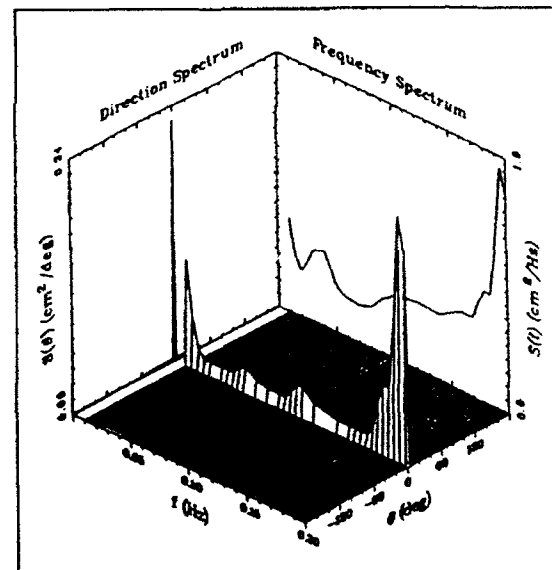
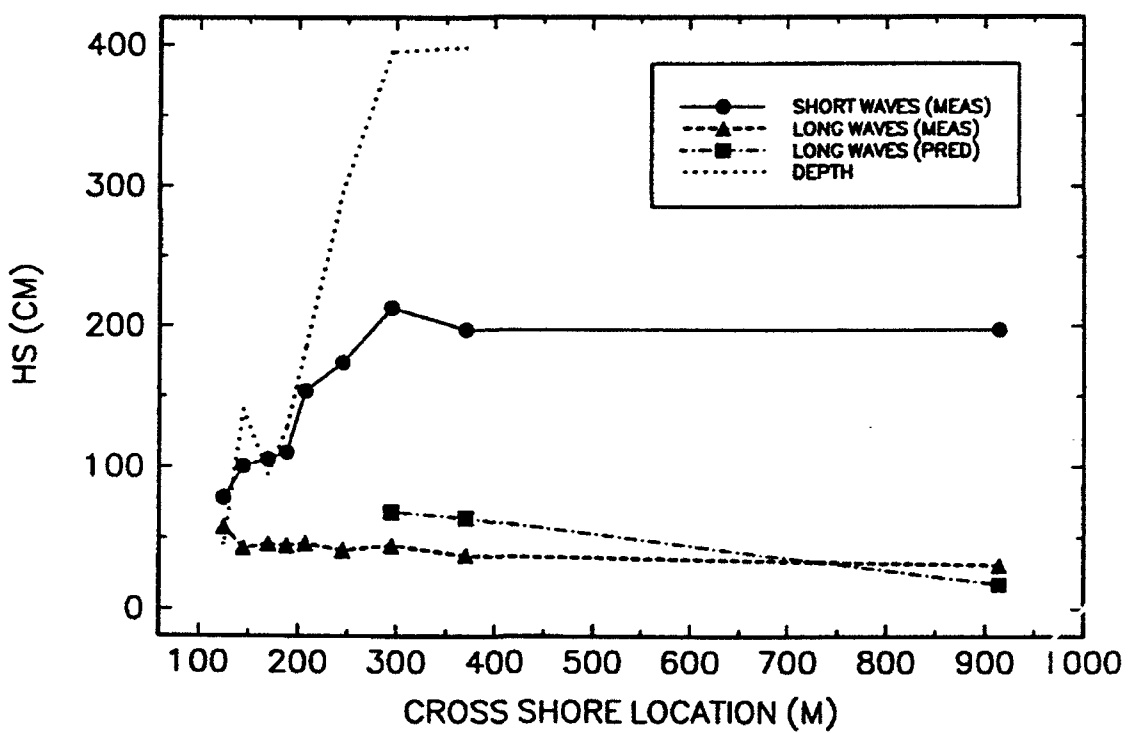


Figure B4. OGA, S0905, long waves

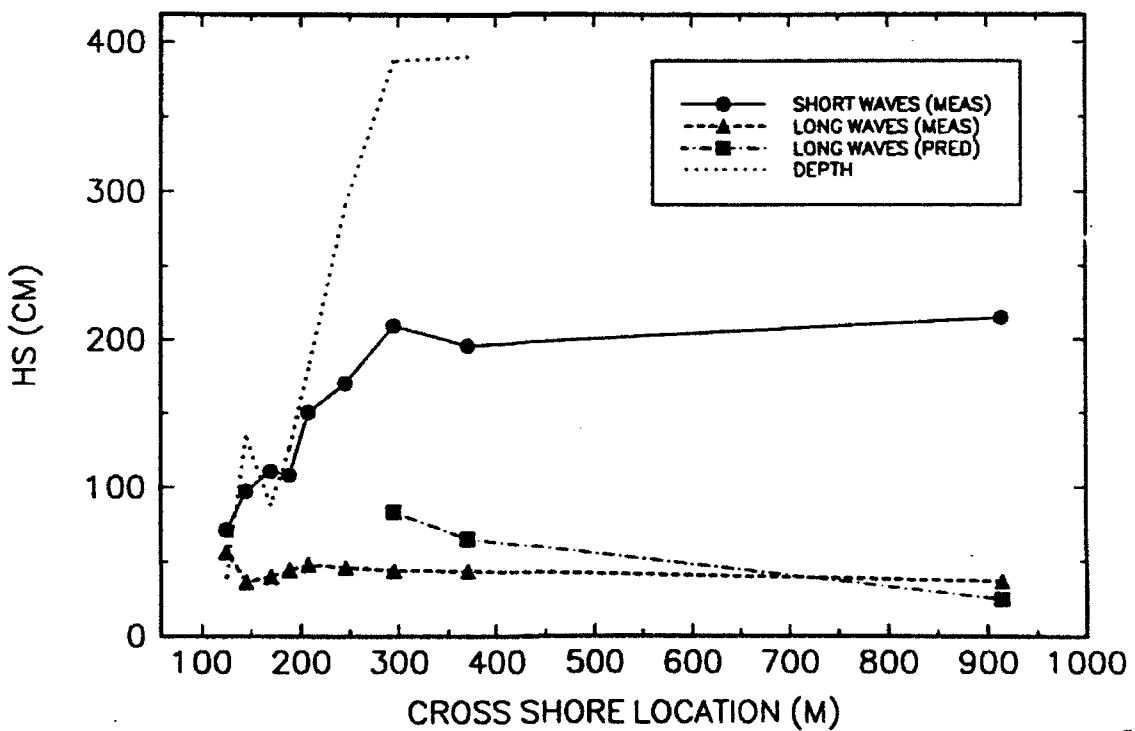
Appendix C

Short and Long Wave Significant Heights from Field Data

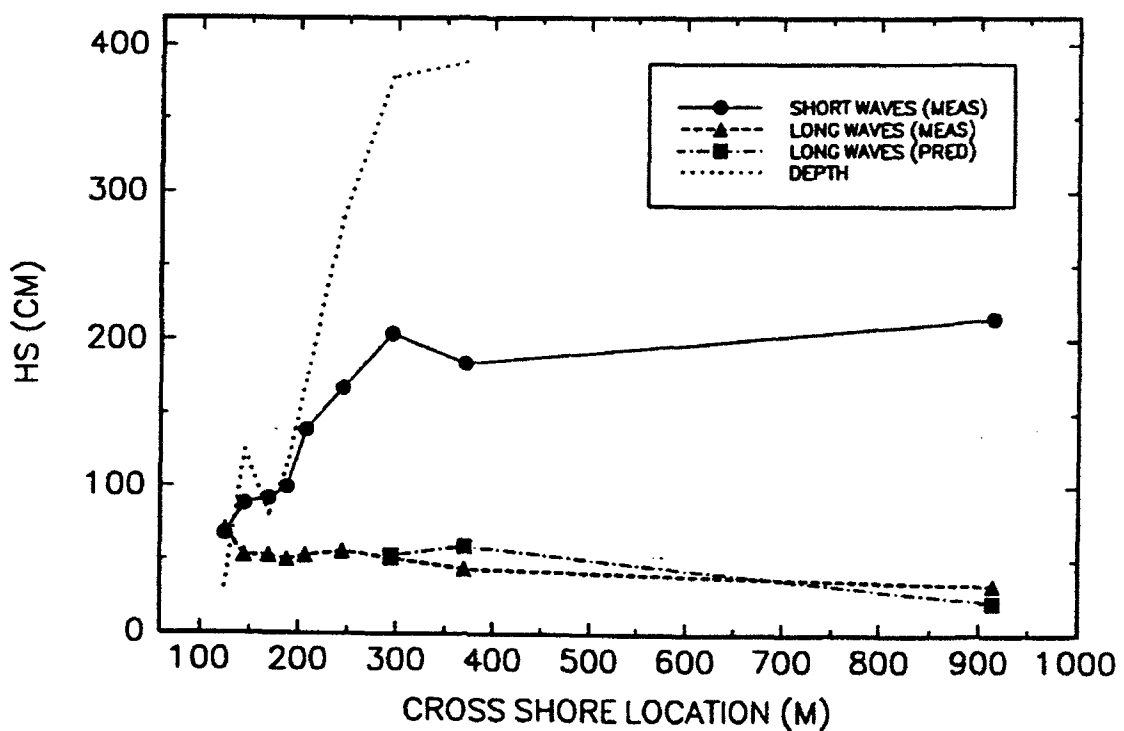
17-MINUTE RECORD BEGINNING AT 1658



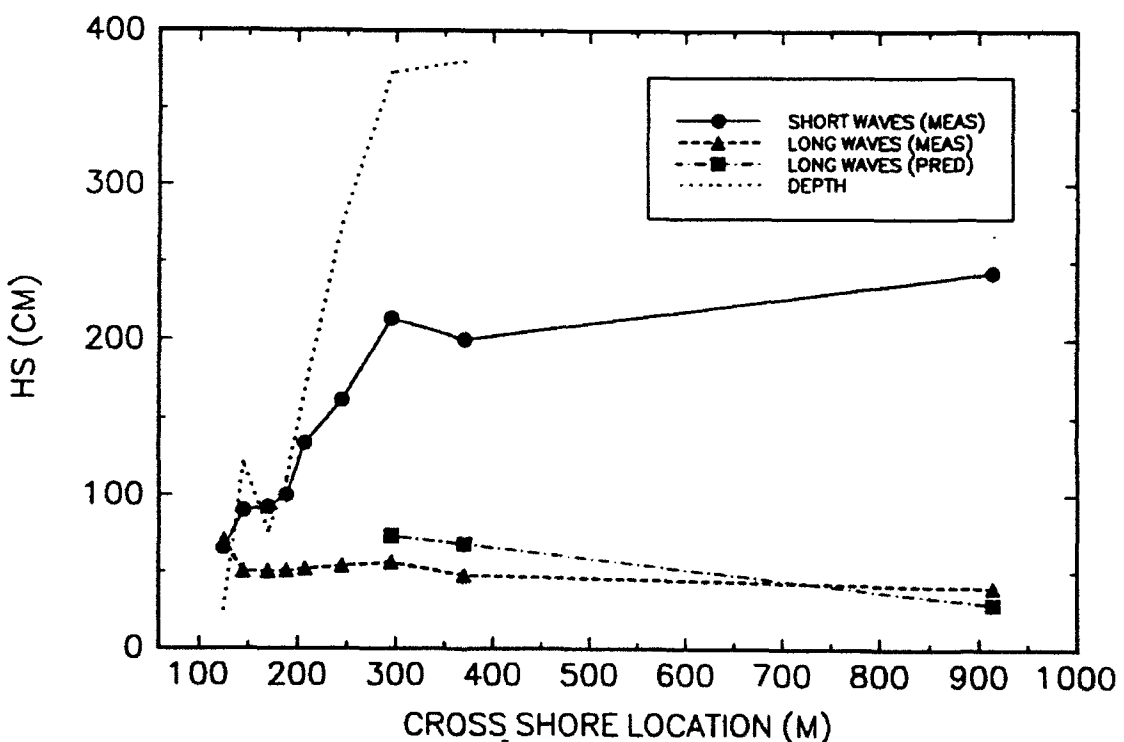
17-MINUTE RECORD BEGINNING AT 1715



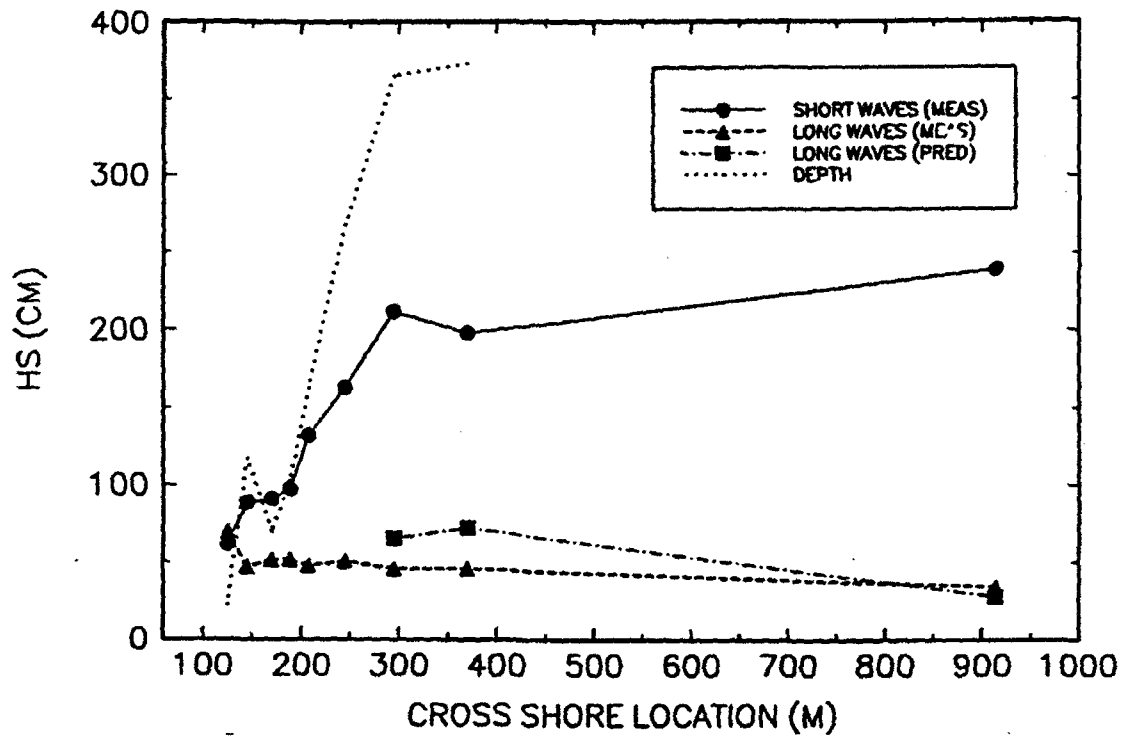
17-MINUTE RECORD BEGINNING AT 1732



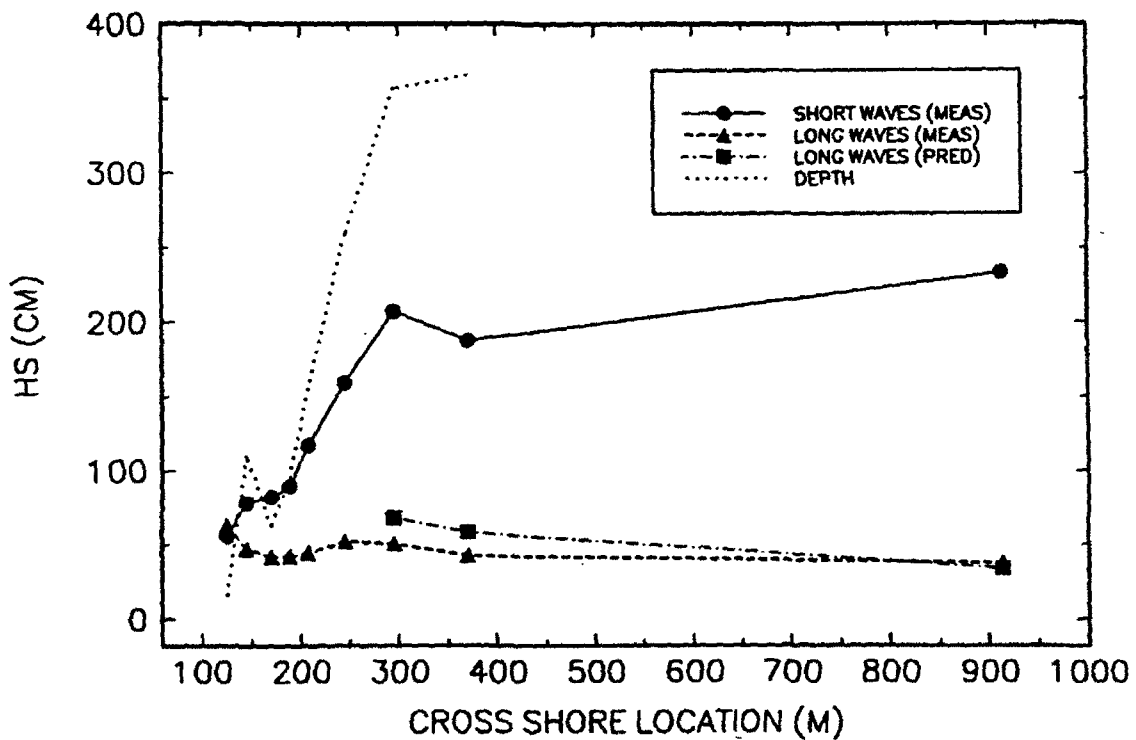
17-MINUTE RECORD BEGINNING AT 1749



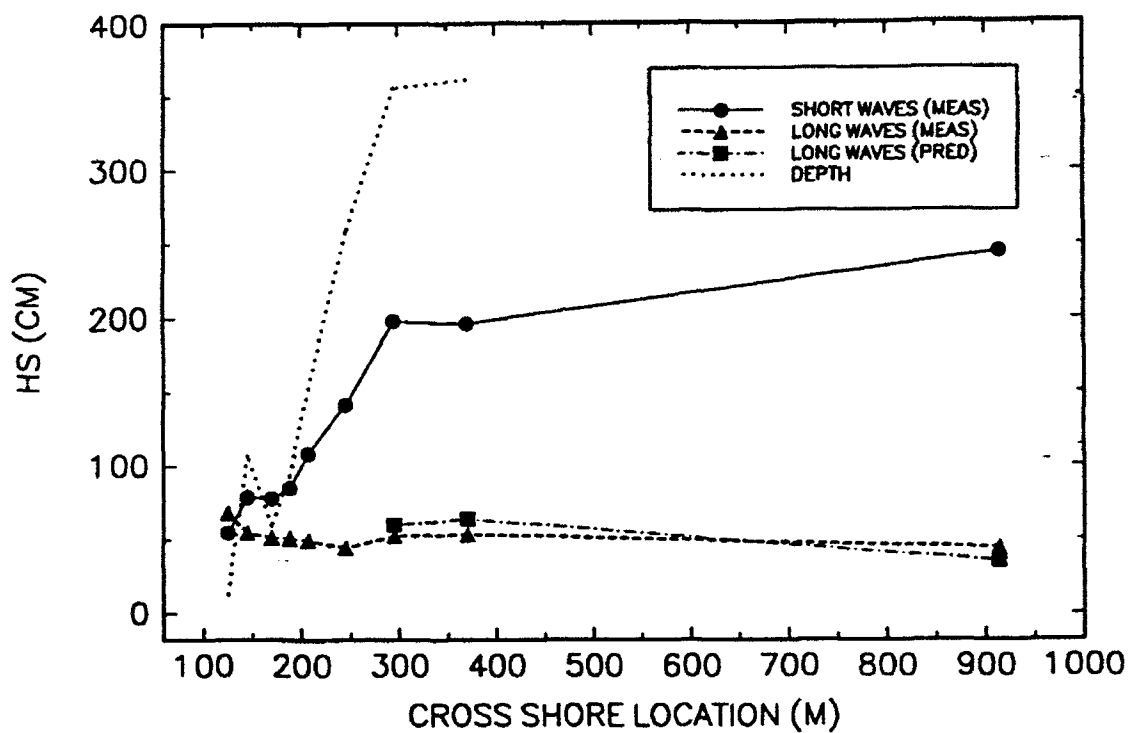
17-MINUTE RECORD BEGINNING AT 1806



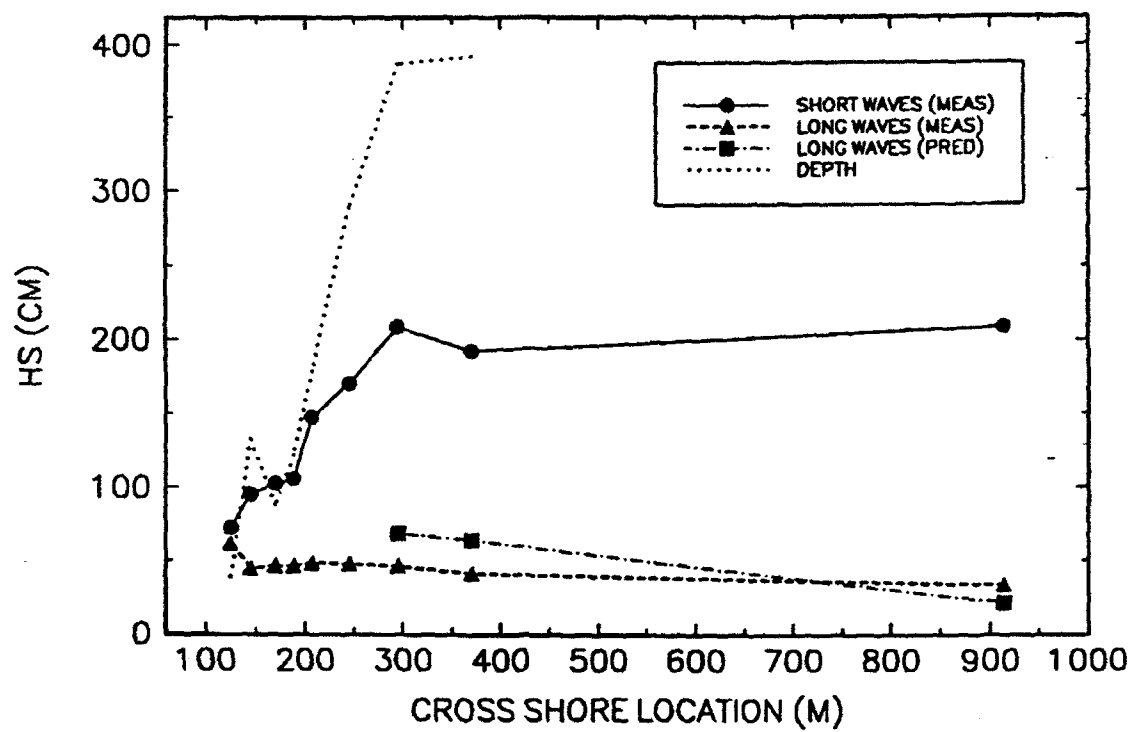
17-MINUTE RECORD BEGINNING AT 1824



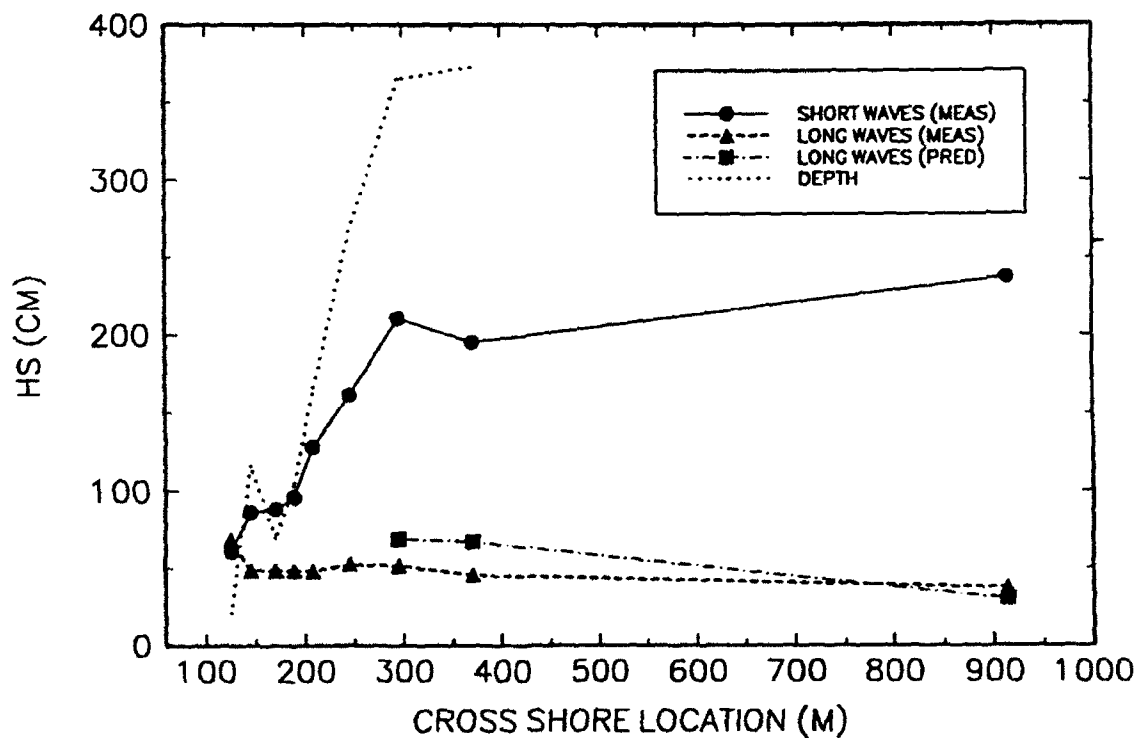
17-MINUTE RECORD BEGINNING AT 1841



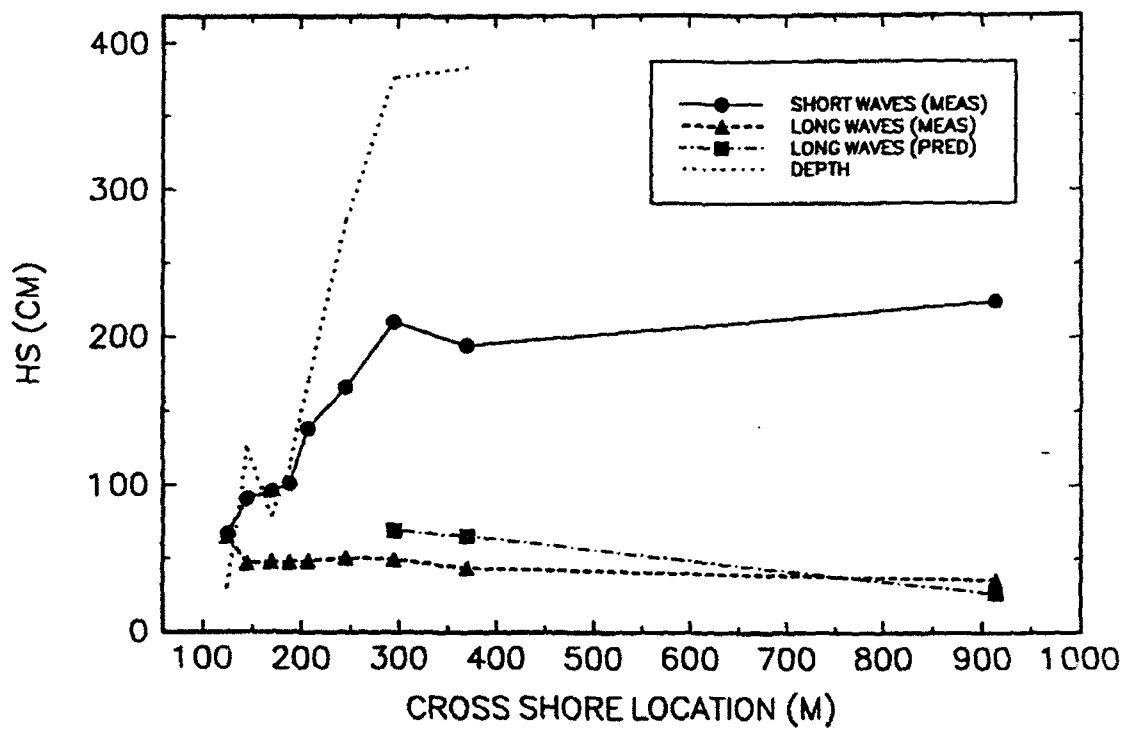
51-MINUTE RECORD BEGINNING AT 1658



51-MINUTE RECORD BEGINNING AT 1749



102-MINUTE RECORD BEGINNING AT 1658

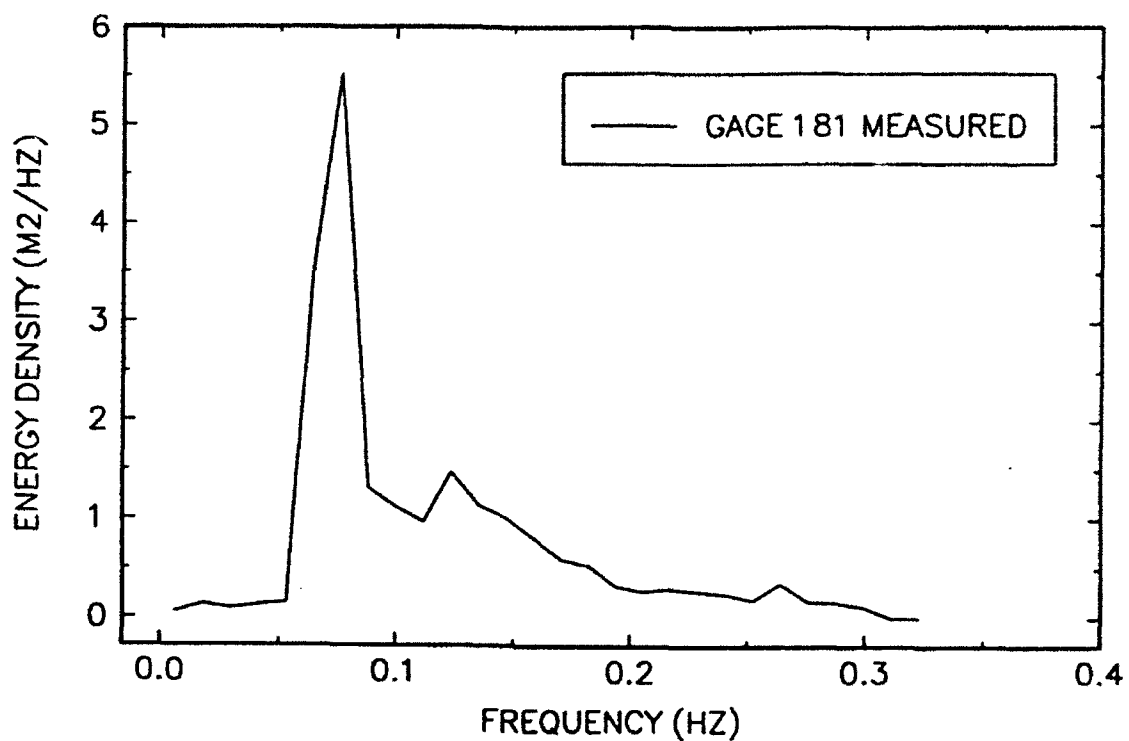


Appendix D

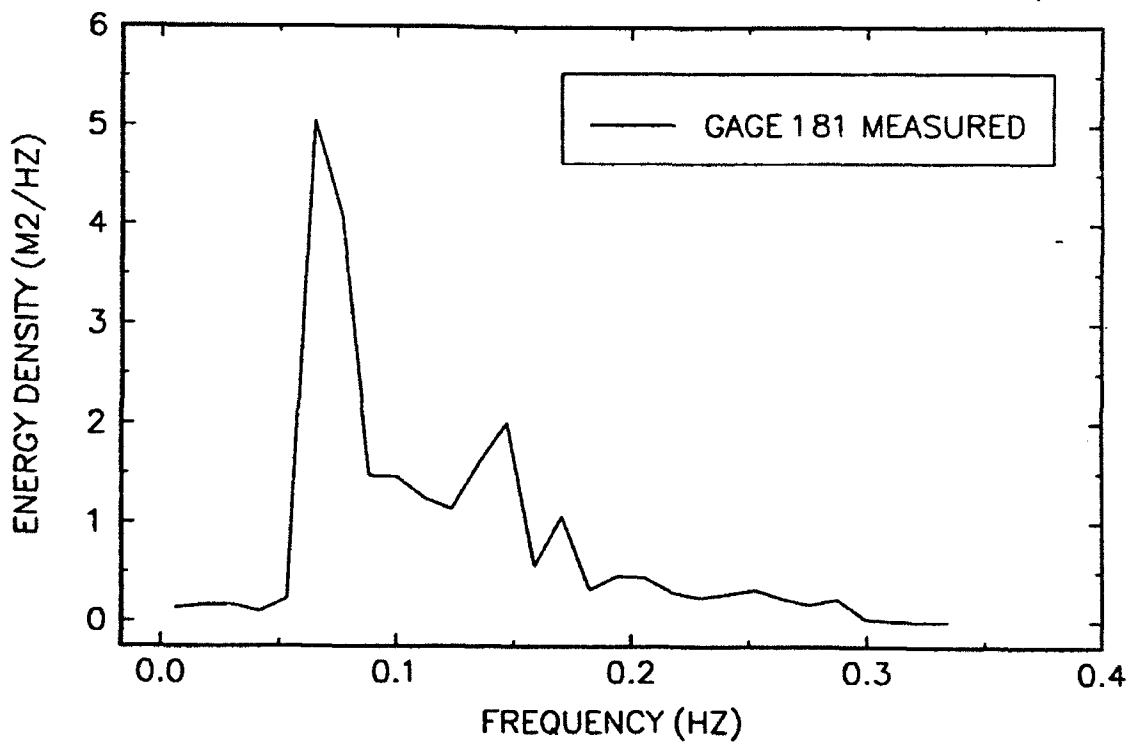
Short and Long Wave Spectra

from Field Data, Gage 181

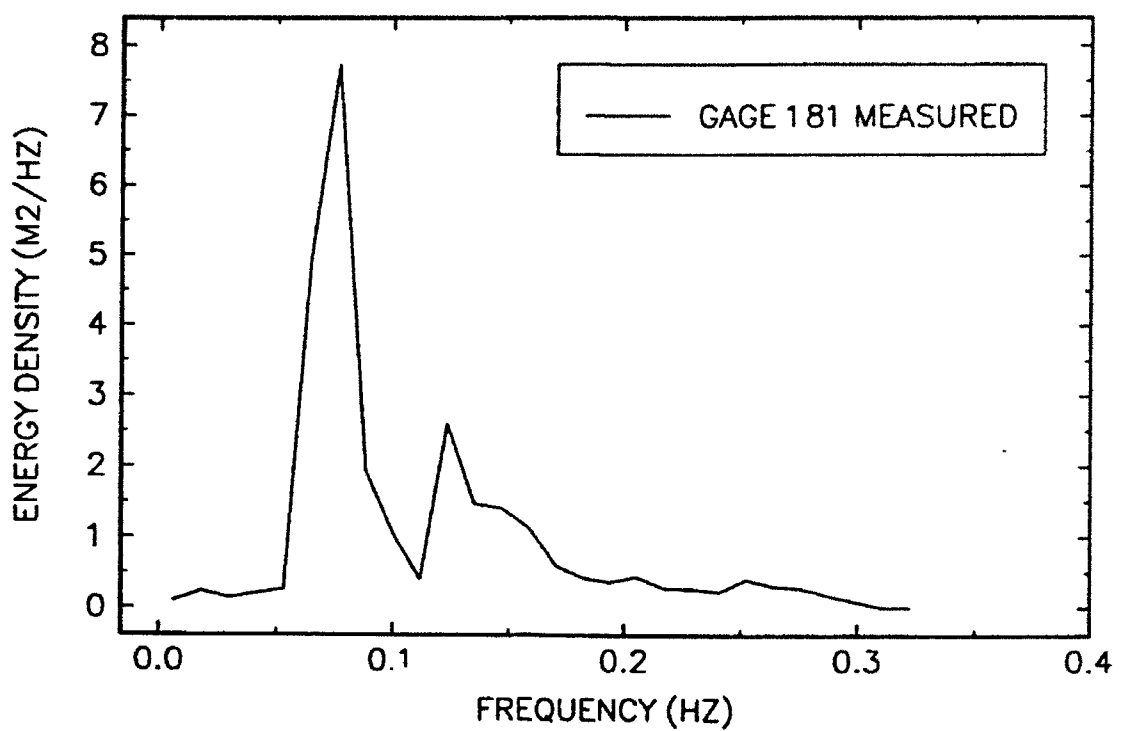
17-MINUTE RECORD BEGINNING AT 1600



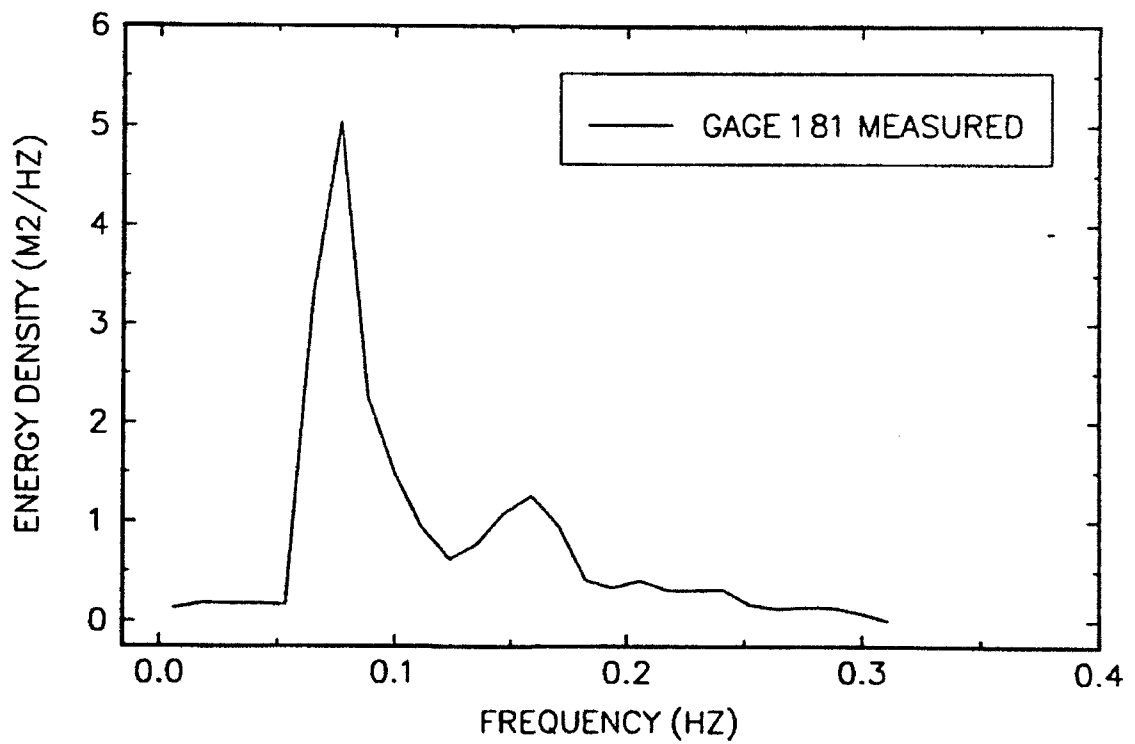
17-MINUTE RECORD BEGINNING AT 1617



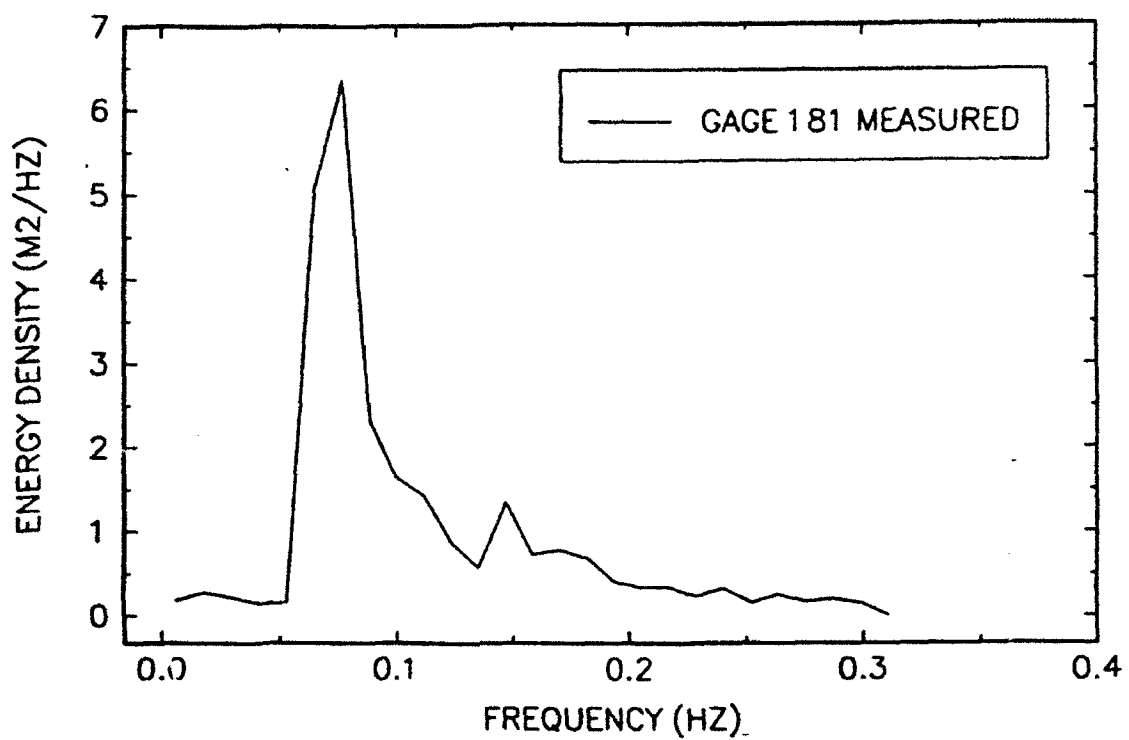
17-MINUTE RECORD BEGINNING AT 1634



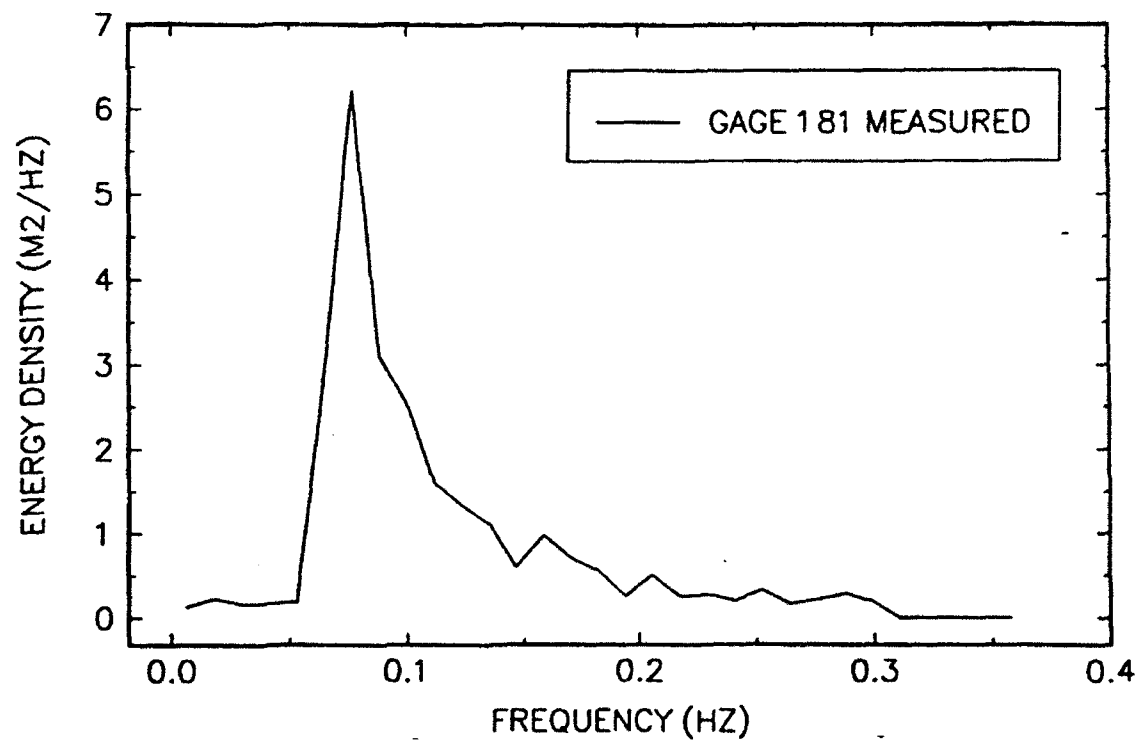
17-MINUTE RECORD BEGINNING AT 1651



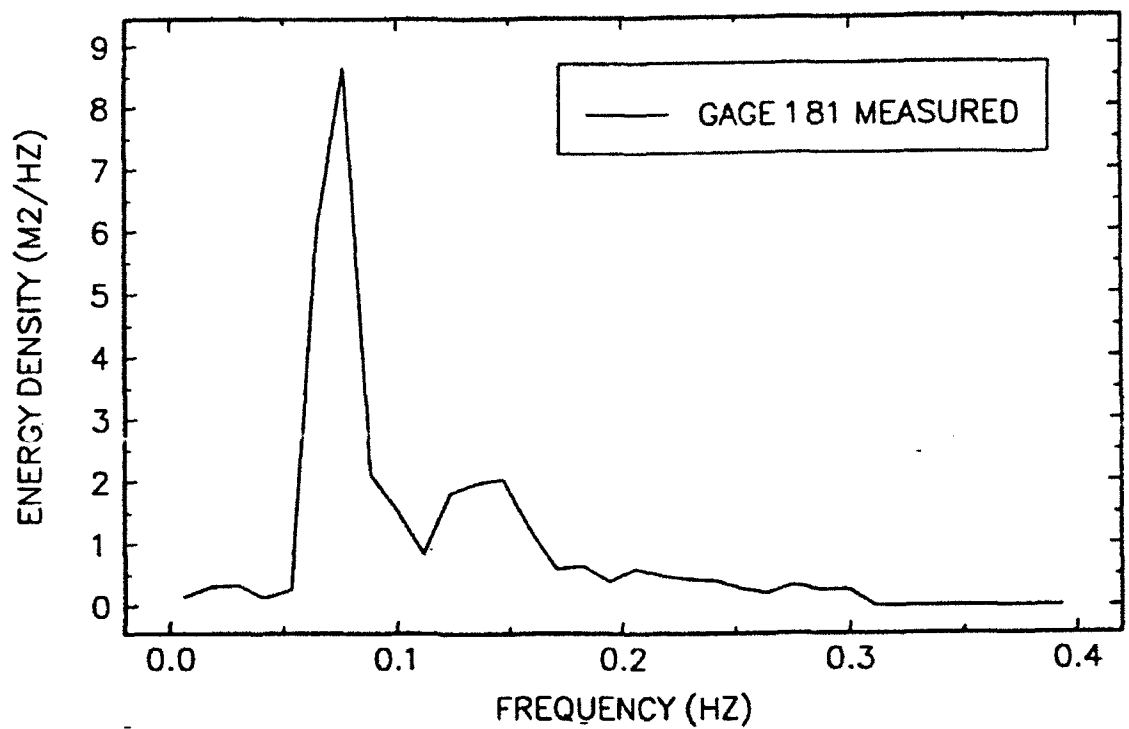
17-MINUTE RECORD BEGINNING AT 1708



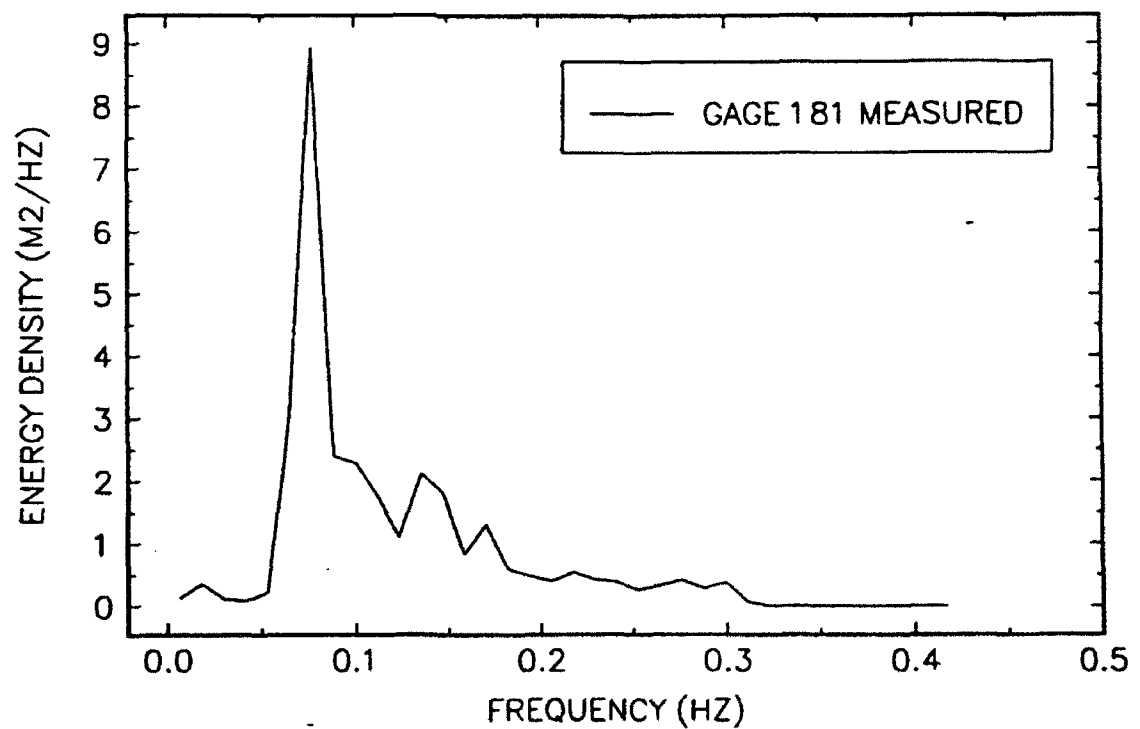
17-MINUTE RECORD BEGINNING AT 1725



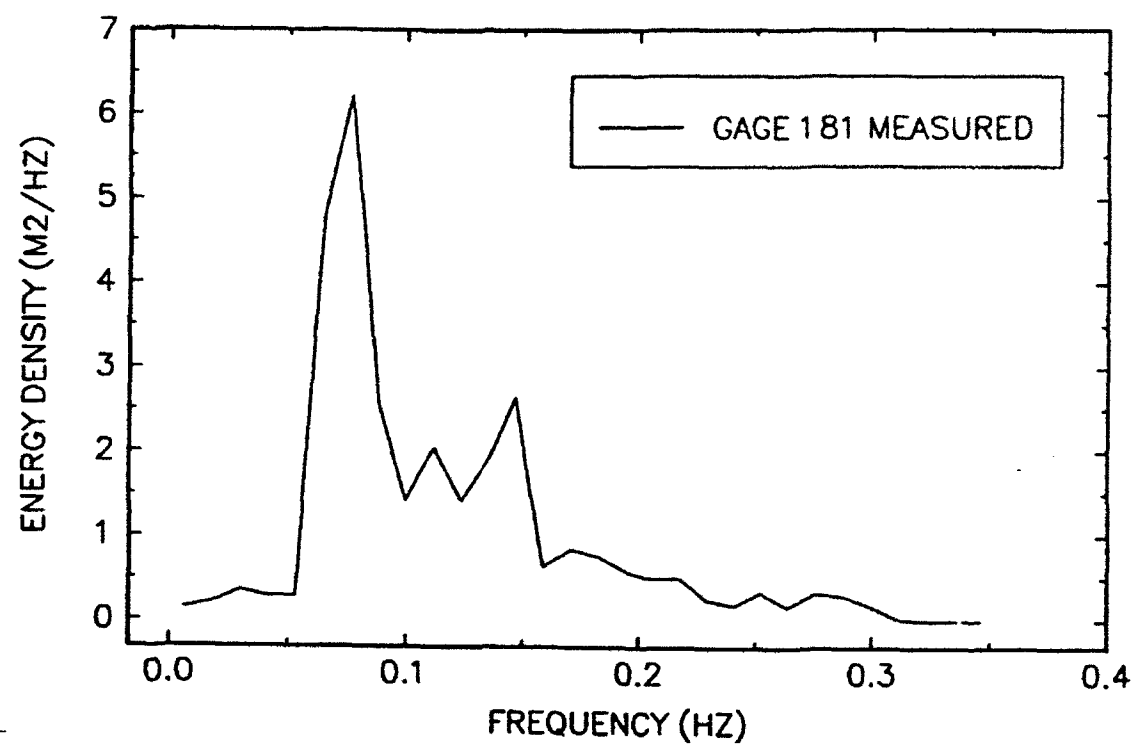
17-MINUTE RECORD BEGINNING AT 1742



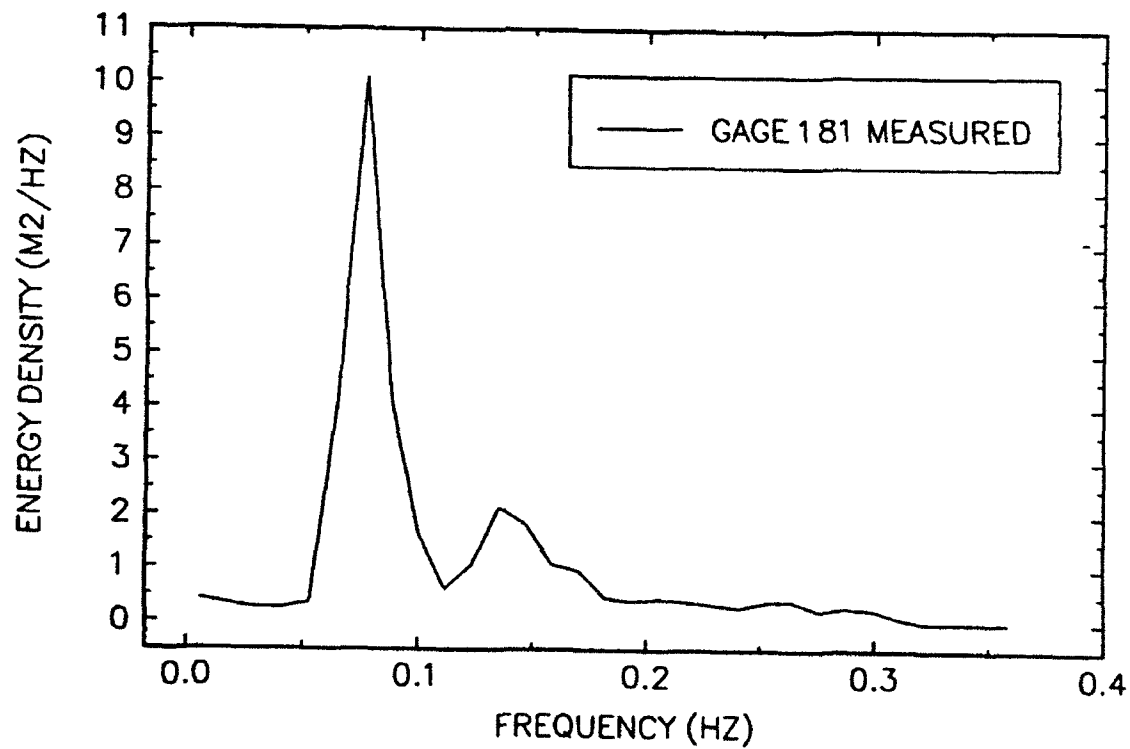
17-MINUTE RECORD BEGINNING AT 1759



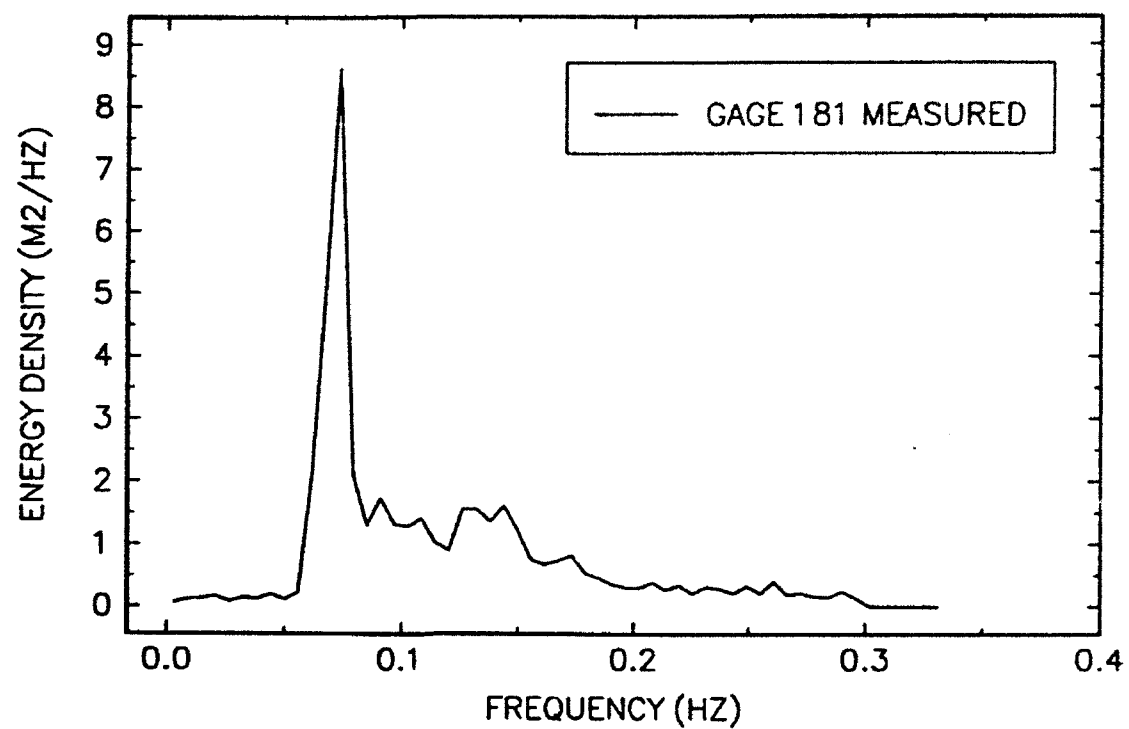
17-MINUTE RECORD BEGINNING AT 1816



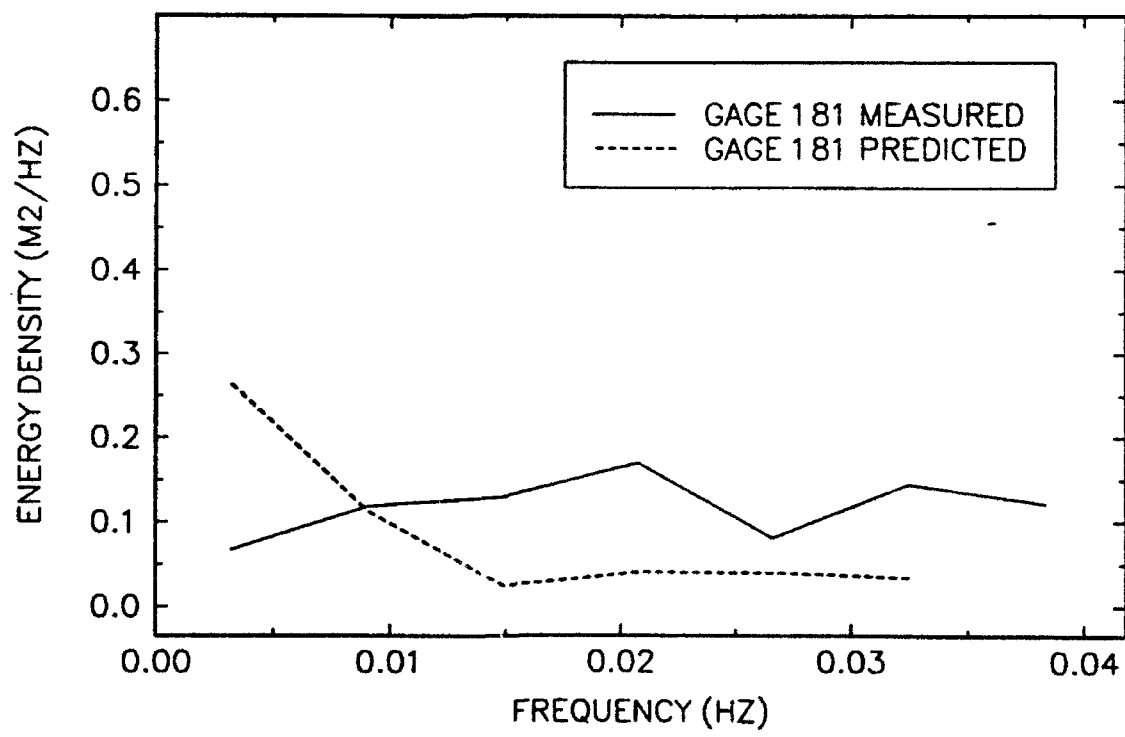
17-MINUTE RECORD BEGINNING AT 1833



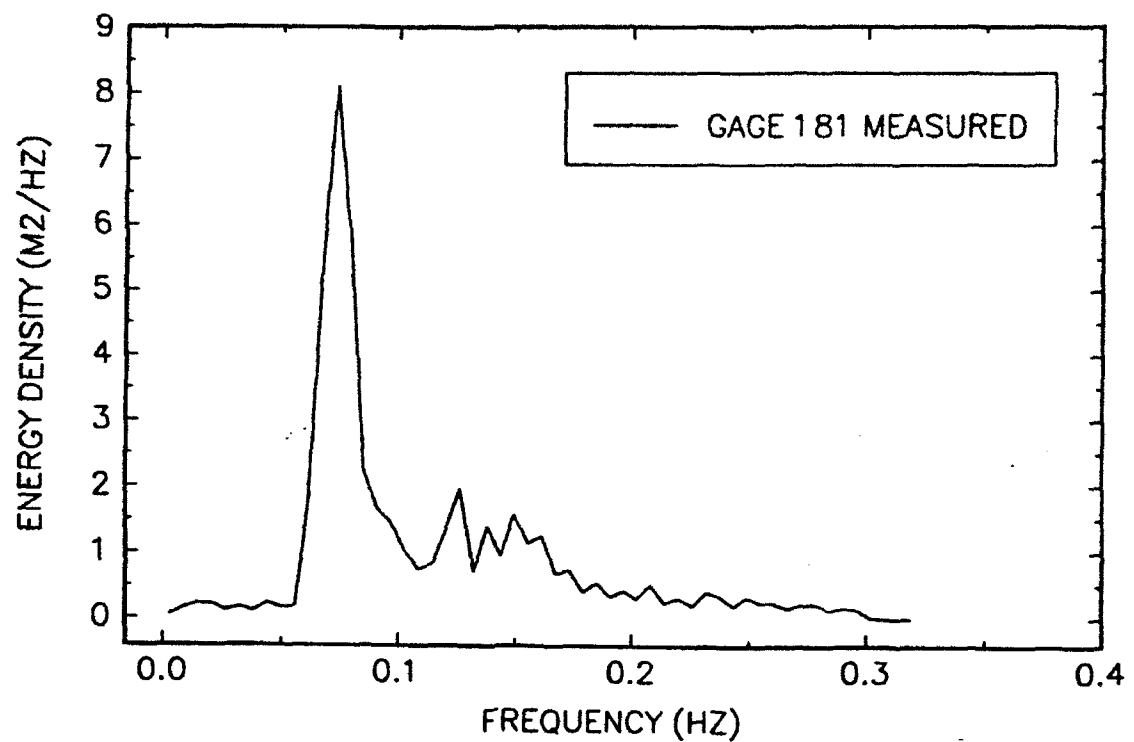
34-MINUTE RECORD BEGINNING AT 1600



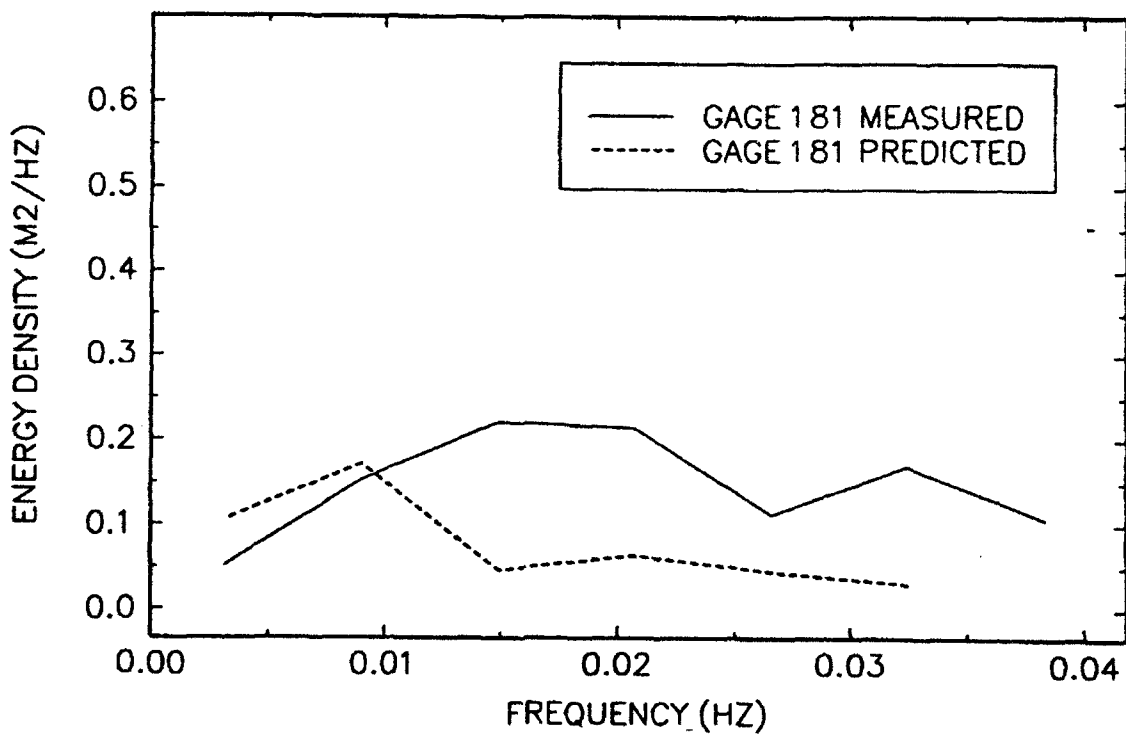
34-MINUTE RECORD BEGINNING AT 1600



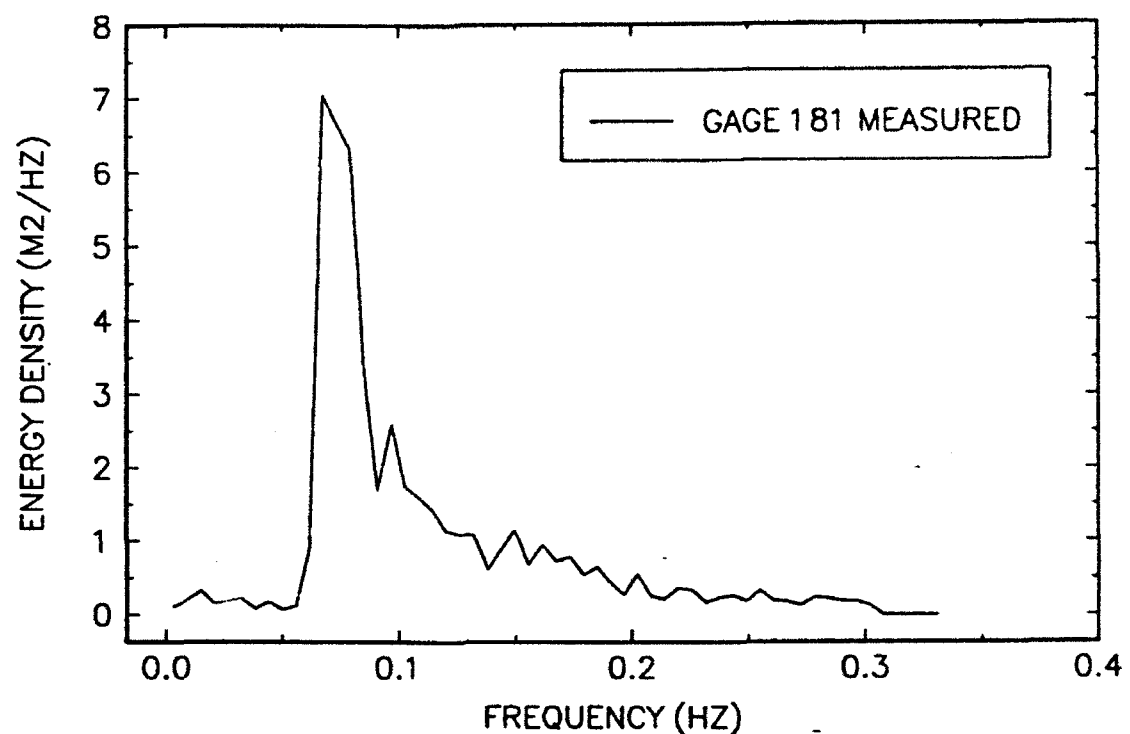
34-MINUTE RECORD BEGINNING AT 1634



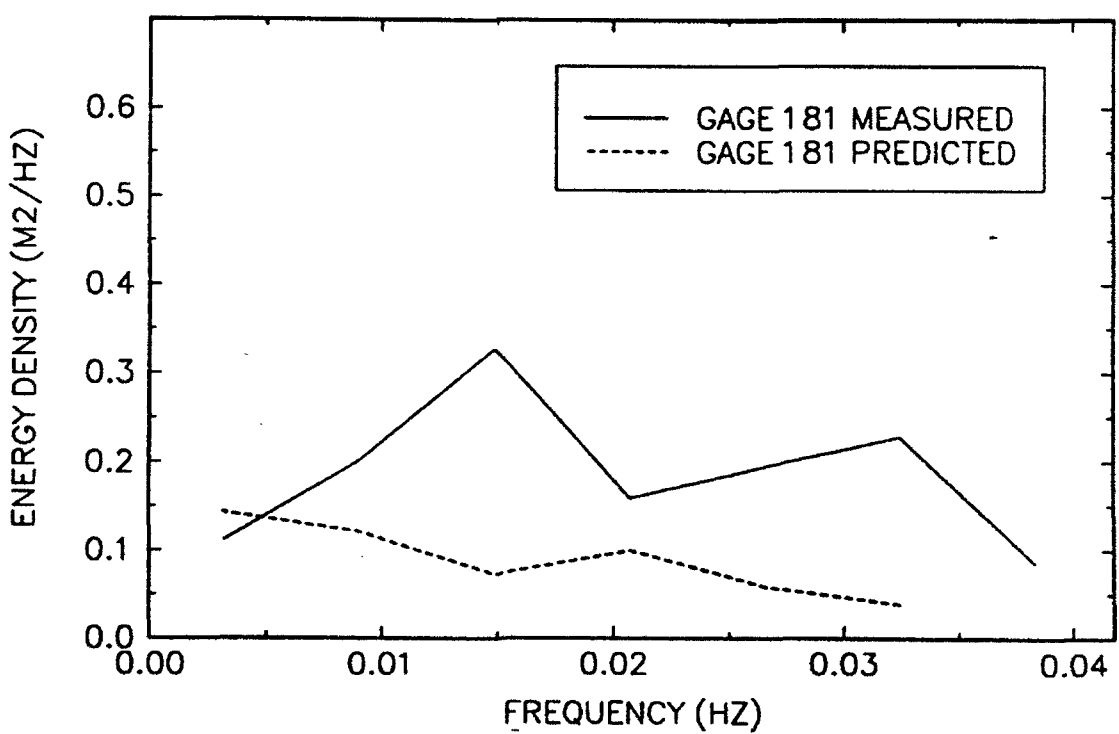
34-MINUTE RECORD BEGINNING AT 1634



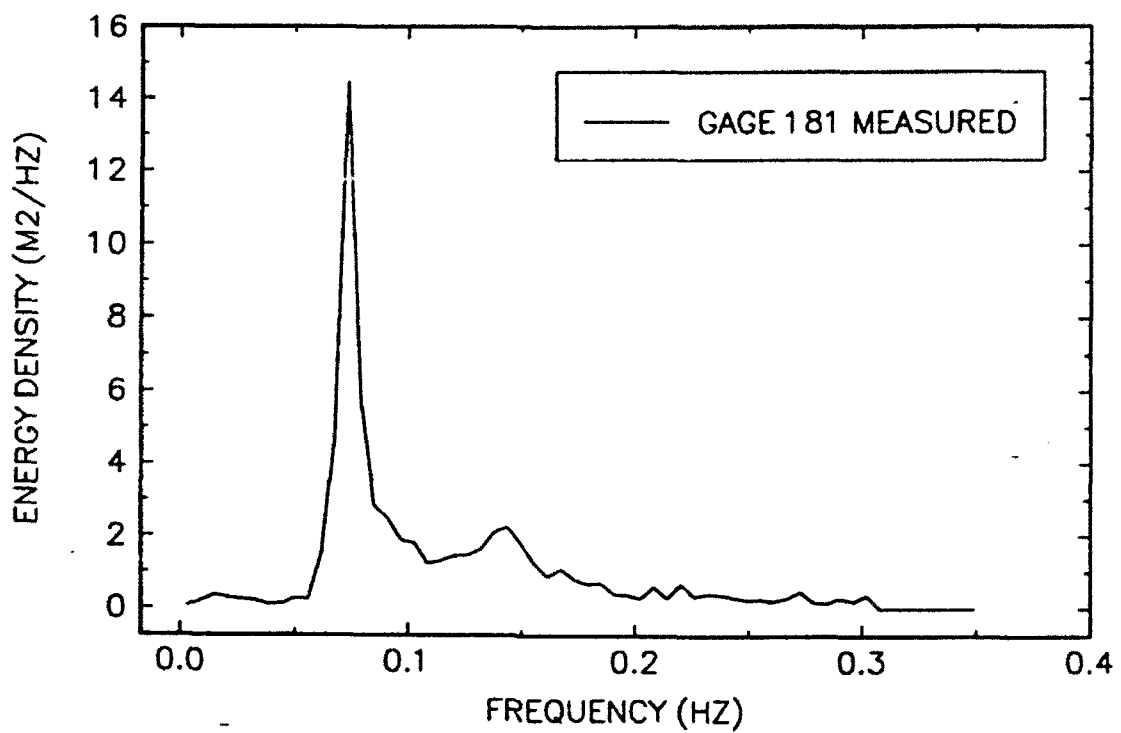
34-MINUTE RECORD BEGINNING AT 1708



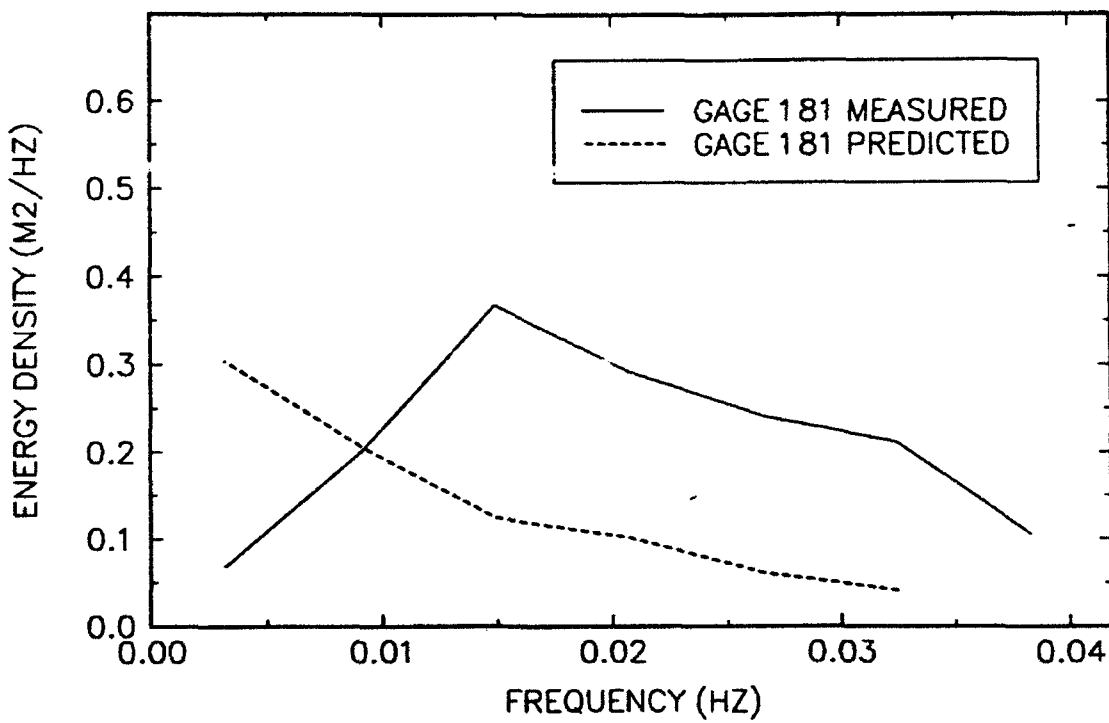
34-MINUTE RECORD BEGINNING AT 1708



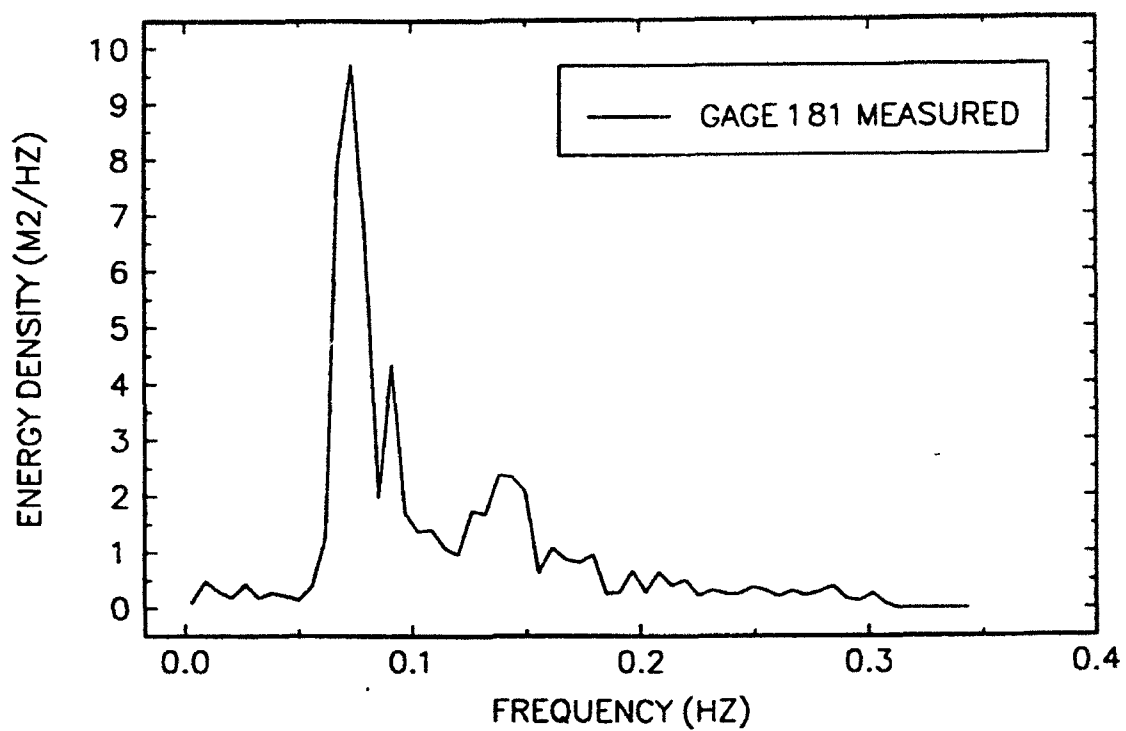
34-MINUTE RECORD BEGINNING AT 1742



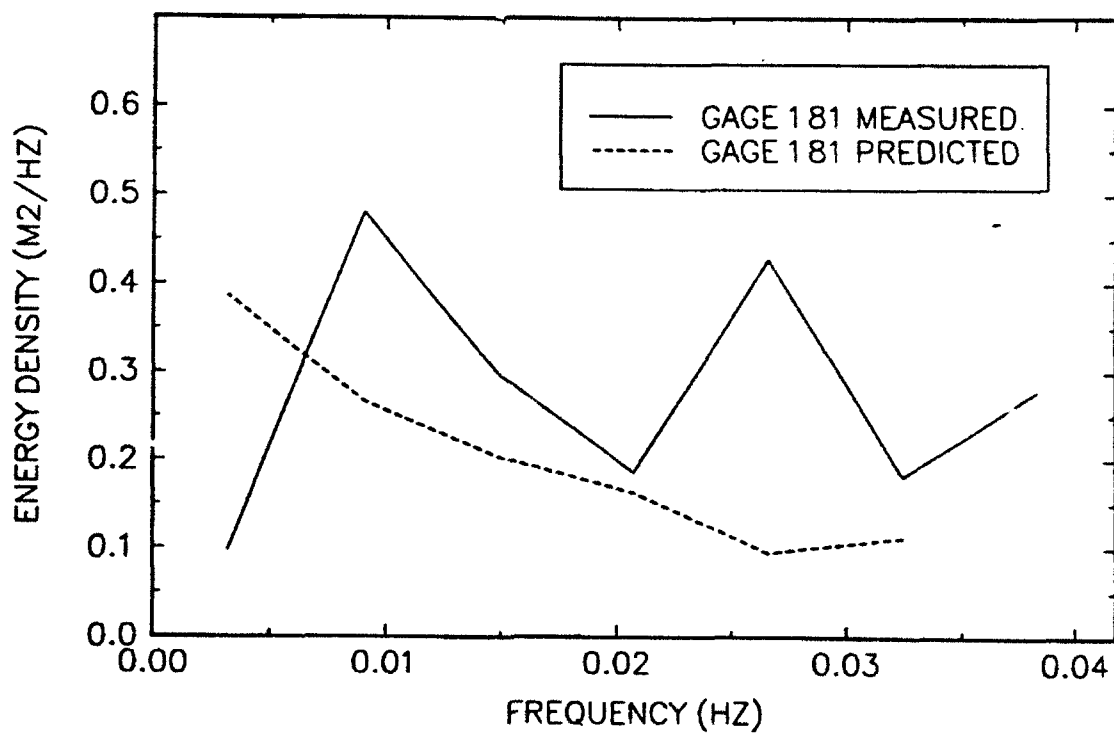
34-MINUTE RECORD BEGINNING AT 1742



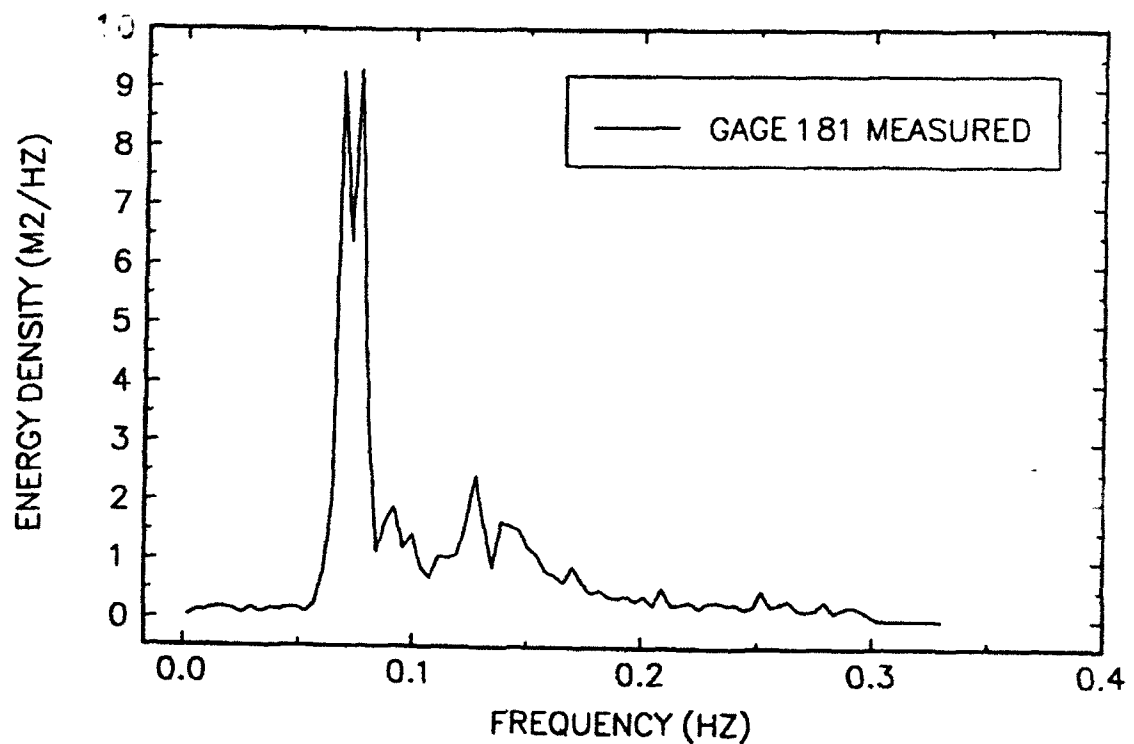
34-MINUTE RECORD BEGINNING AT 1816



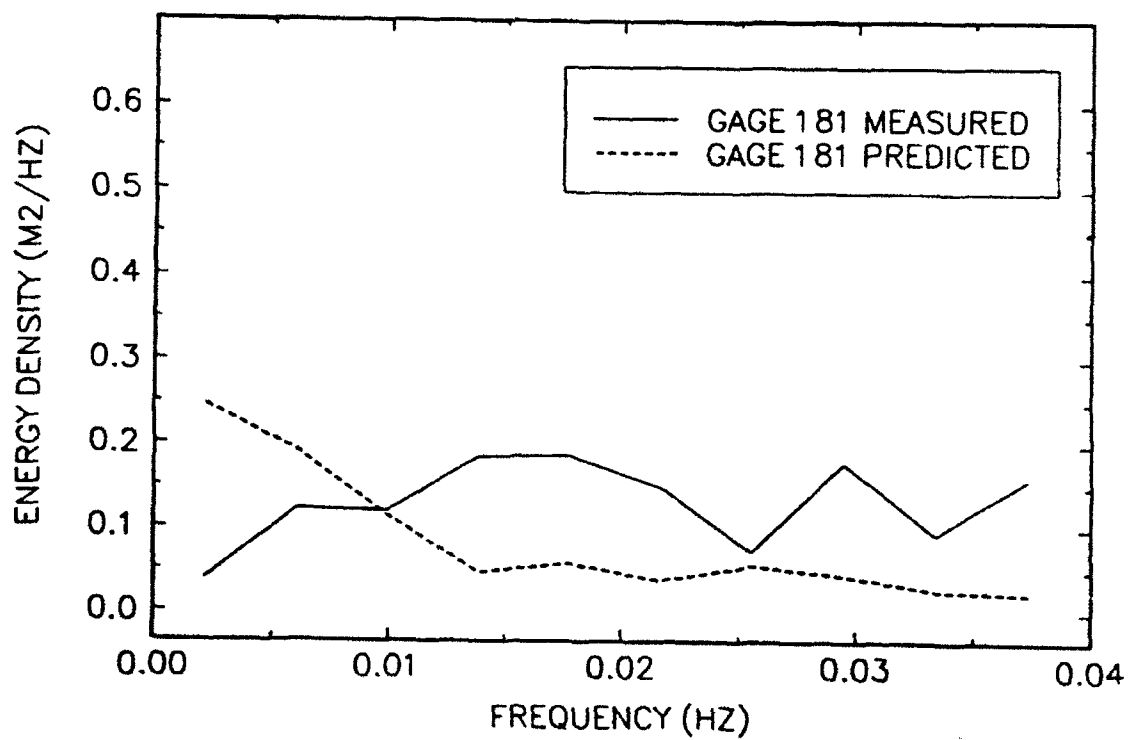
34-MINUTE RECORD BEGINNING AT 1816



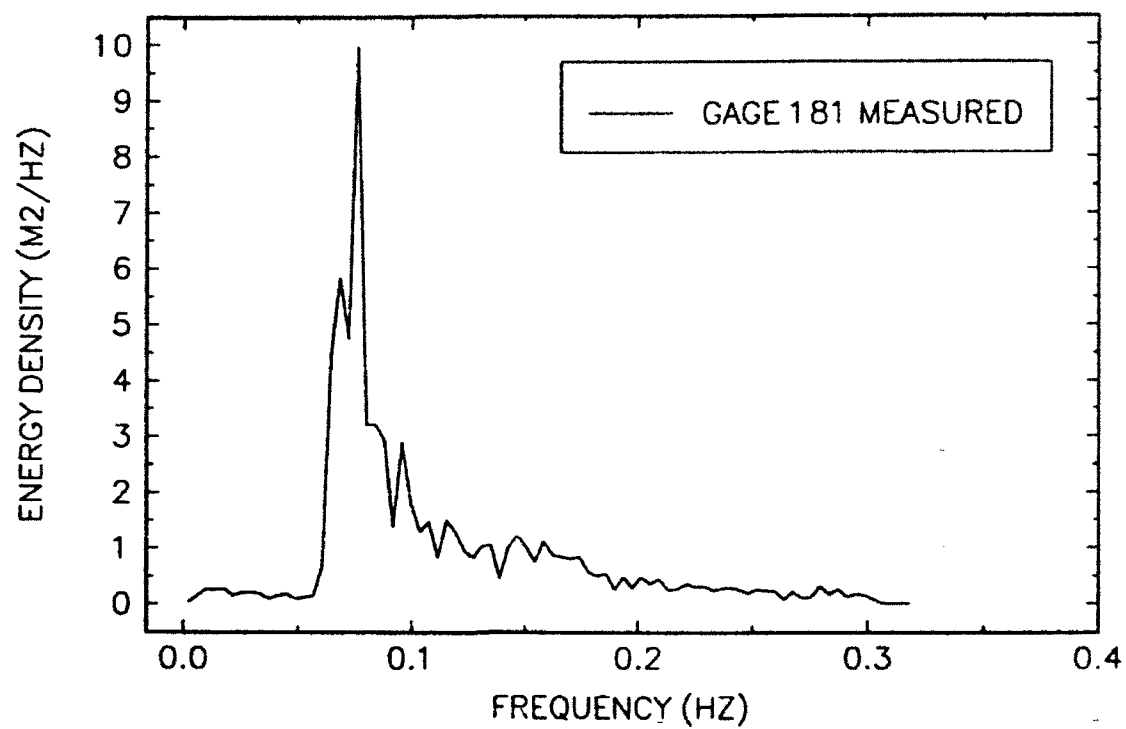
51-MINUTE RECORD BEGINNING AT 1600



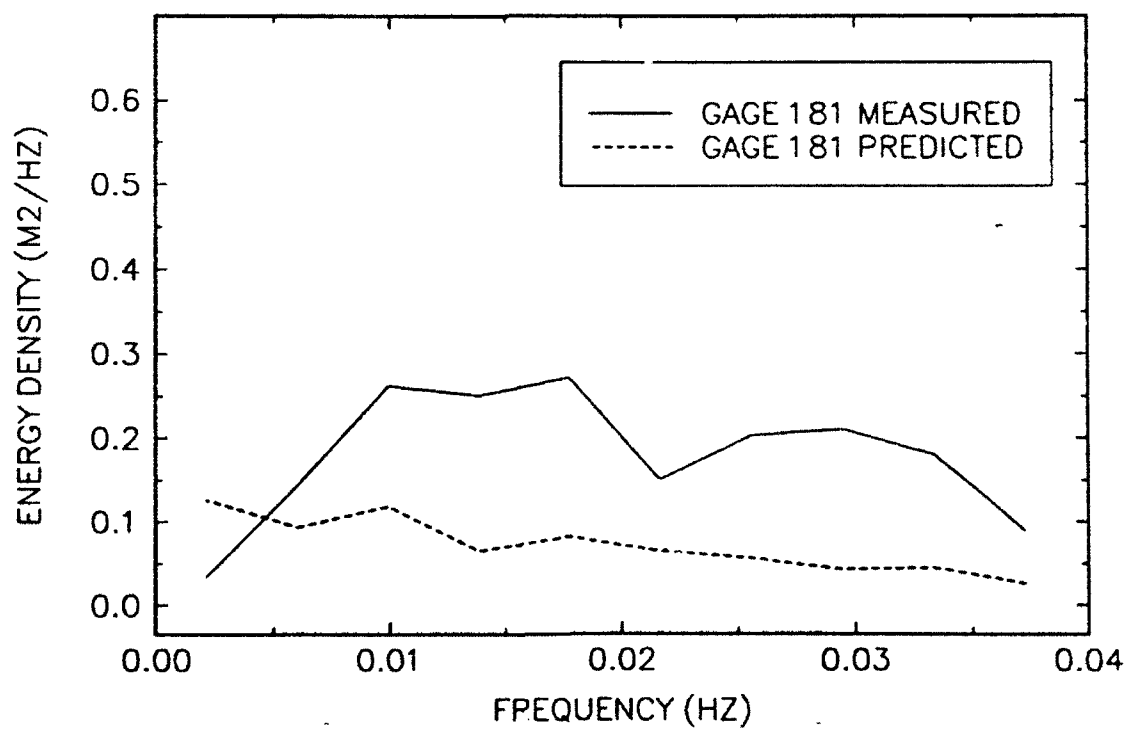
51-MINUTE RECORD BEGINNING AT 1600



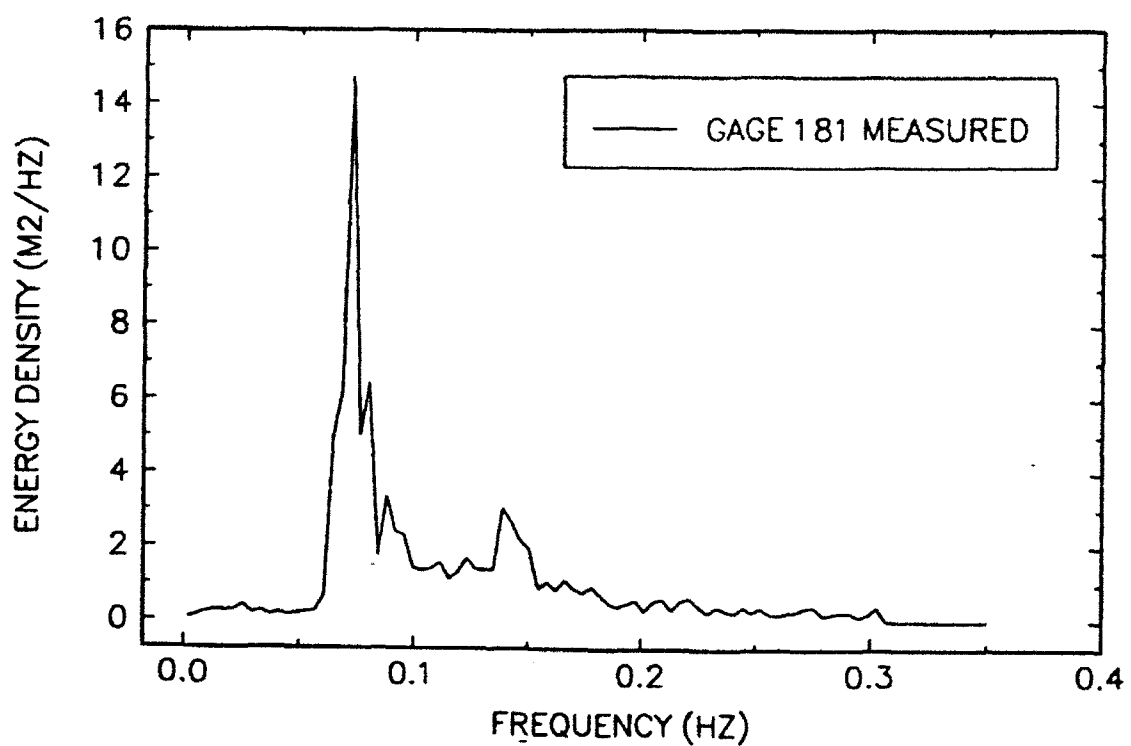
51-MINUTE RECORD BEGINNING AT 1651



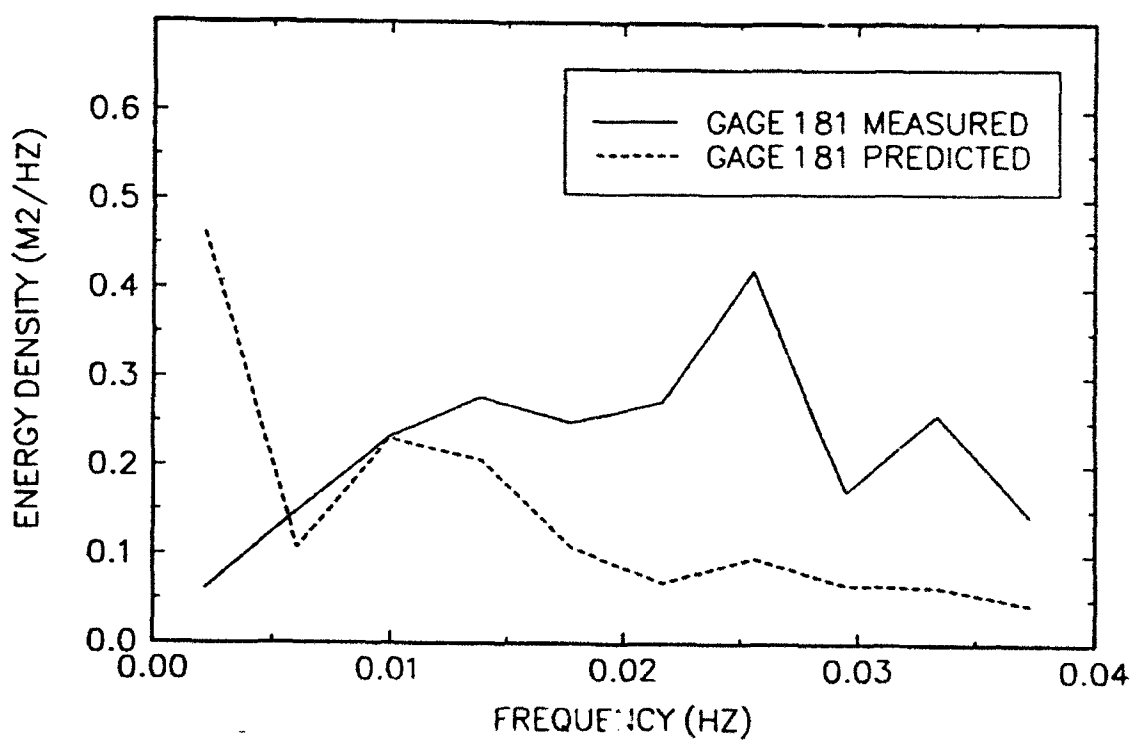
51-MINUTE RECORD BEGINNING AT 1651



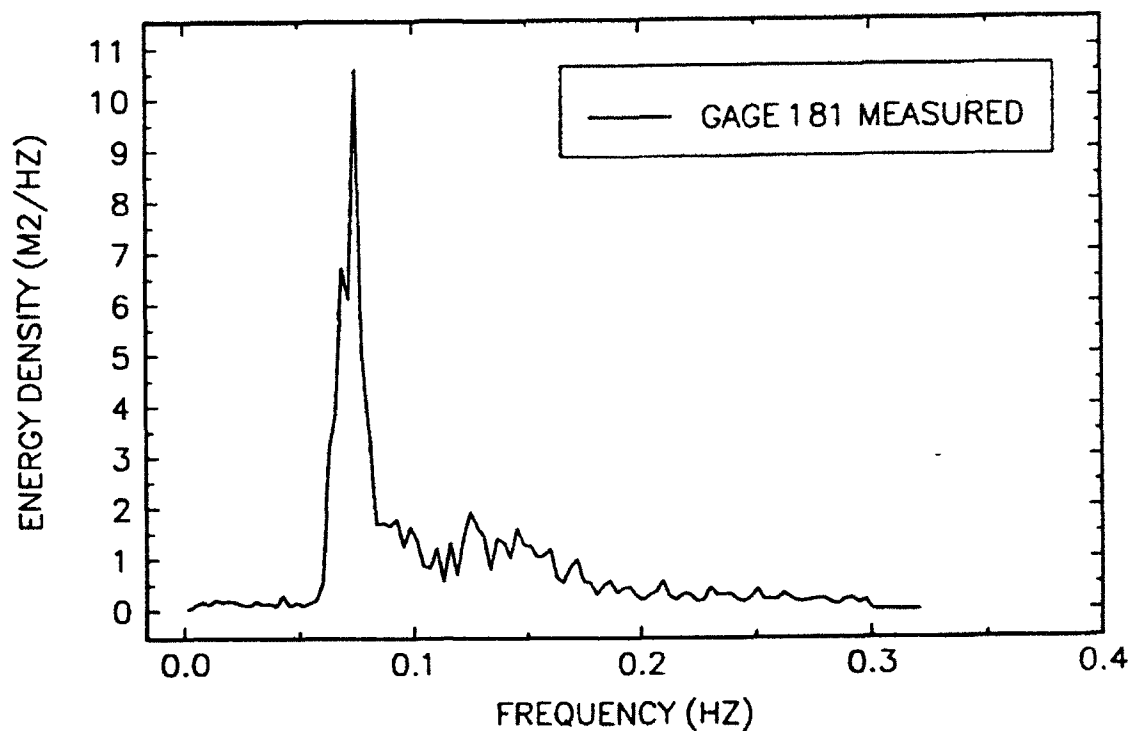
51-MINUTE RECORD BEGINNING AT 1742



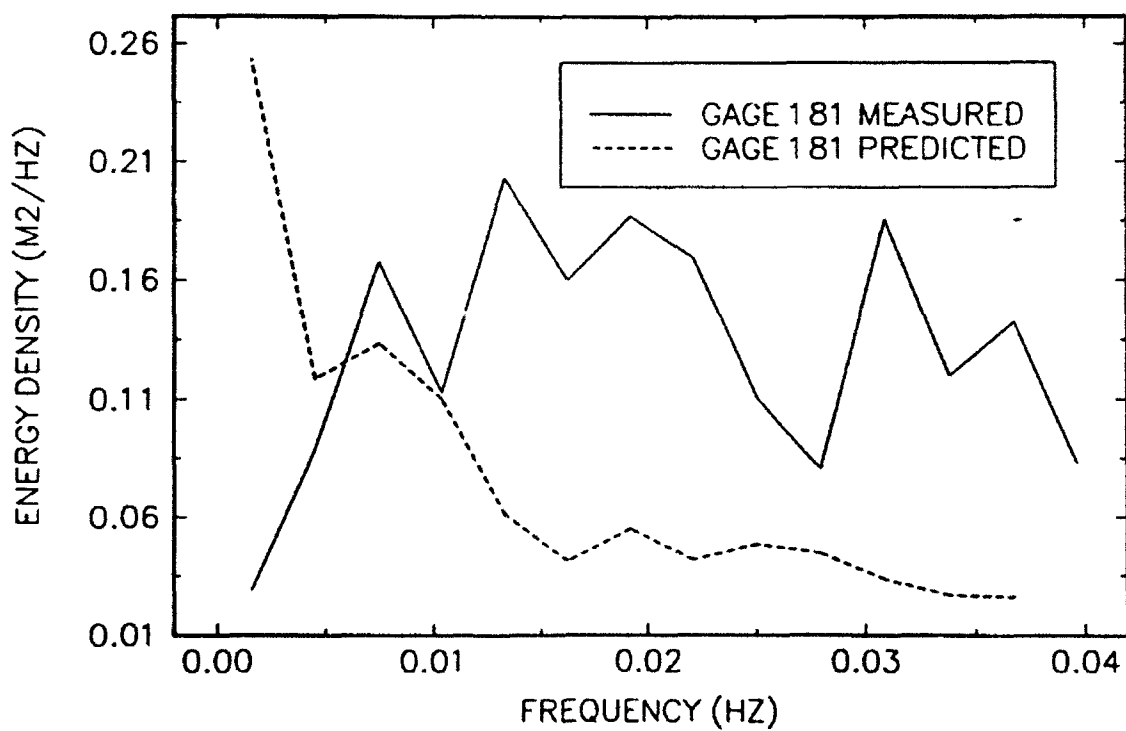
51-MINUTE RECORD BEGINNING AT 1742



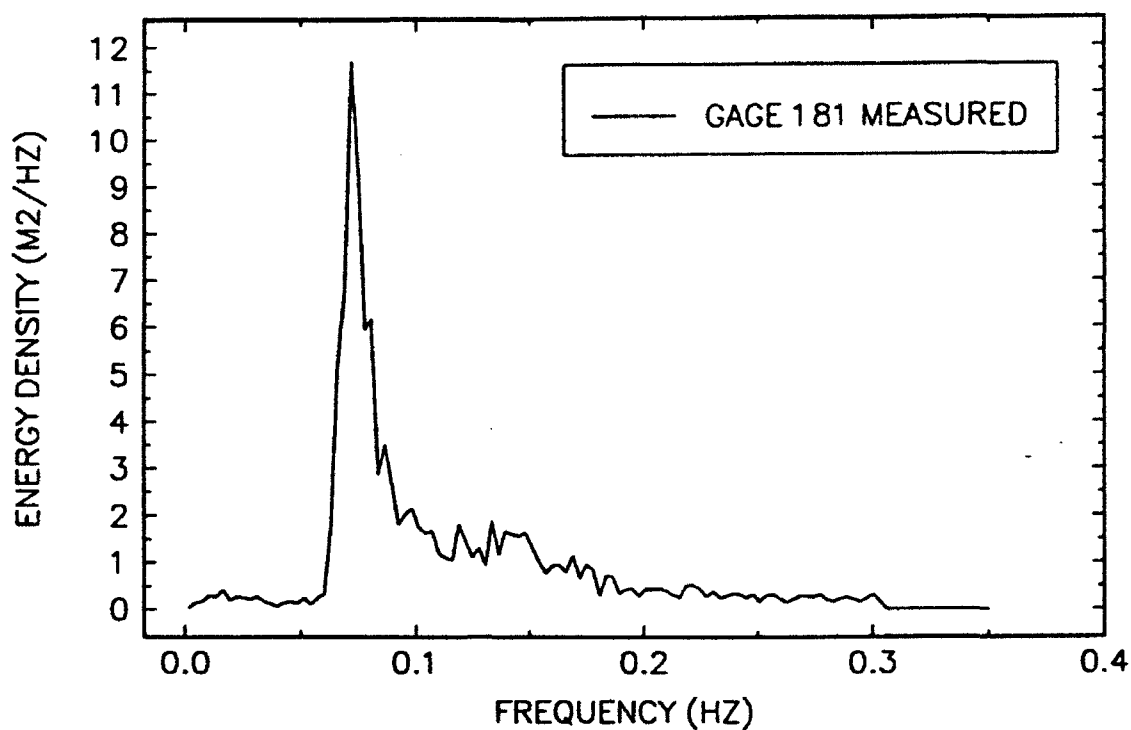
68-MINUTE RECORD BEGINNING AT 1600



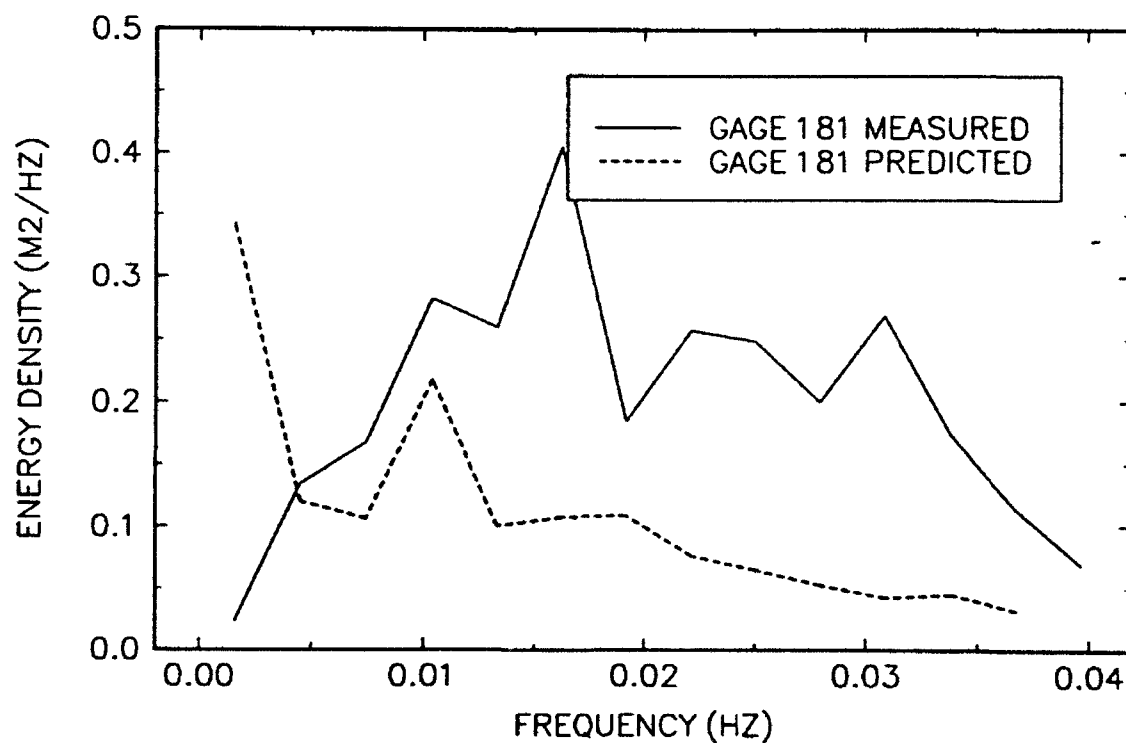
68-MINUTE RECORD BEGINNING AT 1600



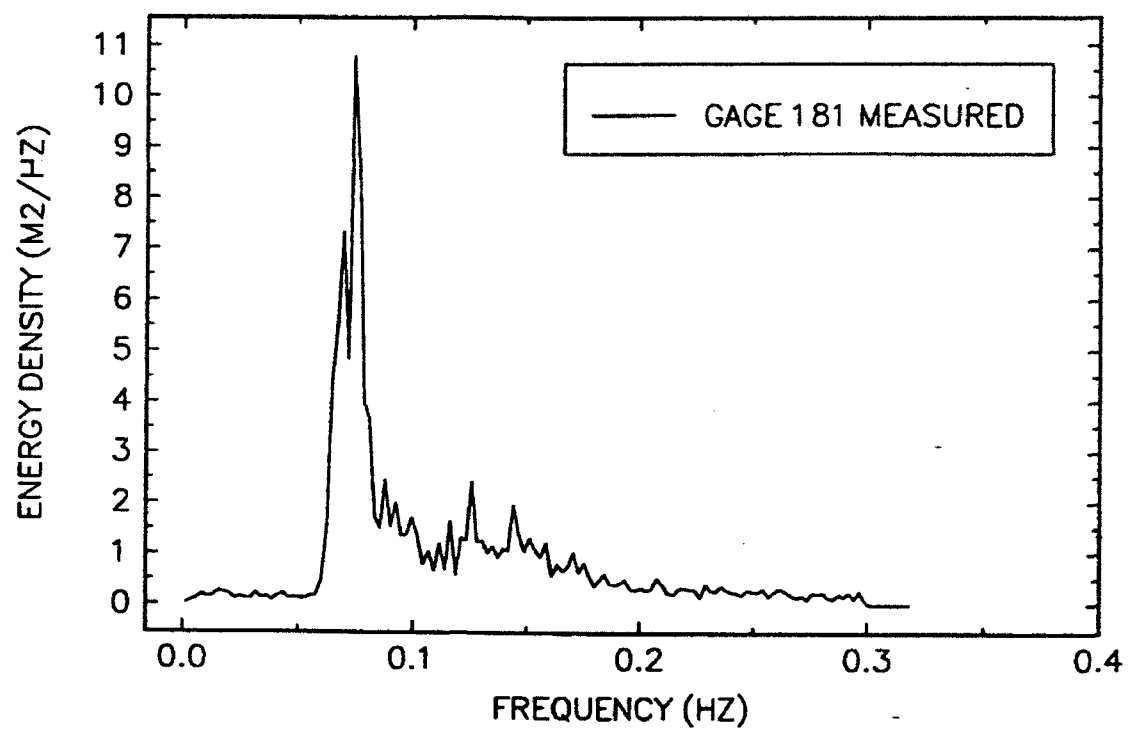
68-MINUTE RECORD BEGINNING AT 1708



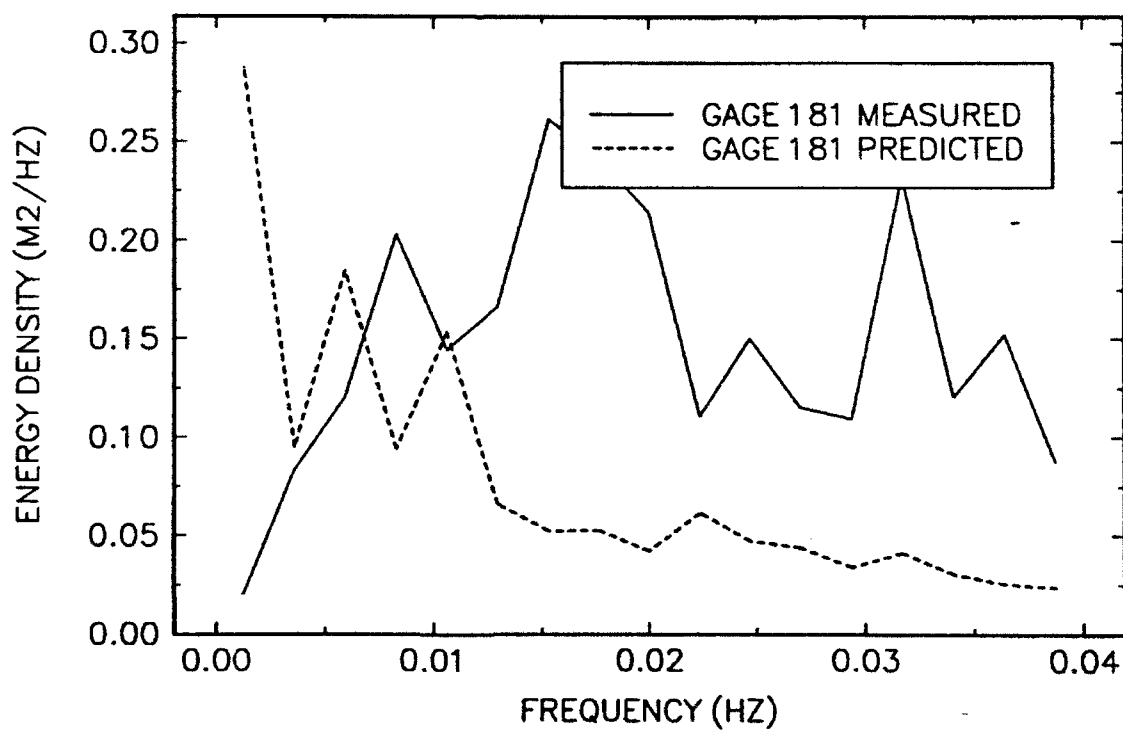
68-MINUTE RECORD BEGINNING AT 1708



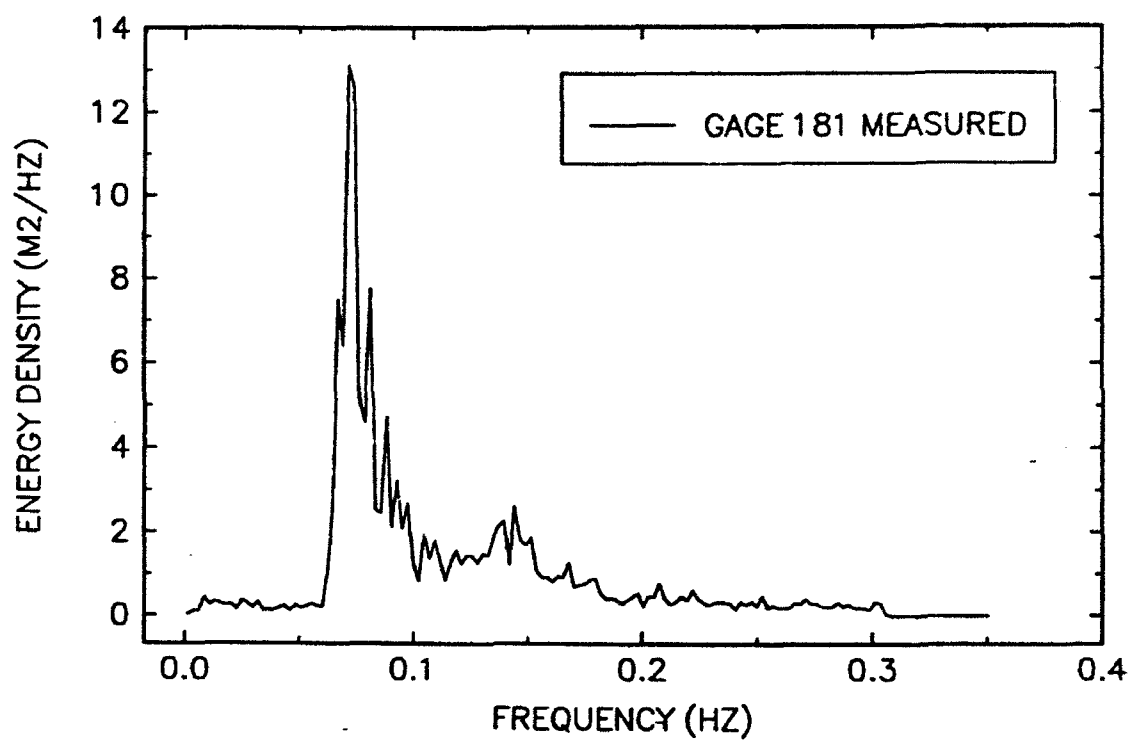
85-MINUTE RECORD BEGINNING AT 1600



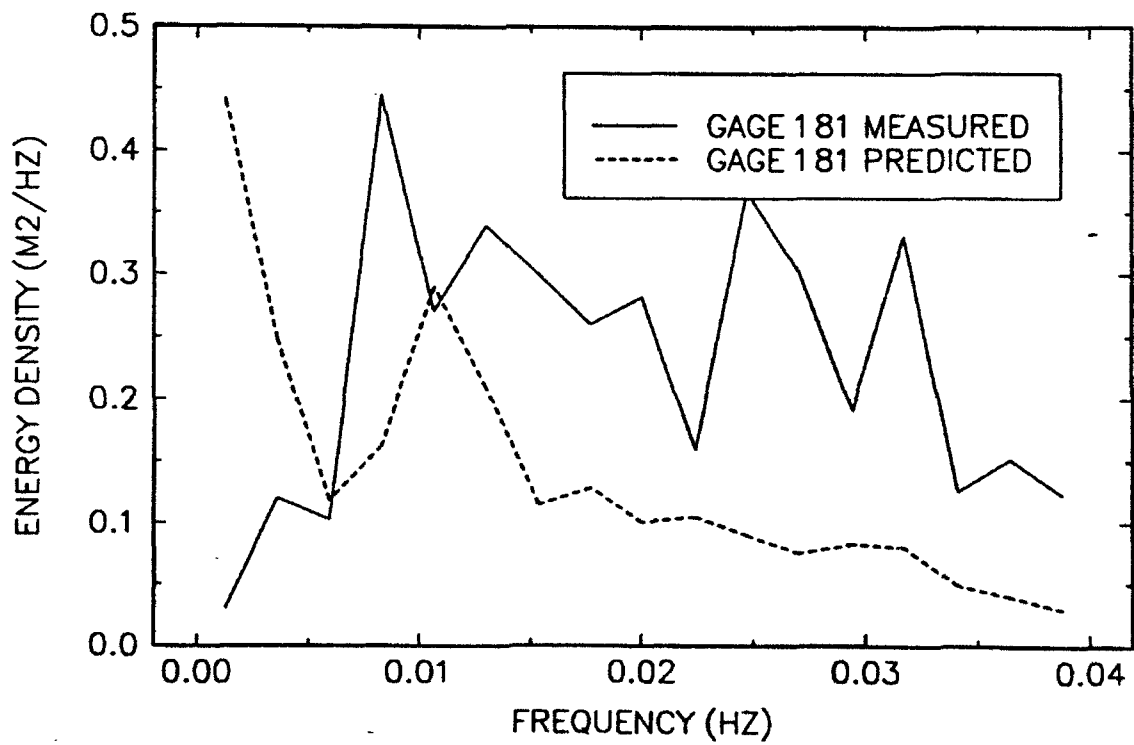
85-MINUTE RECORD BEGINNING AT 1600



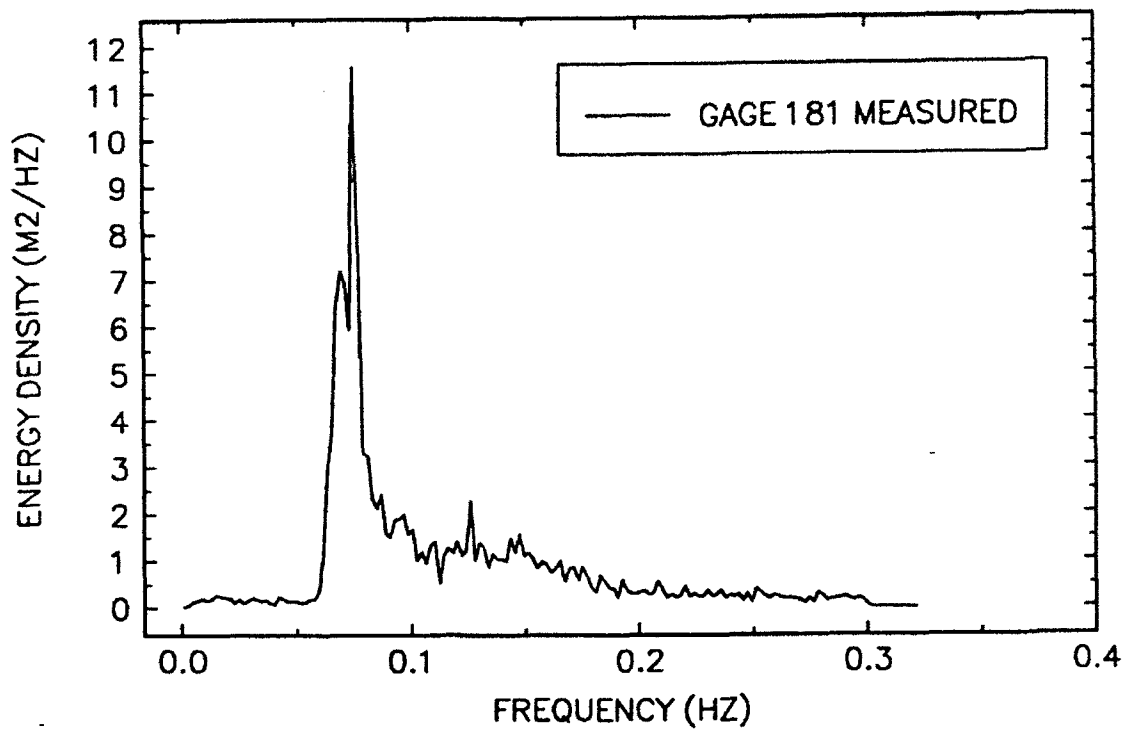
85-MINUTE RECORD BEGINNING AT 1725



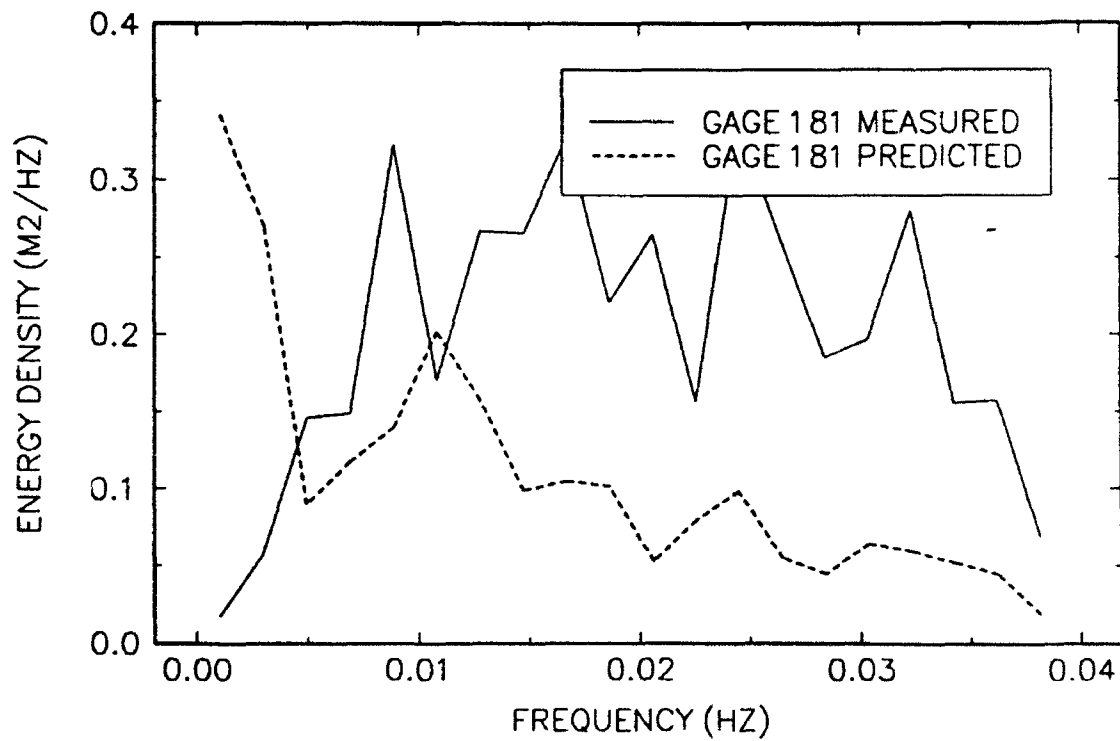
85-MINUTE RECORD BEGINNING AT 1725



102-MINUTE RECORD BEGINNING AT 1600



102-MINUTE RECORD BEGINNING AT 1651

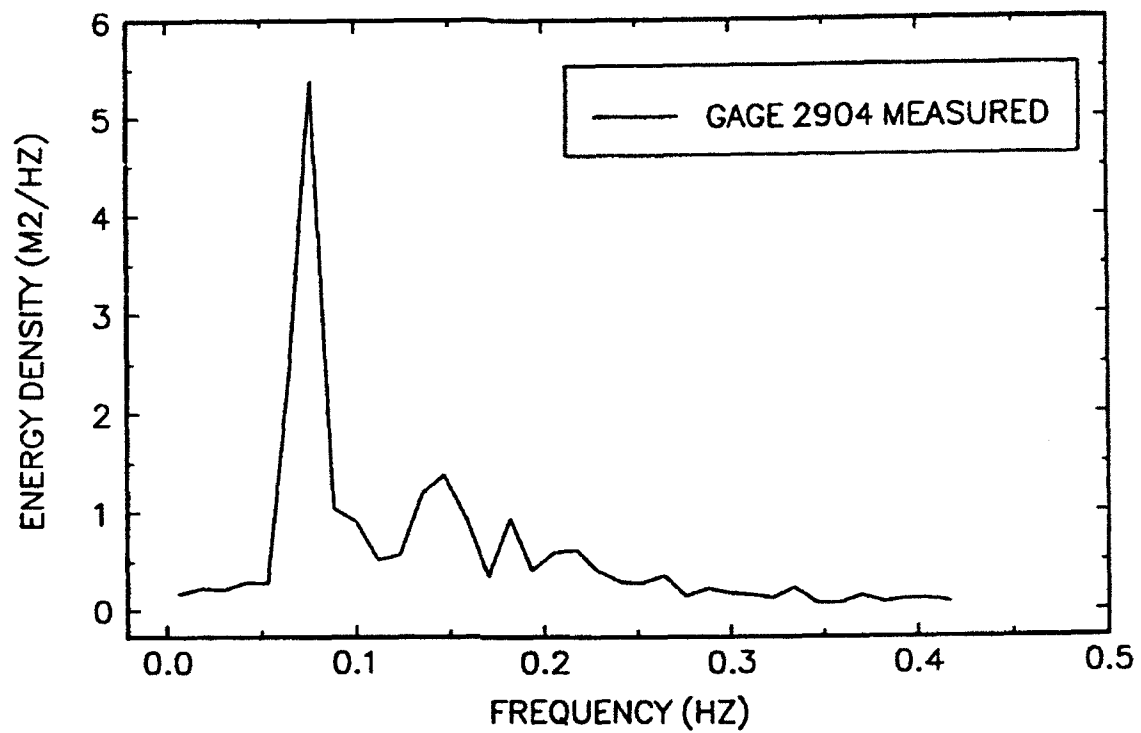


Appendix E

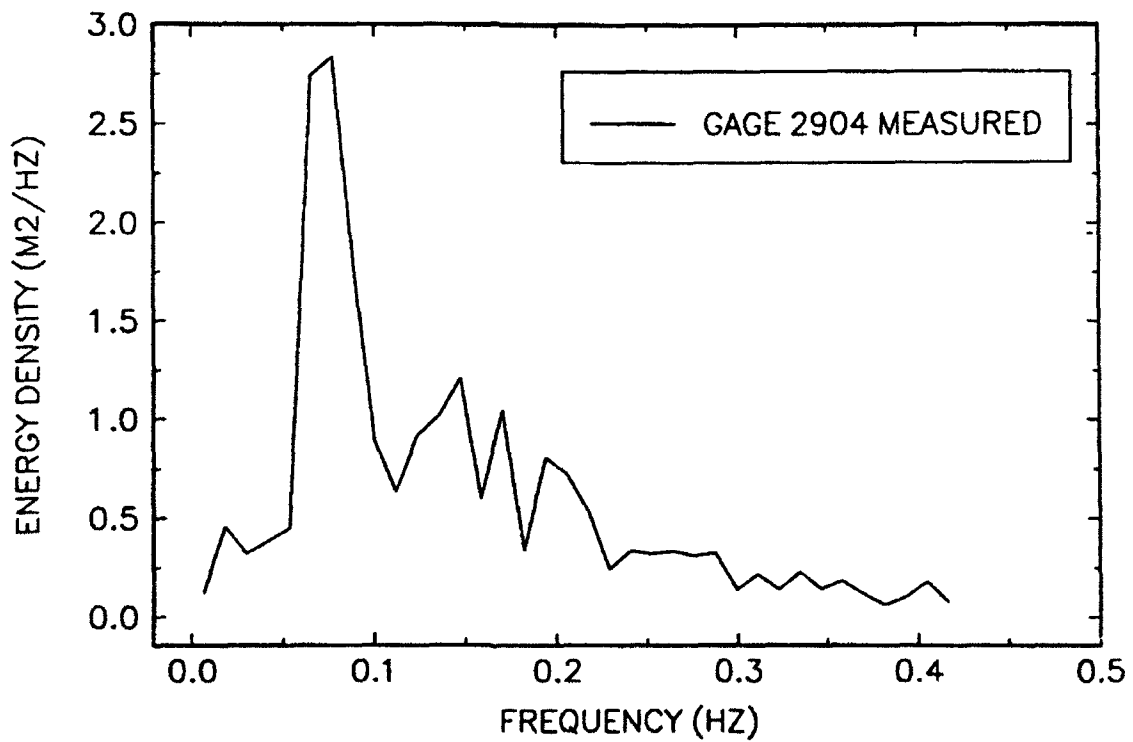
Short and Long Wave Spectra

from Field Data, Gage 2904

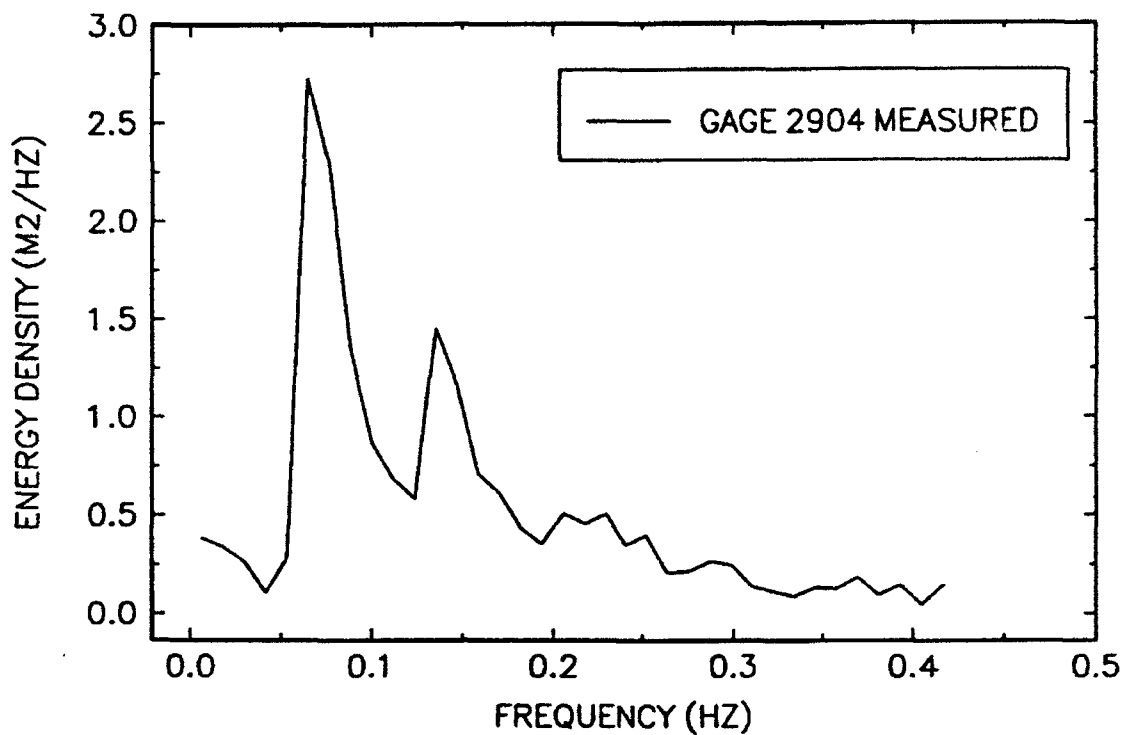
17-MINUTE RECORD BEGINNING AT 1658



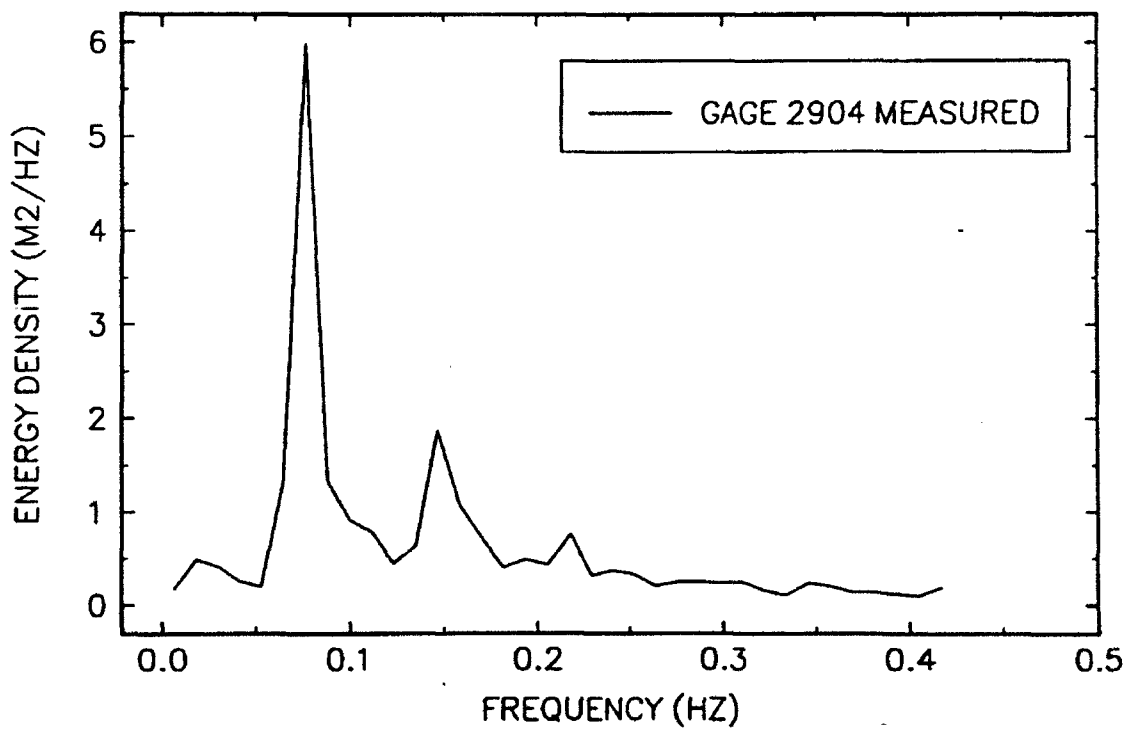
17-MINUTE RECORD BEGINNING AT 1715



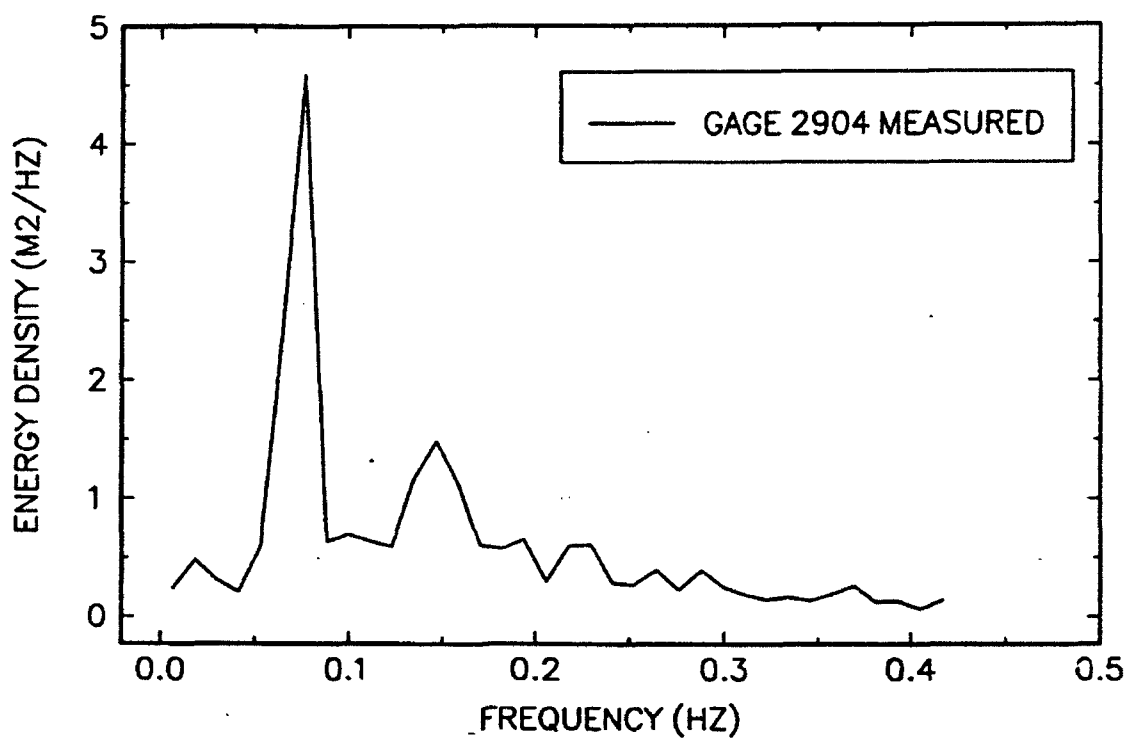
17-MINUTE RECORD BEGINNING AT 1732



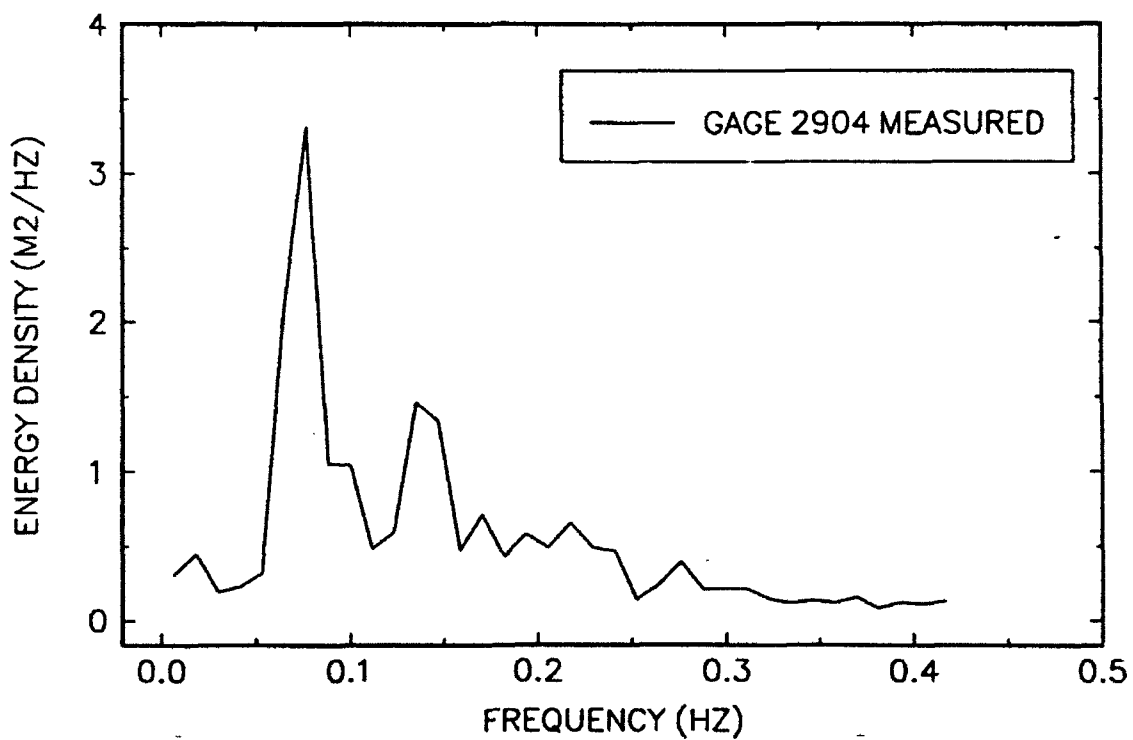
17-MINUTE RECORD BEGINNING AT 1749



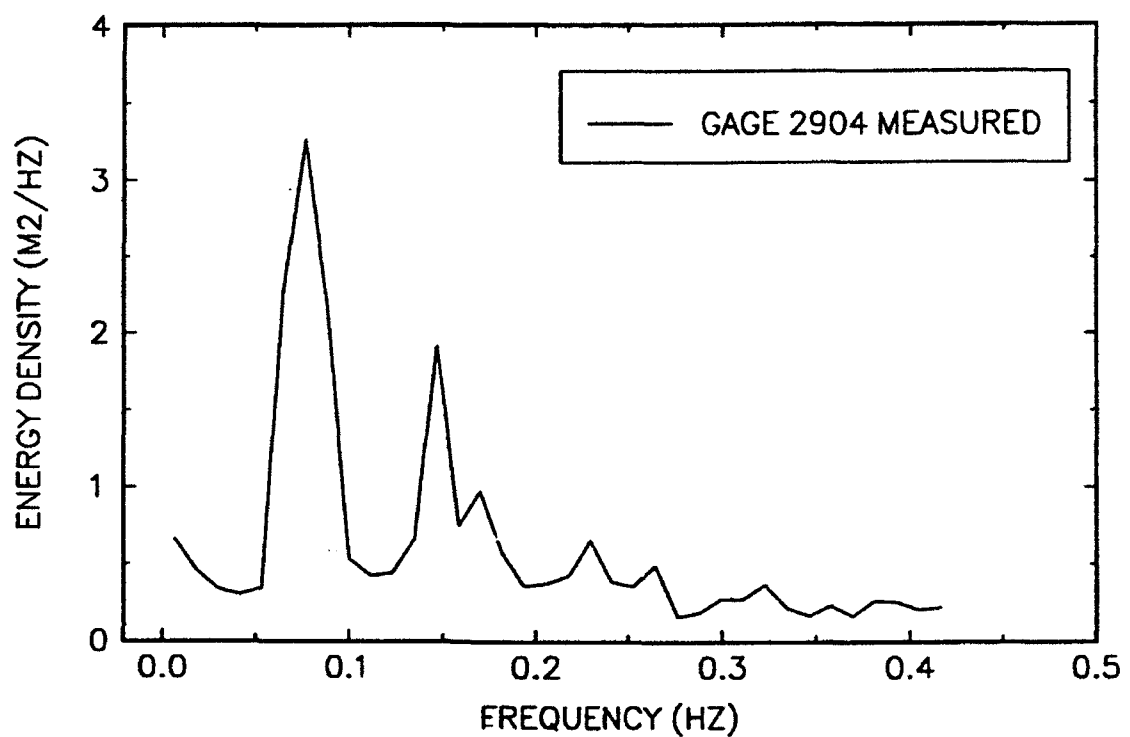
17-MINUTE RECORD BEGINNING AT 1806



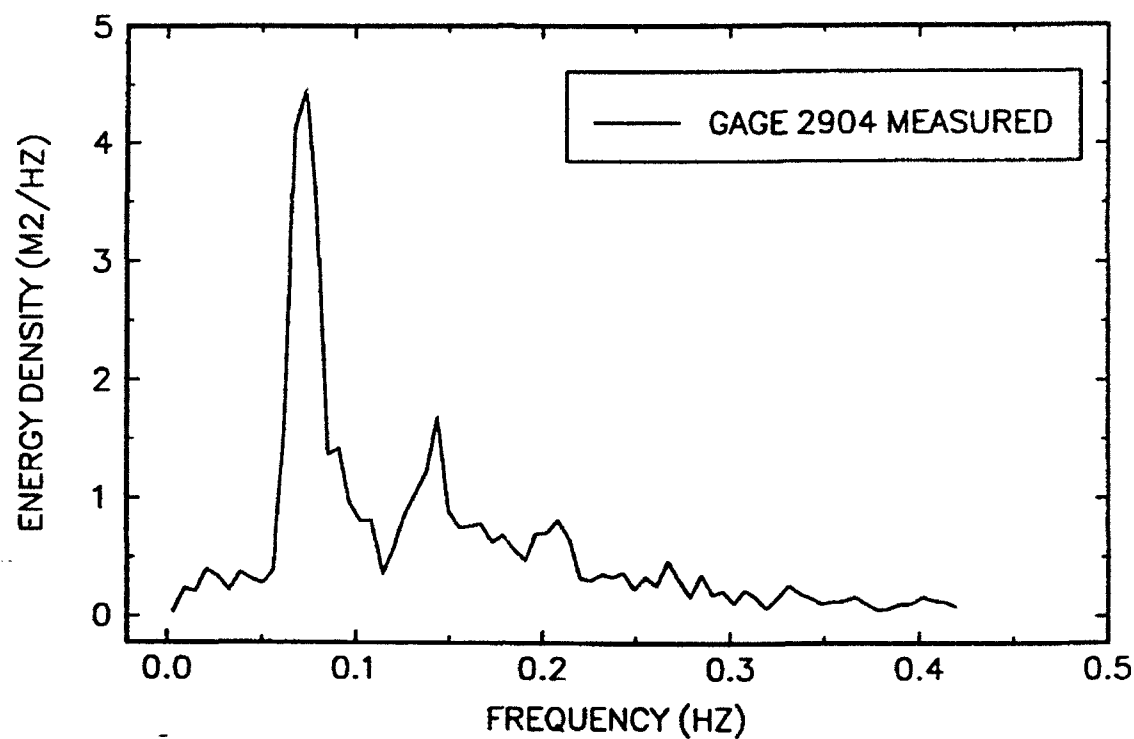
17-MINUTE RECORD BEGINNING AT 1824



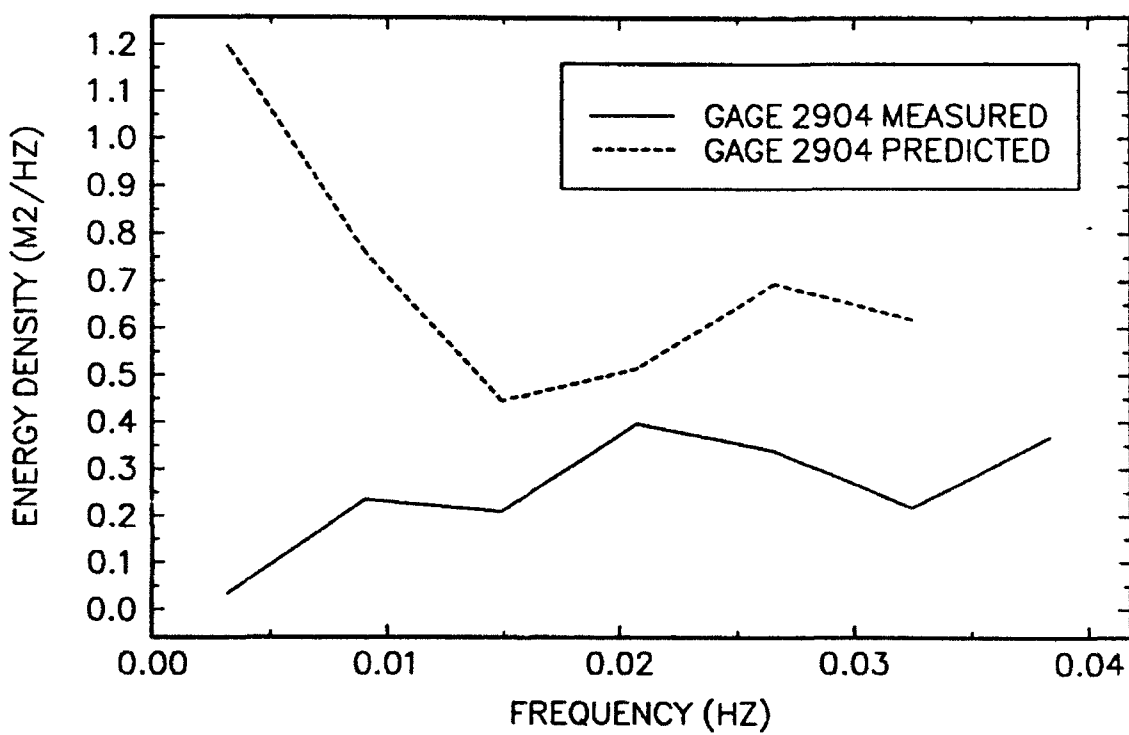
17-MINUTE RECORD BEGINNING AT 1841



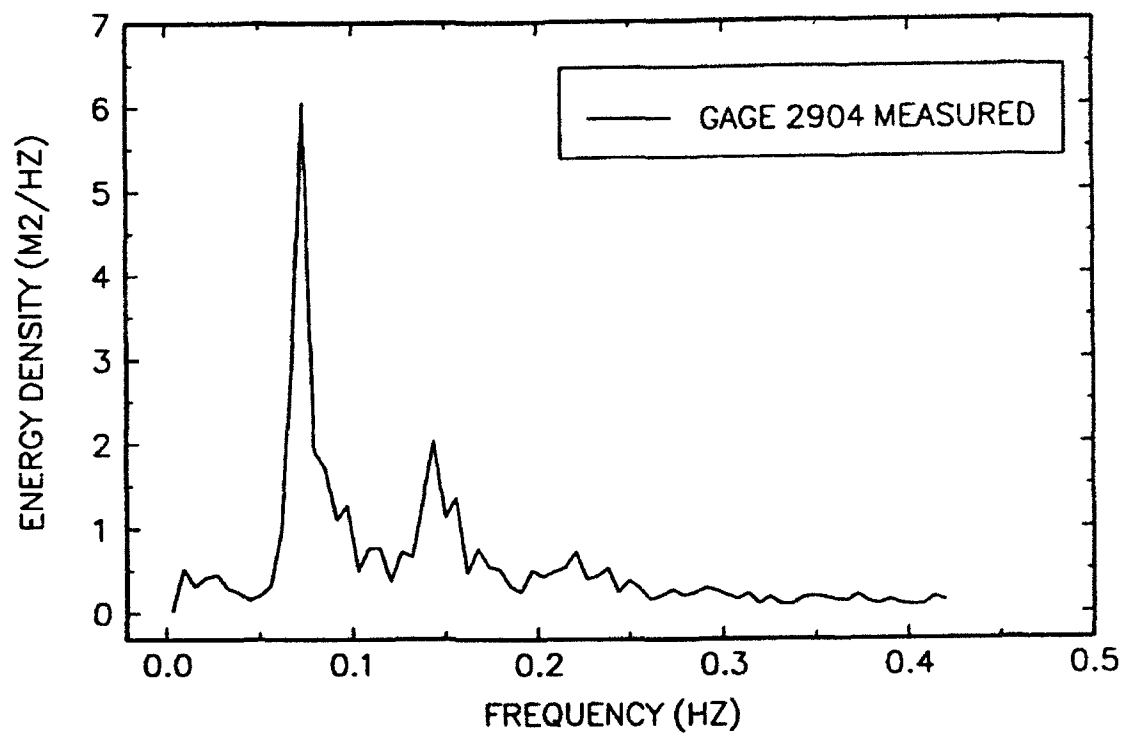
34-MINUTE RECORD BEGINNING AT 1658



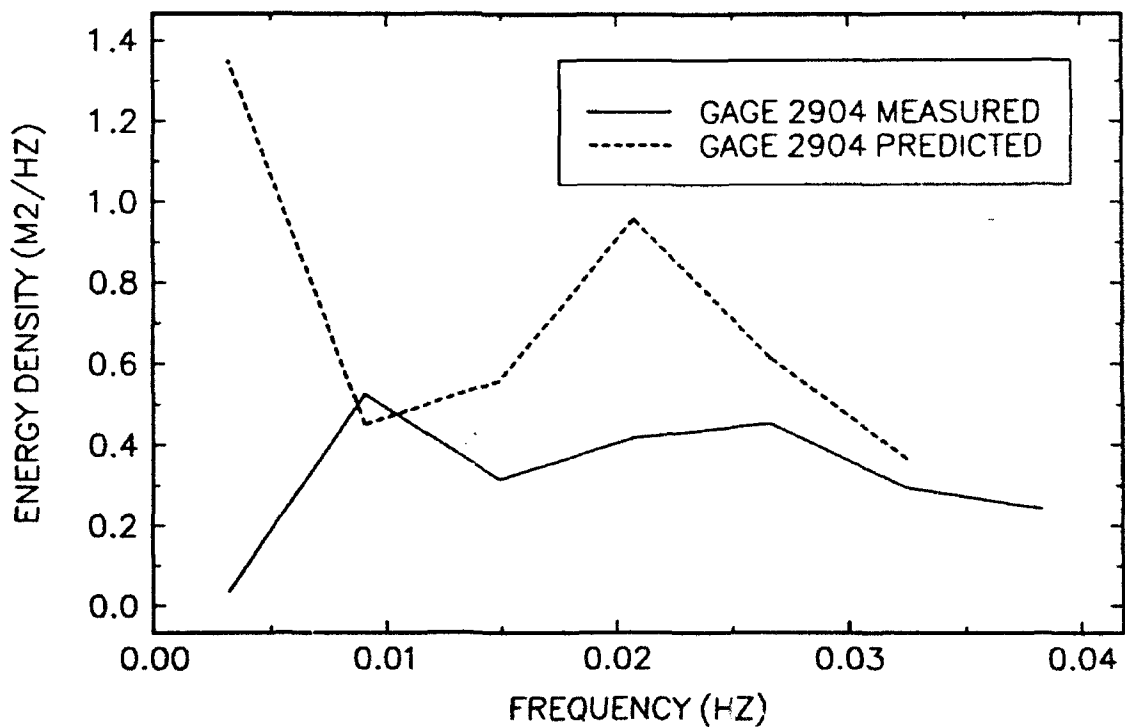
34-MINUTE RECORD BEGINNING AT 1658



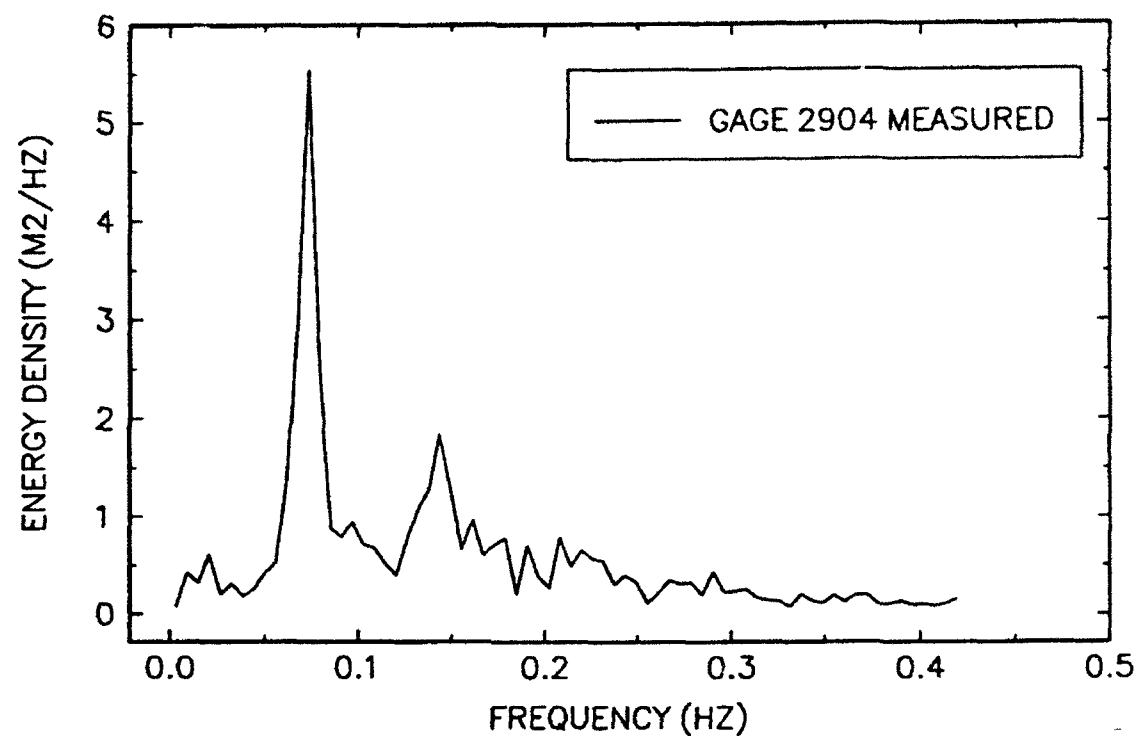
34-MINUTE RECORD BEGINNING AT 1732



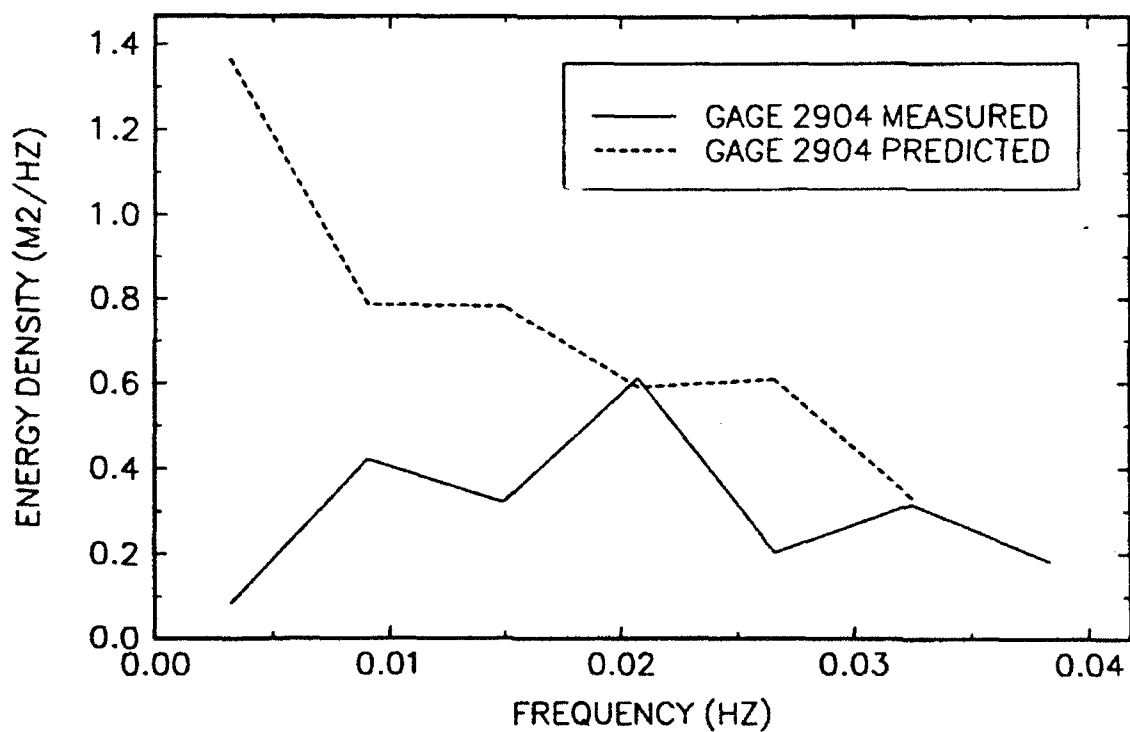
34-MINUTE RECORD BEGINNING AT 1732



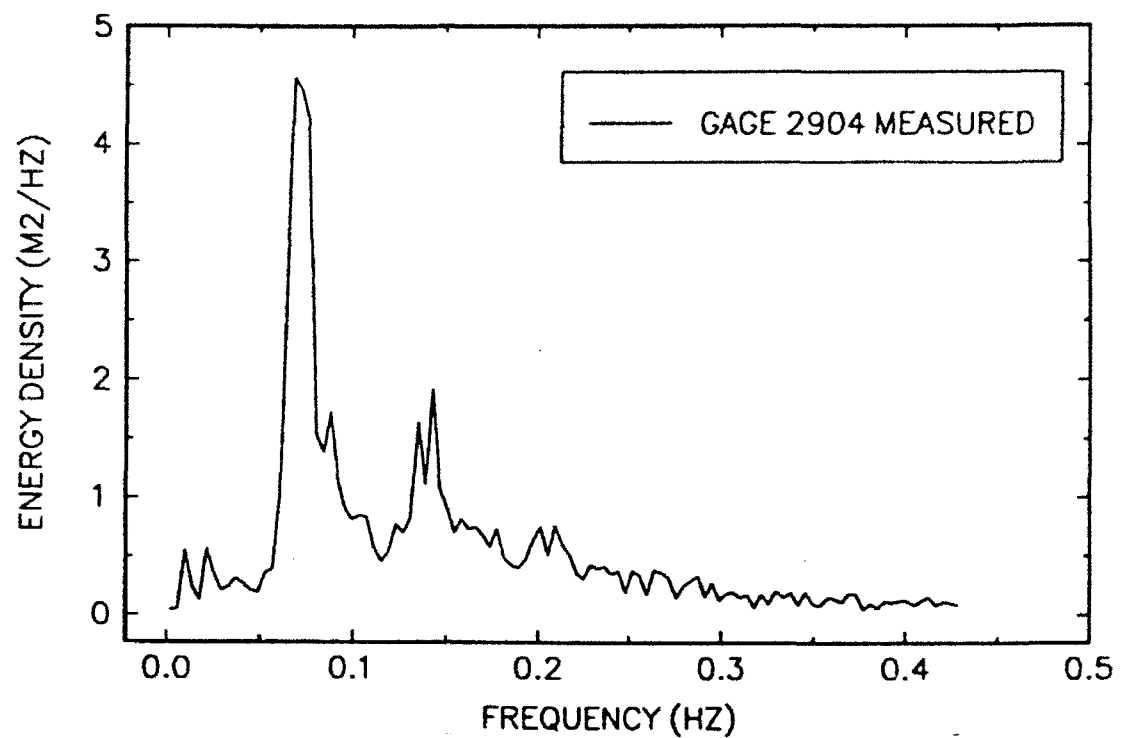
34-MINUTE RECORD BEGINNING AT 1806



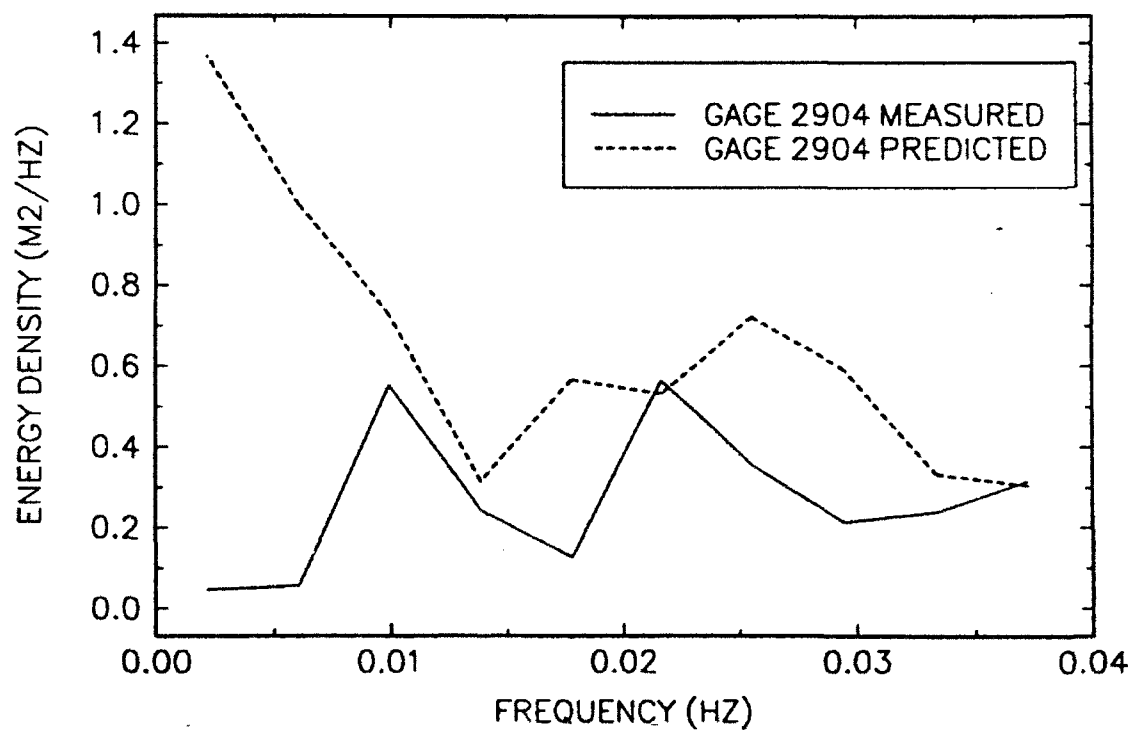
34-MINUTE RECORD BEGINNING AT 1806



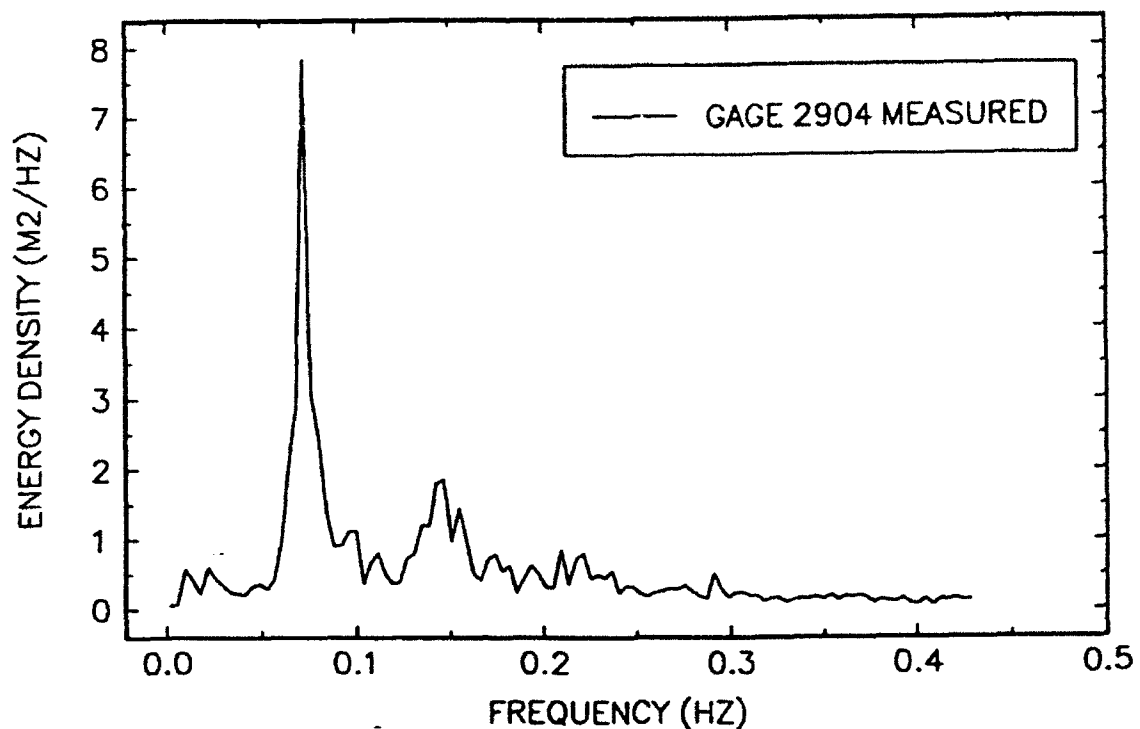
51-MINUTE RECORD BEGINNING AT 1658



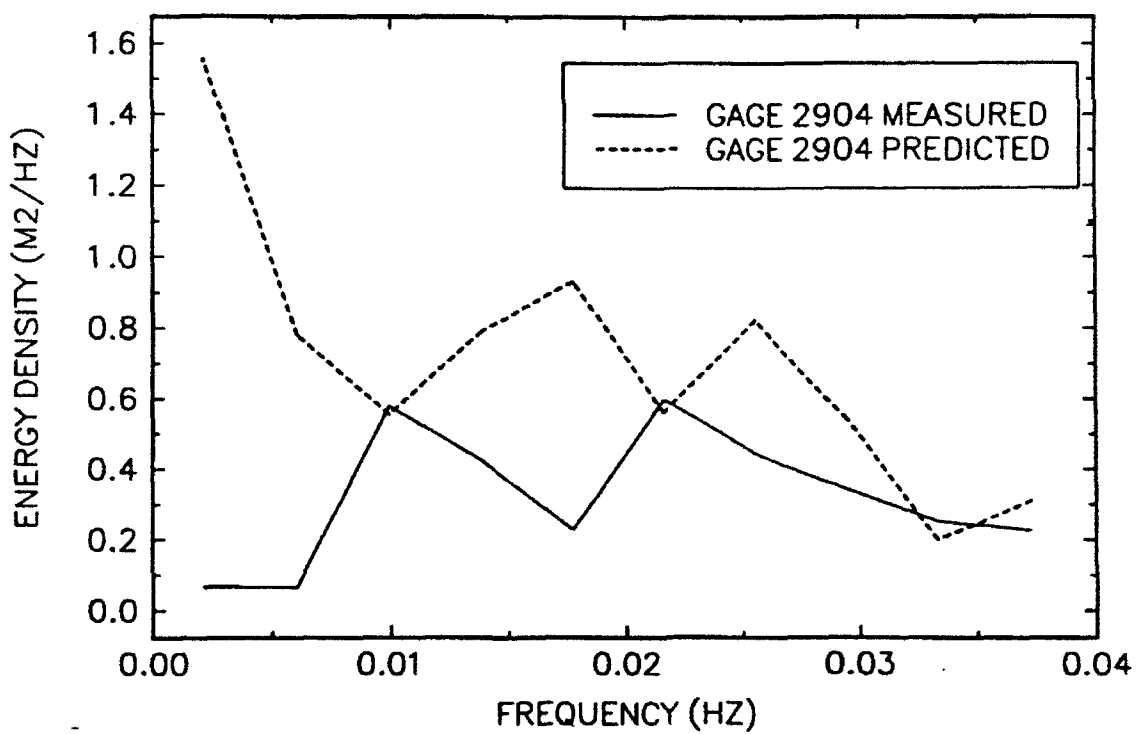
51-MINUTE RECORD BEGINNING AT 1658



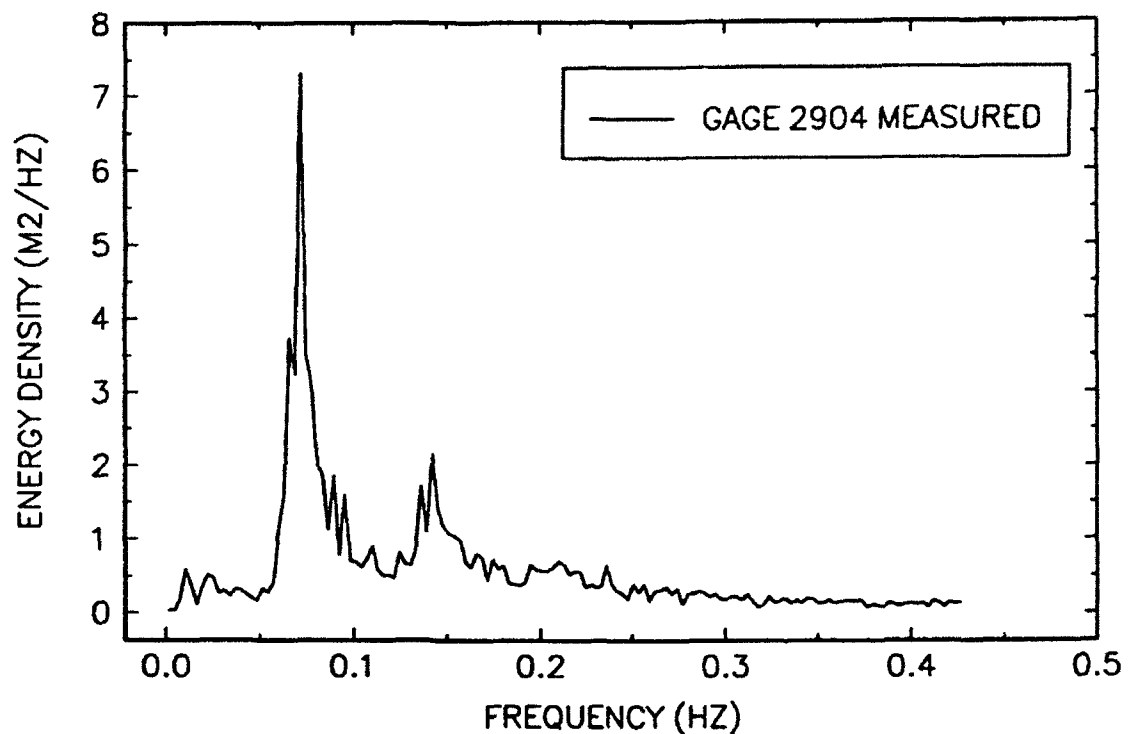
51-MINUTE RECORD BEGINNING AT 1749



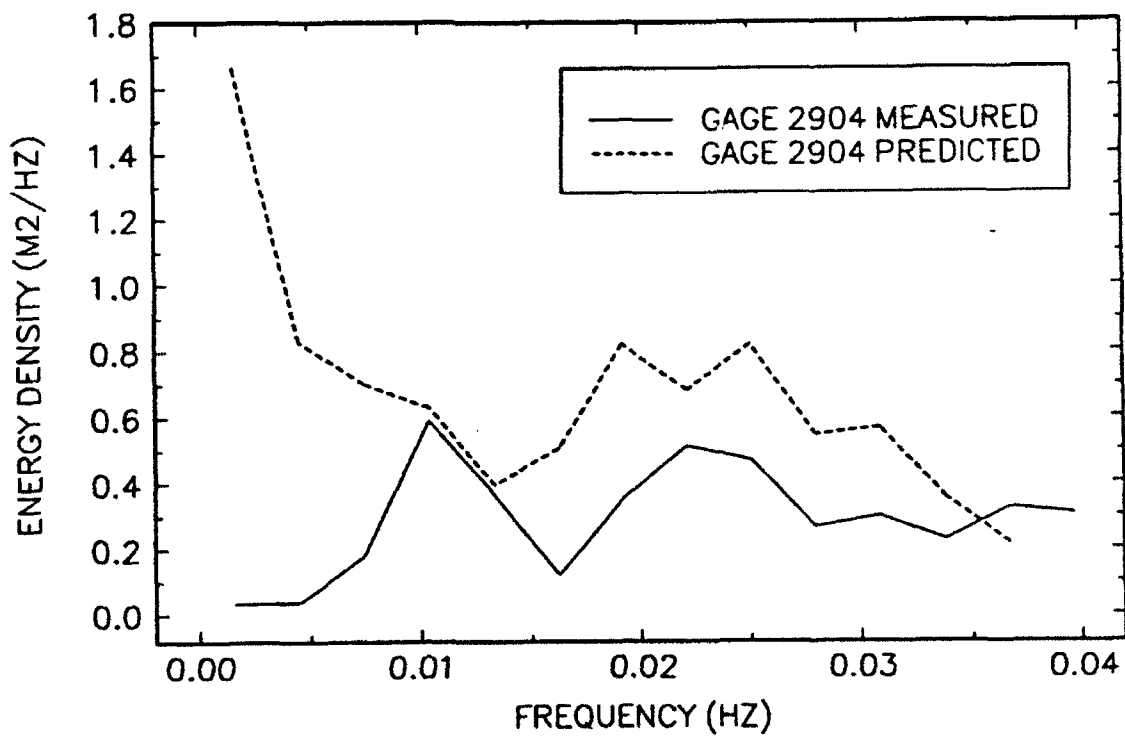
51-MINUTE RECORD BEGINNING AT 1749



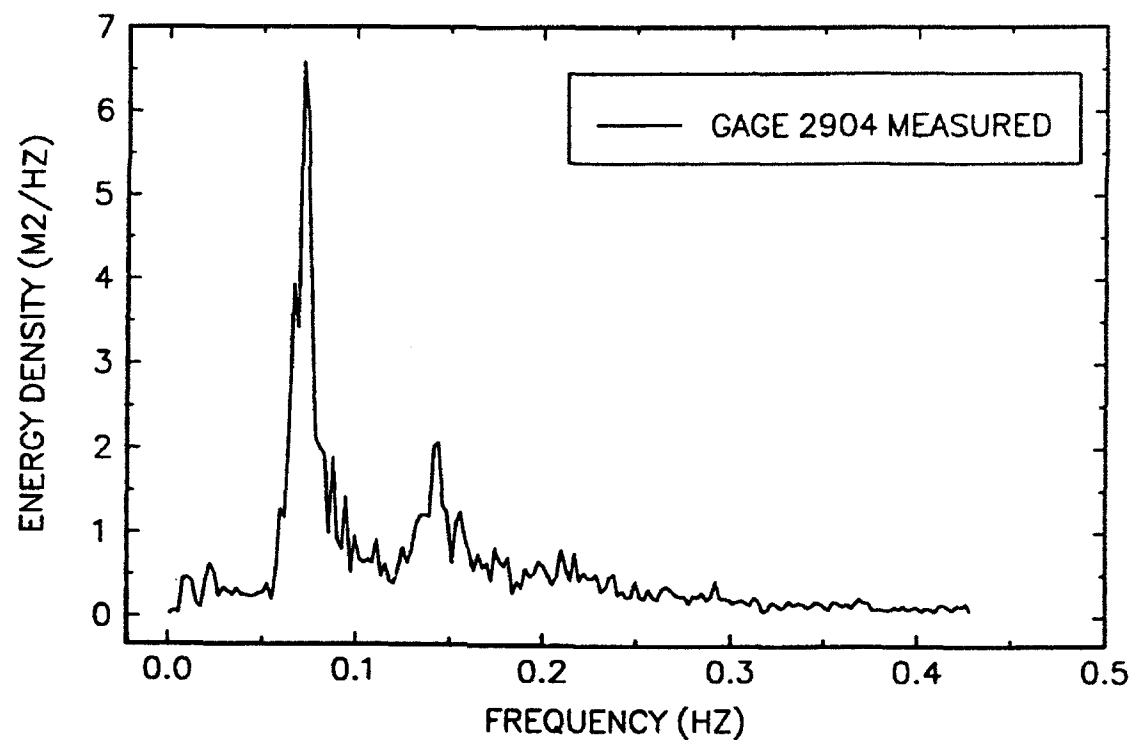
68-MINUTE RECORD BEGINNING AT 1658



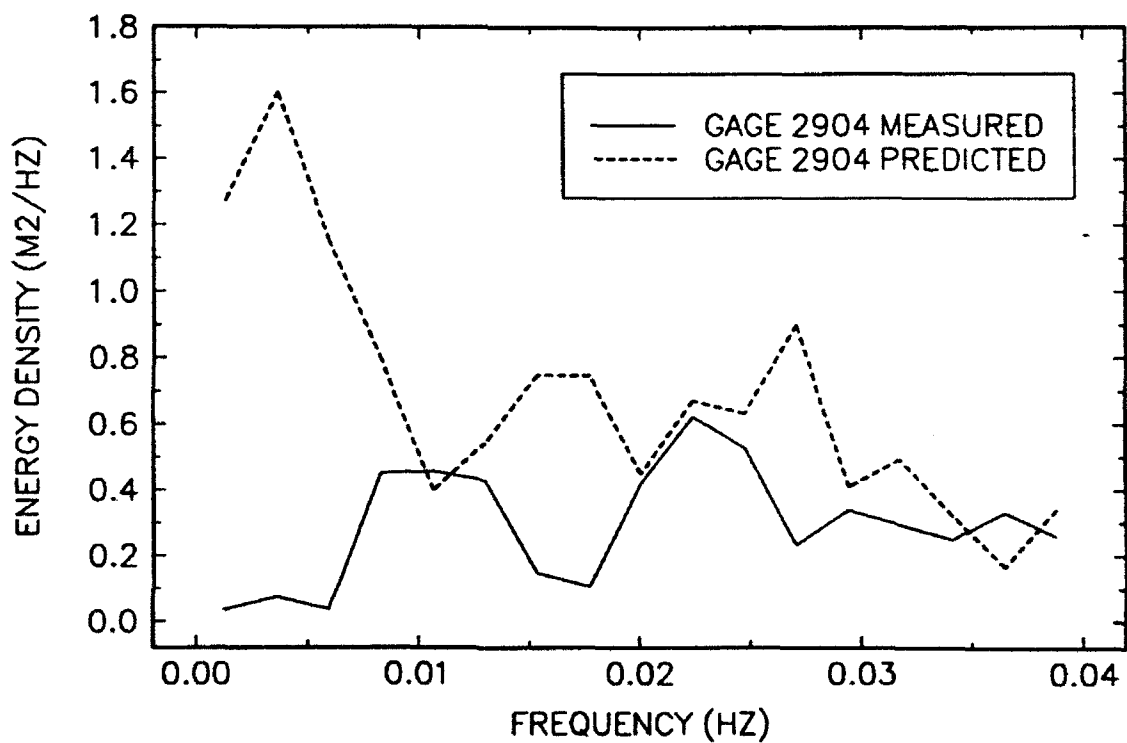
68-MINUTE RECORD BEGINNING AT 1658



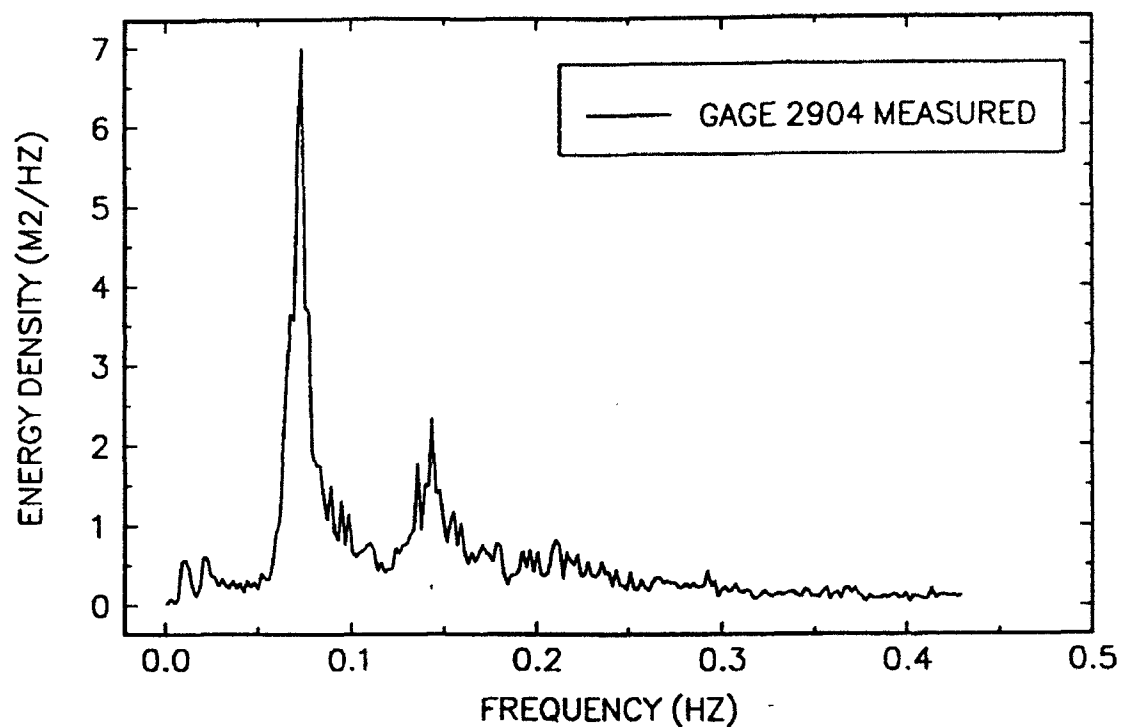
85-MINUTE RECORD BEGINNING AT 1658



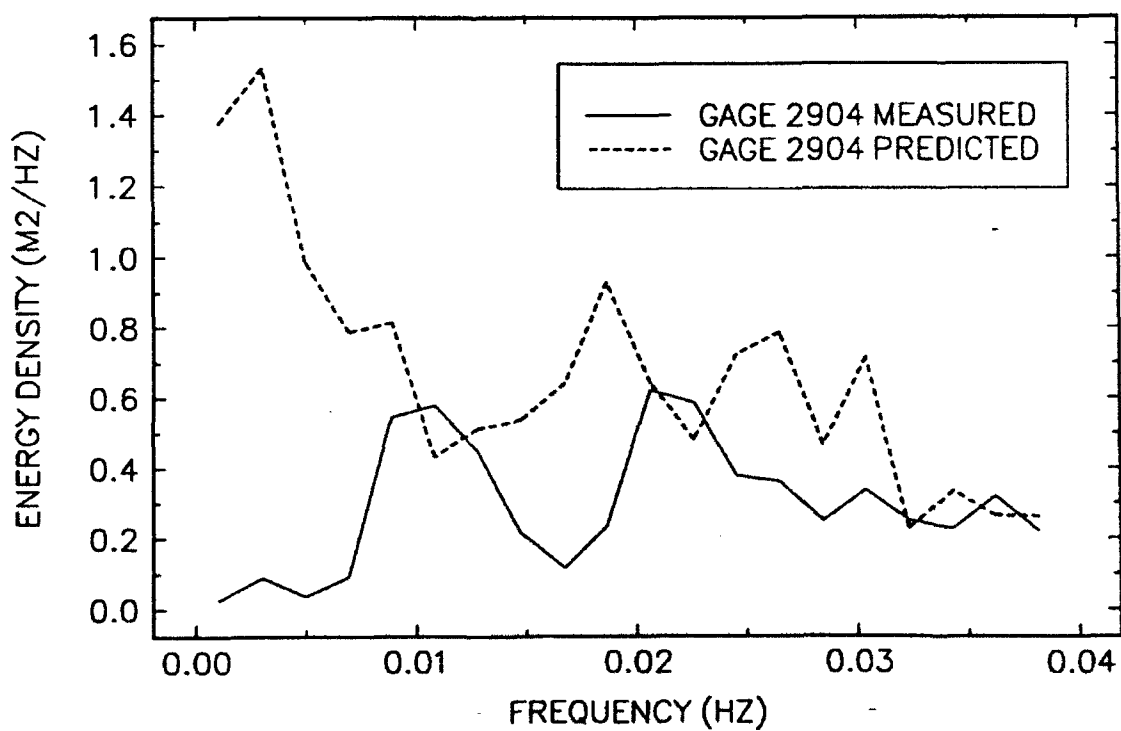
85-MINUTE RECORD BEGINNING AT 1658



102-MINUTE RECORD BEGINNING AT 1658



102-MINUTE RECORD BEGINNING AT 1658

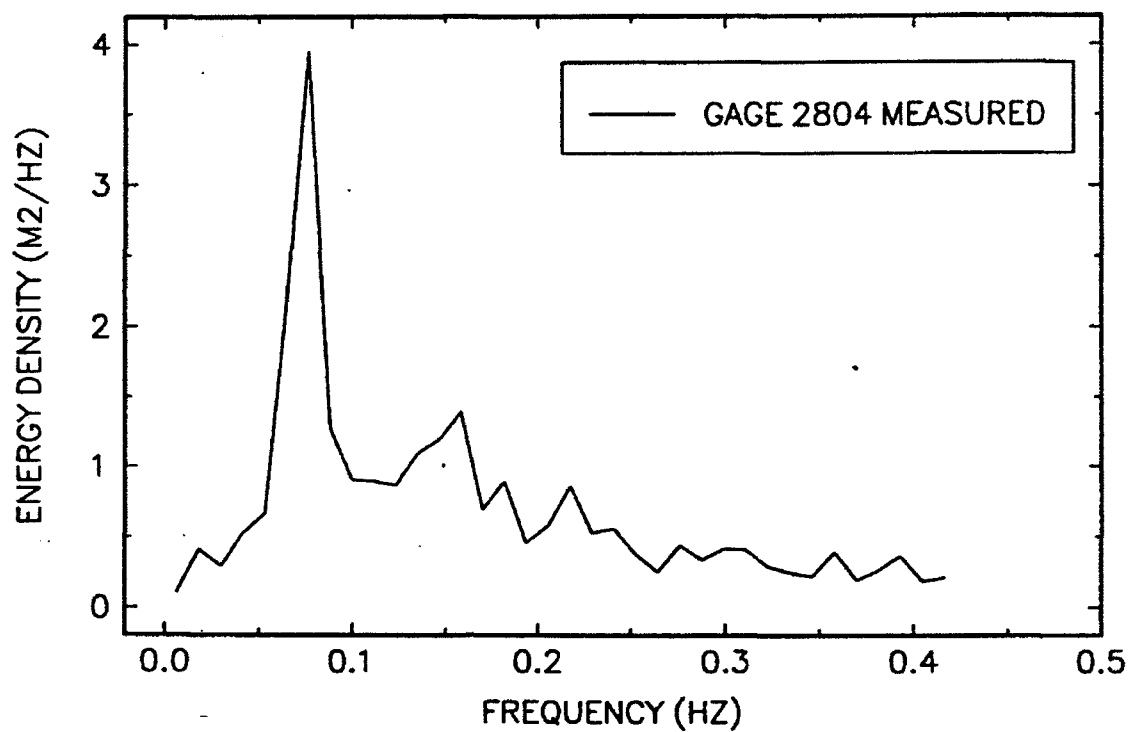


Appendix F

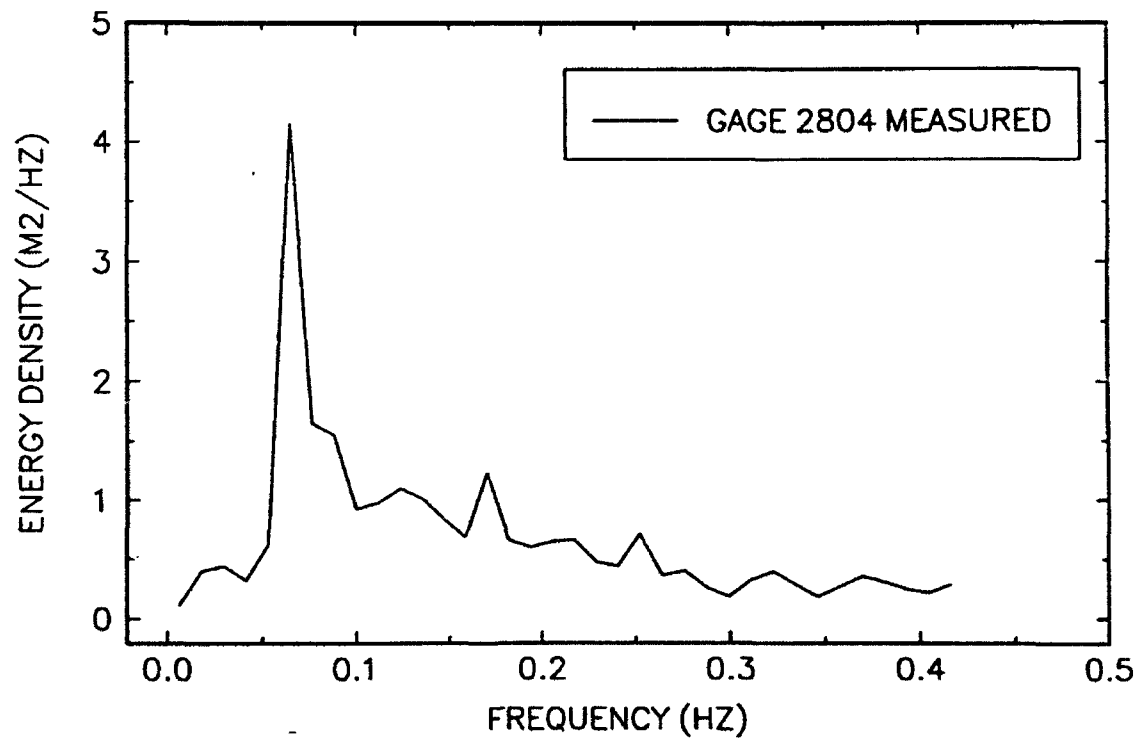
Short and Long Wave Spectra

from Field Data, Gage 2804

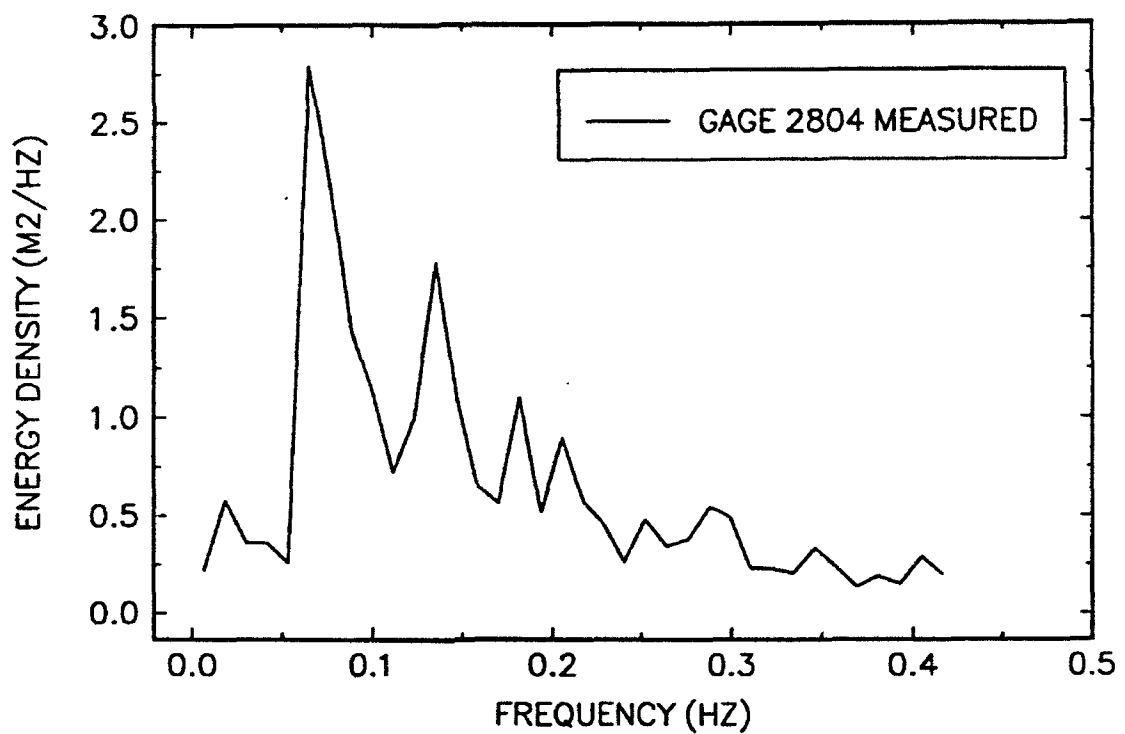
17-MINUTE RECORD BEGINNING AT 1658



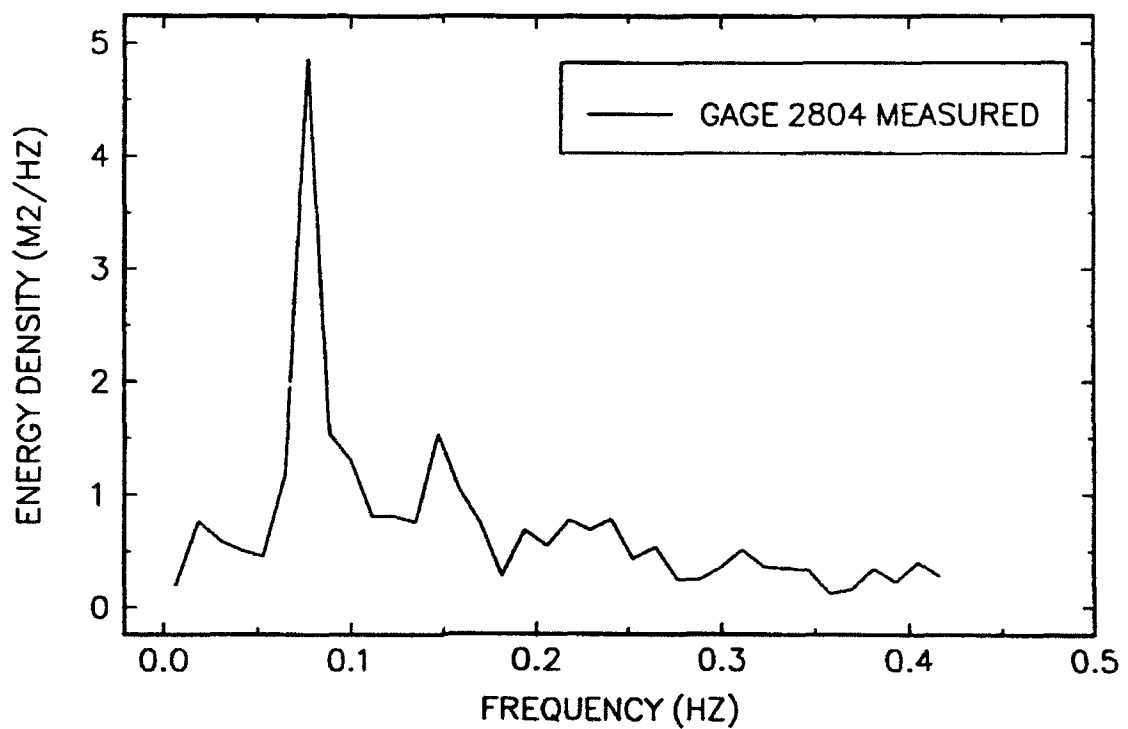
17-MINUTE RECORD BEGINNING AT 1715



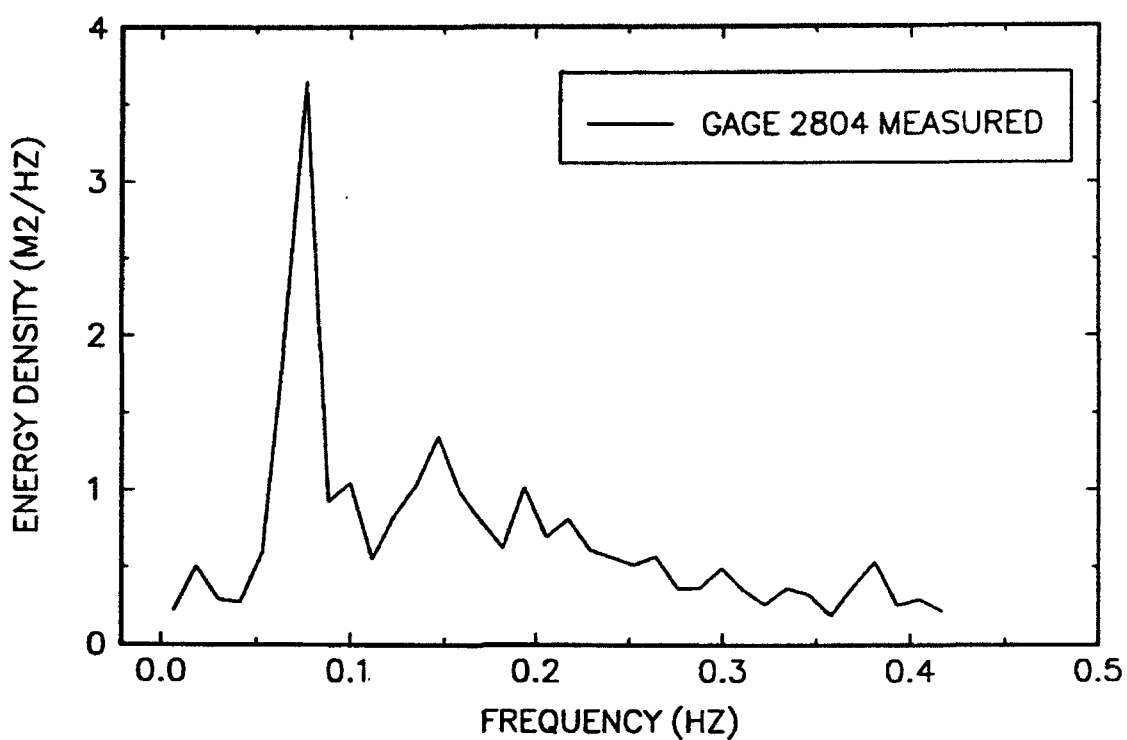
17-MINUTE RECORD BEGINNING AT 1732



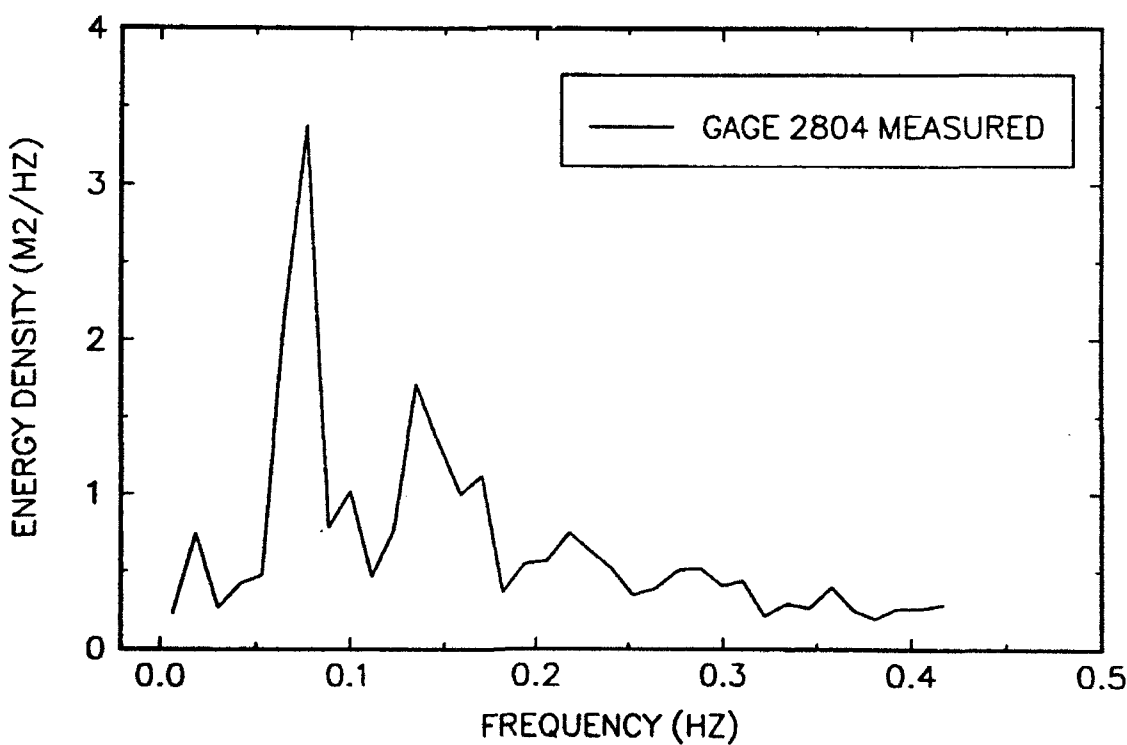
17-MINUTE RECORD BEGINNING AT 1749



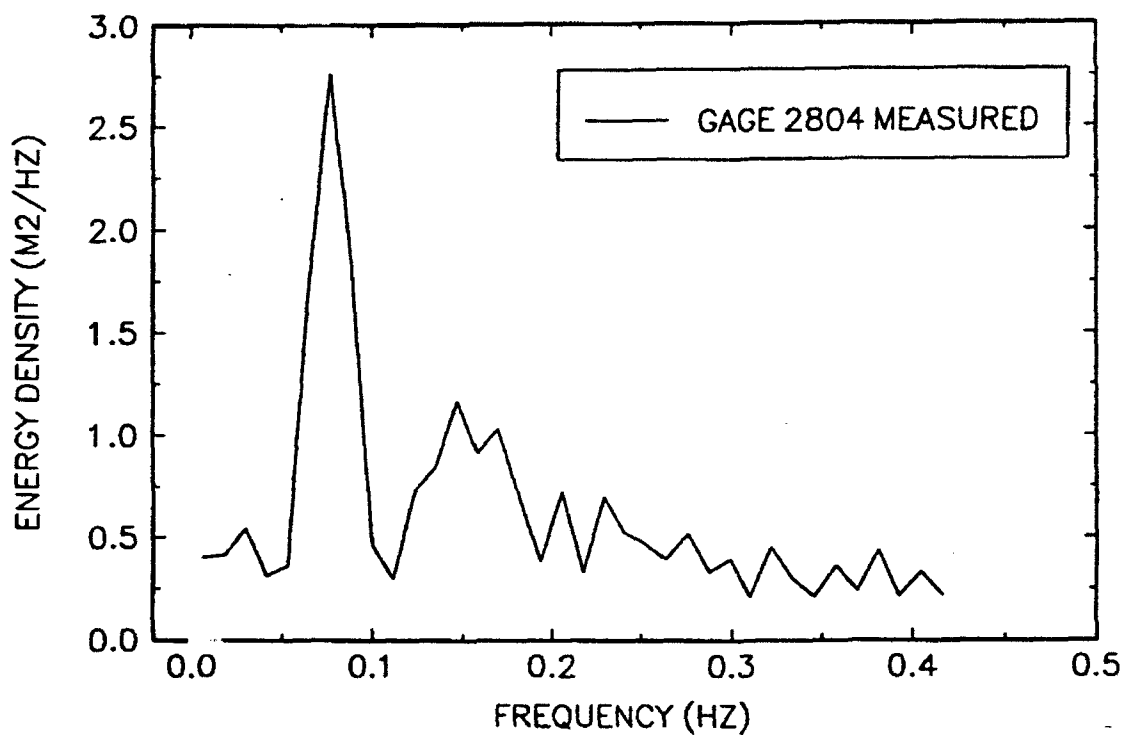
17-MINUTE RECORD BEGINNING AT 1806



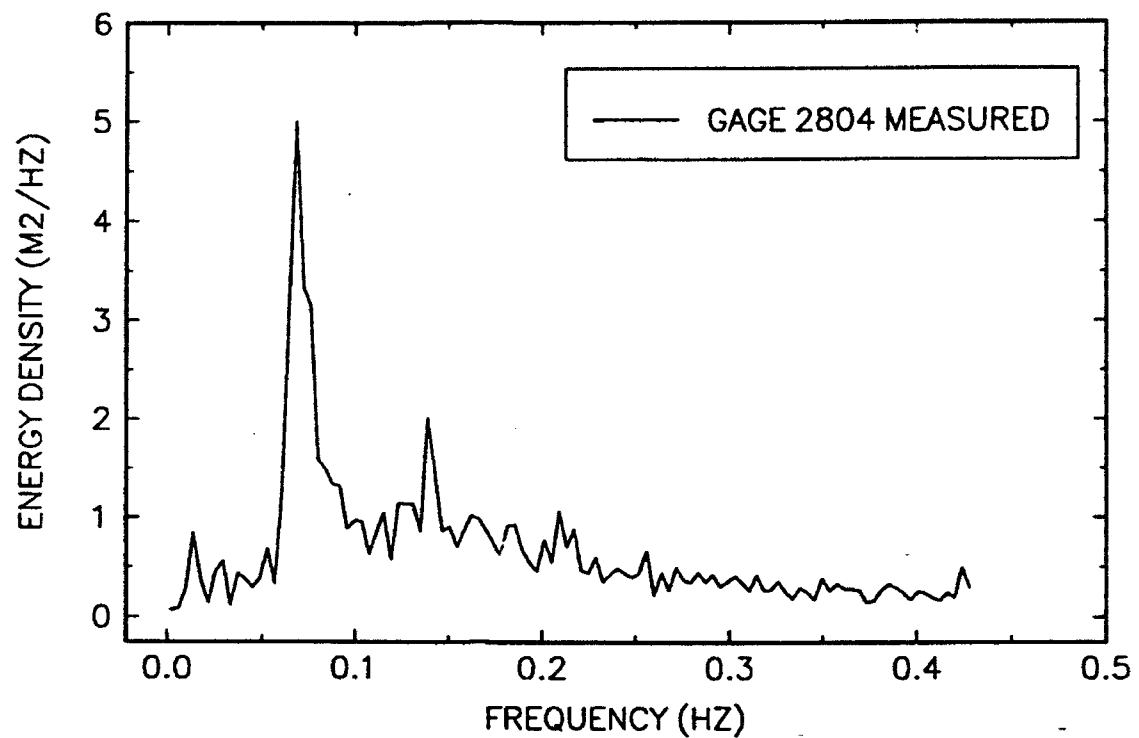
17-MINUTE RECORD BEGINNING AT 1824



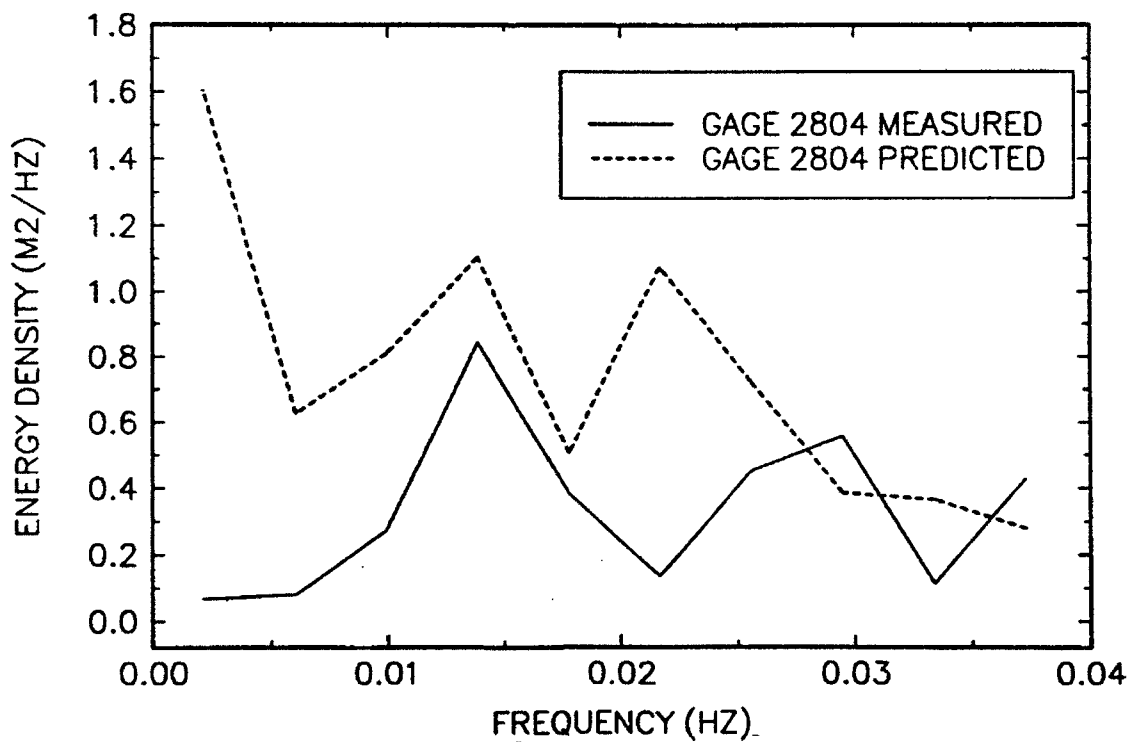
17-MINUTE RECORD BEGINNING AT 1841



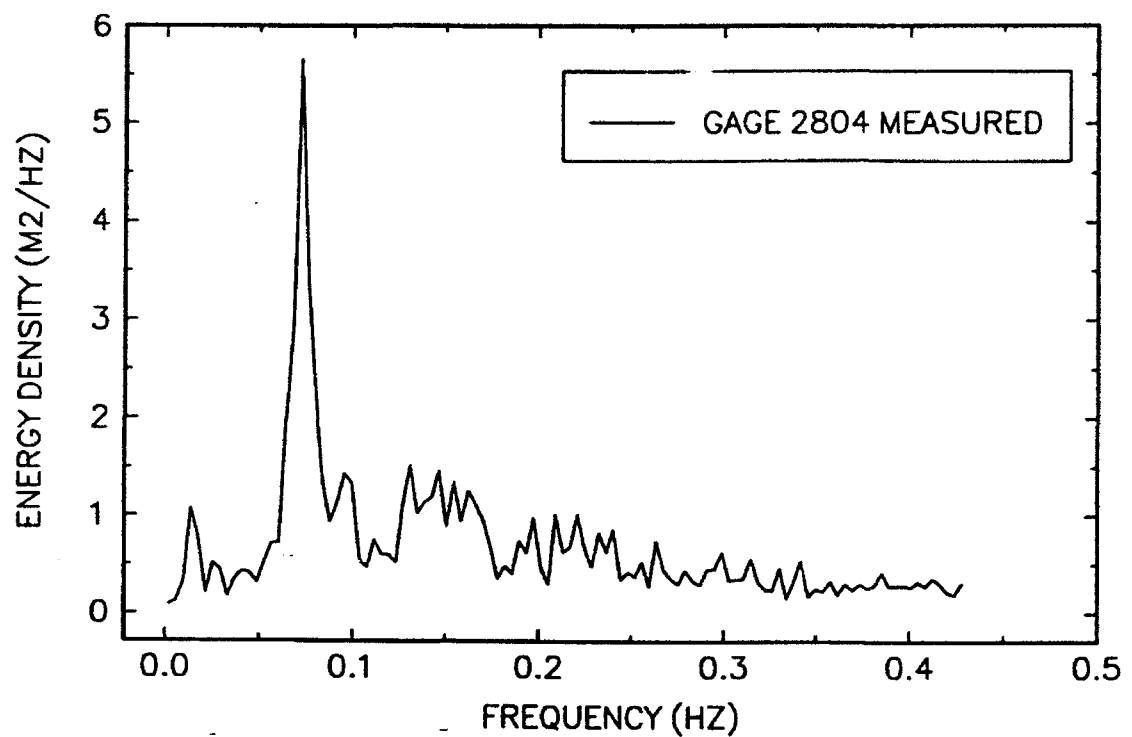
51 -MINUTE RECORD BEGINNING AT 1658



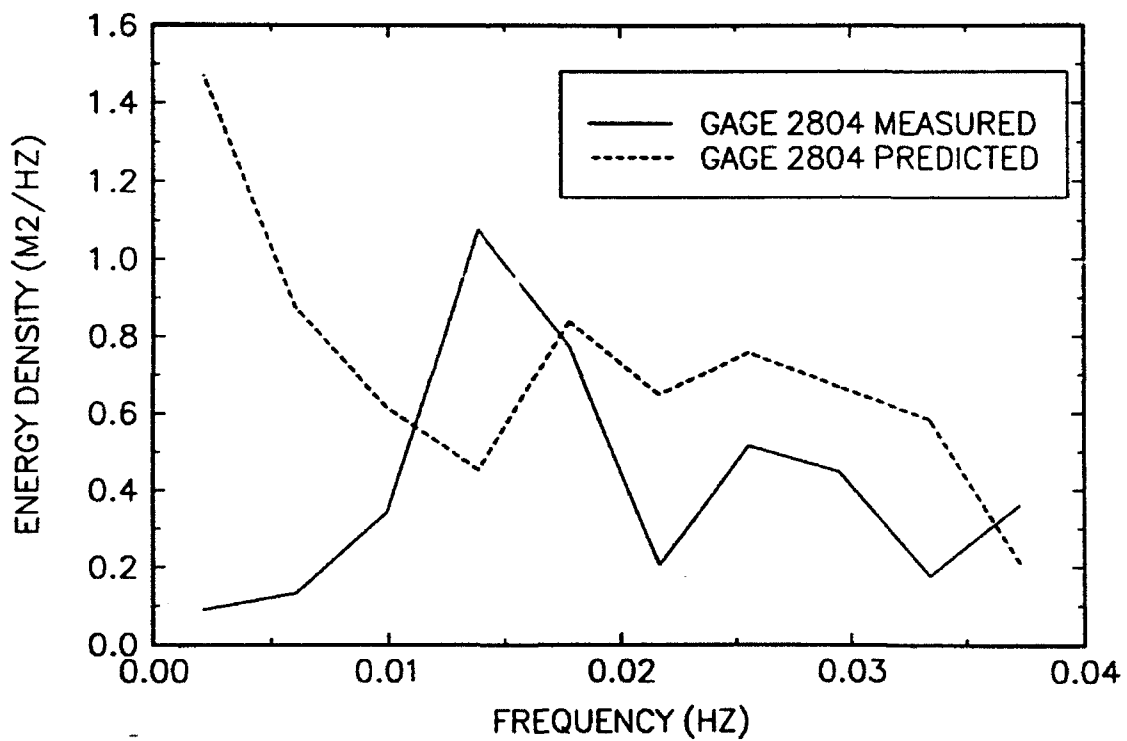
51 -MINUTE RECORD BEGINNING AT 1658



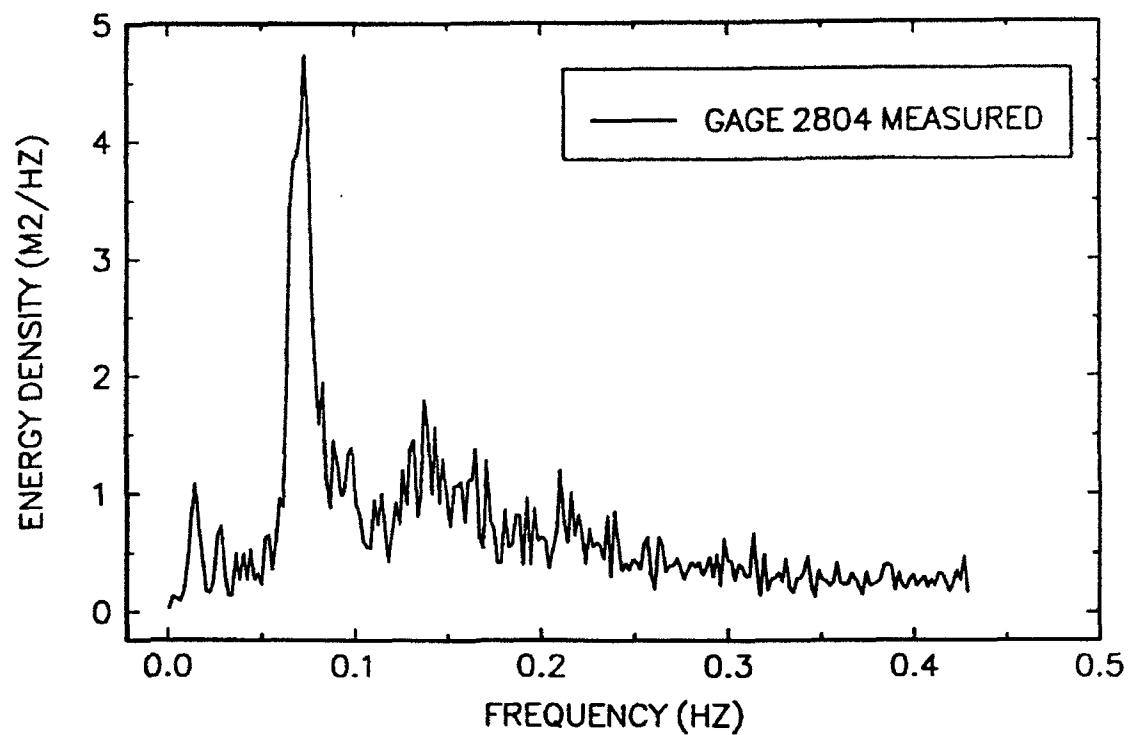
51-MINUTE RECORD BEGINNING AT 1749



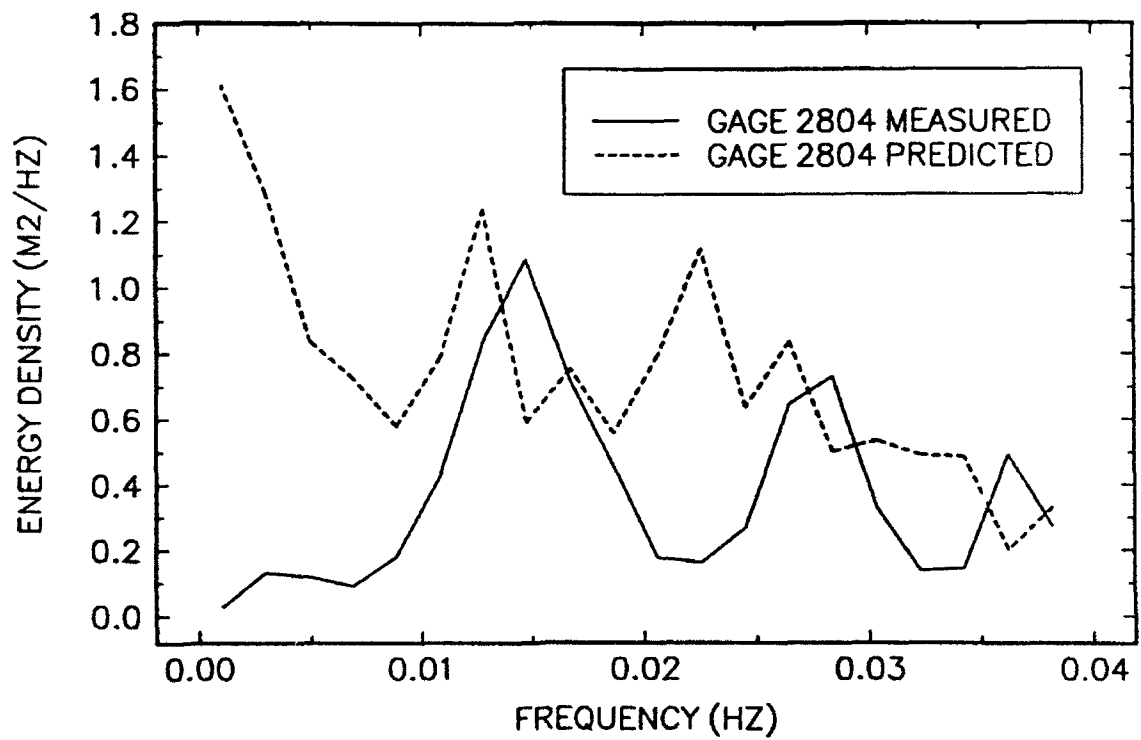
51-MINUTE RECORD BEGINNING AT 1749



102-MINUTE RECORD BEGINNING AT 1658



102-MINUTE RECORD BEGINNING AT 1658

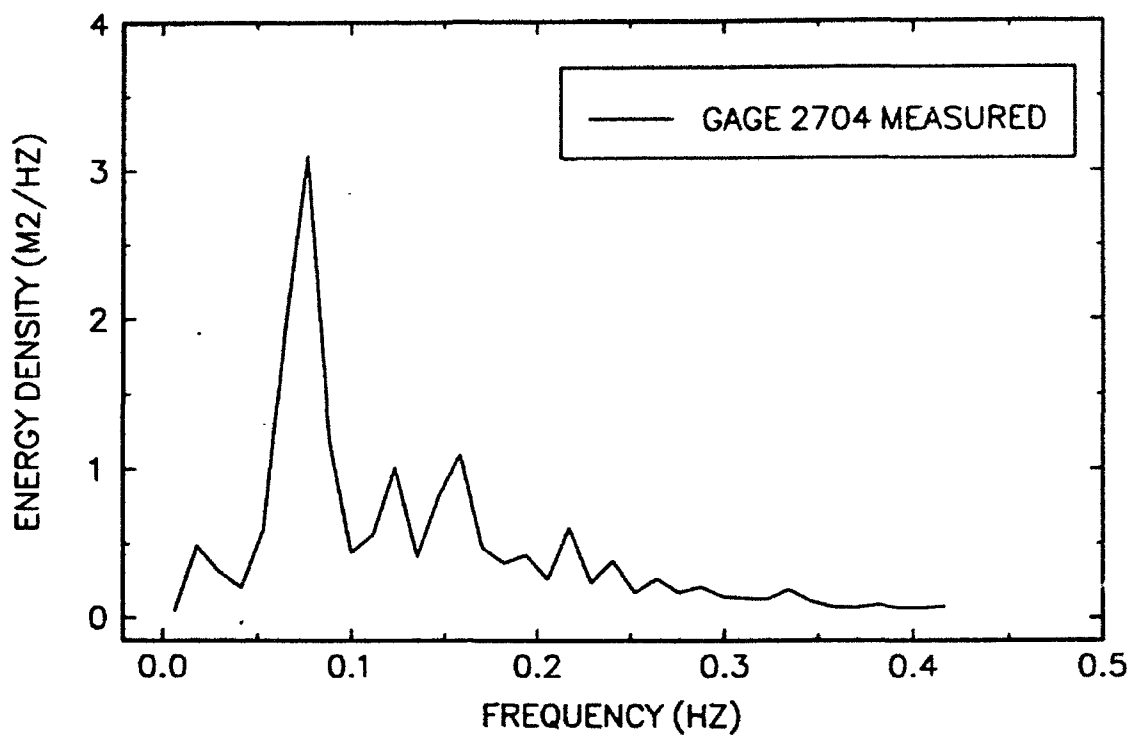


Appendix G

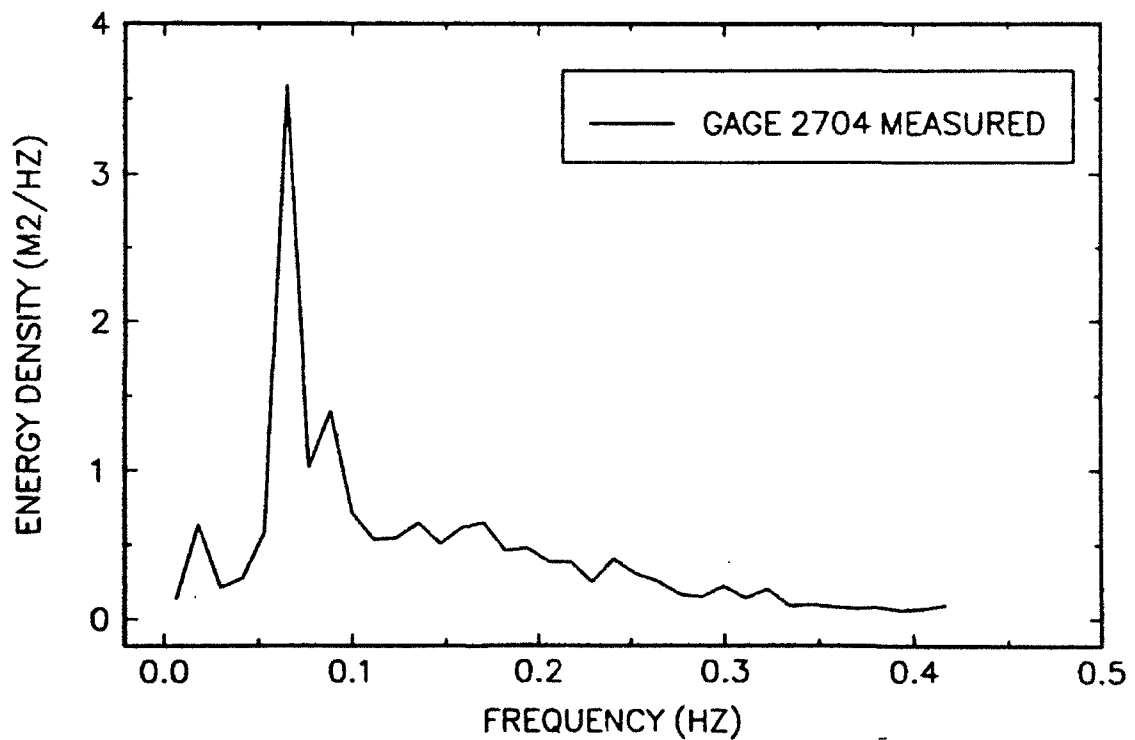
Short and Long Wave Spectra

from Field Data, Gage 2704

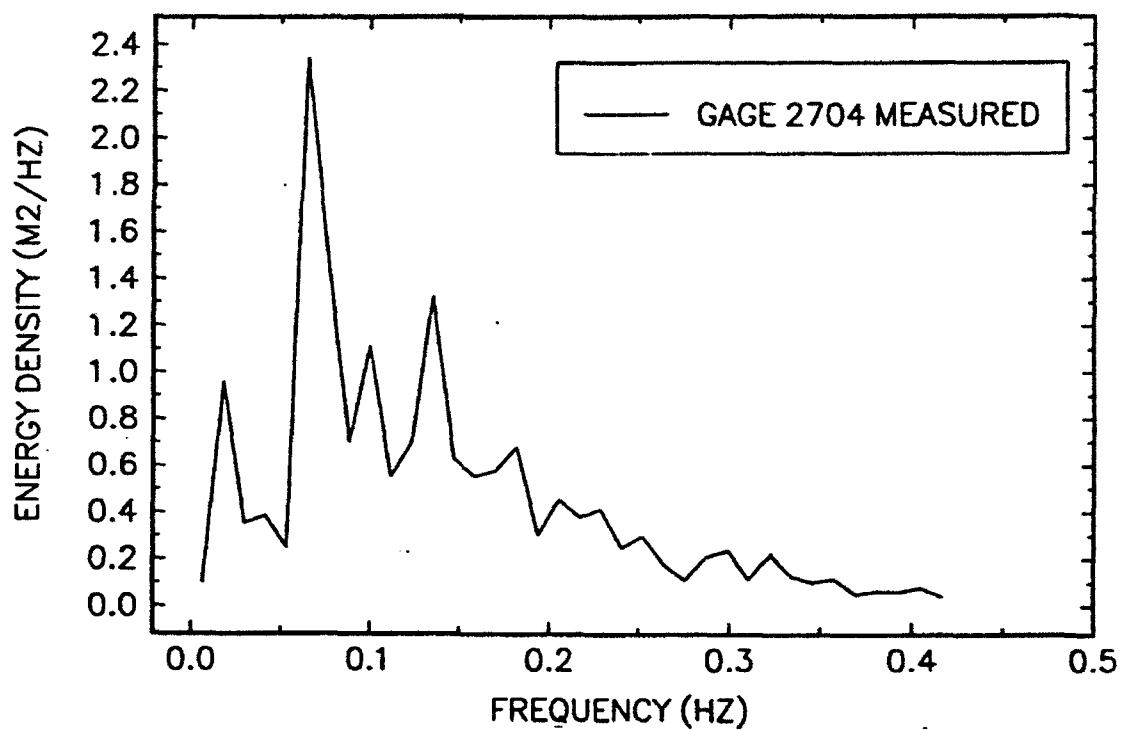
17-MINUTE RECORD BEGINNING AT 1658



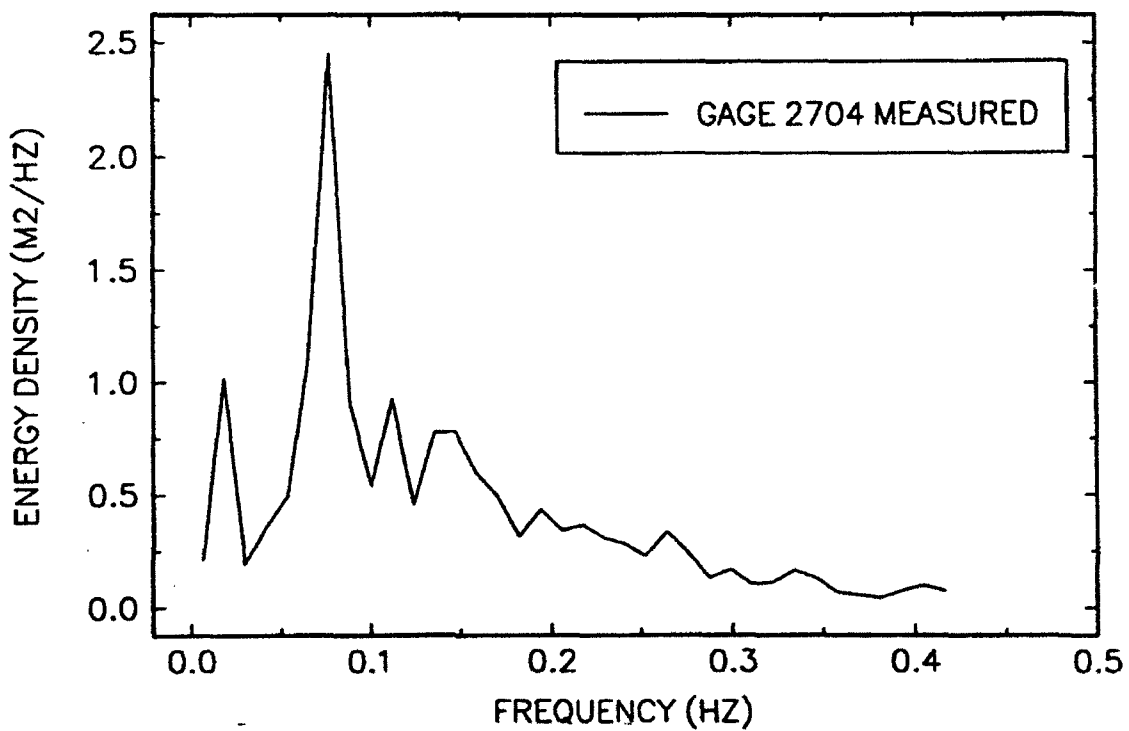
17-MINUTE RECORD BEGINNING AT 1715



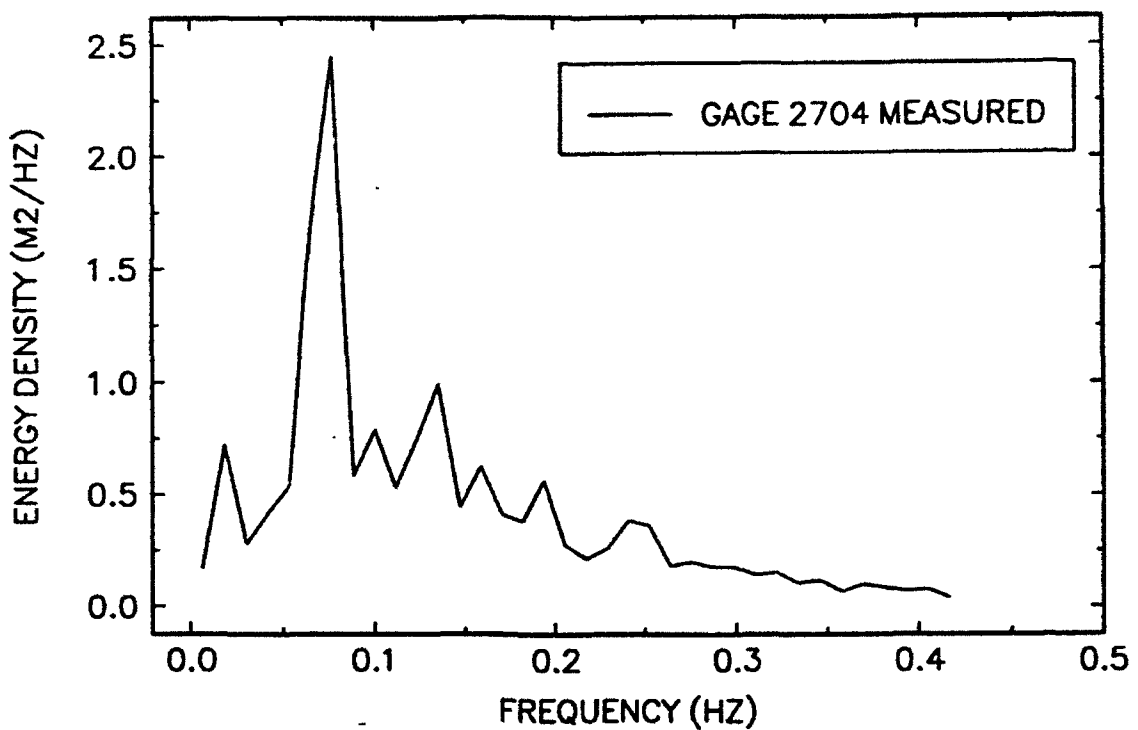
17-MINUTE RECORD BEGINNING AT 1732



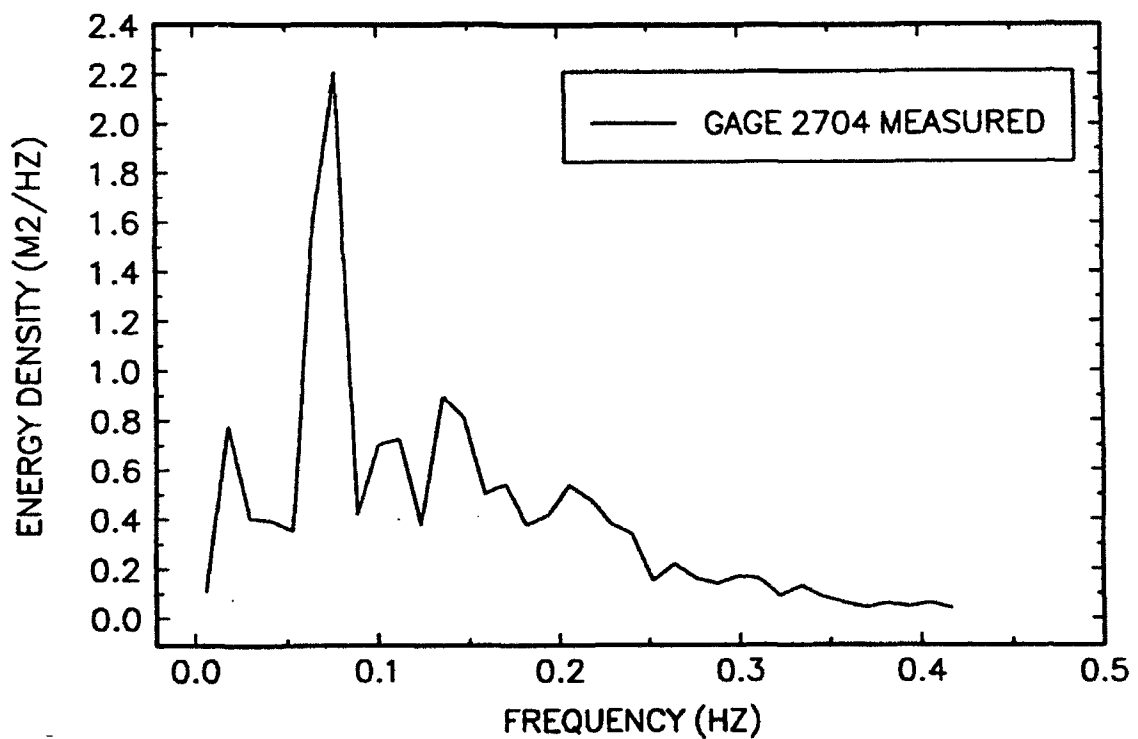
17-MINUTE RECORD BEGINNING AT 1749



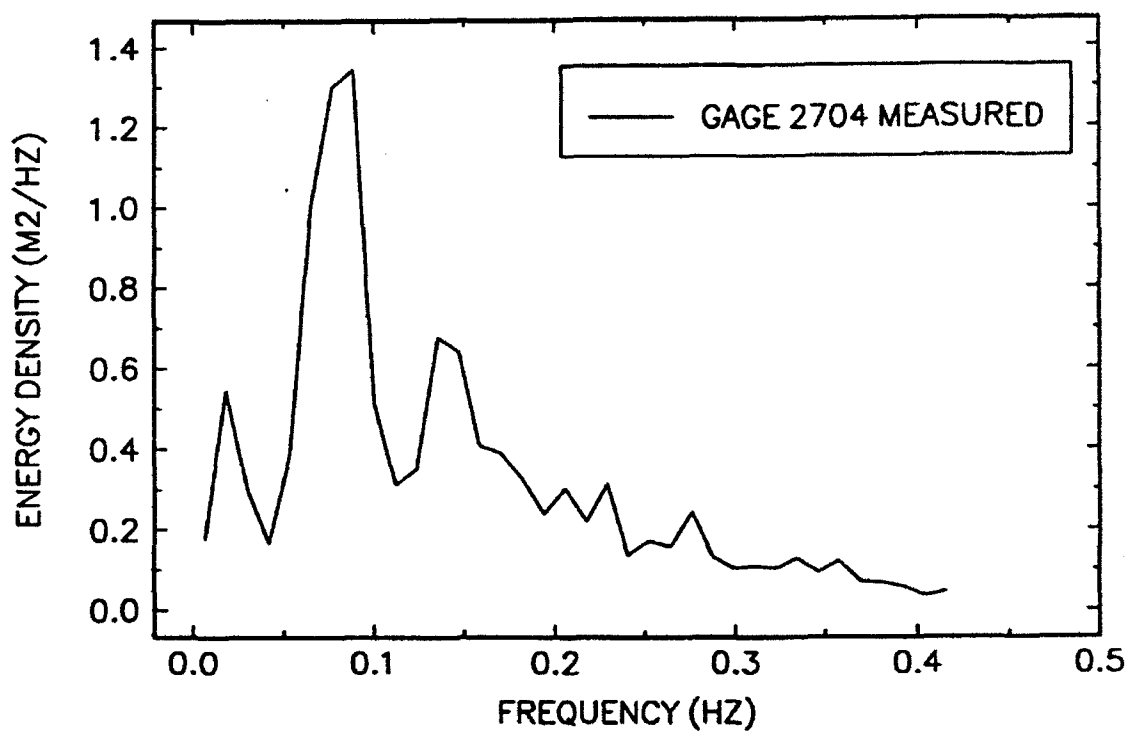
17-MINUTE RECORD BEGINNING AT 1806



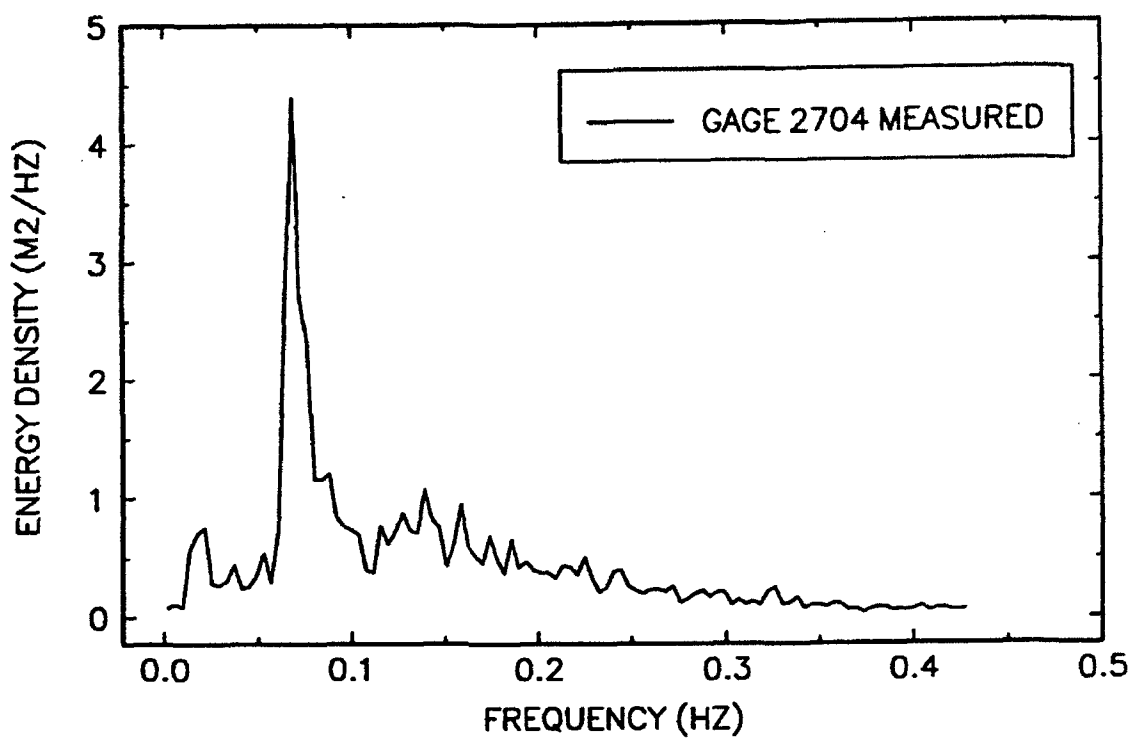
17-MINUTE RECORD BEGINNING AT 1824



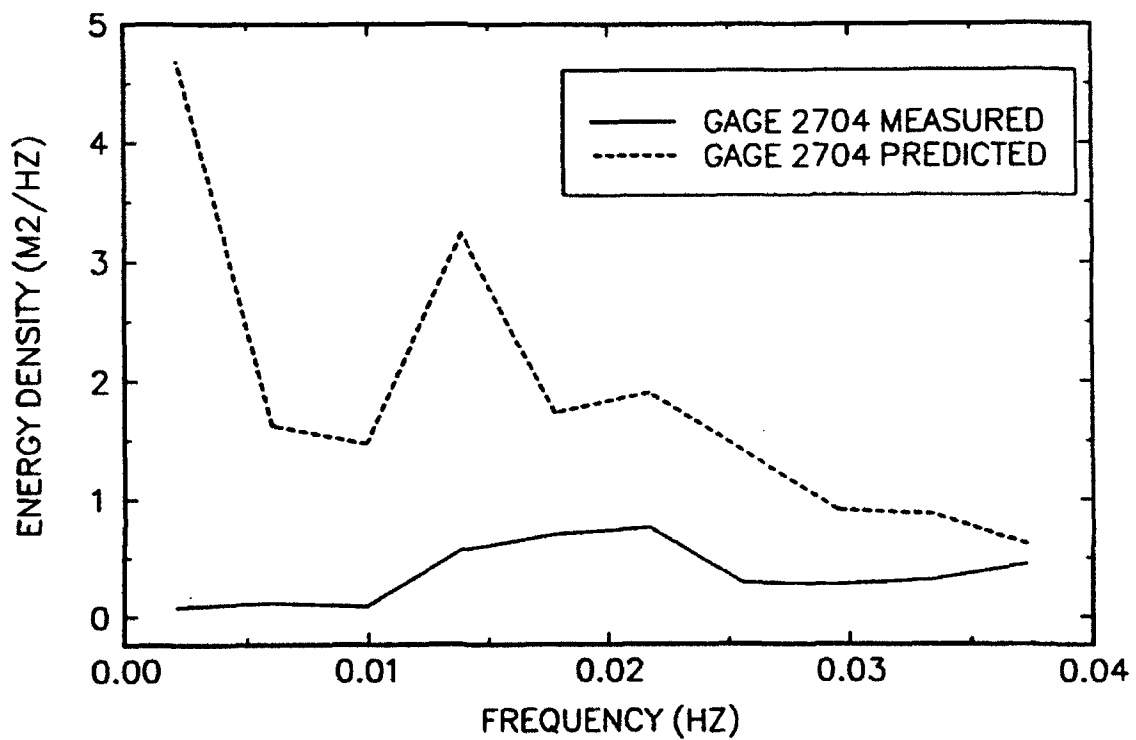
17-MINUTE RECORD BEGINNING AT 1841



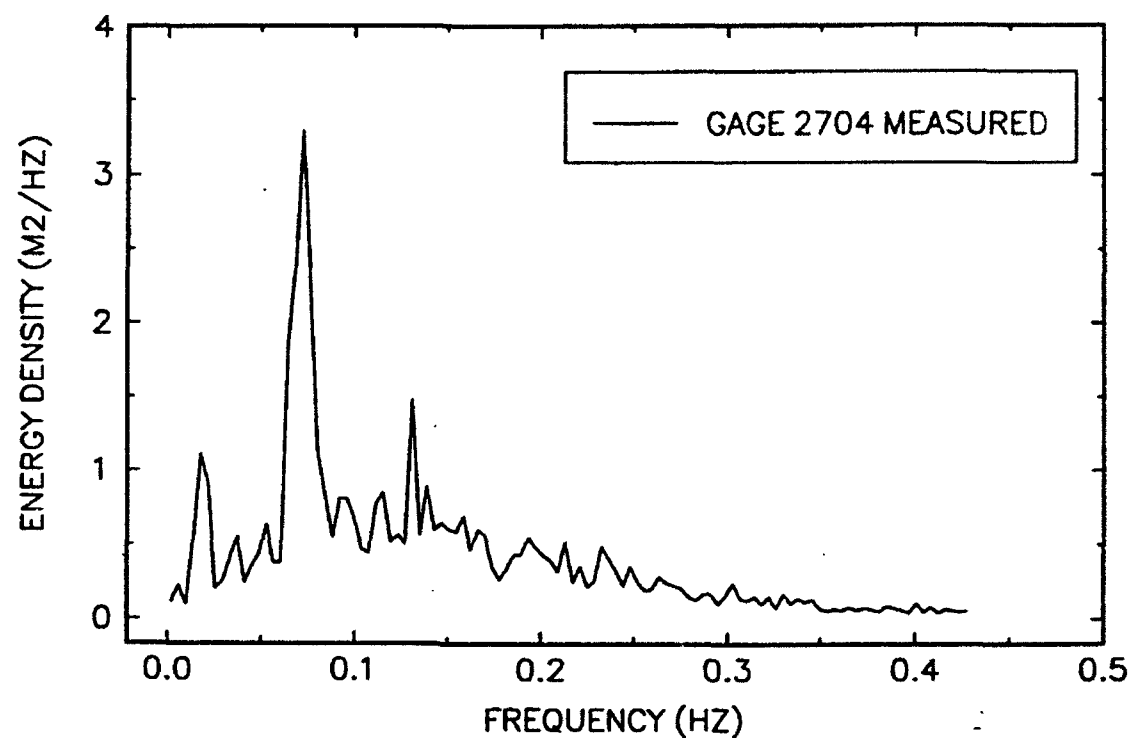
51-MINUTE RECORD BEGINNING AT 1658



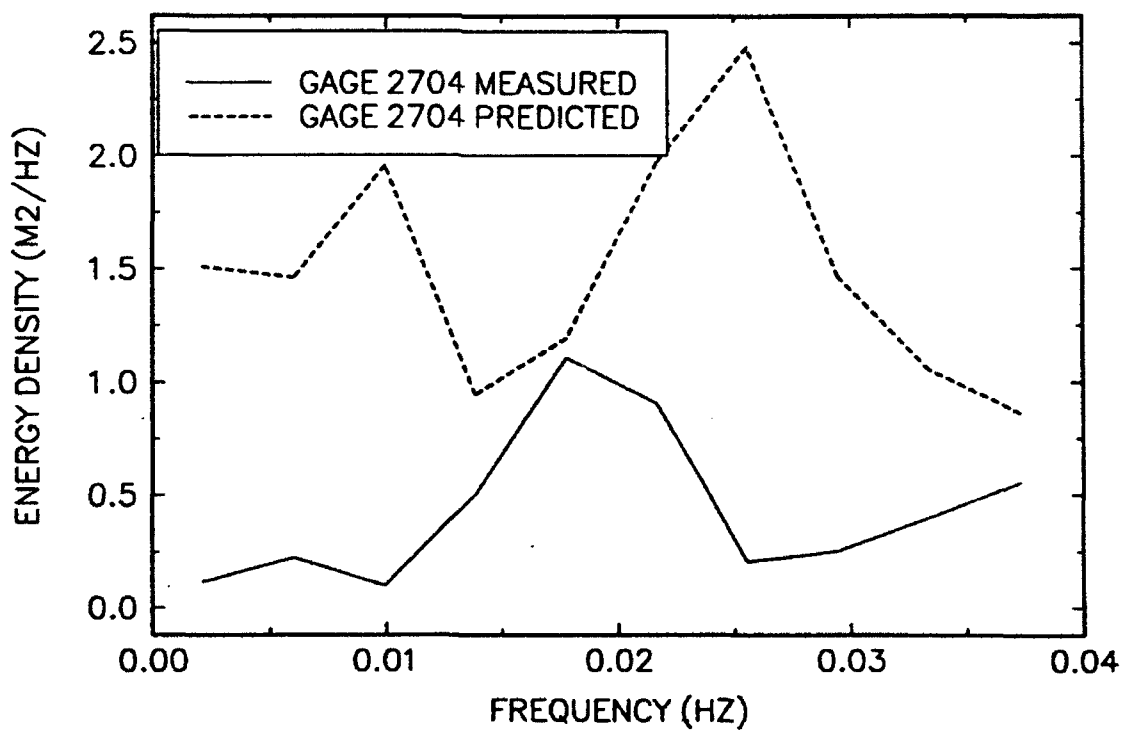
51-MINUTE RECORD BEGINNING AT 1658



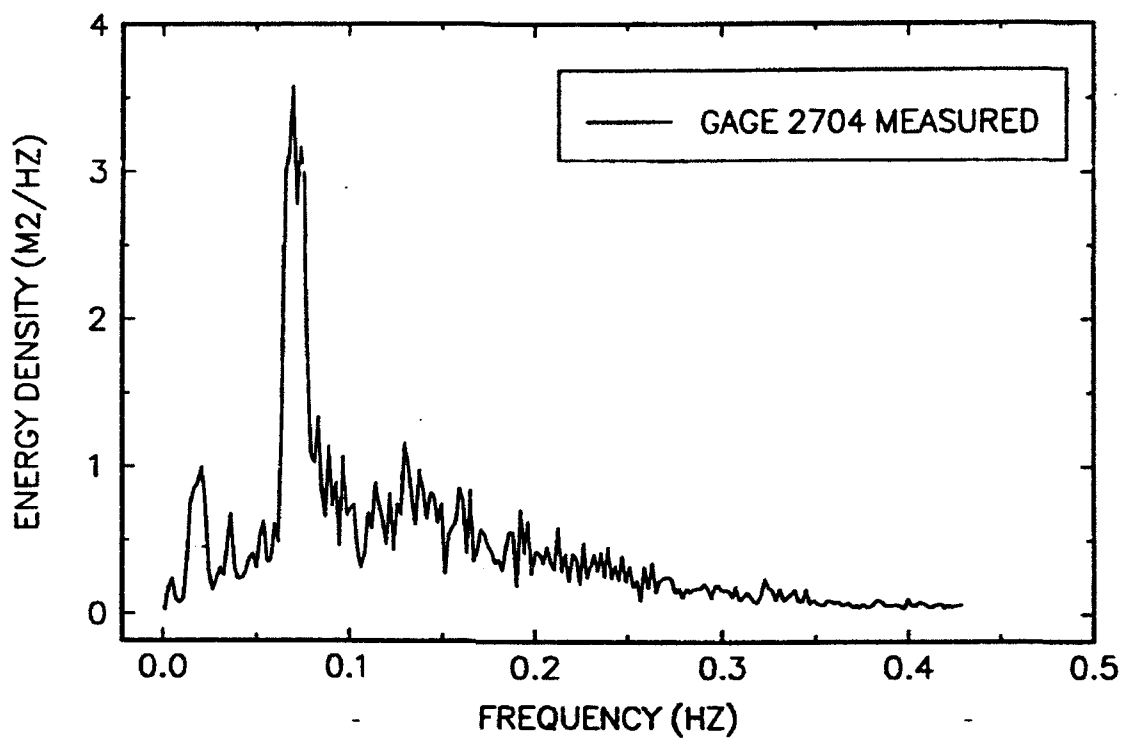
51-MINUTE RECORD BEGINNING AT 1749



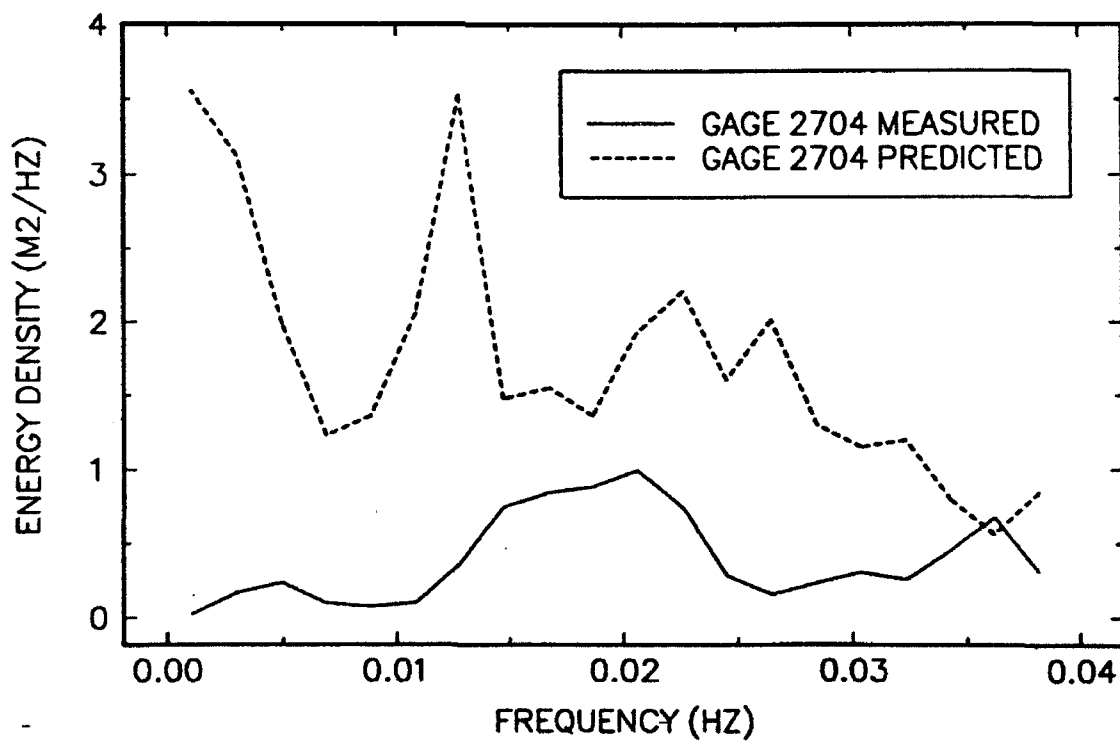
51-MINUTE RECORD BEGINNING AT 1749



102-MINUTE RECORD BEGINNING AT 1658



102-MINUTE RECORD BEGINNING AT 1658

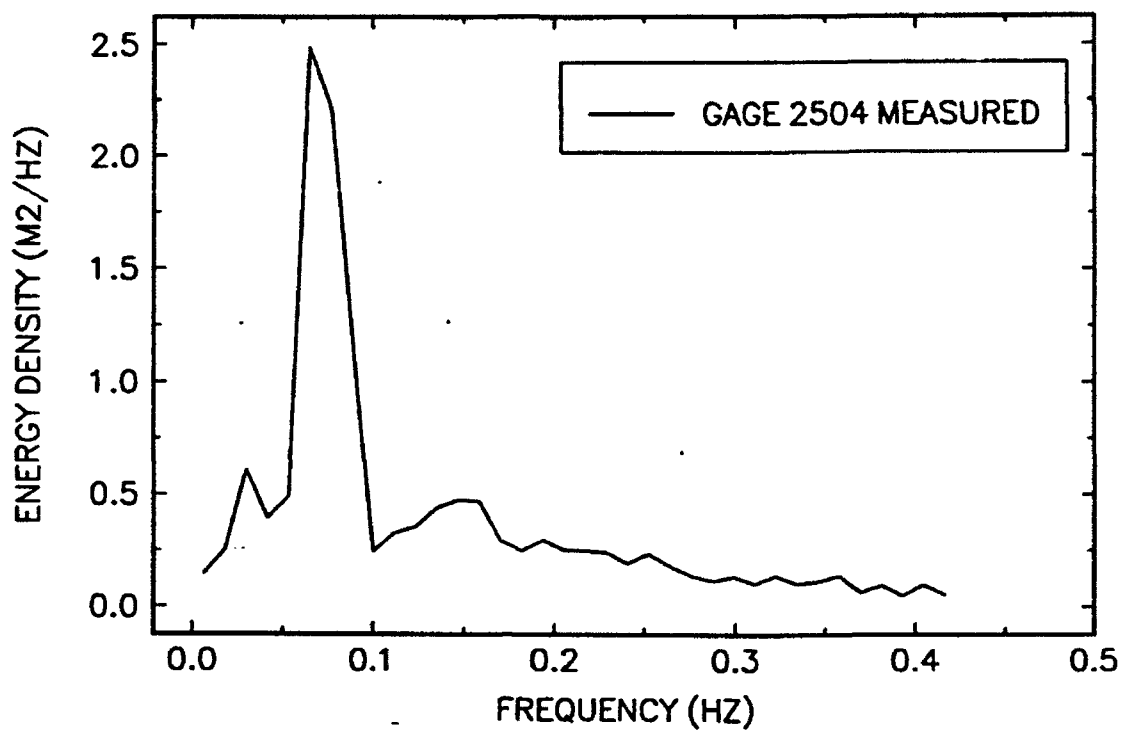


Appendix H

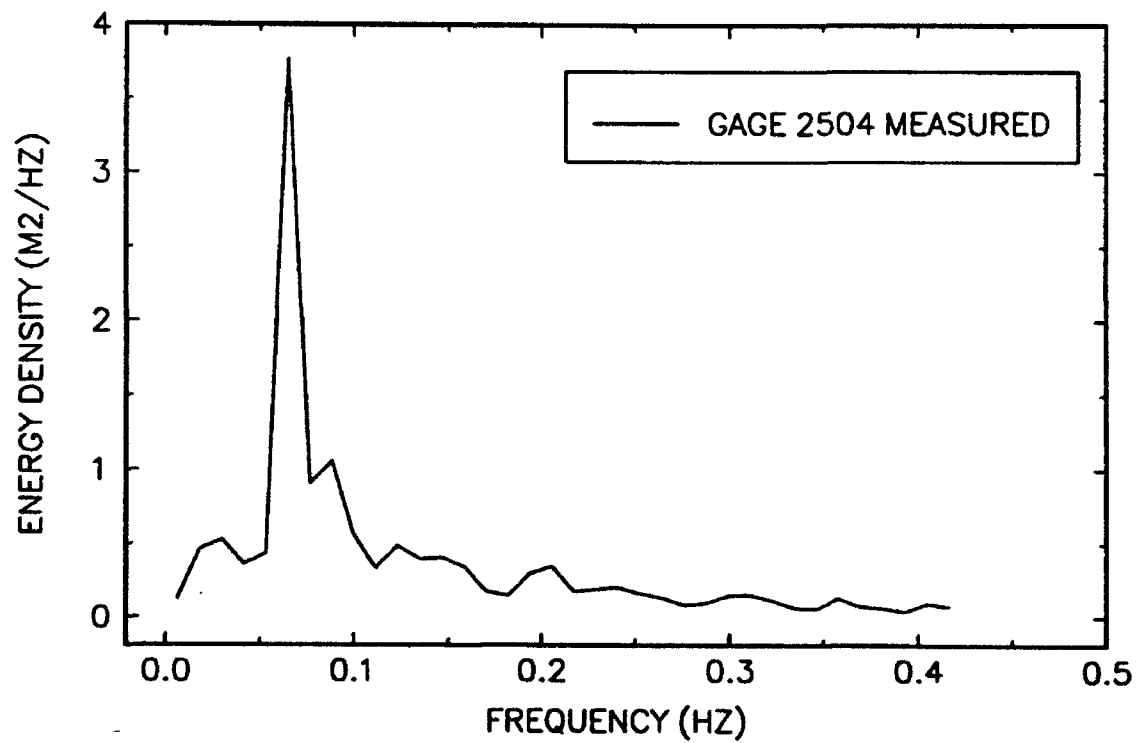
Short and Long Wave Spectra

from Field Data, Gage 2504

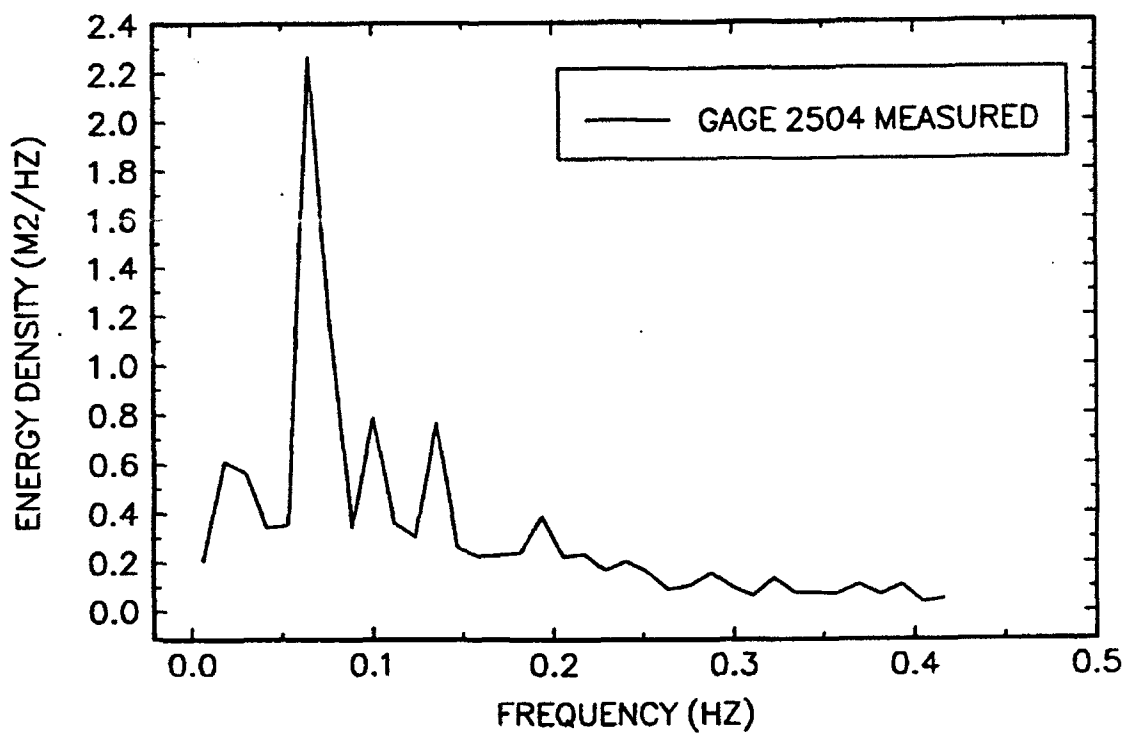
17-MINUTE RECORD BEGINNING AT 1658



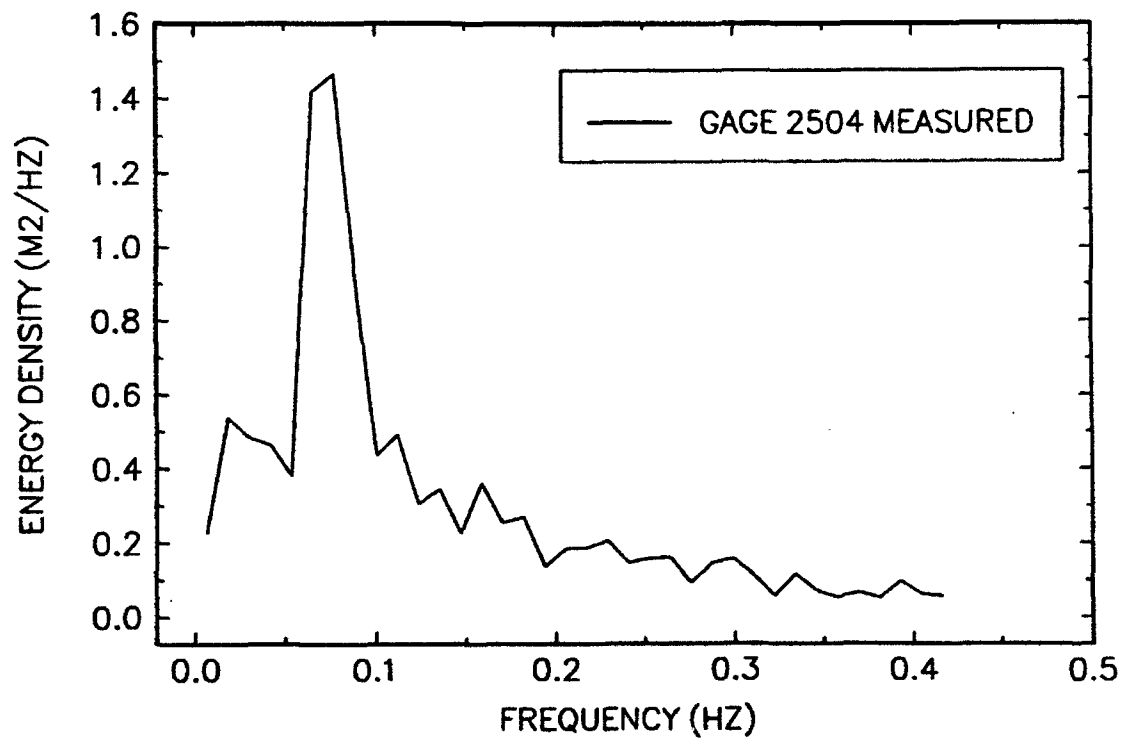
17-MINUTE RECORD BEGINNING AT 1715



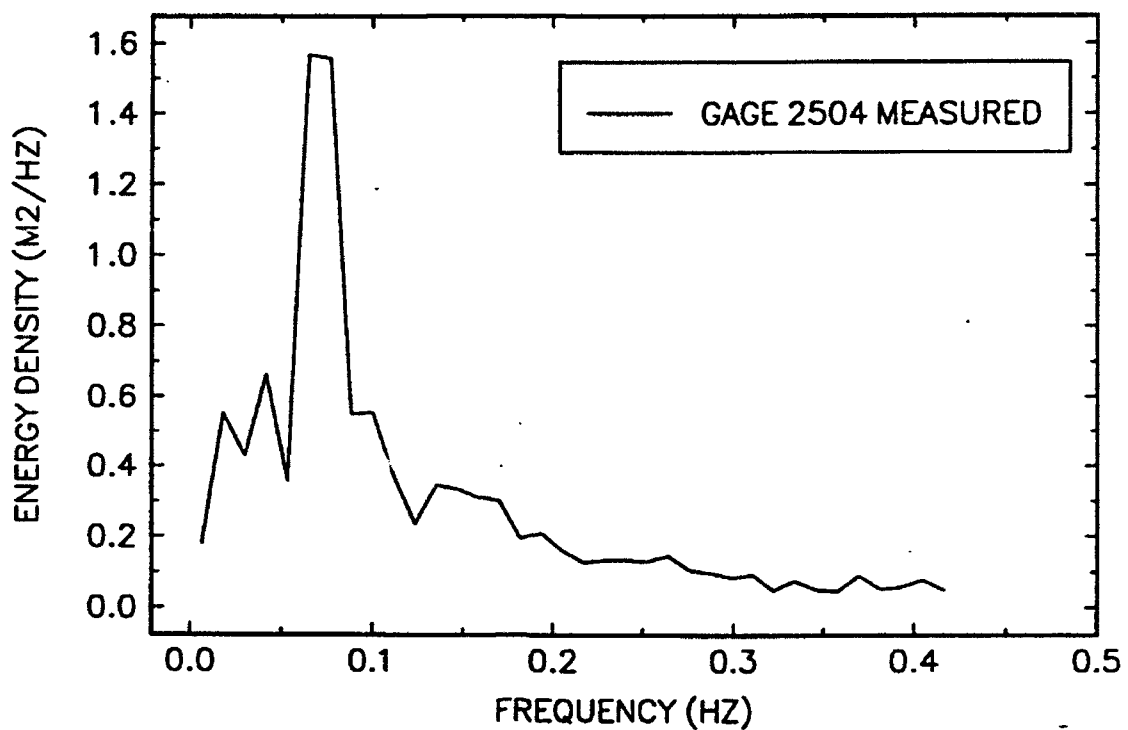
17-MINUTE RECORD BEGINNING AT 1732



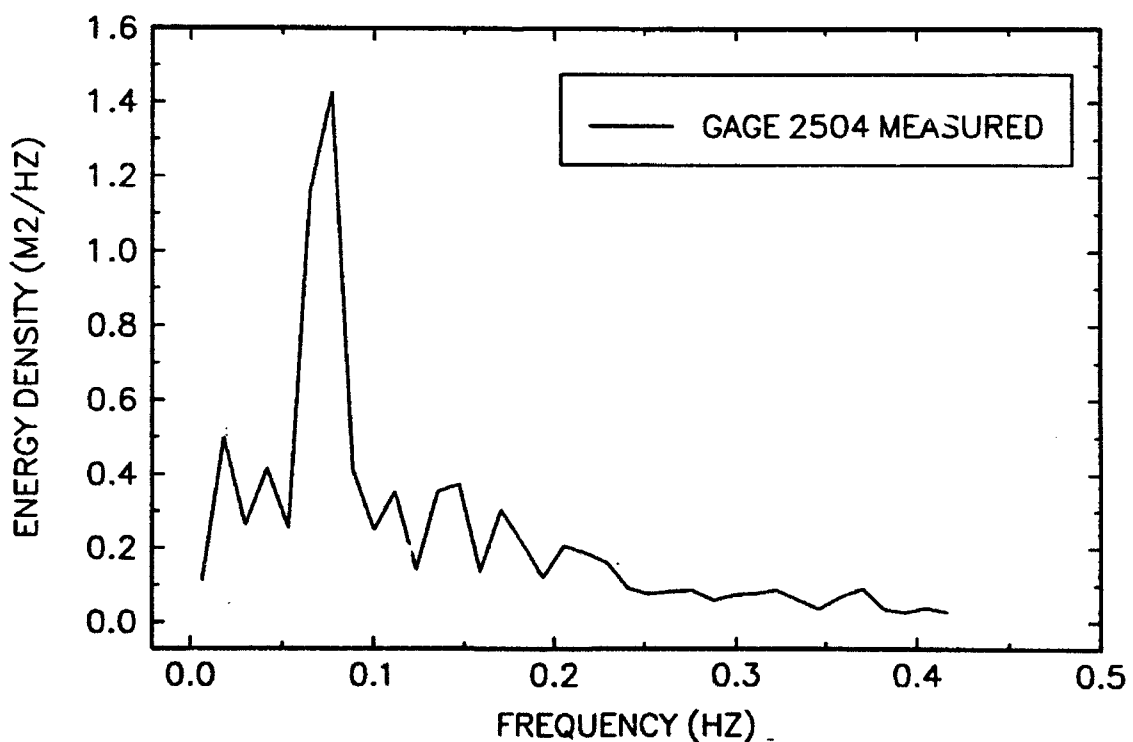
17-MINUTE RECORD BEGINNING AT 1749



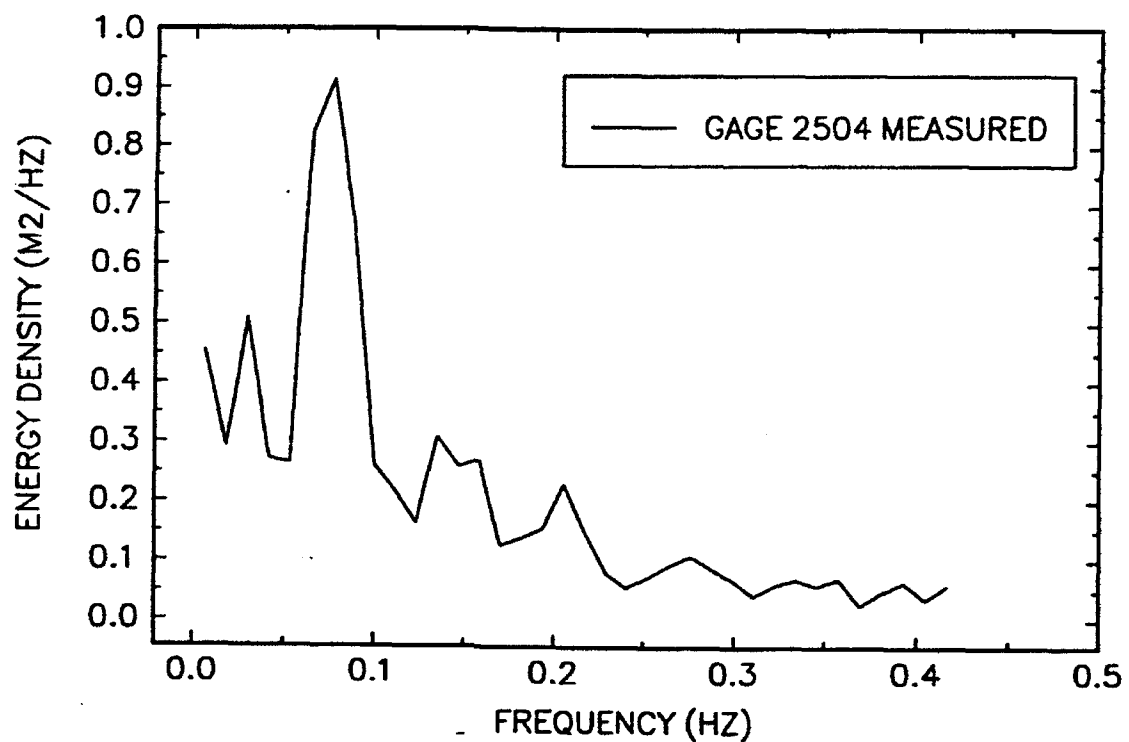
17-MINUTE RECORD BEGINNING AT 1806



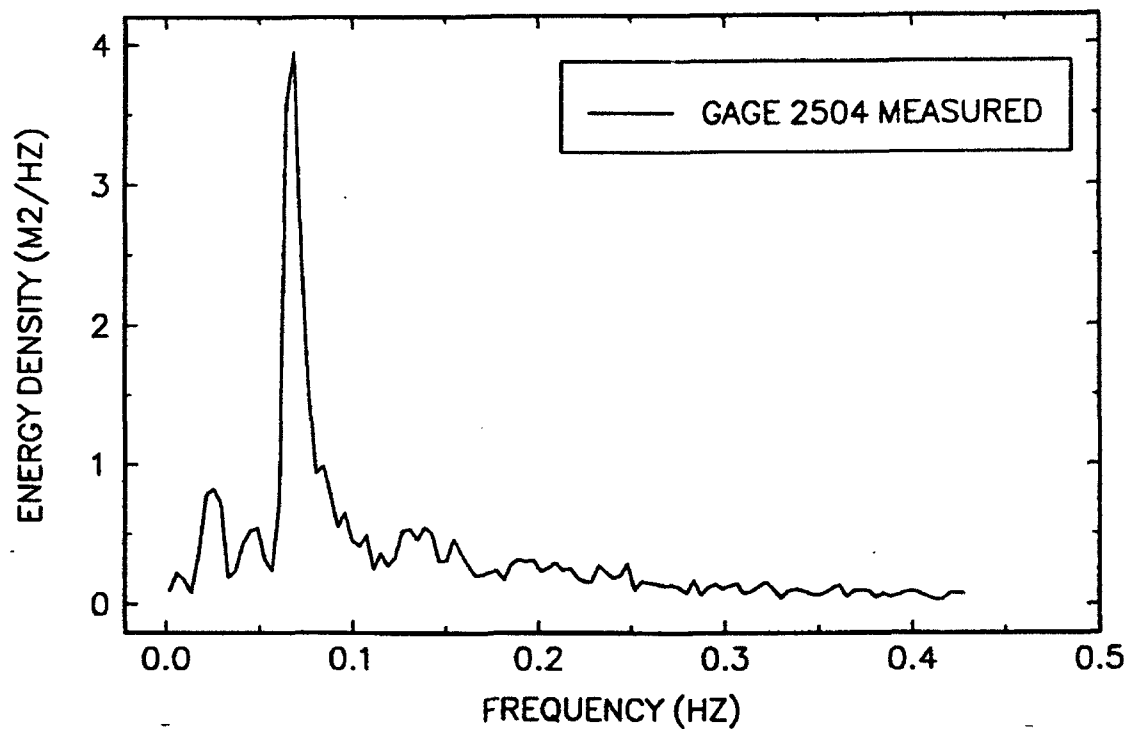
17-MINUTE RECORD BEGINNING AT 1824



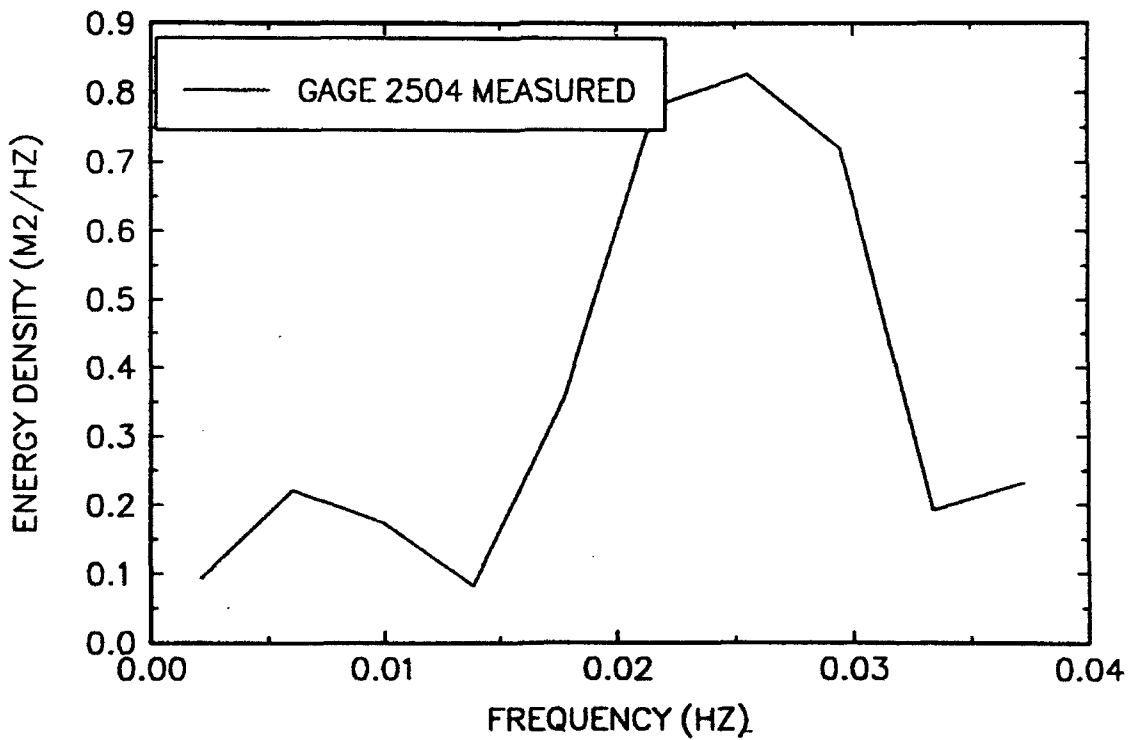
17-MINUTE RECORD BEGINNING AT 1841



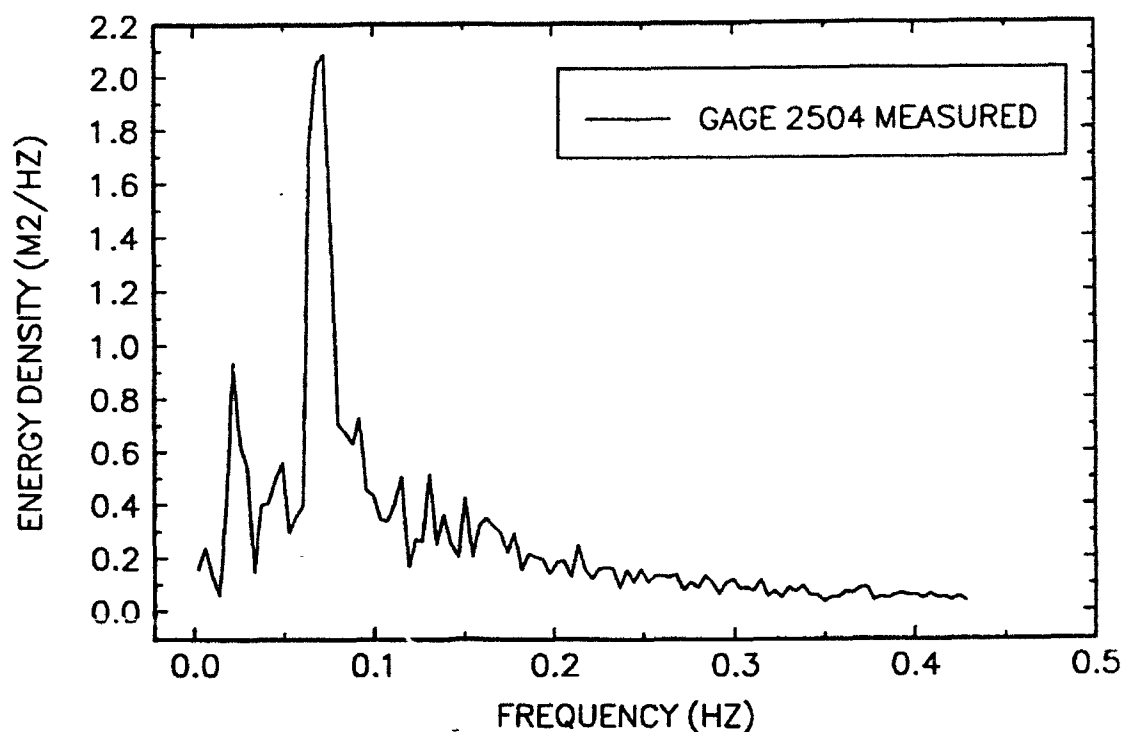
51-MINUTE RECORD BEGINNING AT 1658



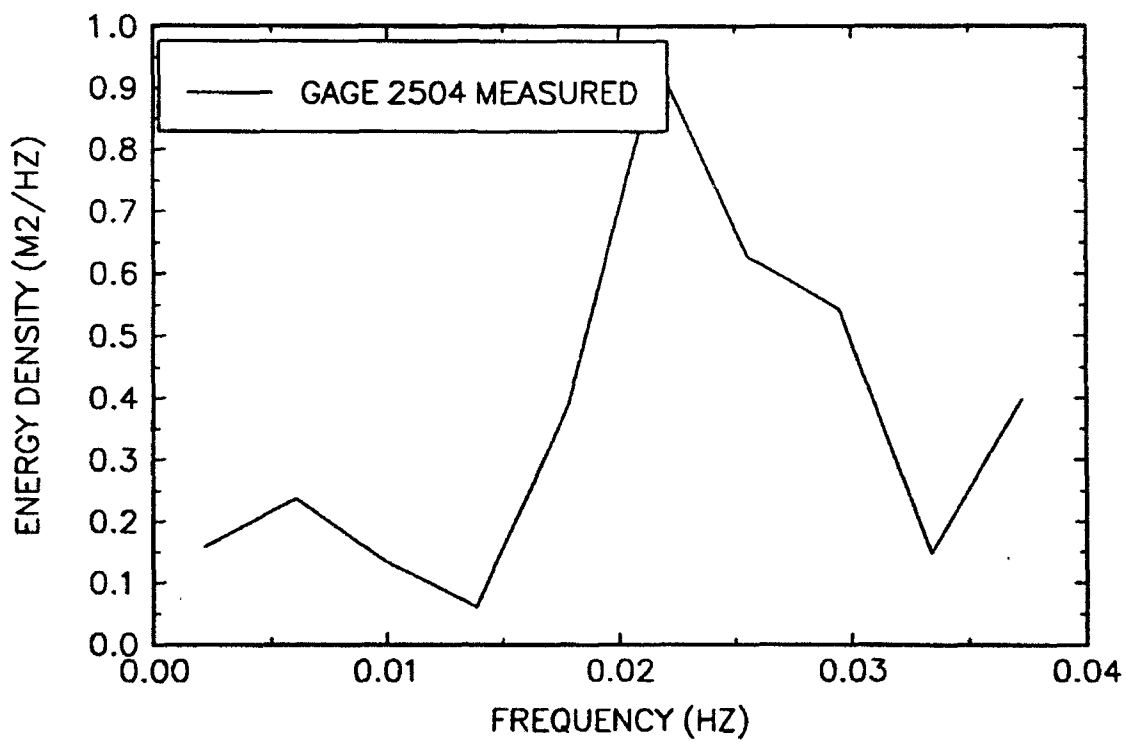
51-MINUTE RECORD BEGINNING AT 1658



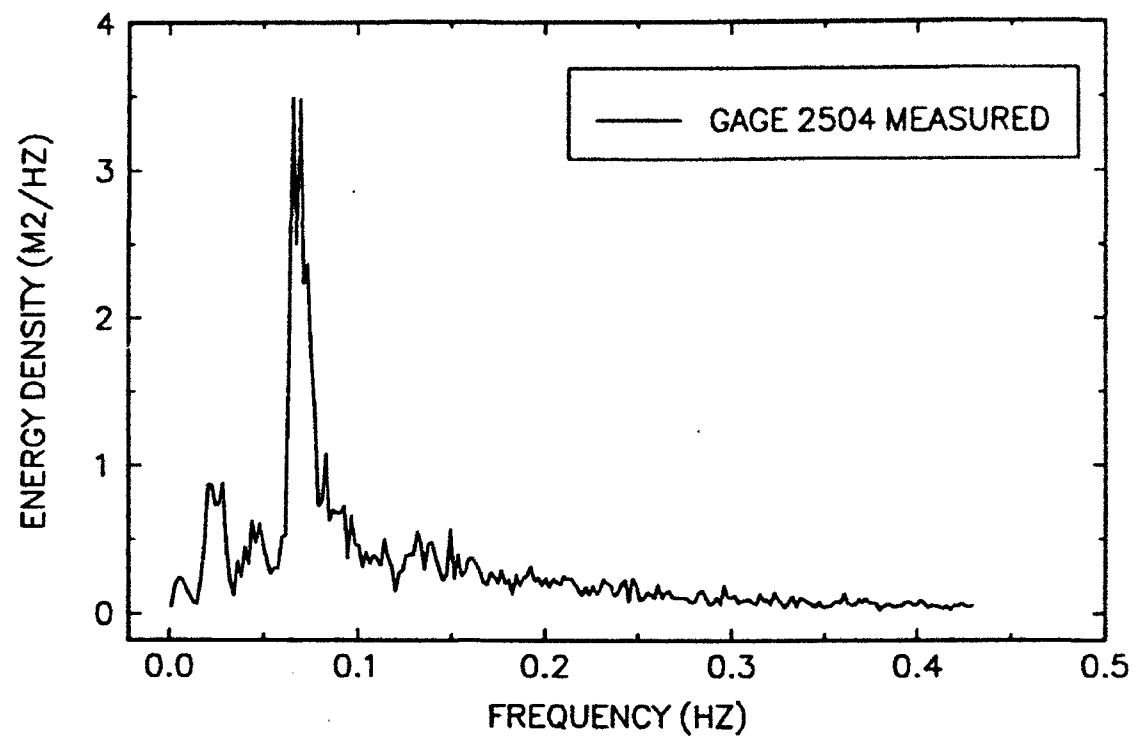
51-MINUTE RECORD BEGINNING AT 1749



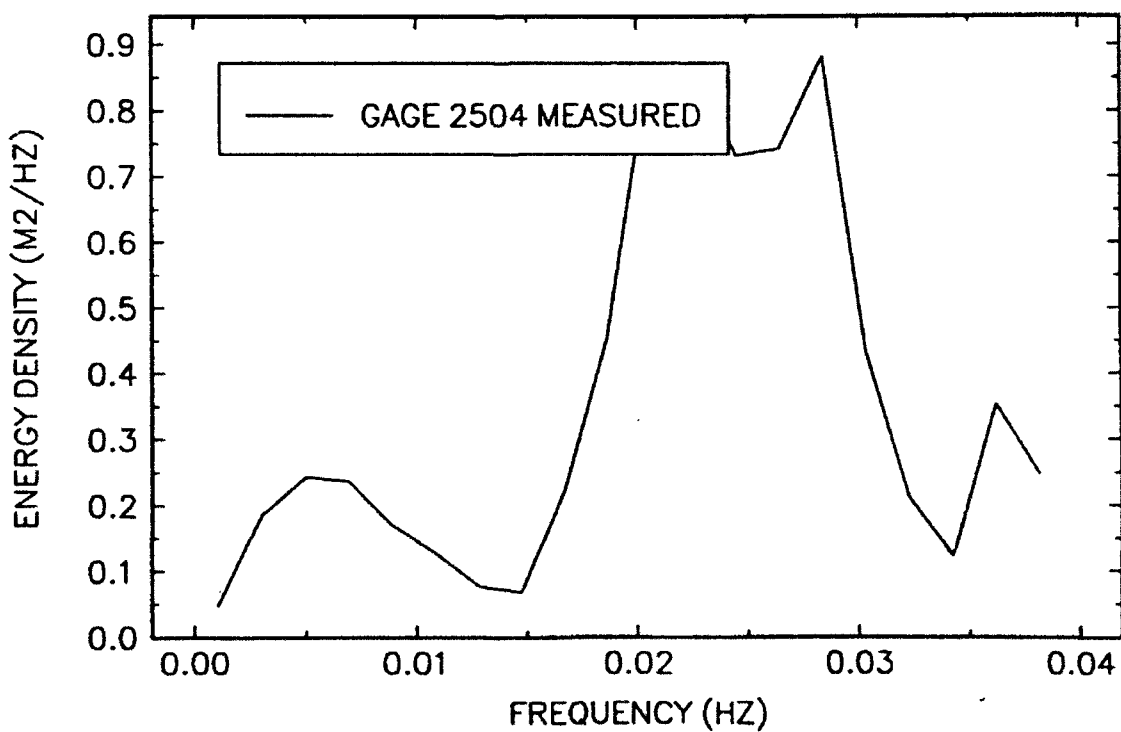
51-MINUTE RECORD BEGINNING AT 1749



102-MINUTE RECORD BEGINNING AT 1658



102-MINUTE RECORD BEGINNING AT 1658

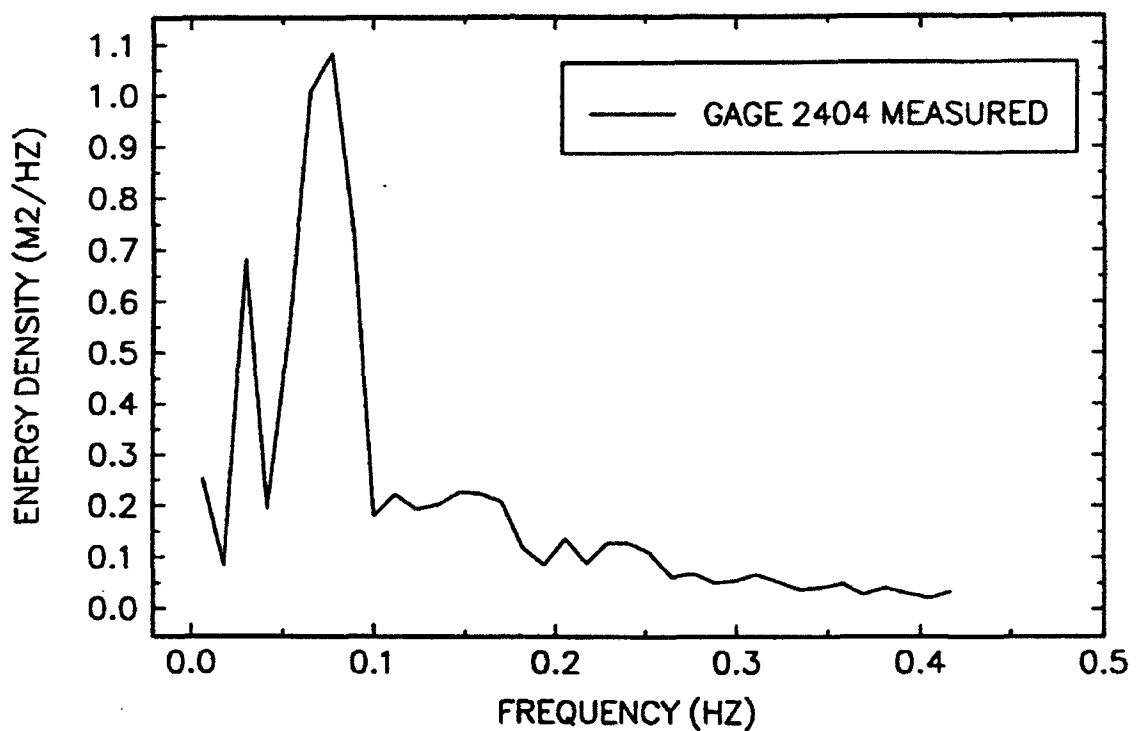


Appendix I

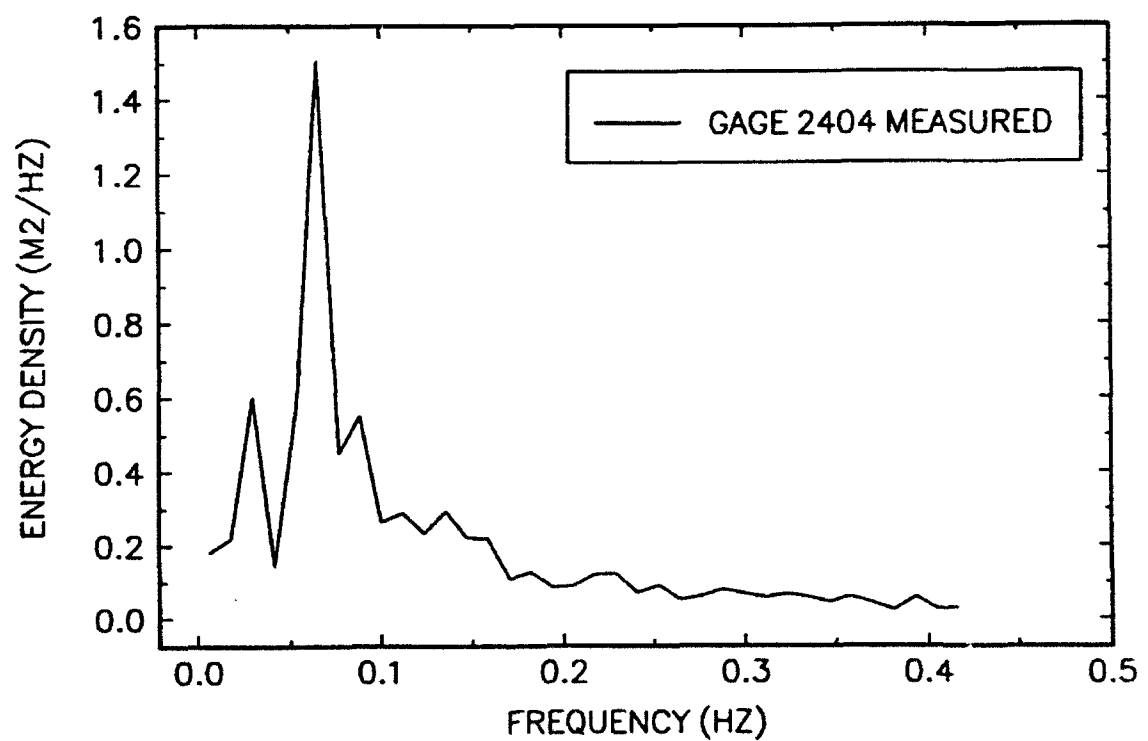
Short and Long Wave Spectra

from Field Data, Gage 2404

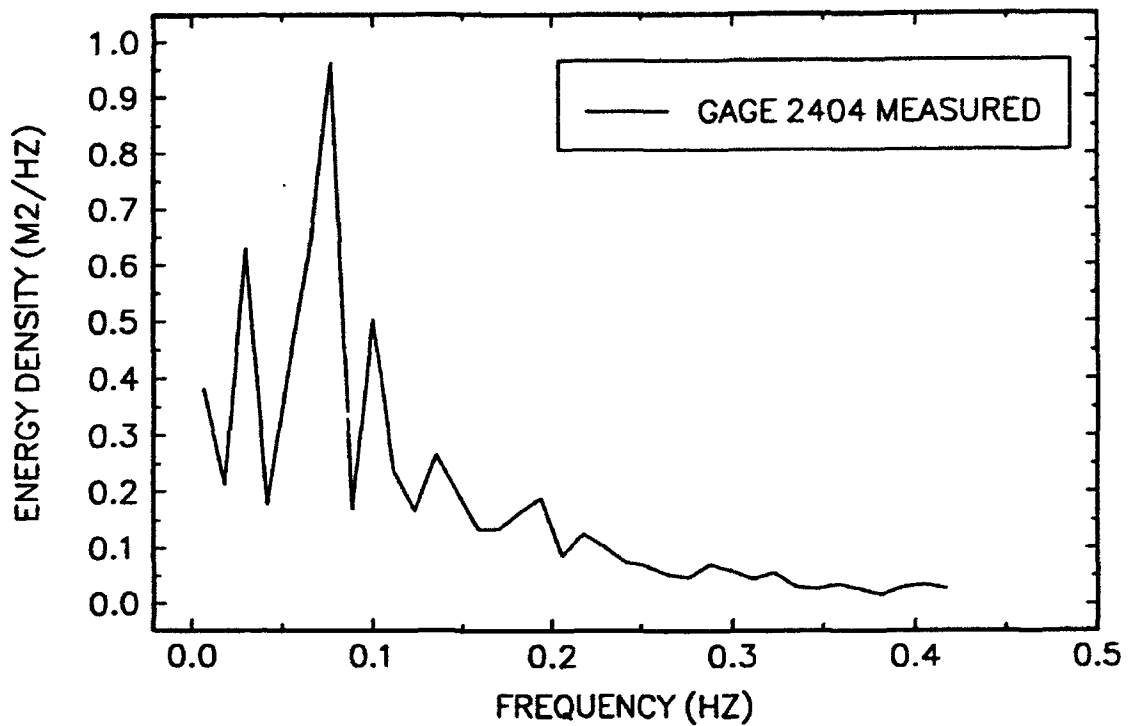
17-MINUTE RECORD BEGINNING AT 1658



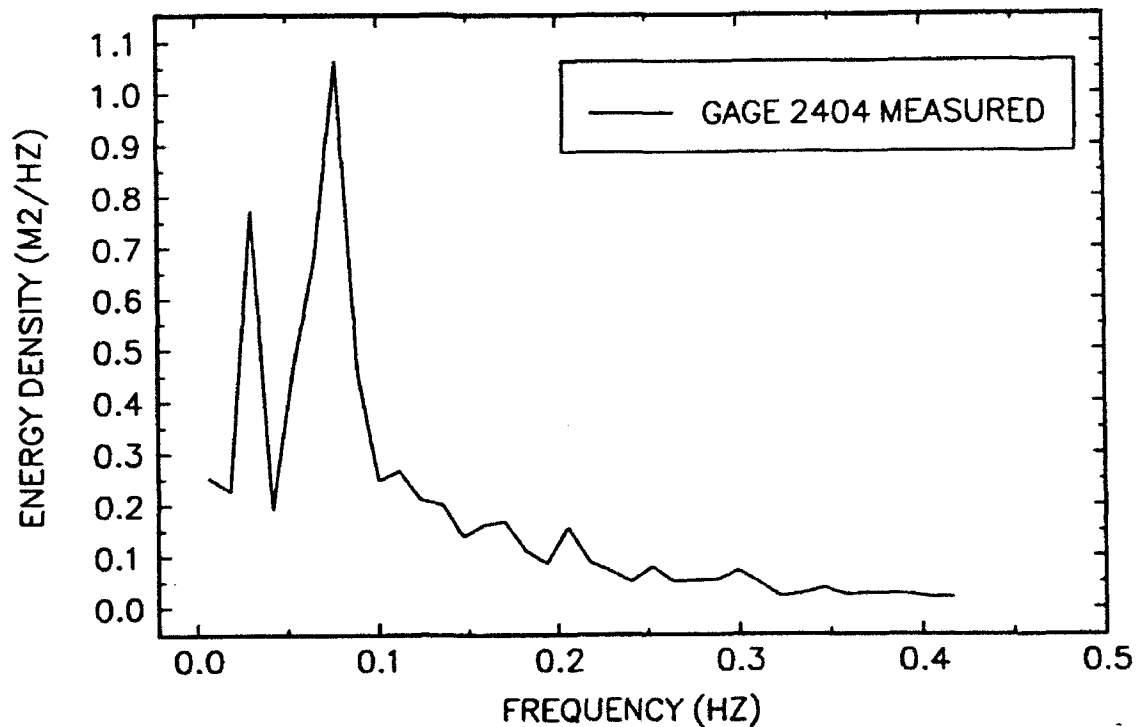
17-MINUTE RECORD BEGINNING AT 1715



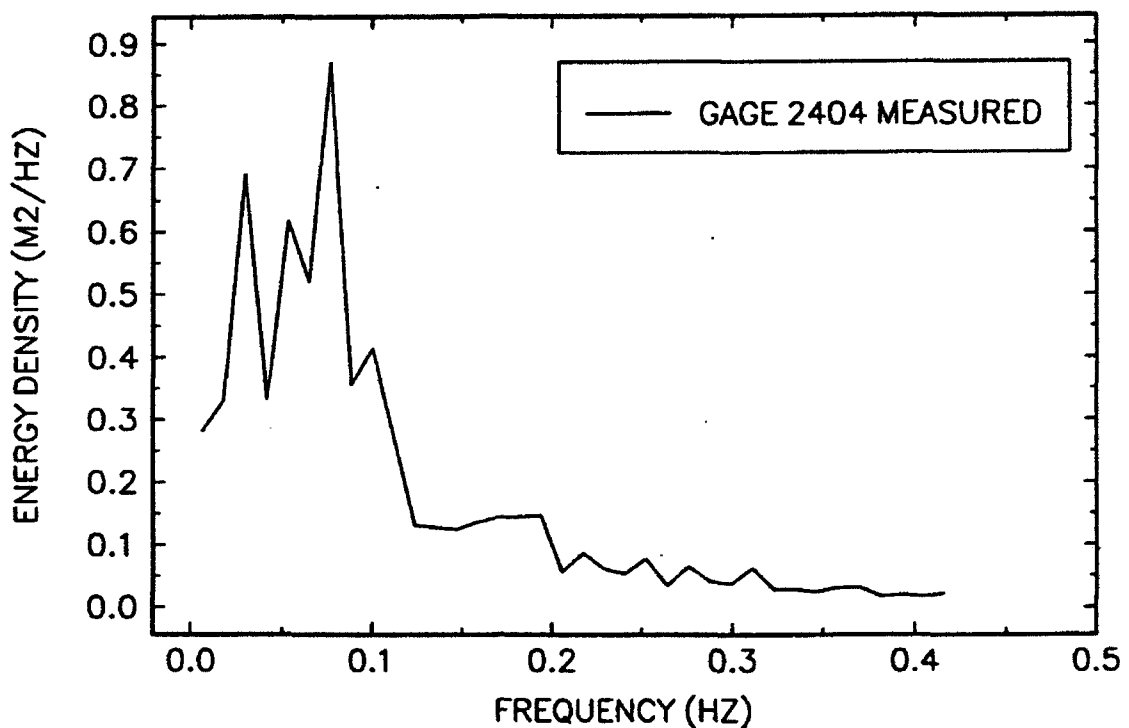
17-MINUTE RECORD BEGINNING AT 1732



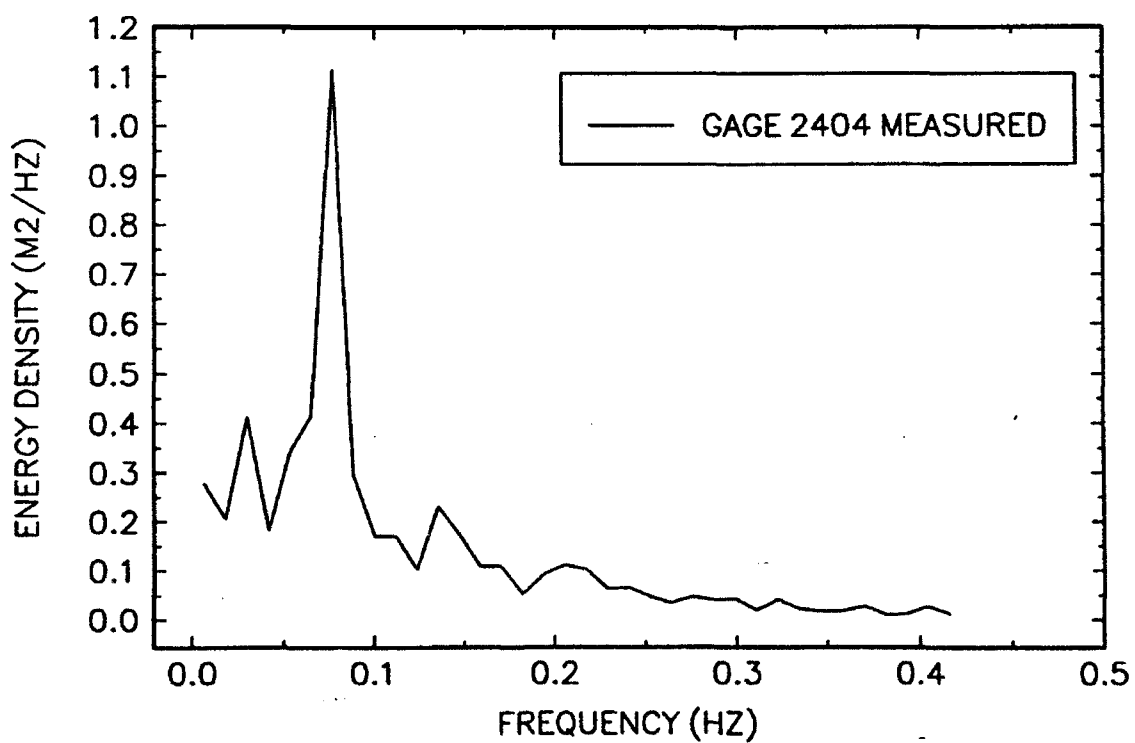
17-MINUTE RECORD BEGINNING AT 1749



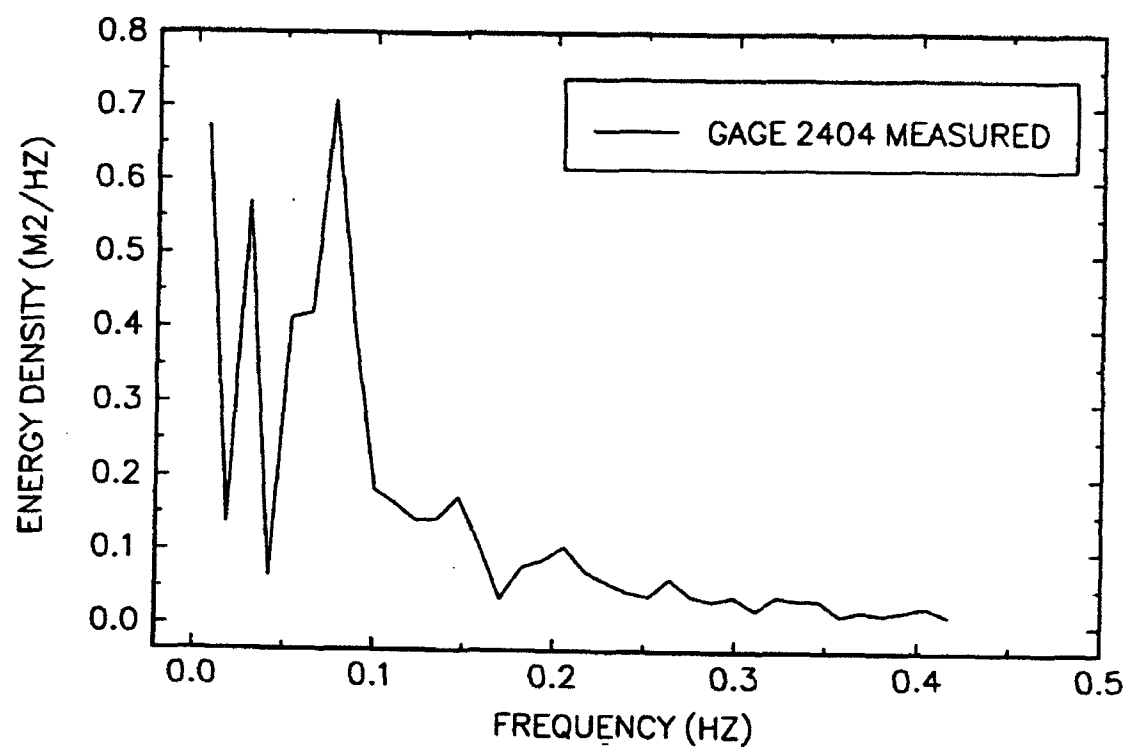
17-MINUTE RECORD BEGINNING AT 1806



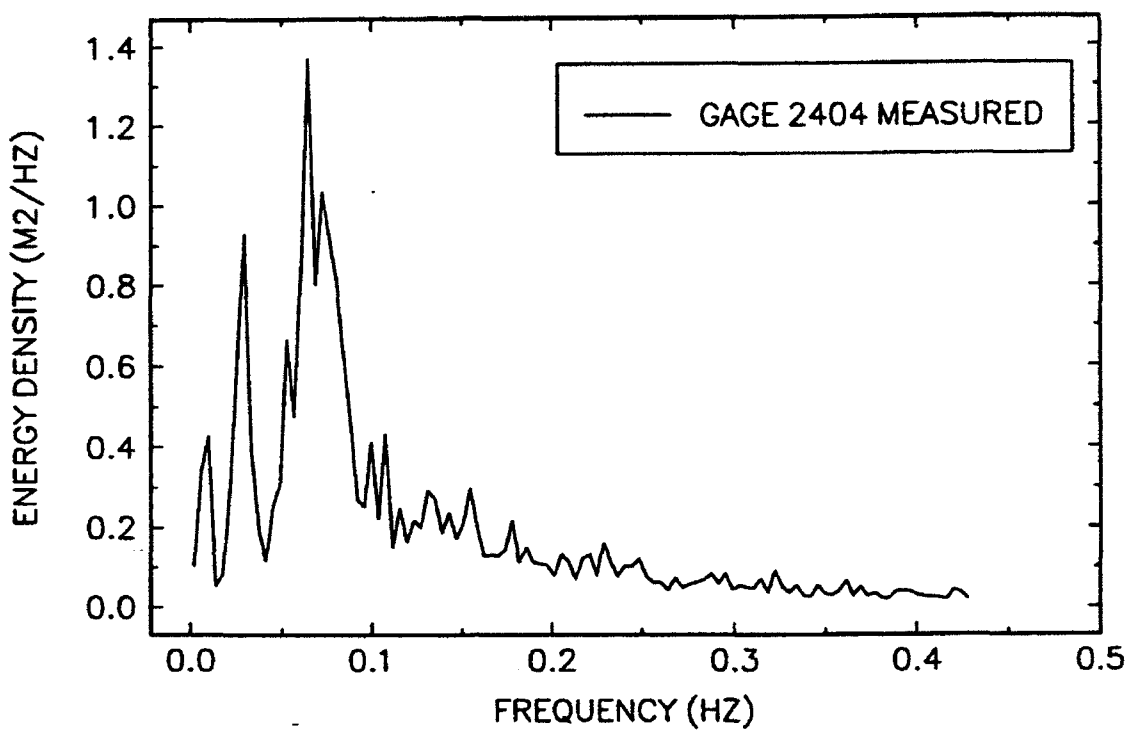
17-MINUTE RECORD BEGINNING AT 1824



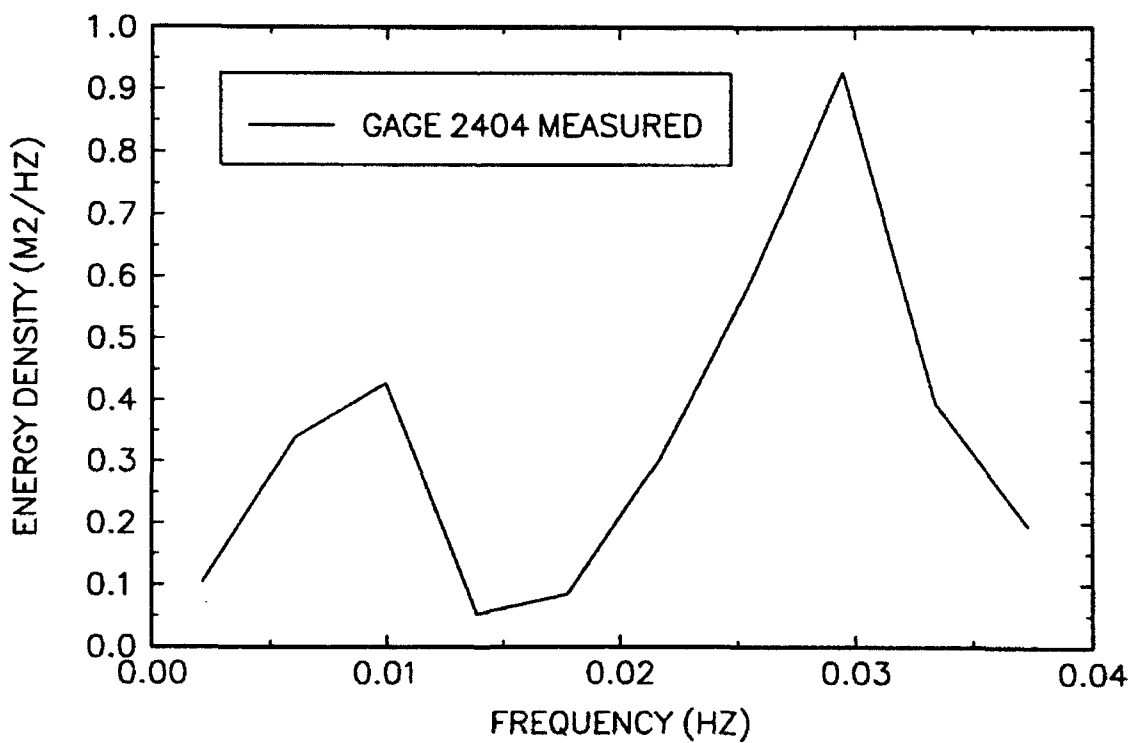
17-MINUTE RECORD BEGINNING AT 1841



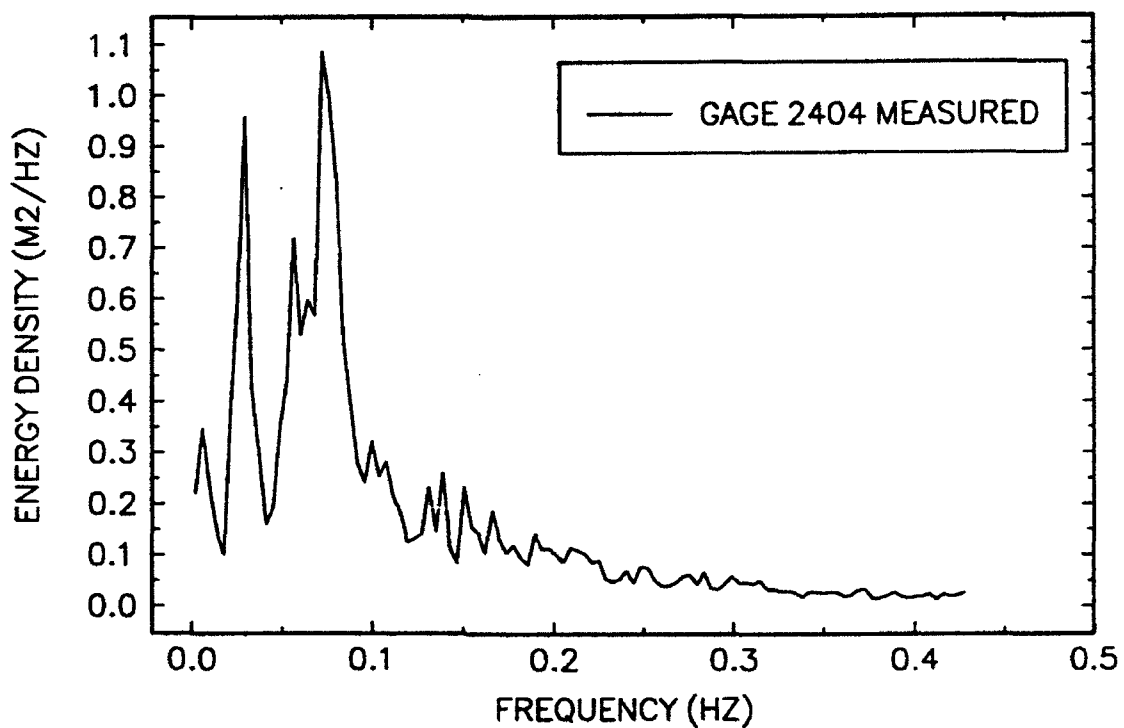
51-MINUTE RECORD BEGINNING AT 1658



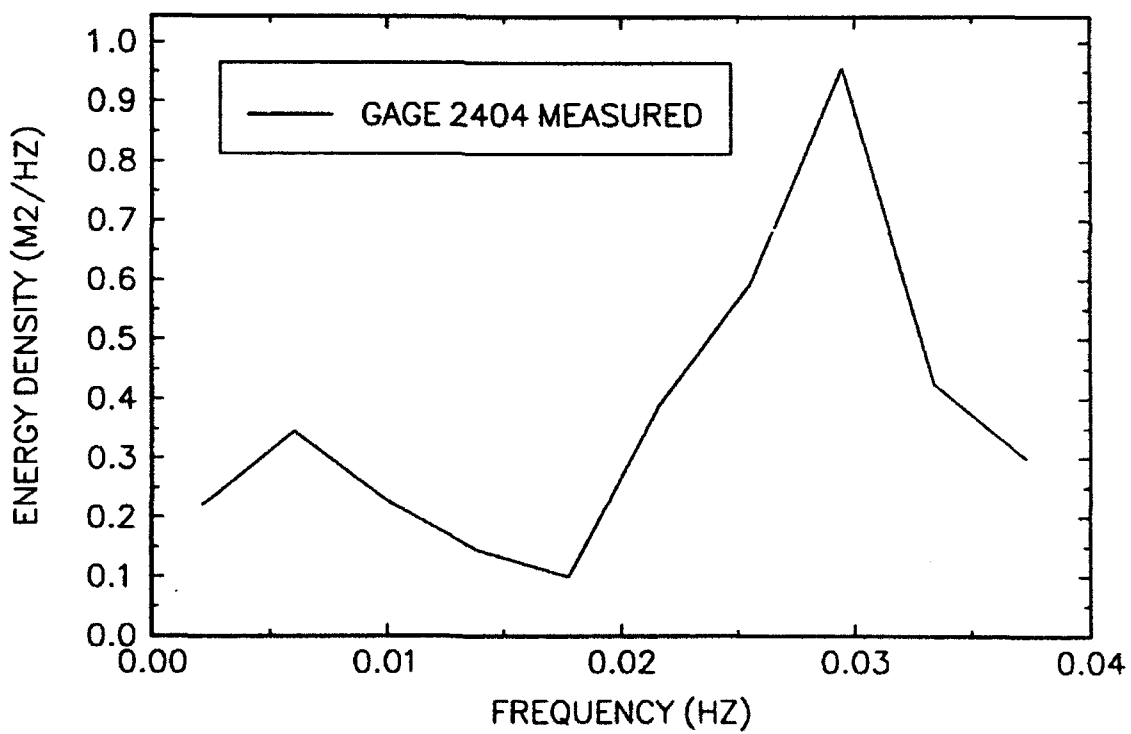
51-MINUTE RECORD BEGINNING AT 1658



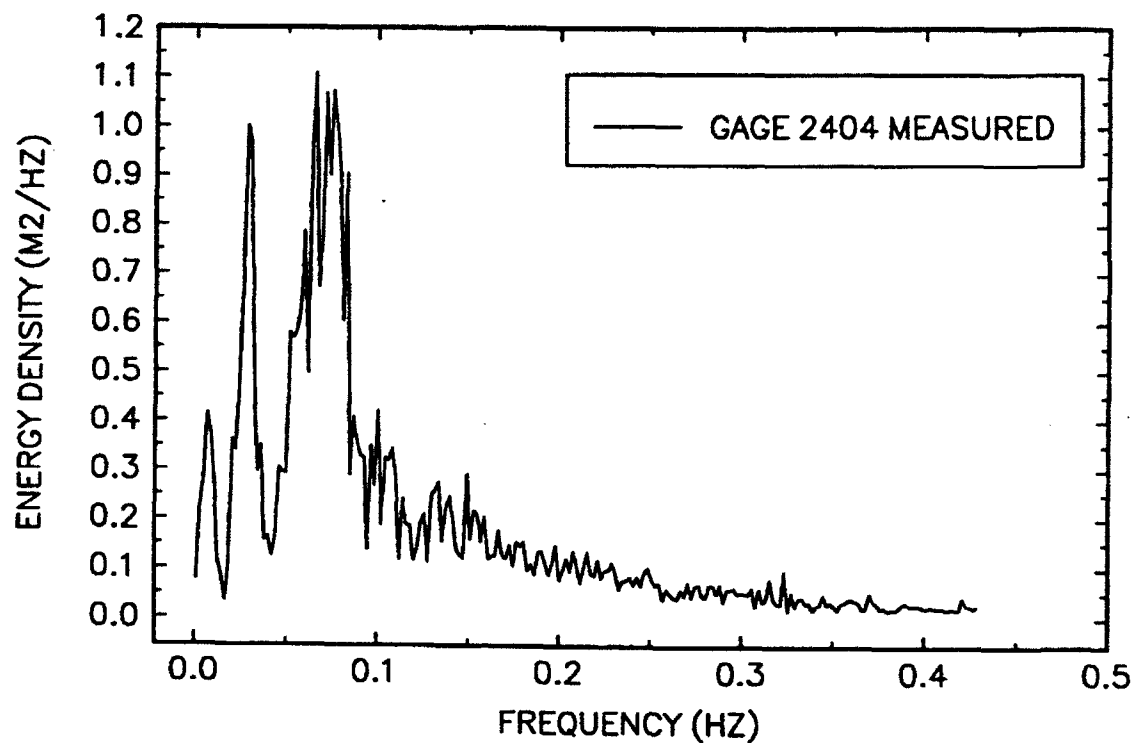
51-MINUTE RECORD BEGINNING AT 1749



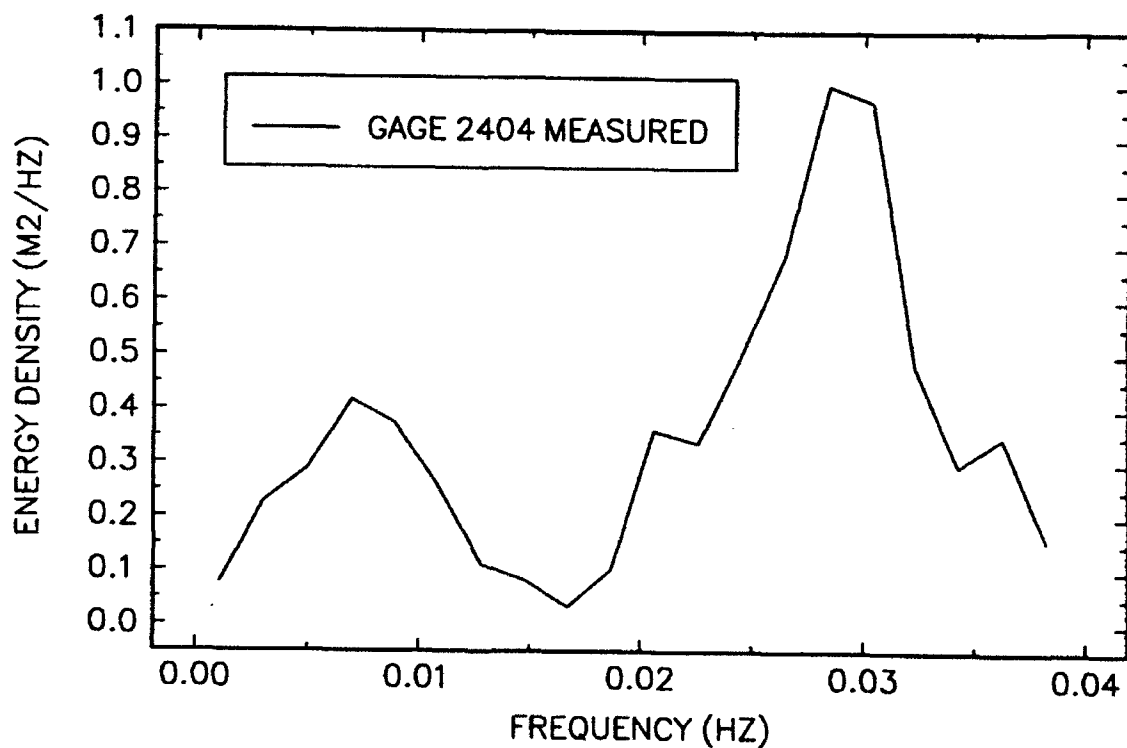
51-MINUTE RECORD BEGINNING AT 1749



102-MINUTE RECORD BEGINNING AT 1658



102-MINUTE RECORD BEGINNING AT 1658

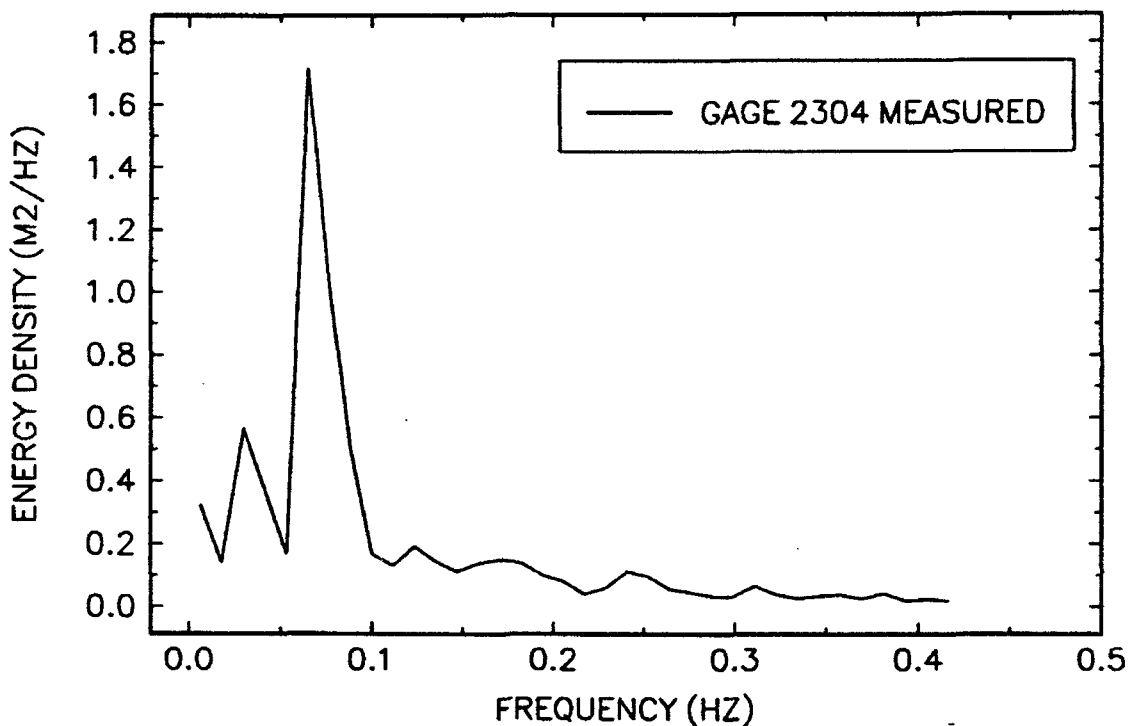


Appendix J

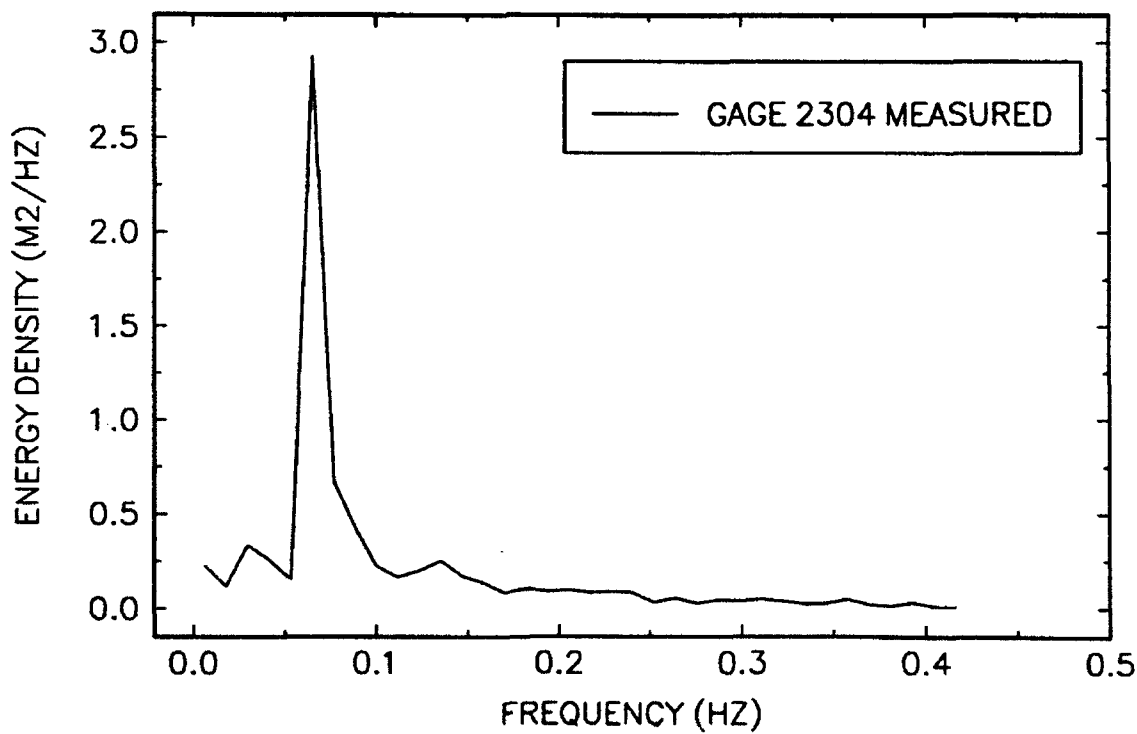
Short and Long Wave Spectra

from Field Data, Gage 2304

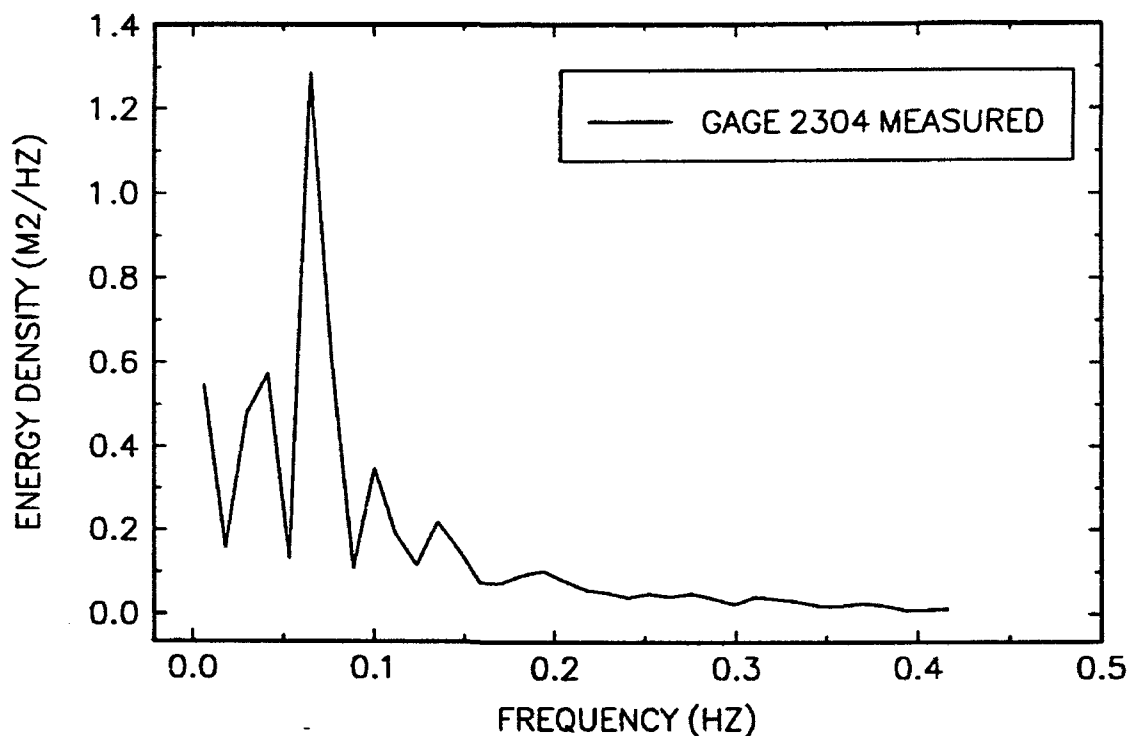
17-MINUTE RECORD BEGINNING AT 1658



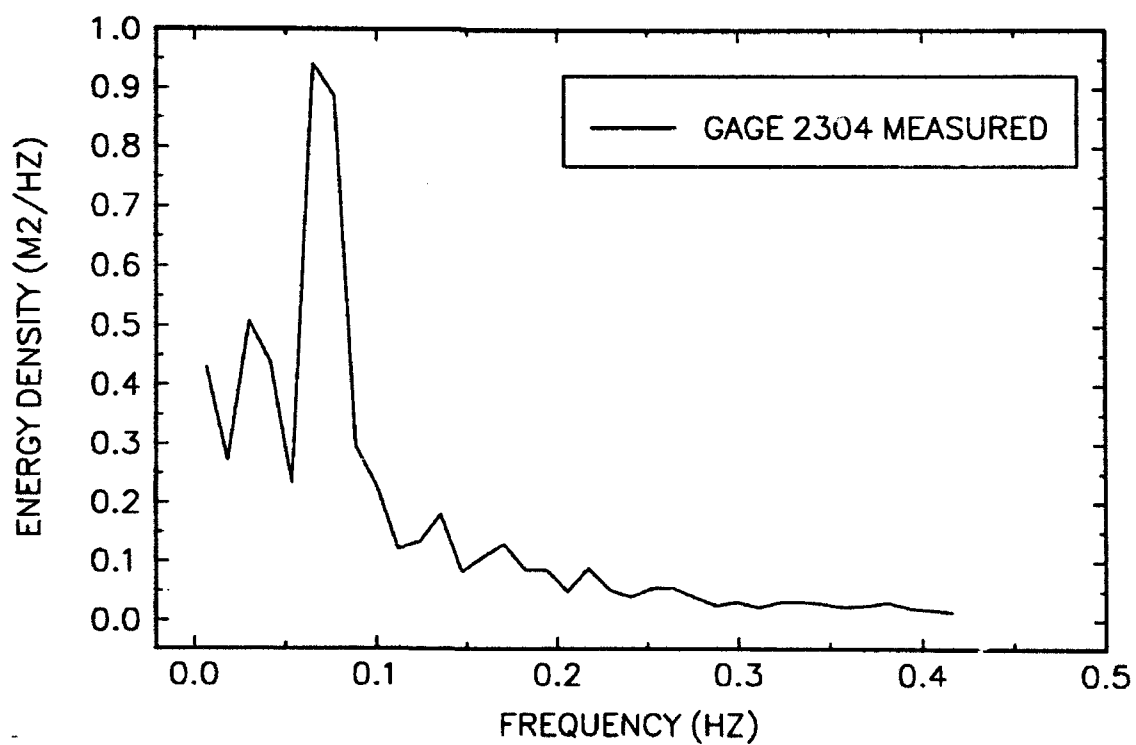
17-MINUTE RECORD BEGINNING AT 1715



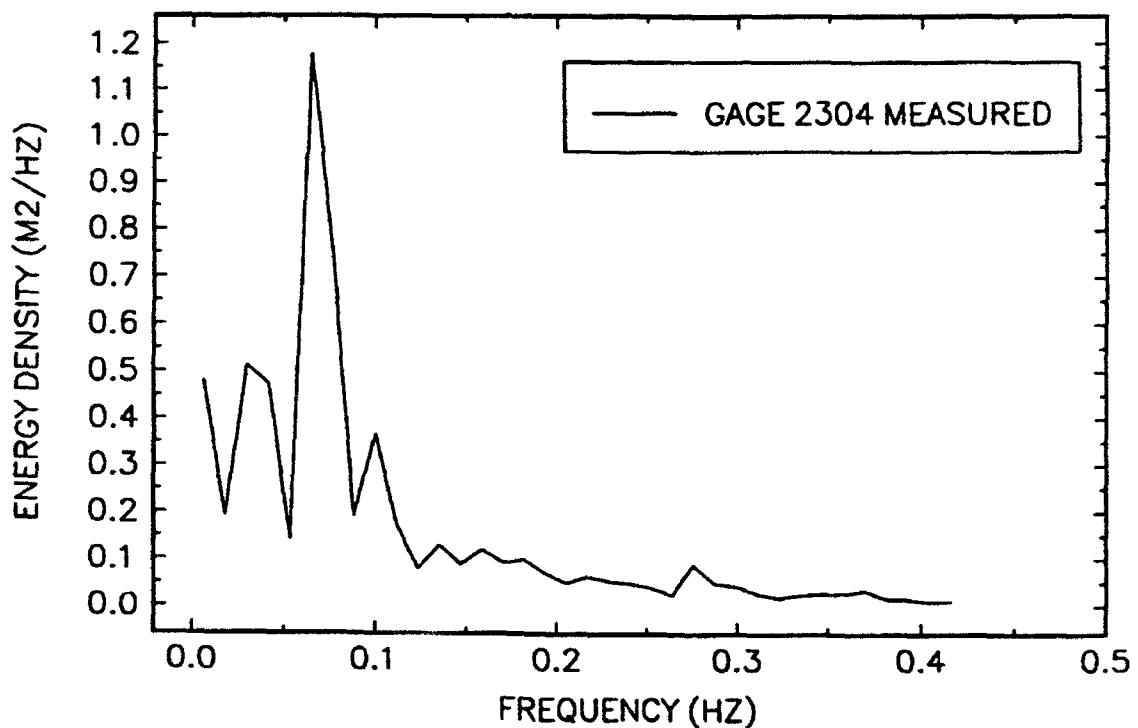
17-MINUTE RECORD BEGINNING AT 1732



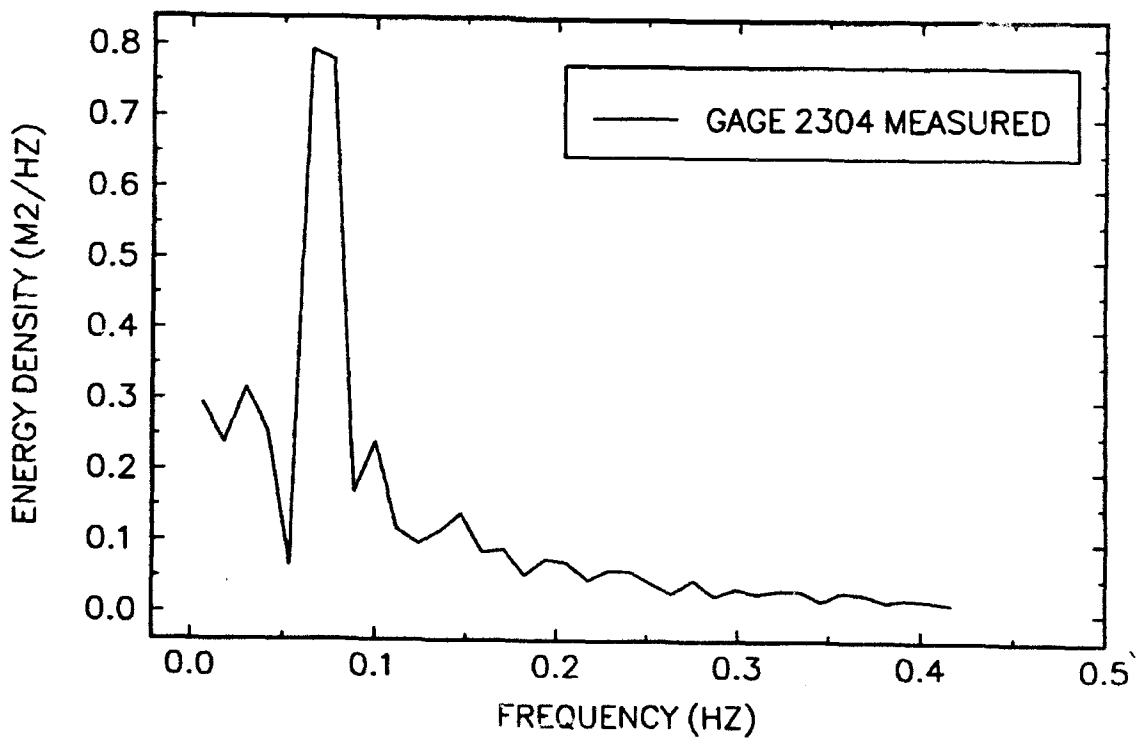
17-MINUTE RECORD BEGINNING AT 1749



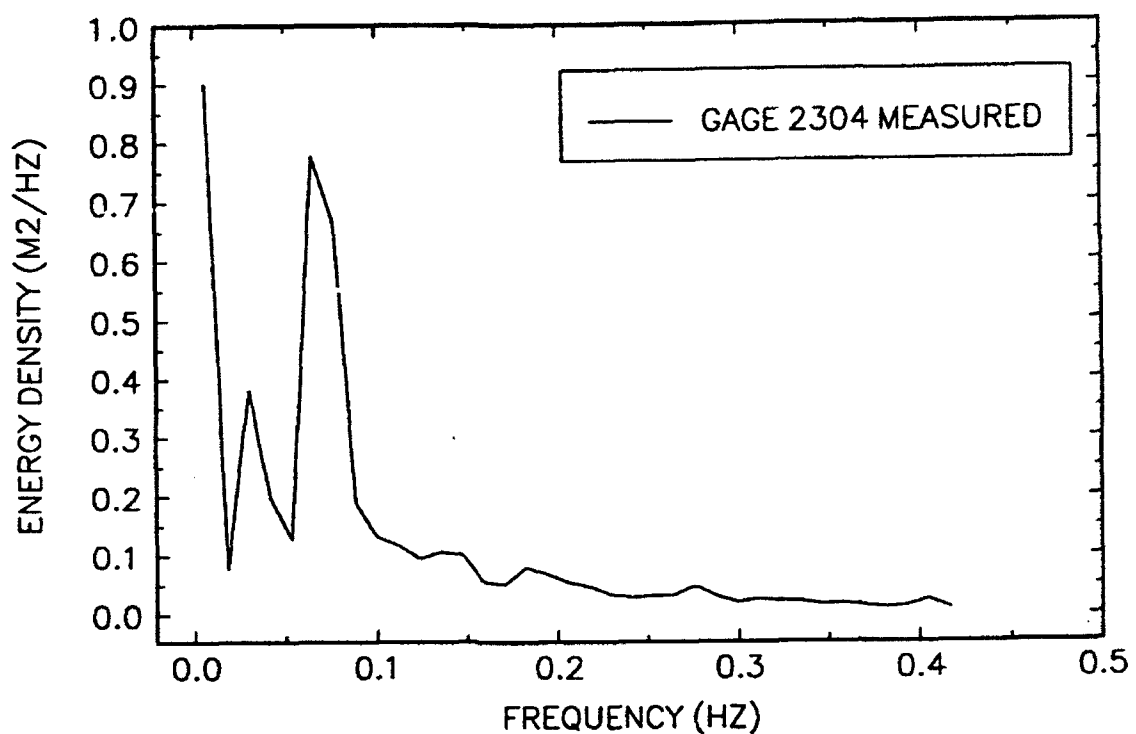
17-MINUTE RECORD BEGINNING AT 1806



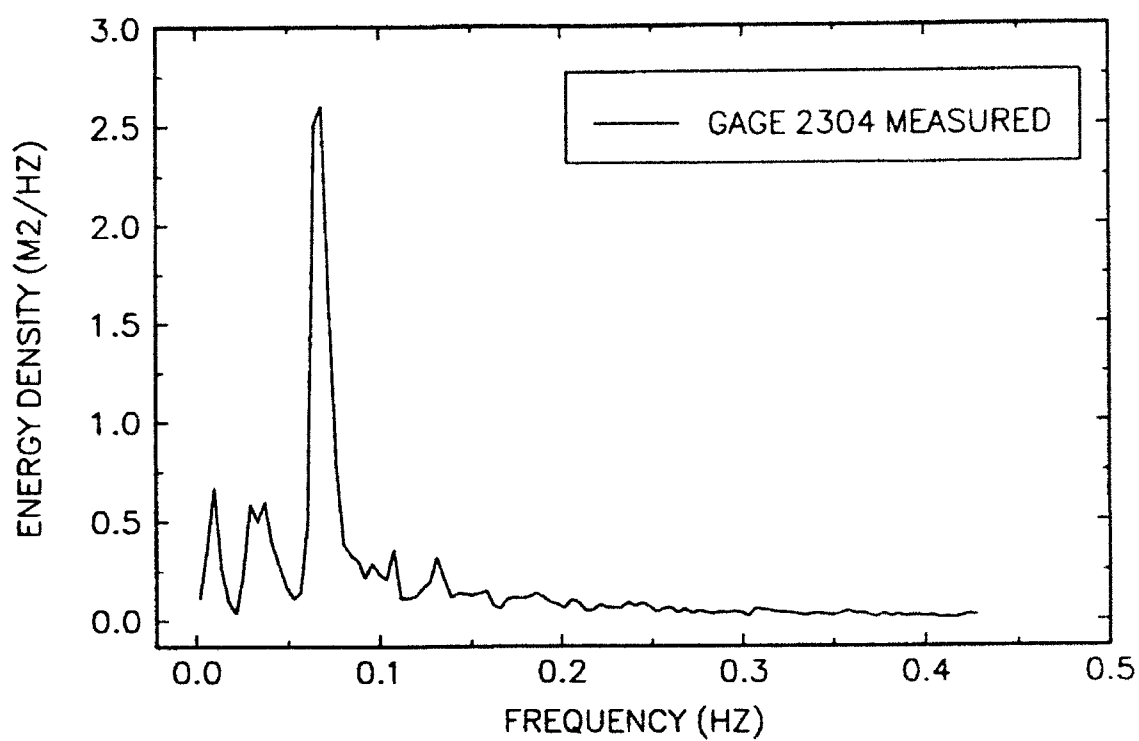
17-MINUTE RECORD BEGINNING AT 1824



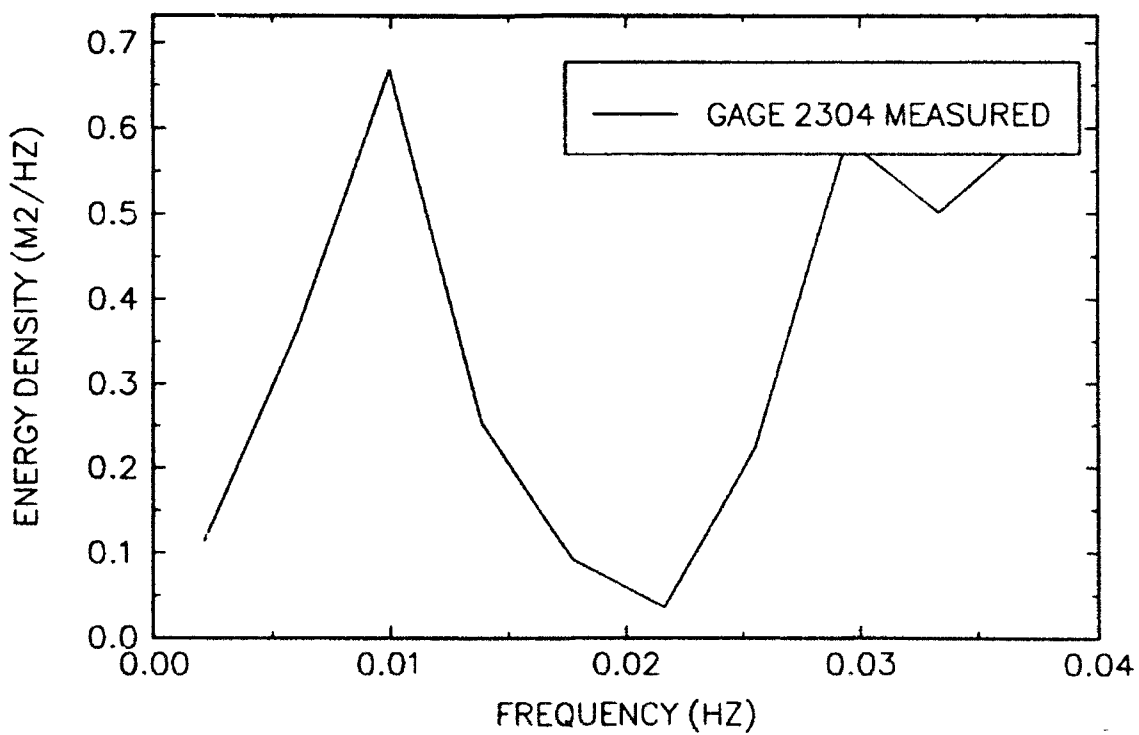
17-MINUTE RECORD BEGINNING AT 1841



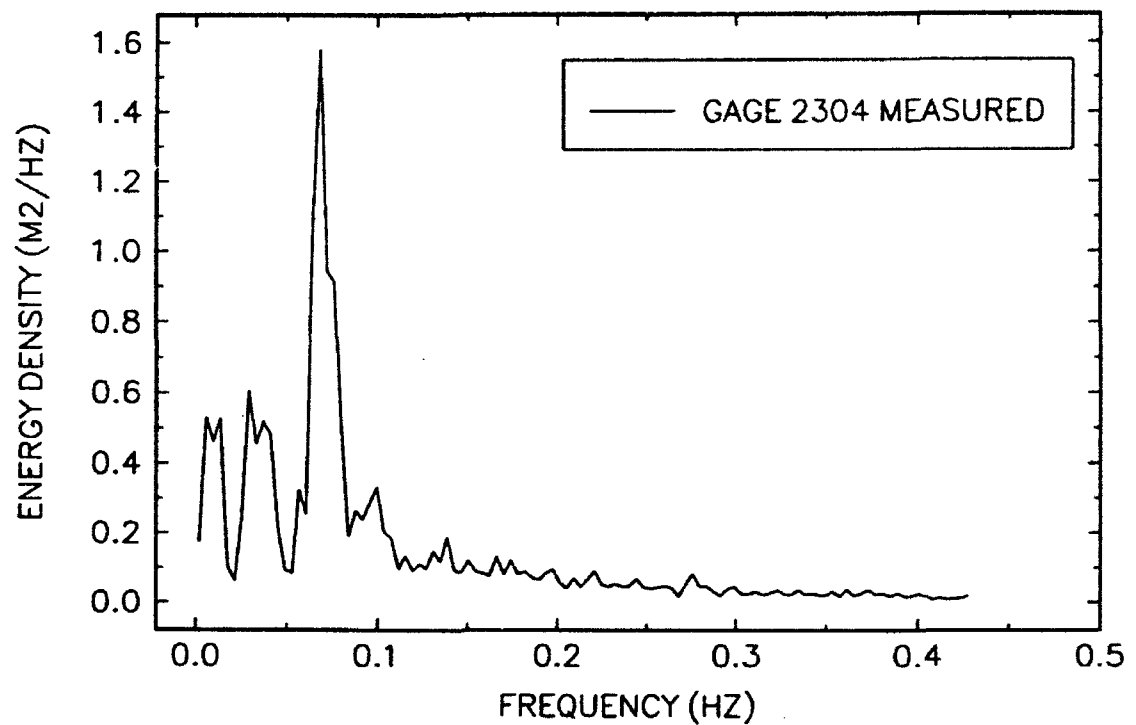
51-MINUTE RECORD BEGINNING AT 1658



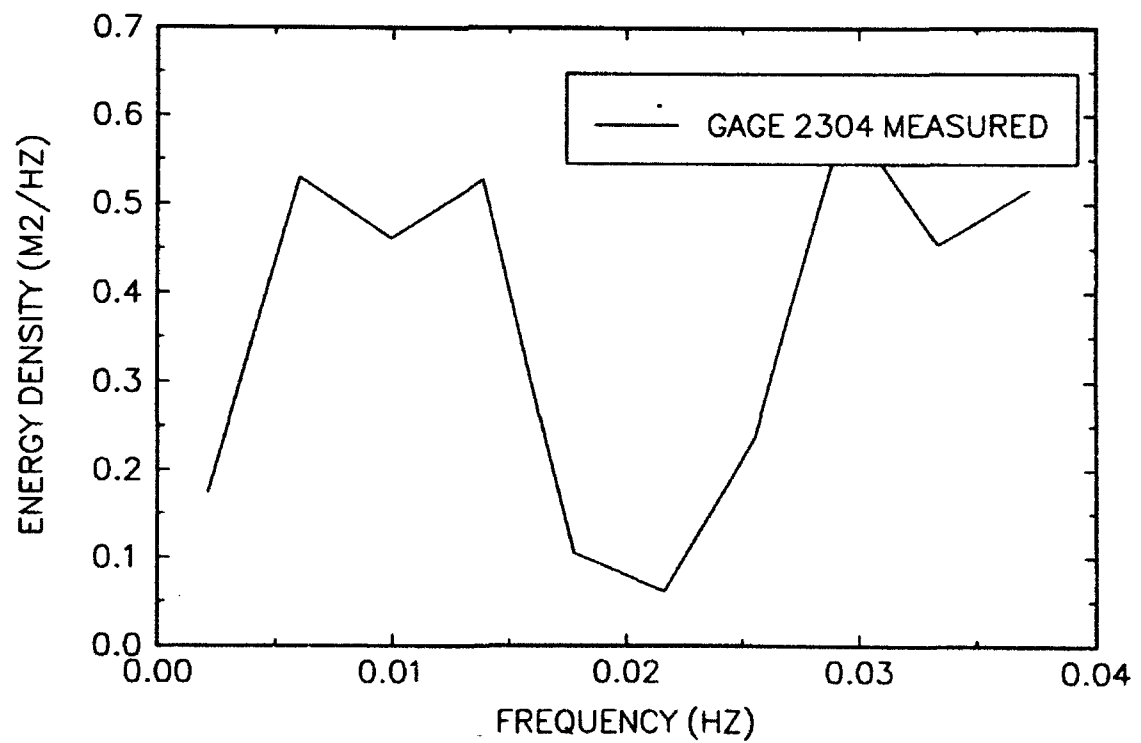
51-MINUTE RECORD BEGINNING AT 1658



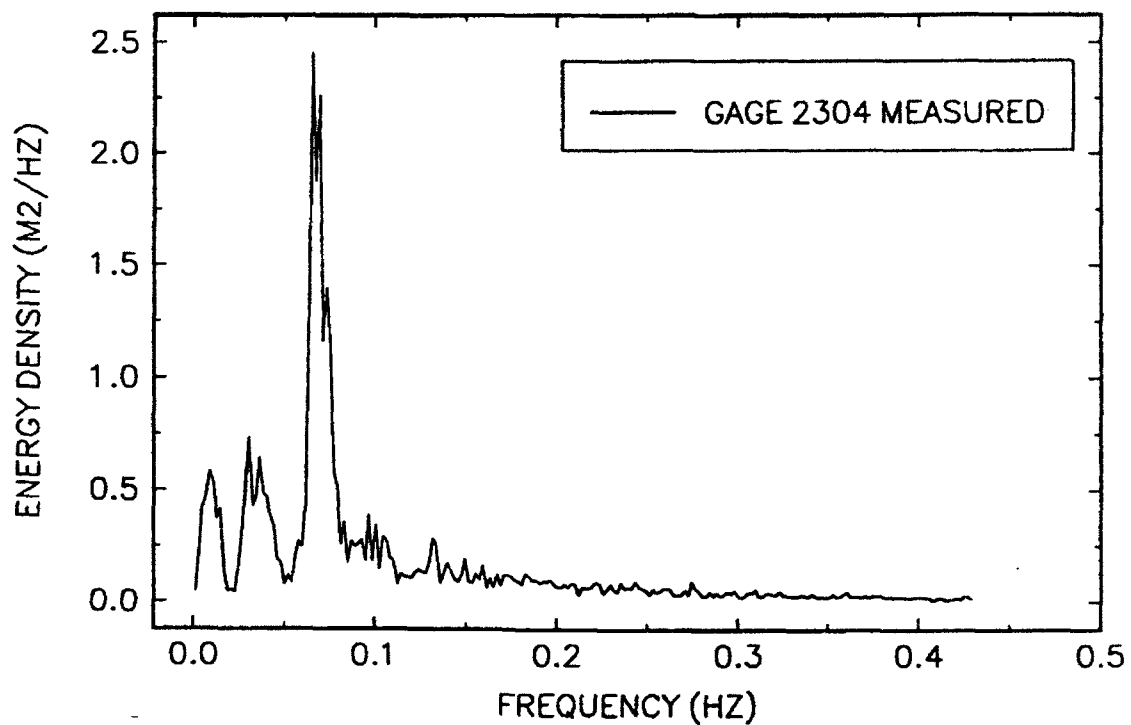
51-MINUTE RECORD BEGINNING AT 1749



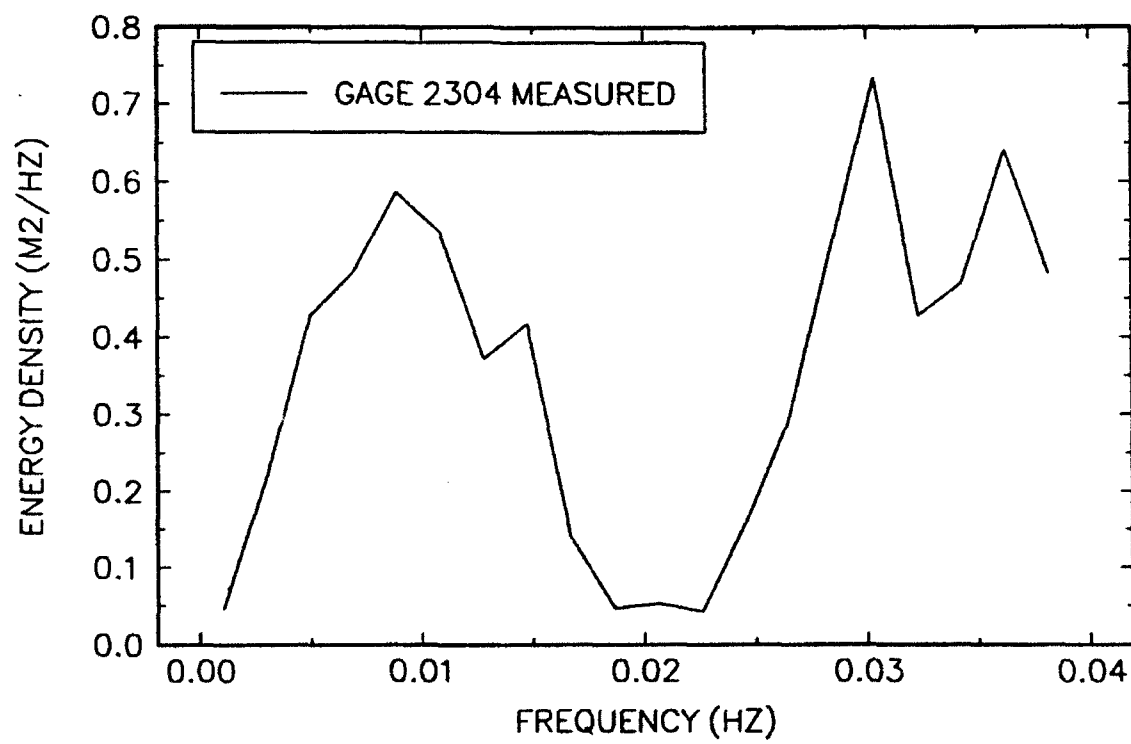
51-MINUTE RECORD BEGINNING AT 1749



102-MINUTE RECORD BEGINNING AT 1658



102-MINUTE RECORD BEGINNING AT 1658

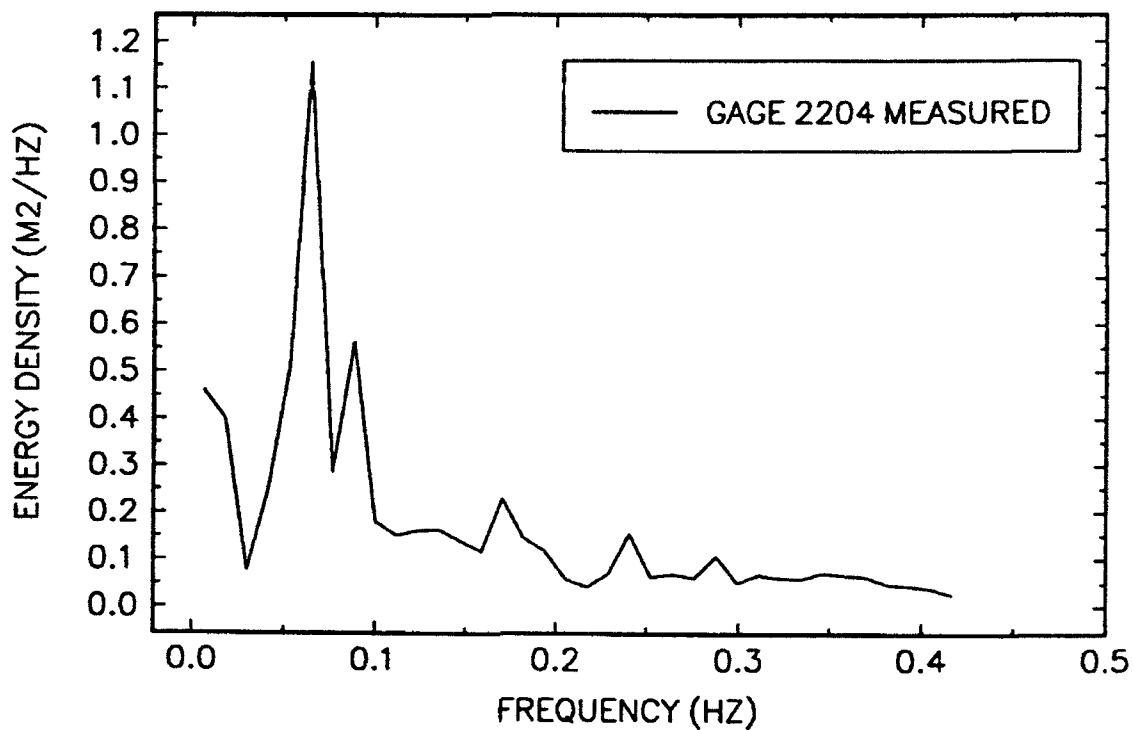


Appendix K

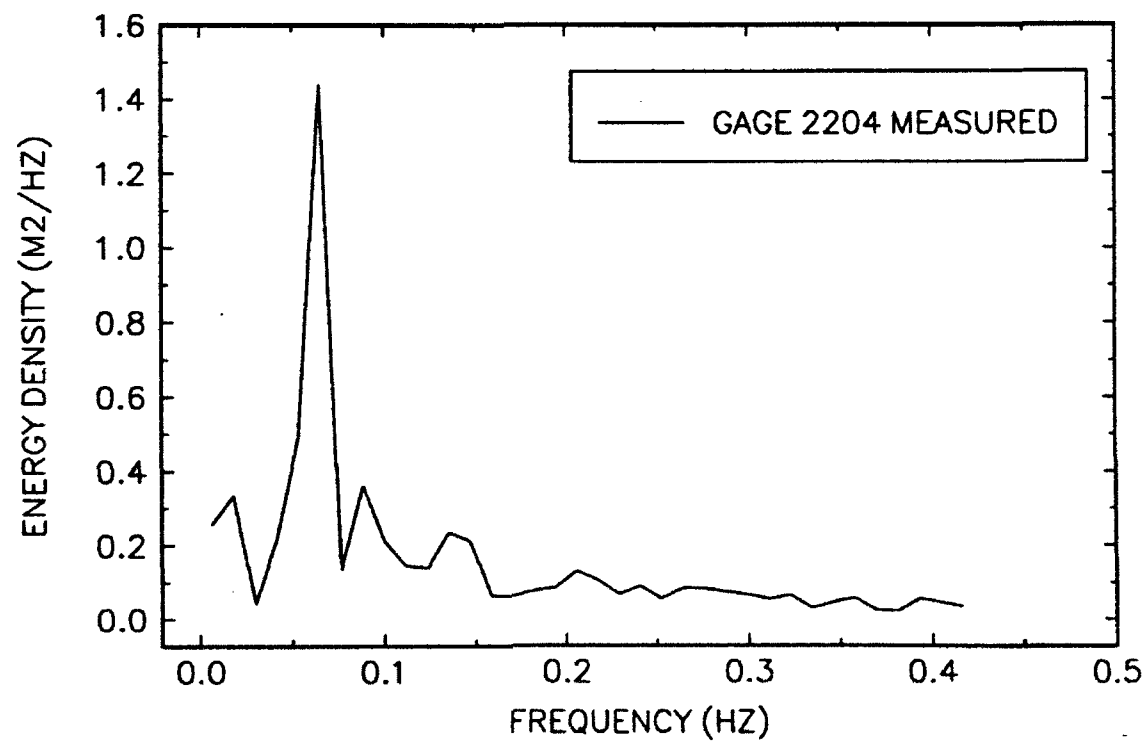
Short and Long Wave Spectra

from Field Data, Gage 2204

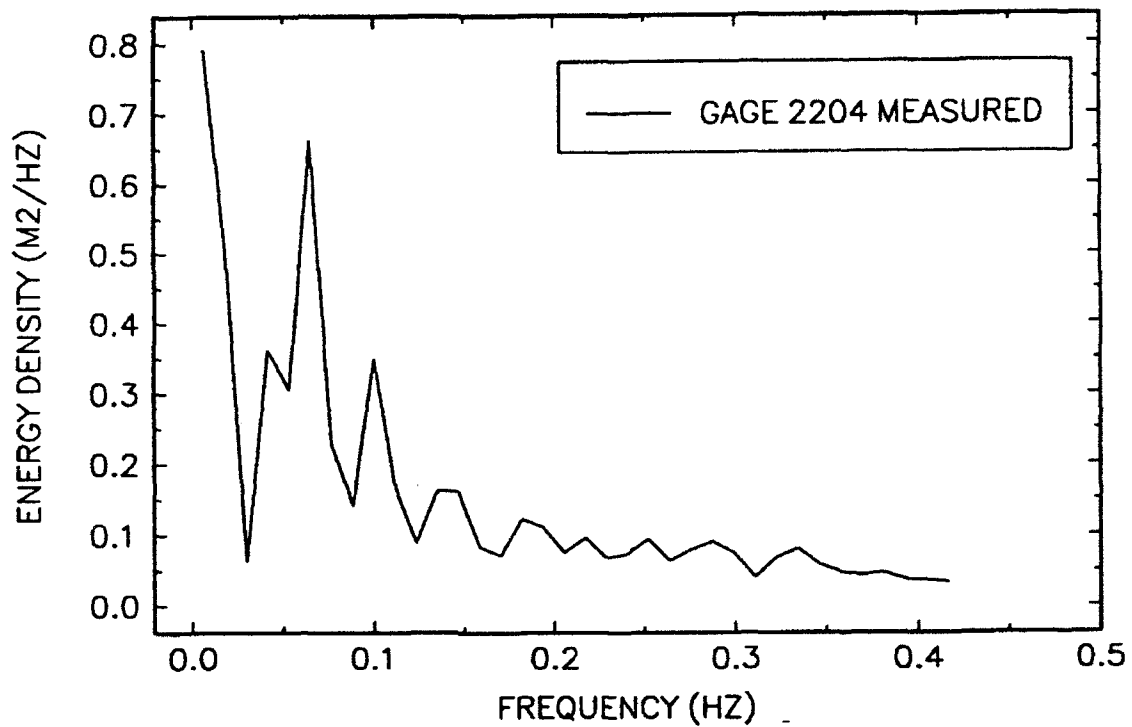
17-MINUTE RECORD BEGINNING AT 1658



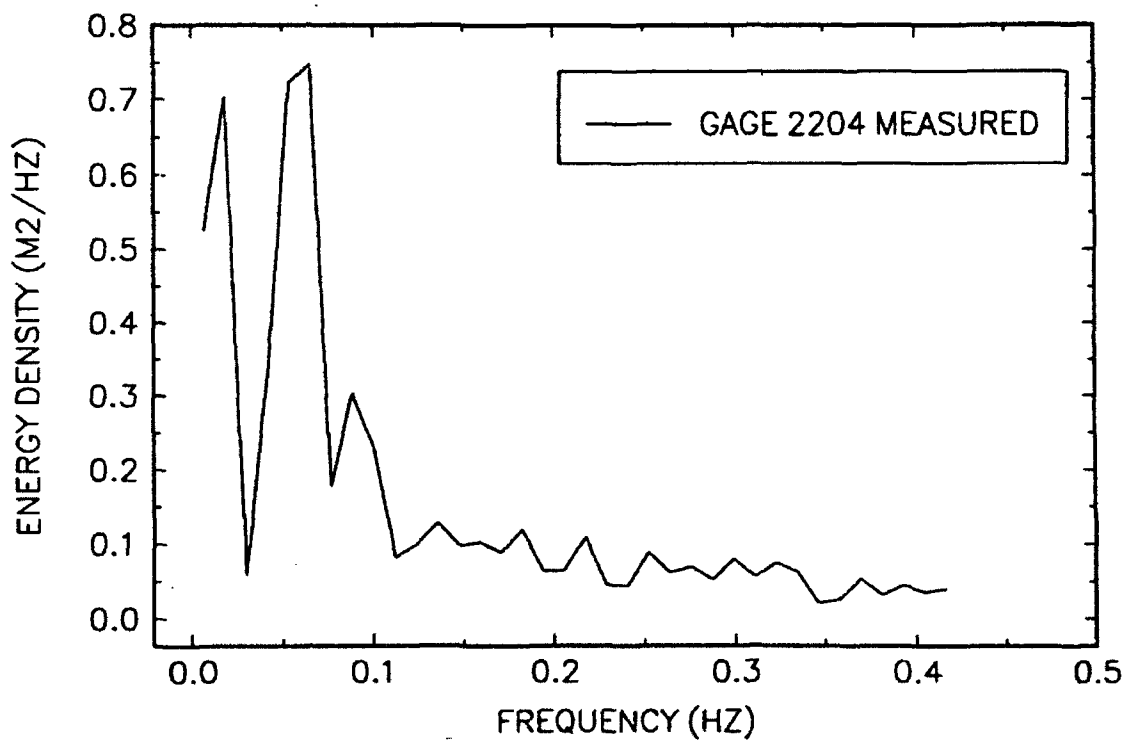
17-MINUTE RECORD BEGINNING AT 1715



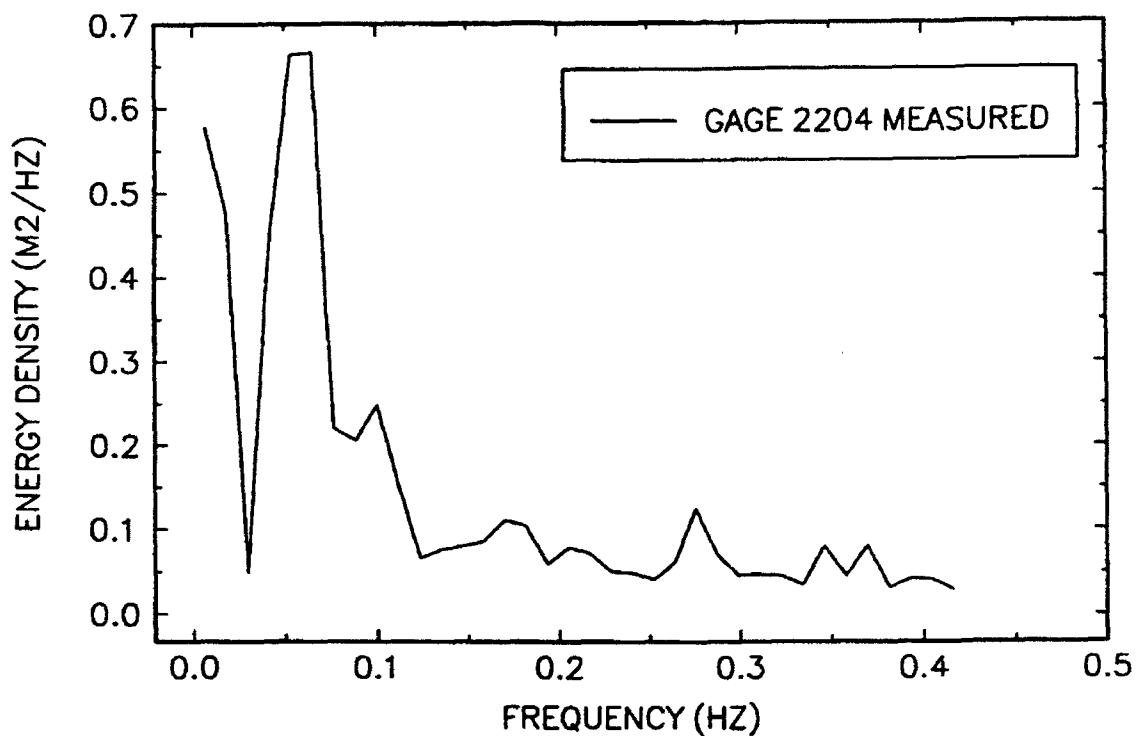
17-MINUTE RECORD BEGINNING AT 1732



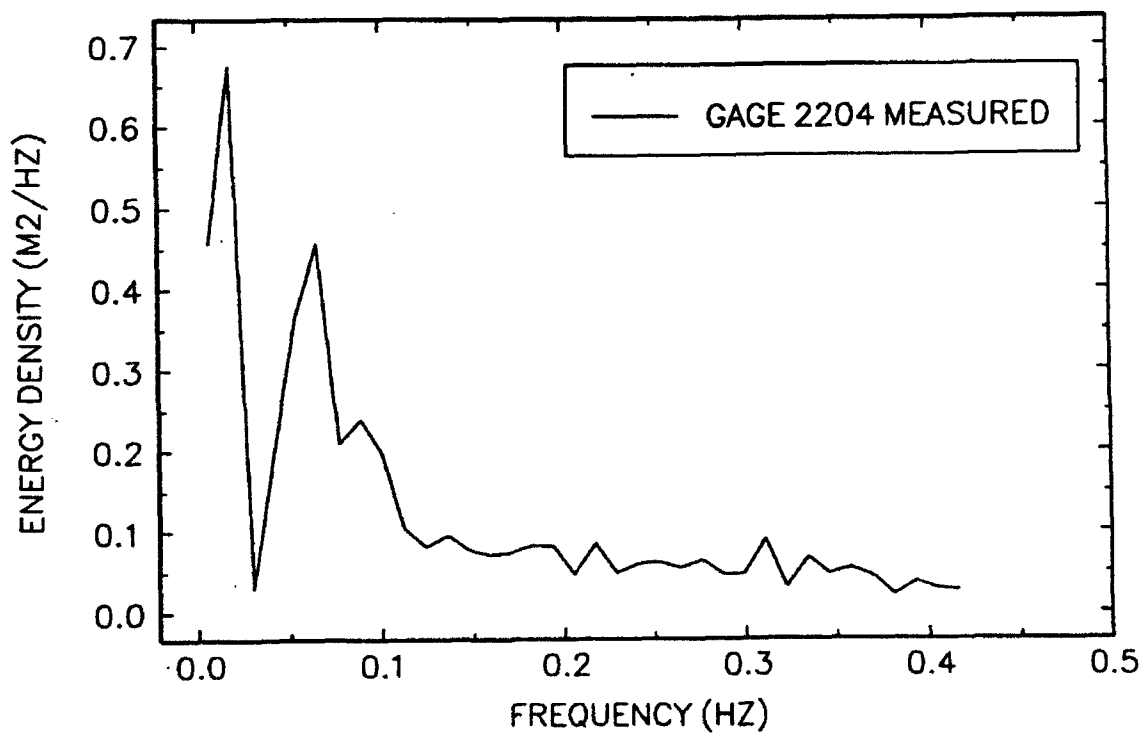
17-MINUTE RECORD BEGINNING AT 1749



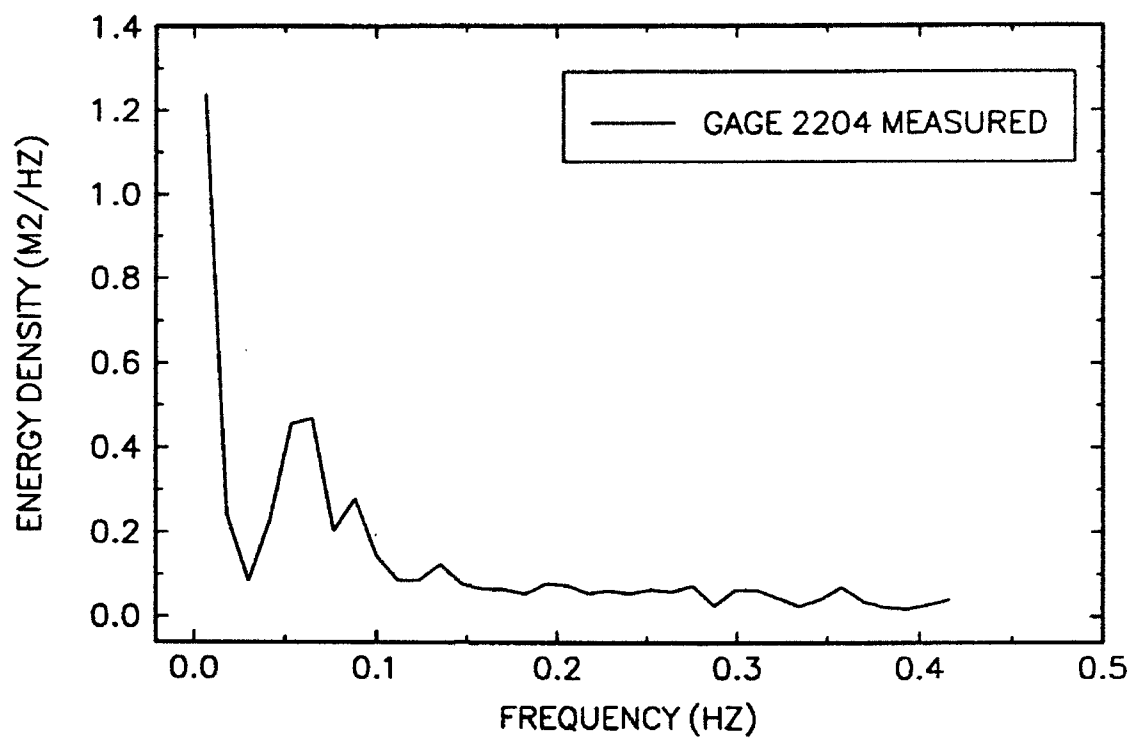
17-MINUTE RECORD BEGINNING AT 1806



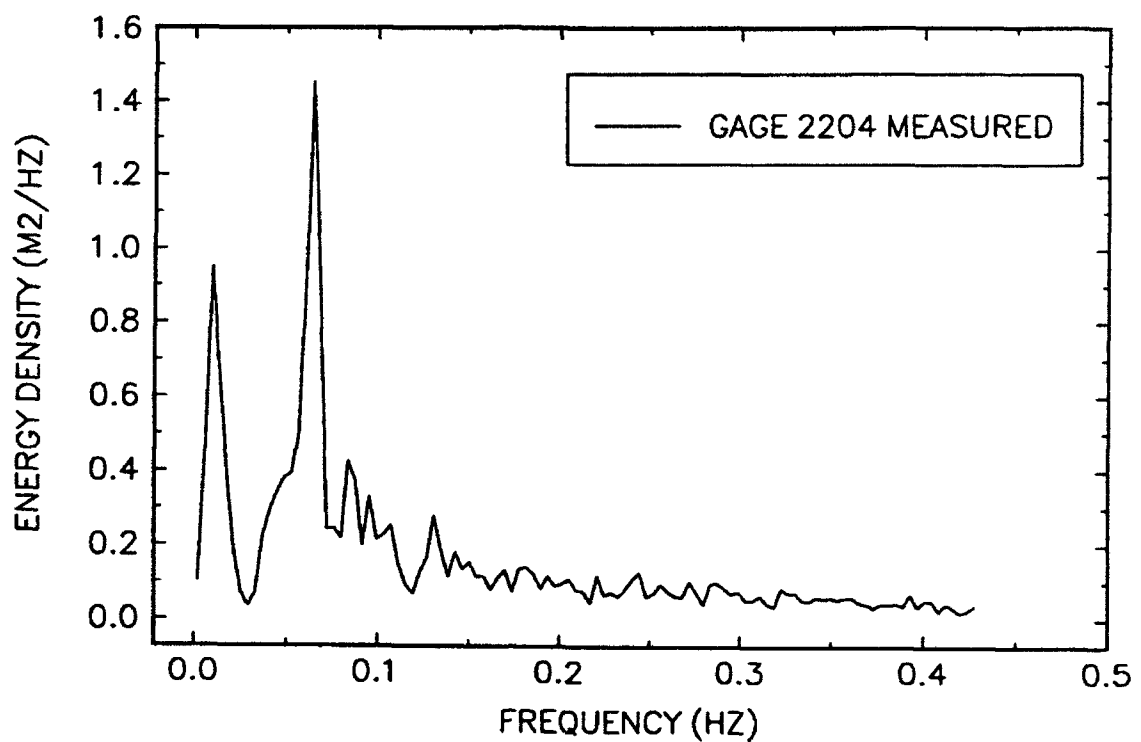
17-MINUTE RECORD BEGINNING AT 1824



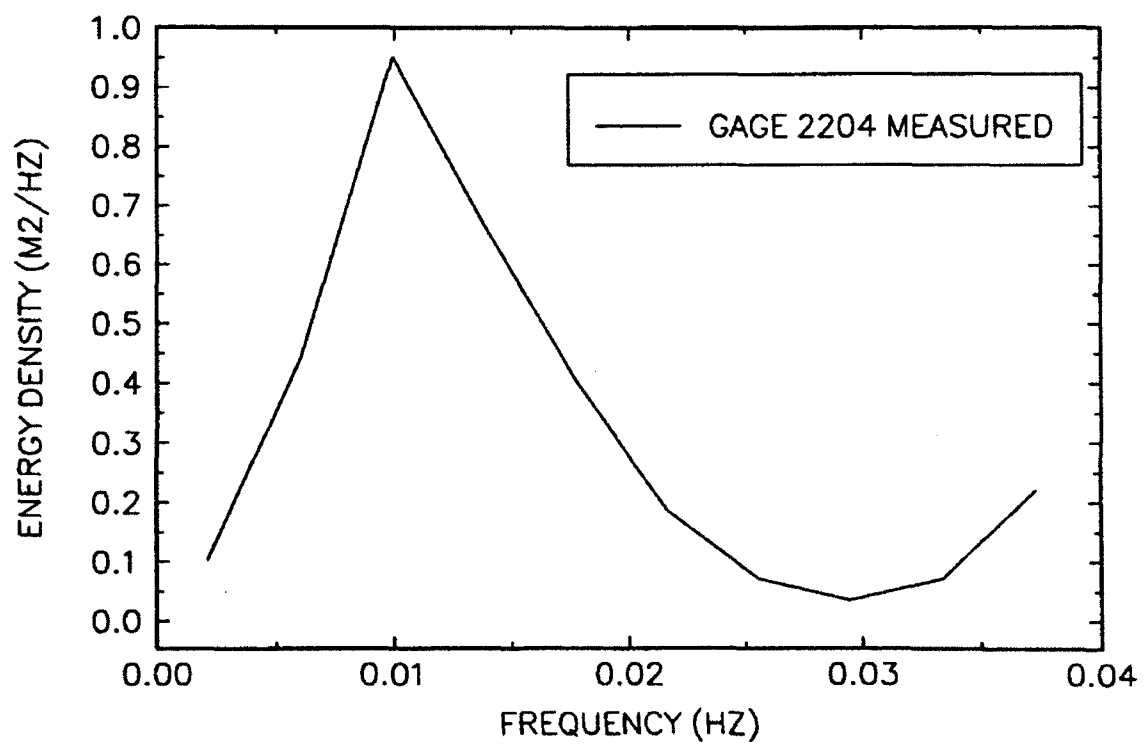
17-MINUTE RECORD BEGINNING AT 1841



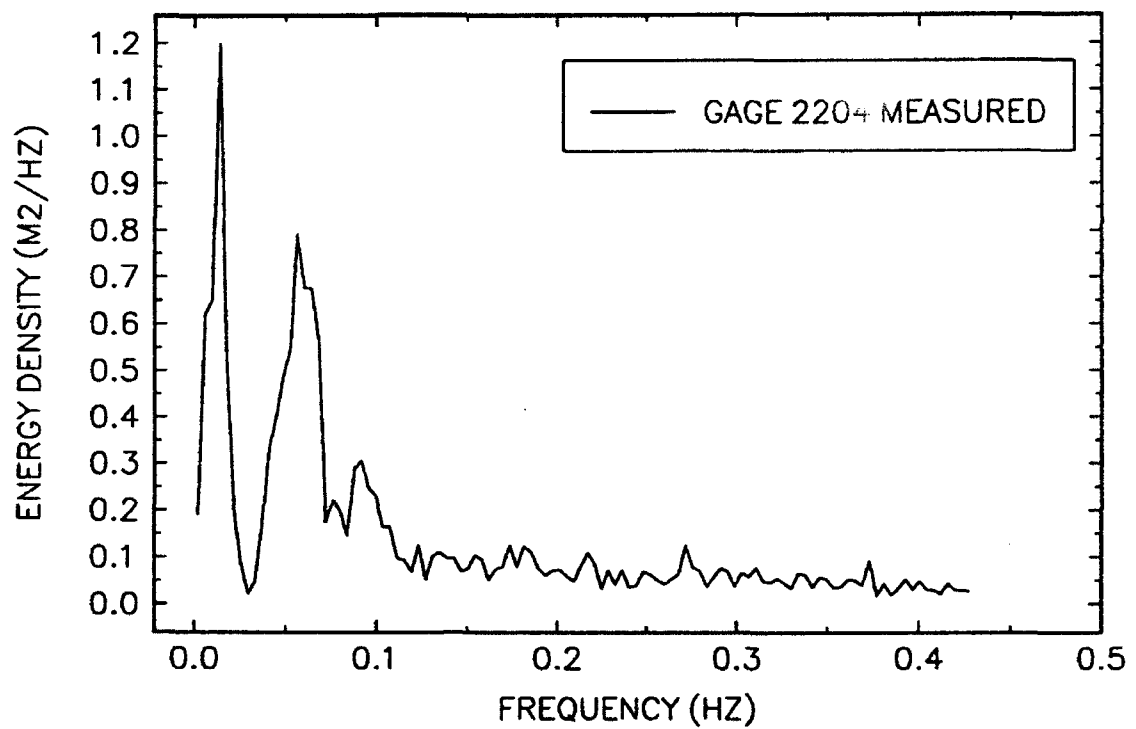
51-MINUTE RECORD BEGINNING AT 1658



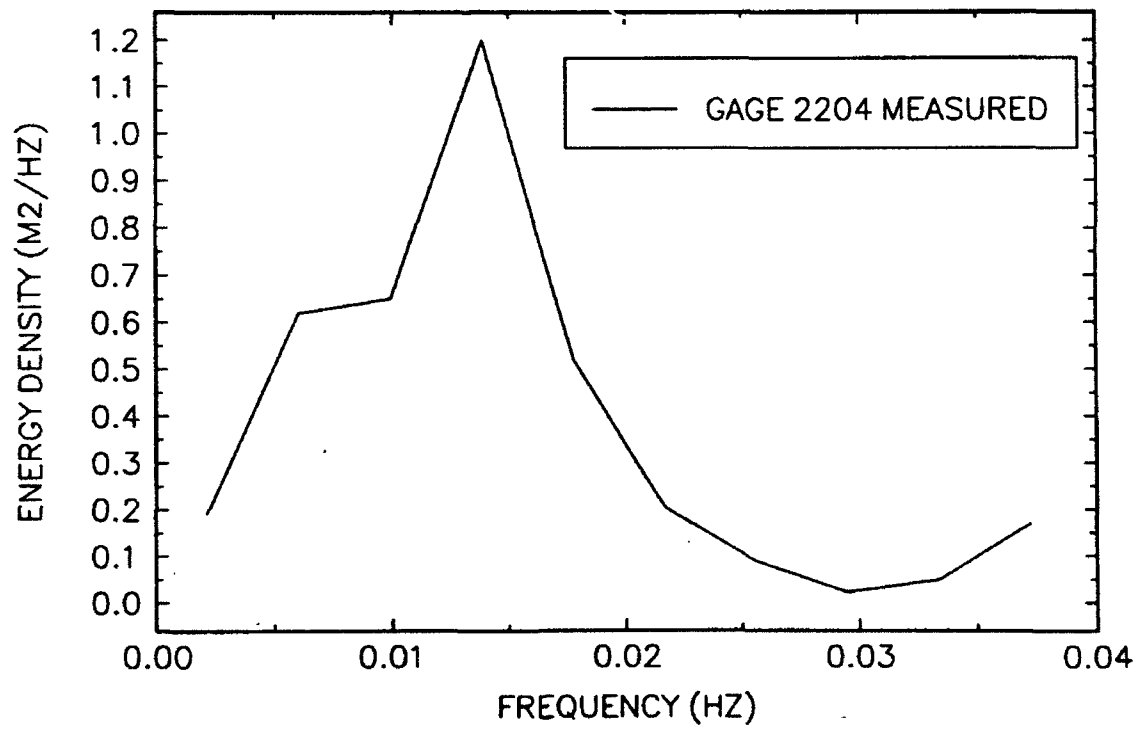
51-MINUTE RECORD BEGINNING AT 1658



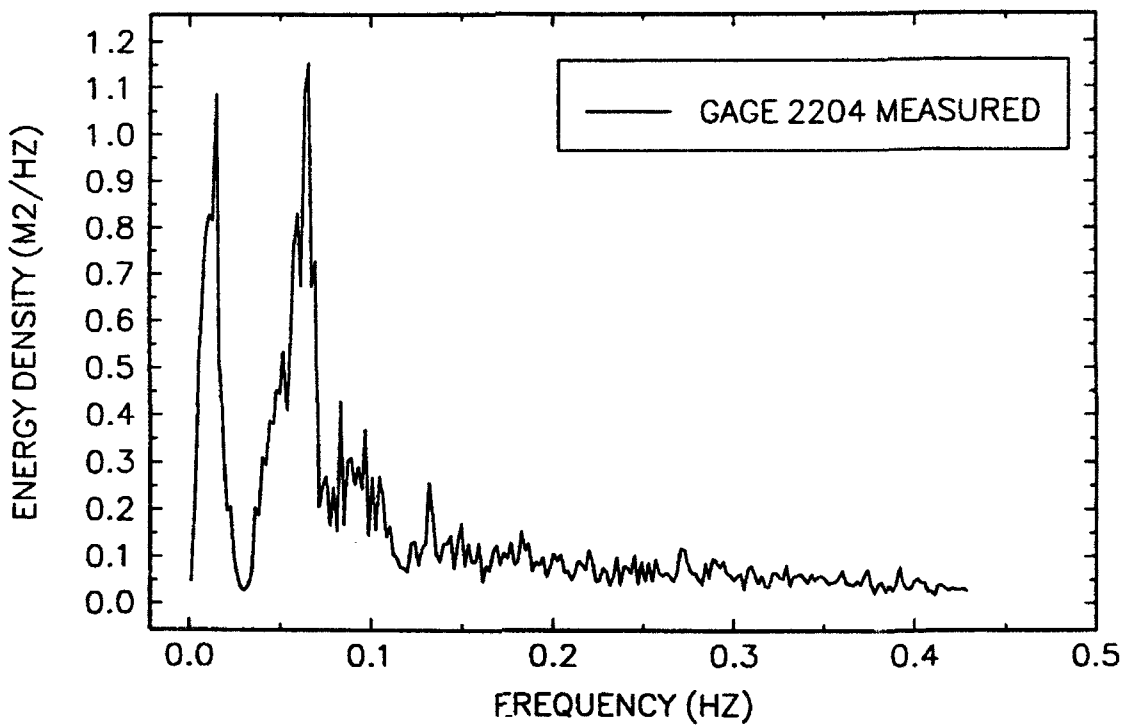
51-MINUTE RECORD BEGINNING AT 1749



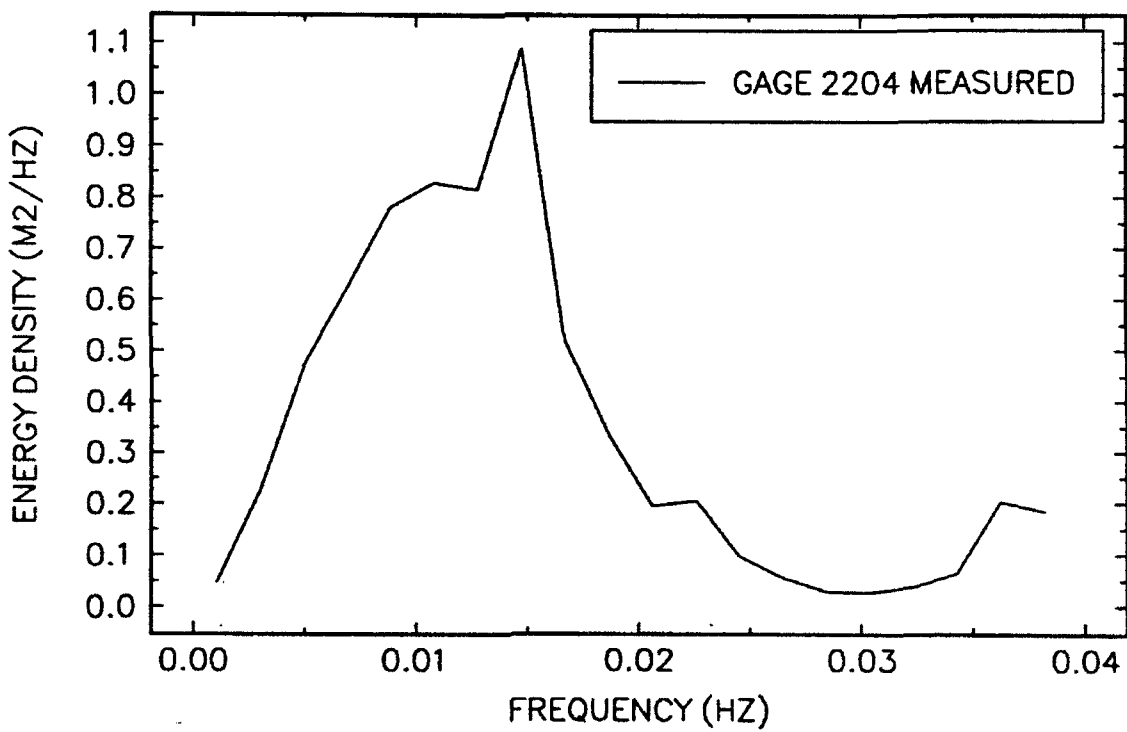
51-MINUTE RECORD BEGINNING AT 1749



102-MINUTE RECORD BEGINNING AT 1658



102-MINUTE RECORD BEGINNING AT 1658

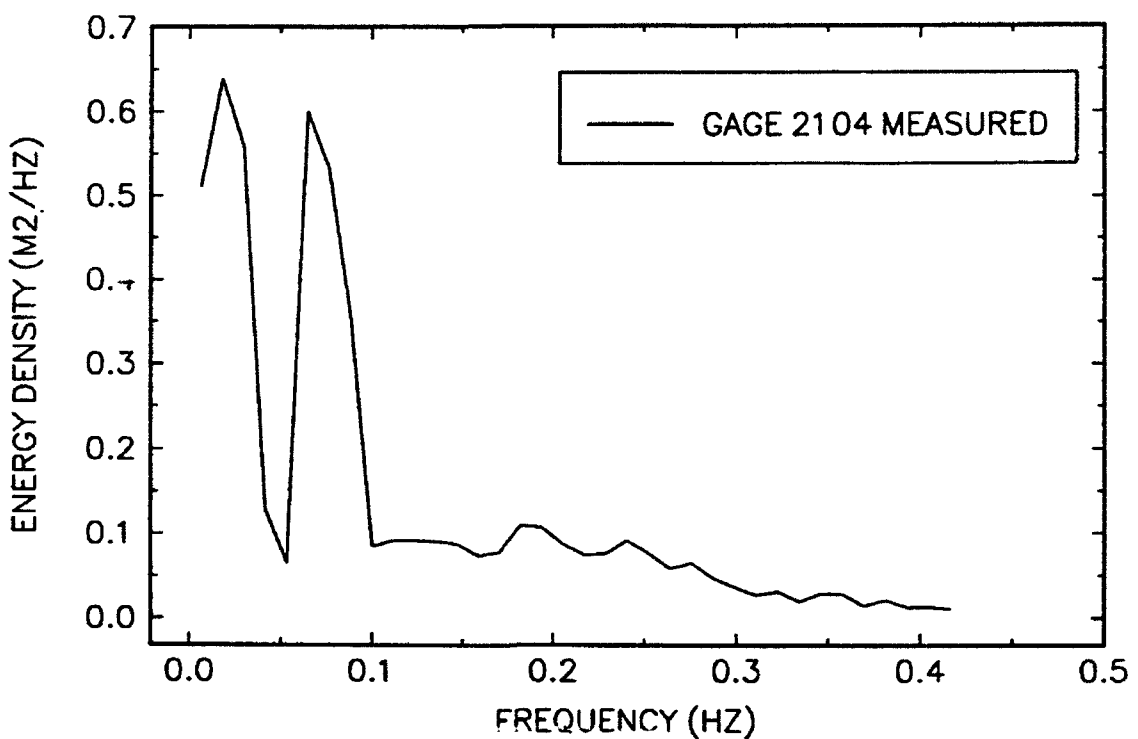


Appendix L

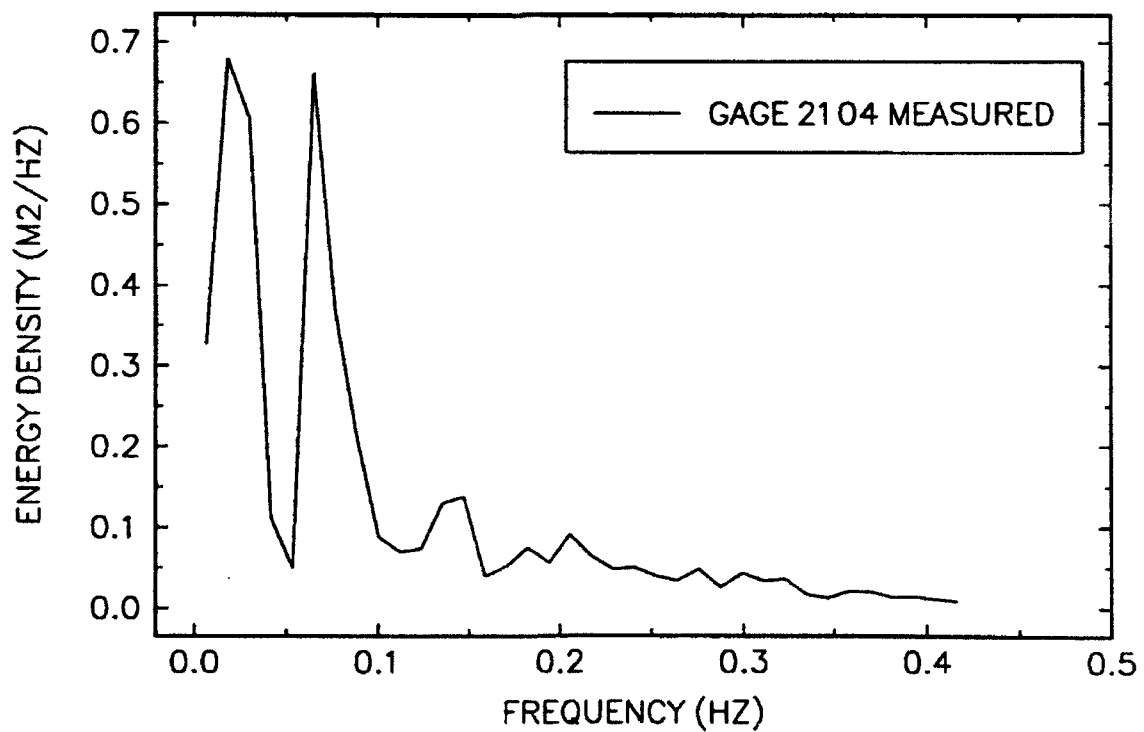
Short and Long Wave Spectra

from Field Data, Gage 2104

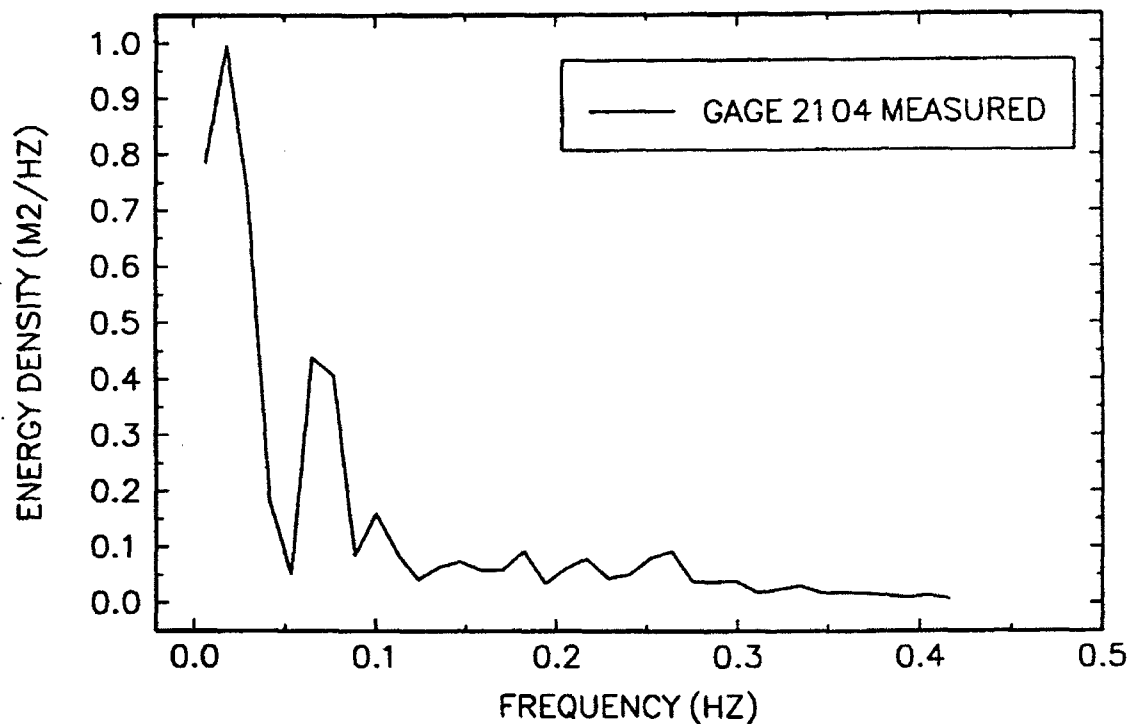
17-MINUTE RECORD BEGINNING AT 1658



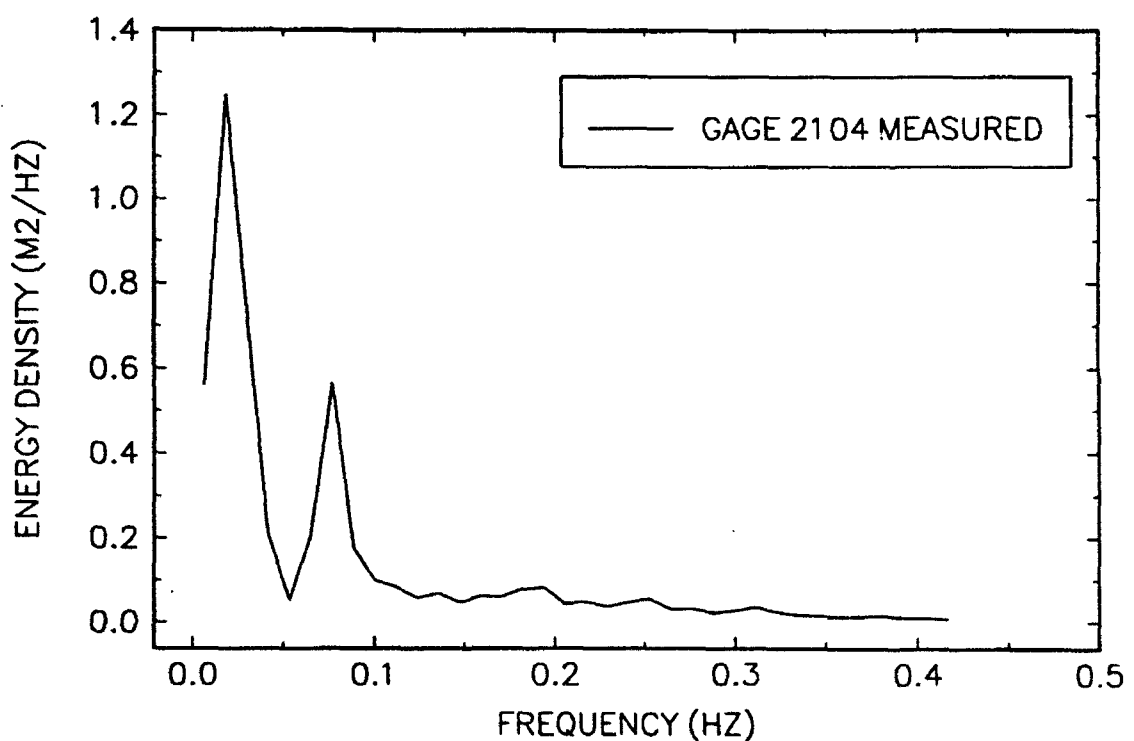
17-MINUTE RECORD BEGINNING AT 1715



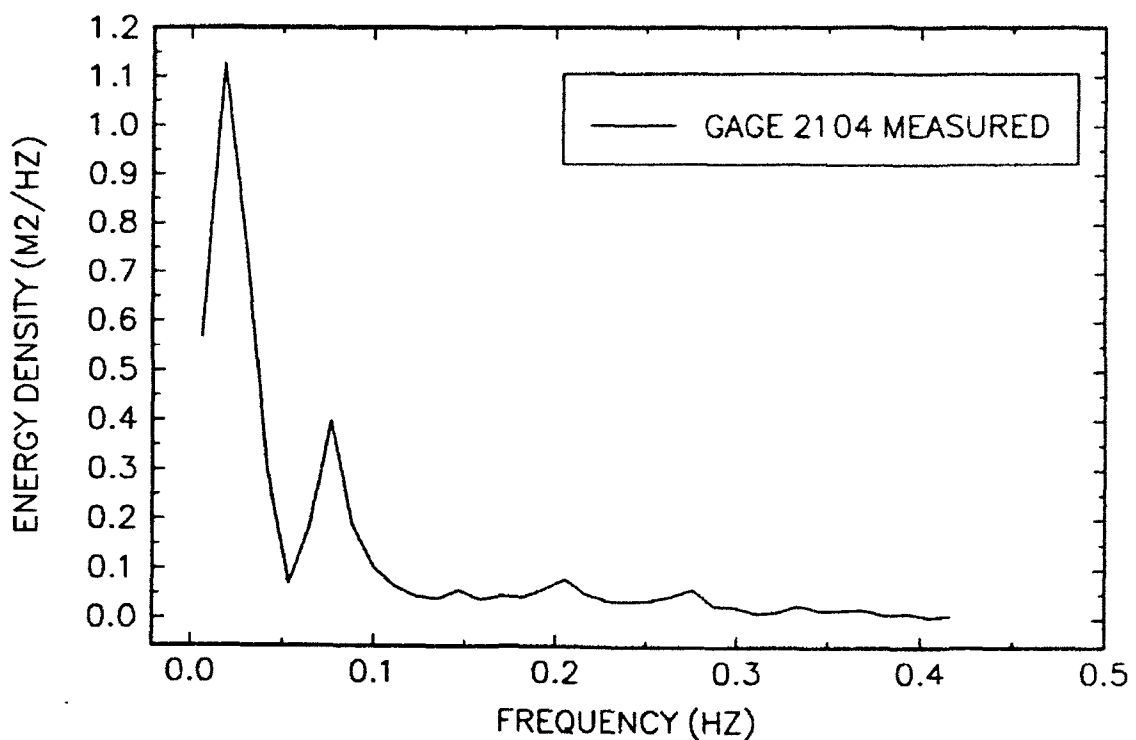
17-MINUTE RECORD BEGINNING AT 1732



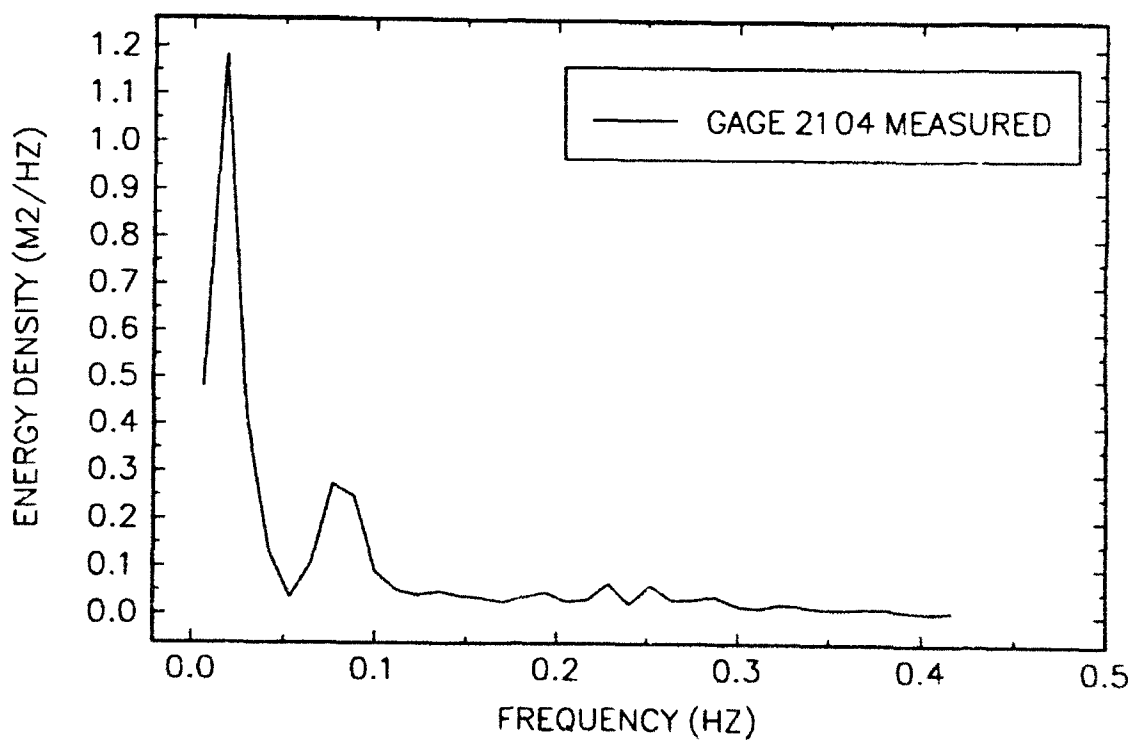
17-MINUTE RECORD BEGINNING AT 1749



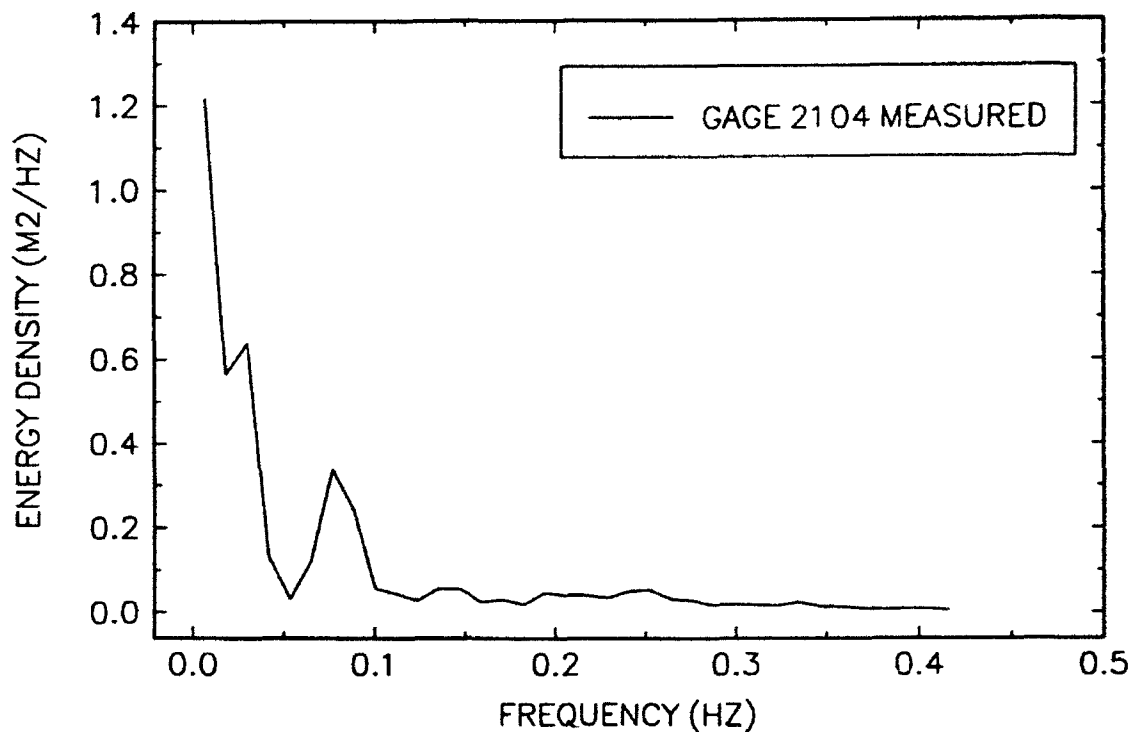
17-MINUTE RECORD BEGINNING AT 1806



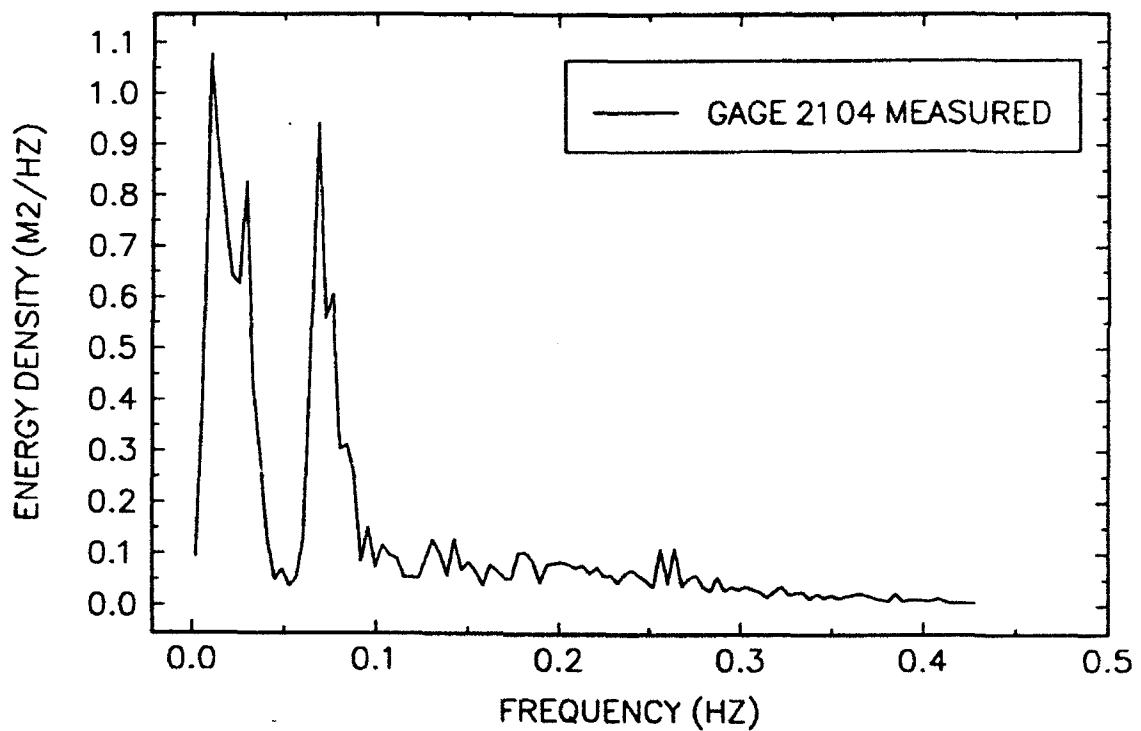
17-MINUTE RECORD BEGINNING AT 1824



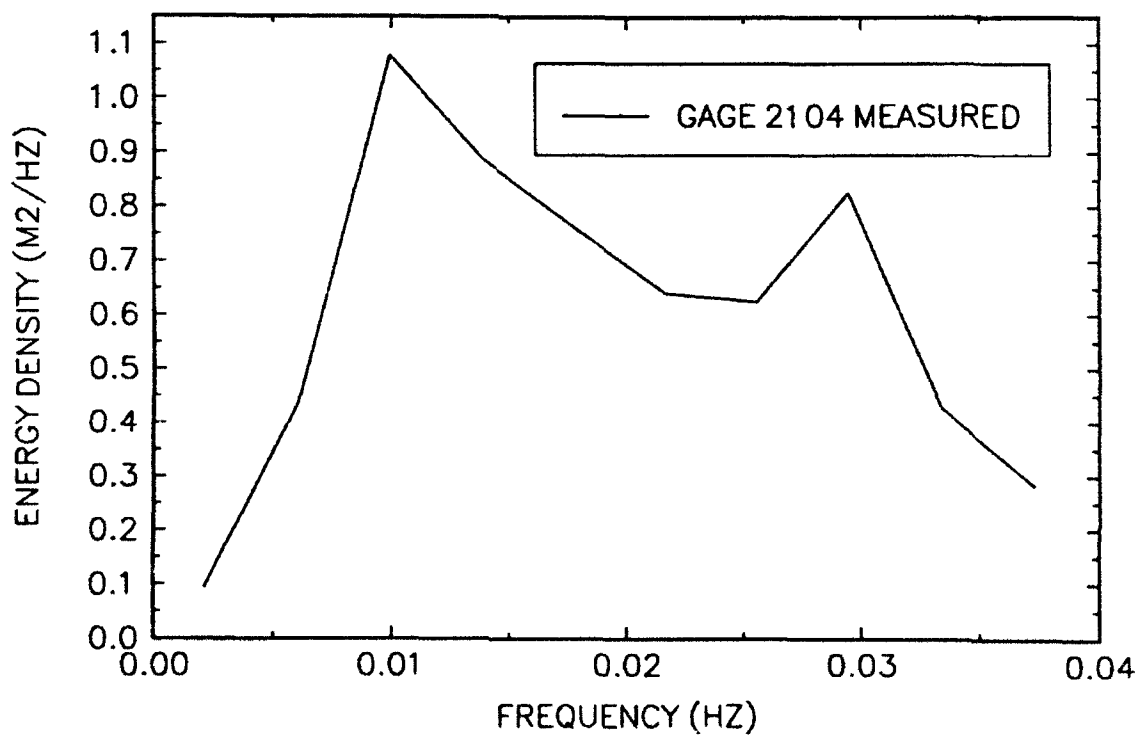
17-MINUTE RECORD BEGINNING AT 1841



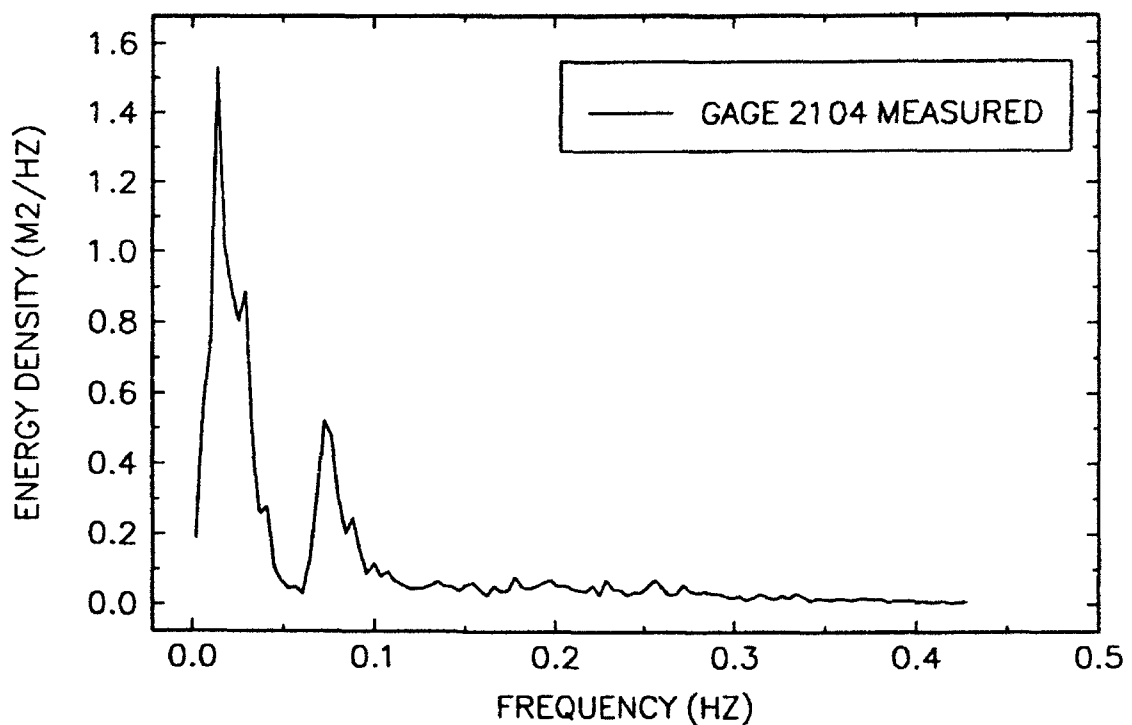
51-MINUTE RECORD BEGINNING AT 1658



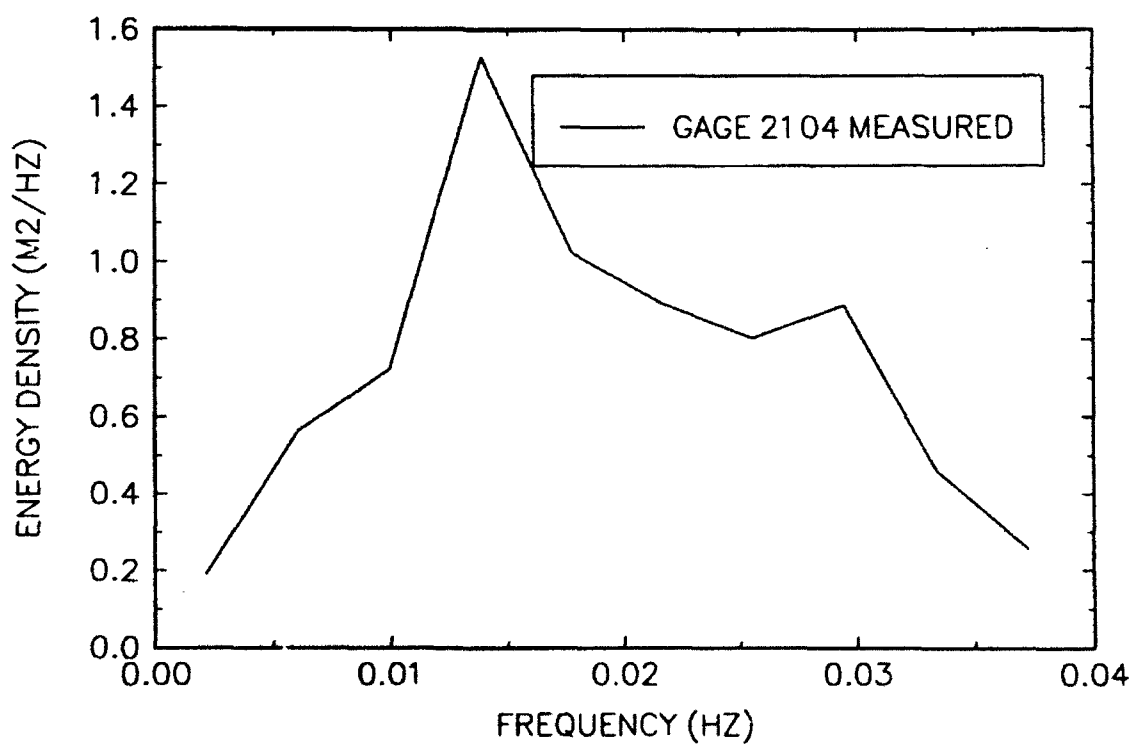
51-MINUTE RECORD BEGINNING AT 1658



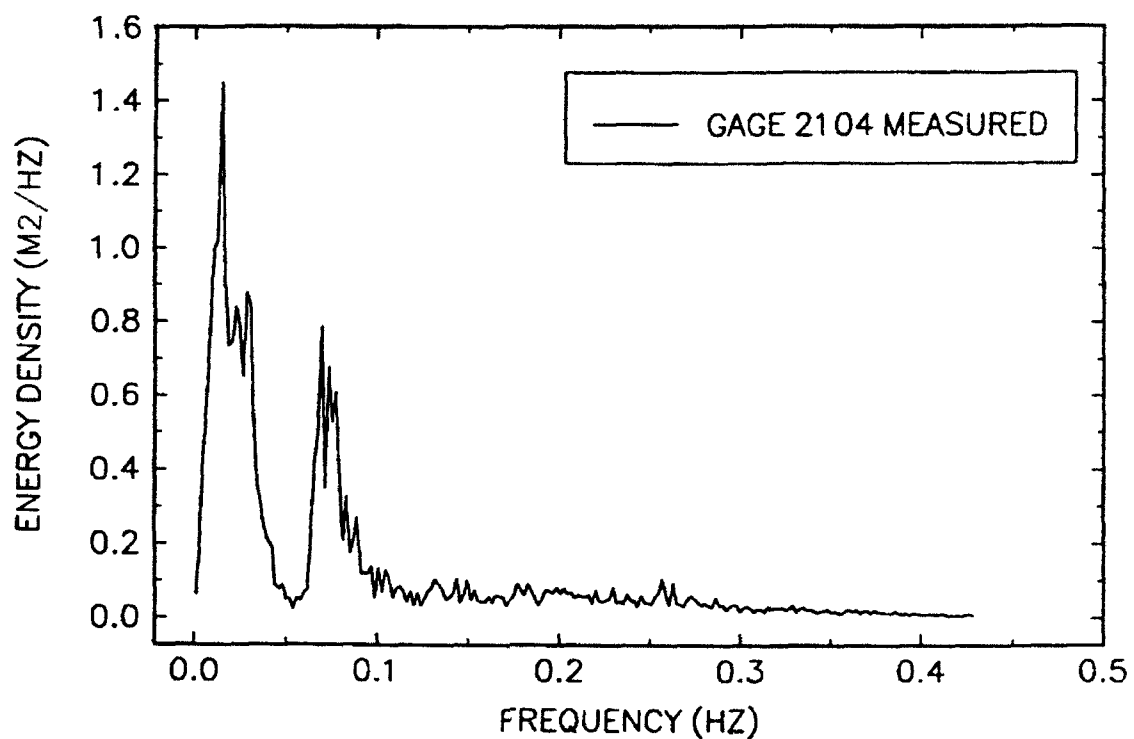
51-MINUTE RECORD BEGINNING AT 1749



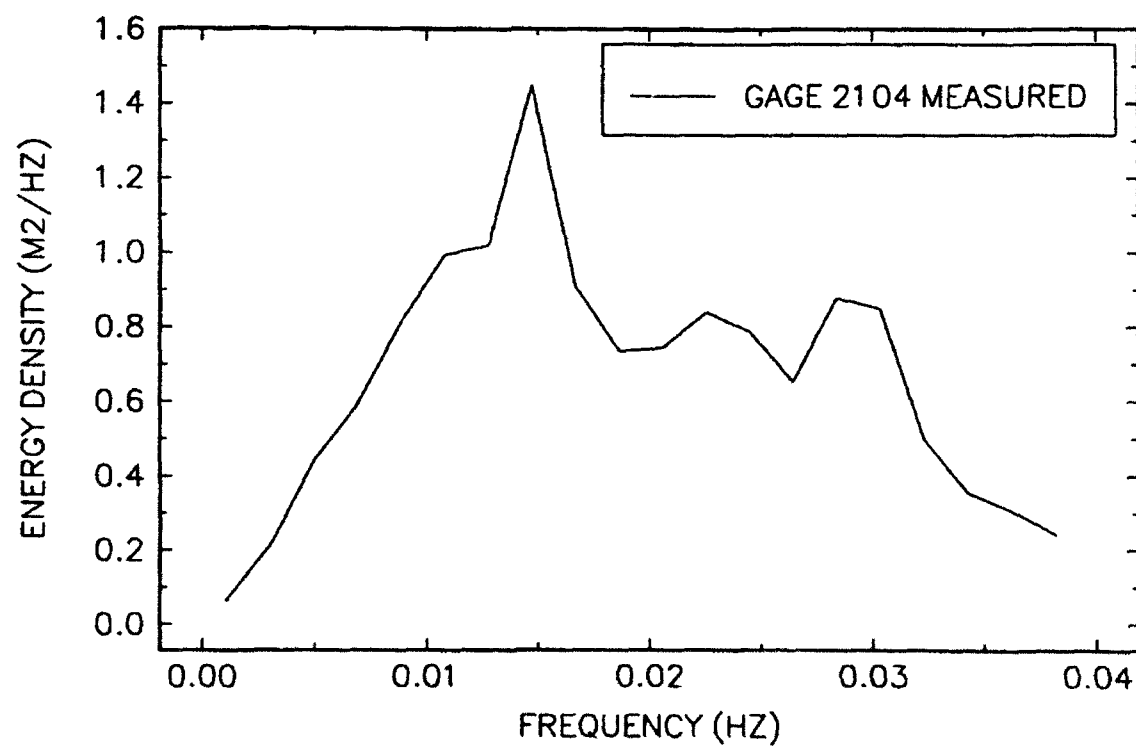
51-MINUTE RECORD BEGINNING AT 1749



102-MINUTE RECORD BEGINNING AT 1658



102-MINUTE RECORD BEGINNING AT 1658



REPORT DOCUMENTATION PAGE

Form Approved
OMB No. 0704-0188

Public reporting burden for this collection of information is estimated to average 1 hour per response, including the time for reviewing instructions, searching existing data sources, gathering and maintaining the data needed, and completing and reviewing the collection of information. Send comments regarding this burden estimate or any other aspect of this collection of information, including suggestions for reducing this burden, to Washington Headquarters Services, Directorate for Information Operations and Reports, 1215 Jefferson Davis Highway, Suite 1204, Arlington, VA 22202-4302, and to the Office of Management and Budget, Paperwork Reduction Project (0704-0188), Washington, DC 20503.

1. AGENCY USE ONLY (Leave blank)	2. REPORT DATE	3. REPORT TYPE AND DATES COVERED	
	August 1993	Final report	
4. TITLE AND SUBTITLE Surf Beat in Coastal Waters			5. FUNDING NUMBERS
6. AUTHOR(S) Edward F. Thompson, Michael J. Briggs			
7. PERFORMING ORGANIZATION NAME(S) AND ADDRESS(ES) U.S. Army Engineer Waterways Experiment Station Coastal Engineering Research Center 3909 Halls Ferry Road, Vicksburg, MS 39180-6199			8. PERFORMING ORGANIZATION REPORT NUMBER Technical Report CERC-93-12
9. SPONSORING/MONITORING AGENCY NAME(S) AND ADDRESS(ES)			10. SPONSORING/MONITORING AGENCY REPORT NUMBER
11. SUPPLEMENTARY NOTES Available from National Technical Information Service, 5285 Port Royal Road, Springfield, VA 22161.			
12a. DISTRIBUTION/AVAILABILITY STATEMENT Approved for public release; distribution is unlimited.		12b. DISTRIBUTION CODE	
13. ABSTRACT (Maximum 200 words) As ocean waves propagate into shallow water, they exhibit increasingly strong nonlinearities. One important nonlinear effect is the emergence of low-frequency energy as a consequence of interactions between higher frequency incident wave components. The low-frequency components can dominate the inner surf zone during storm conditions. Amphibious and LOTS operations can be seriously impacted by currents, water level variations, and runup induced by surf beat. Data were obtained from the U.S. Army Engineer Waterways Experiment Station laboratory and field facilities. A theoretical formulation for the growth of low-frequency energy in shallow water is evaluated against the data sets and used to develop guidelines for predicting surf beat.			
14. SUBJECT TERMS Laboratory experiments Numerical modeling Spectral wave modeling			15. NUMBER OF PAGES 182
16. PRICE CODE			
17. SECURITY CLASSIFICATION OF REPORT UNCLASSIFIED	18. SECURITY CLASSIFICATION OF THIS PAGE UNCLASSIFIED	19. SECURITY CLASSIFICATION OF ABSTRACT	20. LIMITATION OF ABSTRACT